Nonlinear optimal control methods for eco-driving and complete vehicle energy management

Nonlinear Optimal Control Methods for Eco-driving and Complete Vehicle Energy Management

GIOVANNY PAUL PADILLA CAZAR

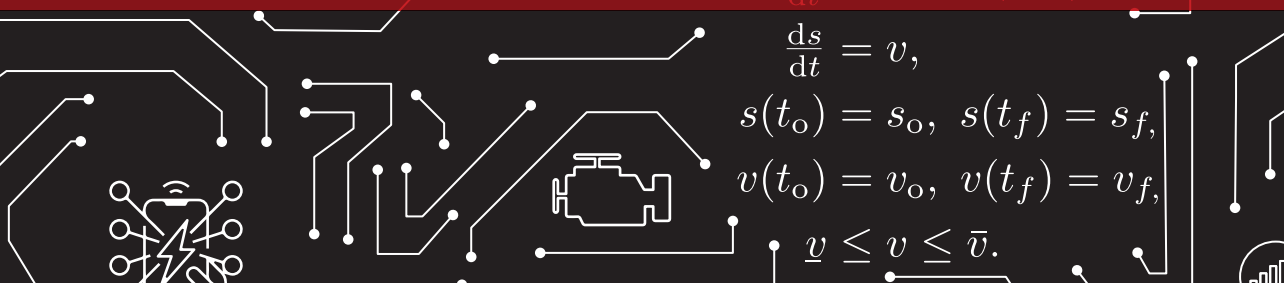

Nonlinear Optimal Control Methods for Eco-driving and Complete Vehicle Energy Management

Proefschrift

ter verkrijging van de graad van doctor aan de Technische Universiteit Eindhiven, op gezag van de rector magnificus prof. dr ir. F.P.T. Baaijens, voor een commissie aangewezen door het College voor Promoties, in het openbaar te verdedigen op dinsdag 1 december 2020 om 13:30 uur

door

Giovanny Paul Padilla Cazar

geboren te Quito, Ecuador

Dit proefschrift is goedgekeurd door de promotoren en de samenstelling van de promotiecommissie is als volgt:

voorzitter:	prof. dr. ir. P.G.M. Baltus
1e promotor:	prof. dr. S. Weiland
copromotor:	dr. ir. M.C.F Donkers
leden:	prof. dr. ir. F.P.T. Willems
	prof. dr. M. Cannon (University of Oxford)
	prof. dr. Antonio Sciarretta (IFP Energies Nouvelles)
	dr. ing. S. Grammatico (Technische Universiteit Delft)
	dr. ir. E. Silvas

Het onderzoek of ontwerp dat in dit proefschrift wordt beschreven is uitgevoerd in overeenstemming met de TU/e Gedragscode Wetenschapsbeoefening.

This work has received financial support from the Horizon 2020 programme of the European Union under the grant 'Electric Vehicle Enhanced Range, Life-time And Safety Through INGenious battery management' (EVERLASTING-713771).

This dissertation has been completed in fulfillment of the requirements of the Dutch Institute of Systems and Control (DISC) for graduate study.

A catalogue record is available from the Eindhoven University of Technology Library
ISBN: 978-90-386-5162-0

This thesis was prepared with the LaTeX documentation system.
Cover Design: Pamela Padilla

Summary

Electrification of transport systems has risen as a promising approach to mitigate environmental effects caused by CO2 emissions and to face the imminent depletion of fossil fuel reserves. Achieving high energy efficiency is crucial for the electrification of vehicles as it leads to a fuel consumption reduction for hybrid vehicles, whereas, for fully electric vehicles, it leads to an extension of the driving range, which reduces range anxiety concerns and contributes to the adoption electric vehicles in the market. An approach to achieve high energy efficiency is the use of well-designed vehicle energy management strategies.

Vehicle energy management strategies can be obtained by solving optimal control problems (OCPs). This thesis focuses on solution methods for nonlinear (and nonconvex) OCPs that emerge from energy optimization applications in vehicles. Specifically, this dissertation discusses modeling approaches and formulations of OCPs for vehicle energy management, global optimality of the solution, scalability of the optimization algorithms and the effects of uncertainty during operation.

The first part of this thesis focusses on eco-driving, which aims to obtain energy optimal velocity profiles. A detailed analysis of the related OCP shows that it has a unique global optimal solution despite the inherent nonconvexity of the problem formulation. This result is exploited to propose a sequential quadratic program that efficiently finds the solution to the eco-driving problem. Additionally, the eco-driving problem formulation is extended to include cornering effects by considering a low complexity model that purely relies in the geometry of the vehicle and the road characteristics. Using a high-fidelity model it is demonstrated that the proposed formulation can improve energy savings up to approximately 8% compared to traditional eco-driving approaches that do not considering cornering effects. This part finalizes with the study of an energy optimal coordination of autonomous vehicles crossing intersections. The proposed formulation aims to obtain the velocity profiles and the priority crossing order that minimize the aggregated energy consumption subject to safety constraints. Simulation results showed that coordinated autonomous vehicles can reduce energy consumption to approximately 16.2% compared to human driven vehicles with lack of coordination.

In the second part of this thesis, contributions are made to the complete vehicle energy management (CVEM) framework. This framework aims to provide strategies to operate all the energy consumers and producers present in the vehicle, which includes all auxiliary systems, possibly in combination with eco-driving. When considering CVEM without eco-driving, a power-based modelling approach is taken, in which the exchange of power between energy consumers and producers is described. This leads to a nonlinear OCP for which it can be shown that it has only global solutions, even though these solutions might be nonunique. This result is exploited to develop a distributed static optimization algorithm based on the Primal-

Dual proximal operator splitting method, leading to a computationally efficient and scalable algorithm that requires little tuning. Numerical examples show that this method can be approximately 3 times faster than off-the-shelf solvers and it can solve problems with a 100 times larger time horizon.

An exploration to include uncertainty due to traffic conditions in the CVEM problem by means of scenario-based optimization is also presented. In this case, the CVEM framework is used in a receding horizon fashion, in which uncertain driving conditions are represented as random constraints. Three methods for velocity prediction in energy management strategies are studied, i.e., a method based on (average) traffic flow information, a Gaussian process regression approach, and the combination of both. Numerical examples show deviations from optimality of approximately 0.75% to 1.79% for the proposed methods. Subsequently, an alternative modeling framework for CVEM is presented, which is based on a port-Hamiltonian approach. This description is suitable to obtain a systematic method to formulate a decomposable OCP for CVEM. A physically insightful cost function that describes the total energy consumption of the vehicle is proposed in terms of internal energy and losses of each system connected to the network. Additionally, it is demonstrated that eco-driving can be incorporated in the CVEM framework in a single OCP formulation, which allows to break, in some degree, the strong dependence on a priori information of the driving cycle, i.e., the velocity profile for a known trajectory in specific time interval. The solution to this unified problem formulation is obtained combining a sequential quadratic programming approach with dual decomposition. Numerical examples show an approximate improvement of 4.7% in energy savings with respect to a non-unified approach.

The final part of the thesis provides experimental results. A shrinking horizon approach to eco-driving for electric city buses is presented, where a reduction of 6.94% in energy consumption is achieved experimentally.

Contents

1

Introduction

1.1. Motivation

Transportation has deeply influenced the evolution of our civilization. Indeed, economic activities and level of welfare fully depend on the transport of raw materials, goods, people and services, and have a major impact on the organization and structural planning of urban and rural areas, public health and the environment. Unfortunately, the transportation has had a negative impact on the society and environment. For instance, the transport sector was responsible for 14% of the global CO_2 emissions from fossil fuel consumption in 2014 [1], Cars and vans in Europe contribute with 14% of the CO_2 emissions [2]. In 2016, it was estimated that 95% of the global transportation energy was based on petroleum fuels [3]. This dependency on fossil fuels is also a sensitive factor that influences the geopolitical stability since petroleum is a finite resource.

Over the last decades, the electrification of transport systems has been raised as a promising approach to reduce the negative effects caused by the environmental role of transportation and to face the imminent depletion of fossil fuels. In the ideal scenario, where electricity consumed by electric transportation systems is produced from renewable energy sources, it is expected that electric transportation will decrease the high oil dependency of modern society [4]. There are also advantages for less idealistic scenarios. For instance, the use of electric vehicles[1] (EV) can attenuate the noise levels, increase safety and significantly reduce CO_2 emissions. In Fig. 1.1, the full life cycle CO_2 emissions for petrol vehicles, diesel vehicles and EV in Europe is presented. This analysis considers CO_2 emissions linked to driving use, electricity production, and battery production. Remarkably, the CO_2 emissions of EV, on average, is 3 times less than petrol and diesel cars. This has motivated the introduction of more strict regulations on CO_2 emissions. For instance, the European Union fleet-wide average emission target for new cars will pass from $130\ g$

[1] Includes battery electric vehicles, plug-in hybrid electric vehicles, solar electric vehicles and fuel-cell electric vehicles.

1

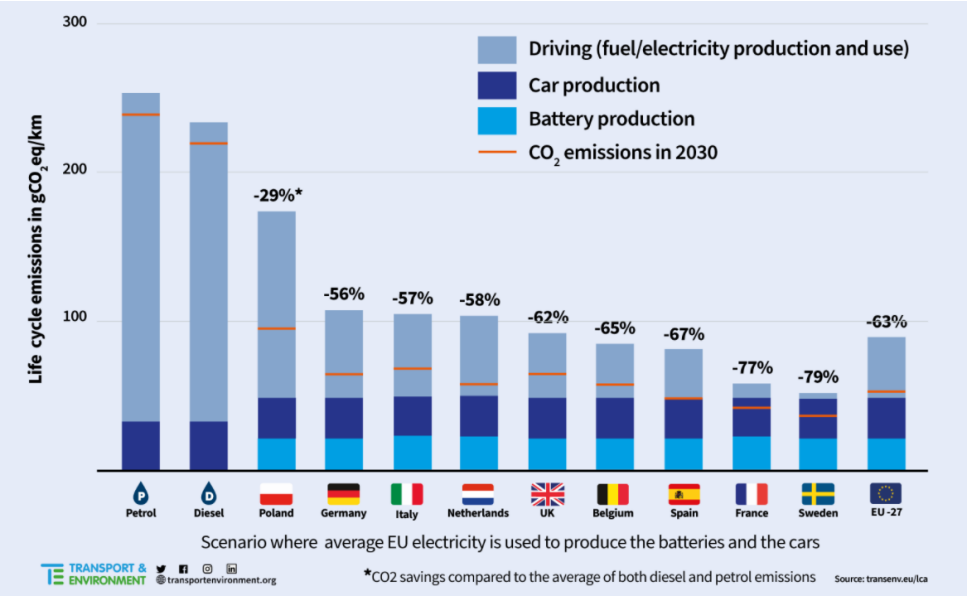

Figure 1.1: Life cycle CO_2 emission for petrol vehicles, diesel vehicles and EV [5].

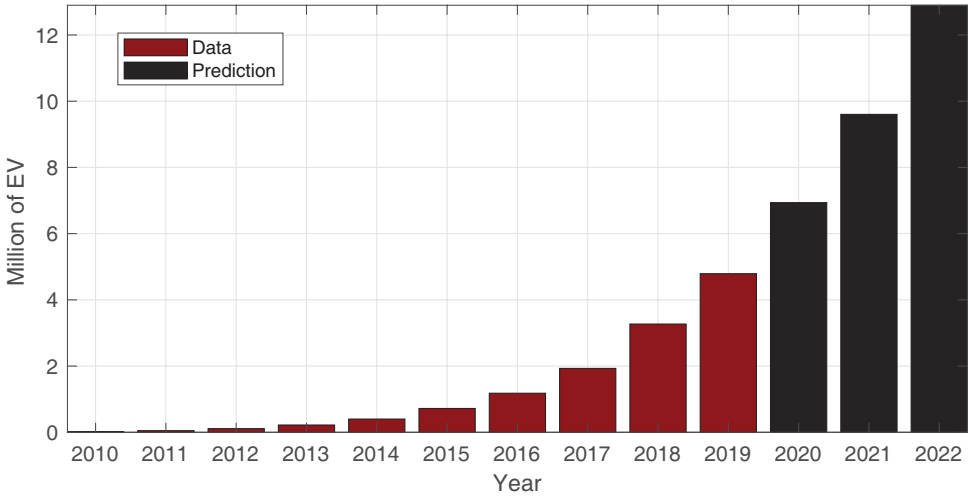

Figure 1.2: Global stock of electric vehicles. Historical data [6] and predictions .

CO_2/km to 95 g CO_2/km in 2021 [2]. Therefore, manufacturers and consequently the general public are actively stimulated to embrace EV in future years.

In recent years, the evolution of the market share for EV, i.e., the percentage of EV related sales in relation to the total automotive market, has opened the door for optimistic predictions about the future for electrified transportation. For instance,

the European market share for EV increased 32% in the period from 2017 to 2018 [7] and by 2019 the growth was of 50% [6] with respect to the previous year. In the Netherlands, the EV market share, was 6% in 2018 and by 2019, it reached 15% [6]. This encouraging tendency can be observed worldwide. For instance, in Fig. 1.2, the global EV stock per year is depicted. Using the historical data from [6], it is possible to estimate that by 2022 the global EV stock, i.e., number or registered EV, will reach approximately 12 million electric vehicles worldwide. All these trends are indicators that allow us to expect that by 2030 electrified transportation might reach a stage of mass market adoption. Scientific research and engineering contributions are at the basis of this development and have helped to accelerate the level of acceptance and the electrification of transport in general. The major contributions are not limited to the vehicles only, but extend to developments and improvements in batteries, charging infrastructure, and truly impressive developments on energy efficiency.

Even though electrified vehicles are entering the market, they have some disadvantages over conventional vehicles. For instance, their inherently limited range and slow charging times lead to range anxiety[2]. There are still many important challenges to be considered to further improve the electrification of the automotive sector, which as consequence contributes to reduce range anxiety concerns and accelerate adoption of electrified vehicles in the market. Some of these challenges are the degrading capacity of batteries to store energy, weather and traffic conditions that drastically affect the prediction of the remaining driving range, limited number of charging stations and the time-consuming charge process [10], [11]. As a response to challenges the following technological approaches are currently being developed:

- Energy dense batteries.
- Extended fast charging infrastructure.
- Accurate driving range prediction.
- Use of light-weight and highly efficient components.
- Energy management strategies.

The use of energy dense batteries implies a range extension that alleviates the range anxiety effects on the users [12]. Currently, Lithium-ion (Li-ion) batteries have been adopted as the market standard for electric vehicles, although their lifetime depends on the operating conditions and they can lead to unsafe situations (e.g., thermal runaway) when misused or due to manufacturing-induced malfunctioning. Significant advances in energy density are expected in the next 5 years by the addition of silicon to the Li-ion batteries, the use of alternative chemistries, introduction of additional energy storage elements such as super-capacitors, or the

[2]Range anxiety is defined as the concern (experienced by users) that the vehicle has insufficient energy to reach the next charging station [7]. Range anxiety has been identified as one of the main reasons that limits the penetration rate of EV in the market [8, 9].

rise of solid-state batteries [13]. Unfortunately, the adoption of these technologies by manufacturers will take longer and the economic impact is still unknown. On the other hand, the extension of charging infrastructure and the development of fast charging technologies aims to reduce the range anxiety by offering the user the possibility to always have a reachable charging station where the charging process is performed in a reduced time, which resembles the functionality of the current gas stations. The changes needed in the grid to support a large number of fast charging power stations are still being discussed [14]. Some estimations [15] indicated that the market was too uncertain to expect a large scale-roll-out of fast charging infrastructure. Nevertheless, the authors in [15] forecast that this scenario might drastically change with a larger adoption of EV in the market. The use of lightweight components in the design of vehicles has been also been considered, e.g., [16]. The main goal is to improve the efficiency of the vehicle, which is translated as range extension. Accurate driving range prediction and the use of energy is an effective way mitigate range anxiety. Accurate predictions of the remaining driving range relieves users' concerns.

Finally, the use of energy management strategies aims to obtain an improved efficiency during operation, which consequently extends the driving range of electrified vehicles. The main advantage to this approach is energy management strategies can, in most of the cases, be implemented in vehicles without requiring additional hardware. Hence, the implementation cost is marginal. For these reasons, energy management strategies that maximize the driving range have been a topic of intensive research in the last years. In this dissertation, energy management strategies are the main research topic and the main goal of this work is to:

Global Objective

Contribute to a clean mobility through accelerating the adoption of electric vehicles in the market using energy management strategies.

This research has been part of the European project EVERLASTING[3], which aims to extend the driving range of electric vehicles by securely exploiting the operating conditions of a given battery technology combined with advanced energy management methodologies.

1.2. Overview of Energy Management Strategies

In this section, the basic concepts of vehicle energy management strategies, i.e., eco-driving and complete vehicle energy management are provided. Special emphasis is put on its formulation as optimal control problems.

[3]The EVERLASTING aims to contribute to solve the issues of range anxiety, cost, reliability and safety of EV battery systems by developing flexible, modular, cost-effective battery management technologies and energy management strategies.

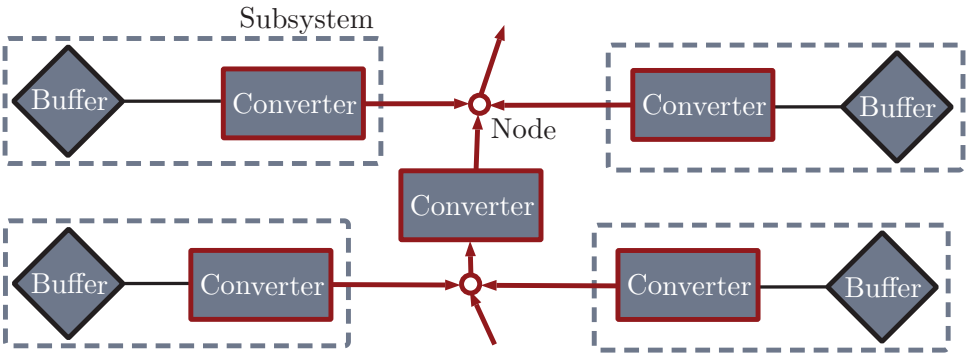

Figure 1.3: General power network topology for electrified vehicles.

1.2.1. Eco-driving

Eco-driving is an energy management strategy that takes advantage of the vehicle inertia to minimize the energy consumption. In general, given an initial and final point of a trajectory, eco-driving aims to find the optimal velocity profile that minimizes the total energy consumed in the trajectory. This optimization process is subject to the longitudinal vehicle dynamics, where the interaction between traction forces and resistive forces is described. In this sense, eco-driving minimizes the energy demanded by the vehicle to cover the desired trajectory and its implementation has a direct effect on the driving behavior. This could lead to significant improvements in energy savings, e.g., in [17] it has been reported that changes in driving behavior could improve the energetic performance of the vehicle more than 30%. It is important to remark that under this definition, the problem of optimizing the velocity profile is often formulated in isolation form the other subsystems in the vehicle, i.e., electric battery, heating ventilation and air conditioning system, etc. Eco-driving is generally considered as an optimal control problem [18].

1.2.2. Complete Vehicle Energy Management

Classic energy management strategies (EMS) have been mainly studied for hybrid electric vehicles. These strategies aim at reducing the energy consumption by an optimal distribution of power among the powertrain components, i.e., the battery, internal combustion engine and electric machine. The Complete Vehicle Energy Management (CVEM) concept was originally introduced in [19] as a holistic extension to classic EMS in vehicles. Later, methodologies to solve the CVEM problem in several automotive applications have been reported in [20–22]. The individual optimization of energy consumption in all the subsystems of a vehicle is incapable to produce a global energy efficient operation. This limitation is consequence of neglecting the iteration that exists between all the energy consumers inside a vehicle. Hence, a holistic approach that optimizes energy consumption of *all the interconnected subsystems* in the vehicle is needed, which is the basis for the CVEM concept.

The energy in the vehicle is transformed between different physical domains,

e.g., chemical energy that is stored as fuel can transformed into electrical energy by an electric generator unit; later, the produced electricity can be either transformed into mechanical energy to propel the vehicle or transformed into thermal energy to modify the temperature of the cabin. For this reason, considering power networks to describe the power iteration between the energy consumers is a useful tool in the CVEM framework. The idea of general power network architecture is presented in Fig. 1.3 and describes the conversion and interaction of power flows between different energy domains [19]. The power network depicted in this figure is composed by energy buffers and converters, which are represented by rhombus and rectangles respectively. The subsystems in the network are constituted by a single converter or by an energy buffer and a converter that are directly connected (gray dashed line). The proposed network has a general configuration that allows to easily describe specific vehicle topologies. The ideal features of CVEM are consequences of its interconnected nature and are summarized bellow:

Ideal Features of CVEM

- **Globally Optimal**
  The methods used to solve the CVEM problem should certify the global optimality of the obtained solutions.
- **Scalable**
  The methods to obtain energy management strategies should be able to handle problem formulations that grow in complexity, i.e., due to the additional subsystems in the network or by considering large time horizons.
- **Flexible**
  Updating or completely removing subsystems or its parameters should not imply major changes in the problem formulation and in the methods that find the energy management strategy.

1.2.3. Eco-driving and CVEMS as Optimal Control Problems

Both the eco-driving problem and the CVEM problem can be described as an optimal control problems. The formulation of the problem depends on the application goals;

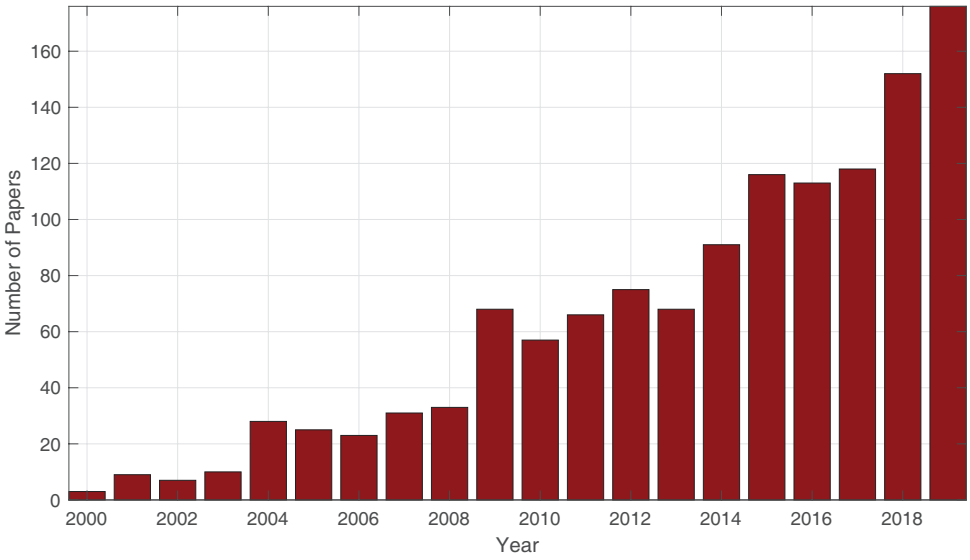

Figure 1.4: Research trend in EMS (number of papers per year published in IEEE that contain the key words "energy management" and "automotive").

however, it is possible to identify a general structure that is given by

$$\min_{\xi(\tau)} \quad \int_{\tau_0}^{\tau_f} J(\xi(\tau))\mathrm{d}\tau \tag{1.1a}$$

$$\text{subject to} \quad \mathcal{D}(\xi(\tau)) = 0, \tag{1.1b}$$

$$\mathcal{H}(\xi(\tau)) = 0, \tag{1.1c}$$

$$\mathcal{N}(\xi(\tau)) = 0, \tag{1.1d}$$

$$\underline{\mathbf{b}}(\xi(\tau)) \leq \mathcal{B}(\xi(\tau)) \leq \overline{\mathbf{b}}(\xi(\tau)), \tag{1.1e}$$

where $\xi(\tau)$ is a time or space dependent vector of decision variables that normally represent power, forces or even velocities in the vehicle. The cost function normally describes the cumulative power consumed from the energy sources in the vehicle over a driving cycle. The problem is subject to the dynamics of all the subsystems (1.1b), the power definition for each converter in the network (1.1c) and to (1.1d) that describes the power balance for all the nodes in the power network. Additionally, the optimal control problem (1.1) is bounded by (1.1e), which often represents power, torque and even velocity bounds. Note that eco-driving can be formulated as a special case of (1.1) that considers a single subsystems, i.e., the inertia of the vehicle.

1.3. State of the Art

A large amount of energy management strategies (EMS) have been reported in the last two decades. As can be seen in Fig. 1.4, the number of papers published in

2019 is approximately three times larger than the amount of papers published in 2010; thus, showing the growing interest of EMS the automotive industry. For the sake of simplicity, the literature that describes the state of the art in this research is divided in four relevant groups that are detailed bellow.

1.3.1. Classic EMS

Traditionally, energy management problems are focused on controlling the power split between the combustion engine and the electric machine of a hybrid electric vehicle. By storing regenerative braking energy and shifting the operating points of the combustion engine, a significant amount of fuel can be saved. In [23], [24, Ch. 4] optimization techniques for energy control on hybrid vehicles are summarized. Additionally, the books [25, 26] present a complete introduction to this research area. Classic EMS literature can be classified in ad hoc solutions and optimal control approaches. Additionally, the optimal control approaches can be subdivided into off-line and on-line control problems.

Heuristic solutions

The set of EMS that are included in this classification are normally characterized to be computationally fast, which make them suitable candidates for on-line implementations. Historically, these type of approaches were the first to appear in EMS literature [27, 28]. Fuzzy logic [29] and neural networks [30] are popular strategies among this classification. The disadvantage of these strategies is that the *performance of the systems is sensitive to changes in operation*, and the *global optimality of the solution cannot be guaranteed*. Nevertheless, some authors are have proposed solutions to properly recalibrate these strategies using dynamic programming (DP) [31], thus obtaining an acceptable approximation of the global solution.

Off-line optimal control problems

EMS under this category are normally used as benchmark solutions for specific applications or configurations of the optimal control problem due to the fact that global optimal solutions can be typically achieved. A representative technique in this category is DP. For instance in [32], applying DP forces the convergence to the global optimum of the energy management problem proposed. However, DP has the inherent disadvantage that *the computational burden increases with the number of states*.

Methods based on the Pontryagin's Maximum Principle (PMP), see, e.g., [33, 34] can handle computational complexity of multi-state energy management problems. In PMP, the problem is reduced to solving a two-point boundary value problem, which can be *difficult to solve in the presence of state constraints*. Moreover, the global optimality of the solutions obtained can only be guaranteed if the formulation of the optimal control problem is convex. Static optimization methods, contrary to PMP, can easily obtain solutions taking into account state constraints in the problem formulation. Additionally, these methods can guarantee *global optimality of the solution only for convex approximations of the energy management problems*, e.g., see [35] and the references therein.

Finally, it is important to remark that the EMS that belong to the offline optimal control problems classification, *need to have a priori complete information related to driving cycle*, i.e., velocity and road gradient.

On-line optimal control problems

In this case, algorithms that requires a low computational effort are described. For these methods, the requirement of a priori information related to the velocity and road profile is relaxed, which normally leads to *suboptimal solutions*. In [36, 37] infinite horizon stochastic DP is used to obtain an EMS off-line policy that is implemented as a look-up table in a embedded system with a low computational power.

A fast computational approach that is based on (approximations of) PMP is known as the equivalent consumption minimization strategy (ECMS) [38]. In this strategy, the energy consumption in the battery is transformed into an equivalent fuel consumption, which is represented by a co-state function related to the battery energy. The co-state can be estimated (which often leads to an approximations) at every time instant, thus eliminating the necessity for the complete driving profile information in advance. Consequently, ECMS can be implemented on-line, but updating the co-state is a delicate task that often leads to suboptimal solutions.

Model predictive control (MPC) is also used to implement on-line EMS [39, 40]. A finite-time horizon prediction of the future energy consumption is used to calculate the optimal control strategy, from which only the first control decision is implemented. A successive execution of this procedure obtains a suboptimal energy management policy, that depending on the quality of the predictions and the length of the receding horizon, can approximate well to the optimal solution.

1.3.2. CVEM Approaches

In general, the classic EMS approaches consider only a reduced set of subsystems, i.e., the power interaction between the the internal combustion engine, electric machine and batteries. This motivated the emergence of the CVEM concept, as it was already discussed in Section 1.2.2. CVEM aims to extend classic EMS approaches to incorporate more subsystems in the optimal control problem, which brings, as consequence, improvements in energy savings. The extra degrees of freedom added to the problem, makes CVEM appealing to be used in fully electric vehicles, where the power split between the electric machine and the combustion engine has disappeared.

CVEM was first proposed in [19] and a deep discussion about the difficulties using classic EMS techniques to solve the CVEM problem was also presented. For instance, DP can provide global optimal solutions to CVEM problems, however, scalability becomes an issue due to the curse of dimensionality observed in this technique. Similarly, the inherent set of state constraints presented in the CVEM problem makes PMP approaches difficult to be used for this application. As a consequence, centralized and decentralized optimization approaches have been proposed to satisfy the requirements imposed by the CVEM concept.

The research conducted within [20] has made some early attempts to incor-

porate auxiliaries into the classic EMS approaches. Due to the use of centralized optimization methods and convexification techniques the optimal control formulations that lead to *global optimality* and *scalability* features for CVEM are satisfied to some degree. However, the approaches reported are not flexible, i.e., *the EMS is not easily reconfigurable when new subsystems are introduced in the optimization problem due to the convexification procedure*. Additionally, some of the results presented in [20] have included the vehicle inertia in the energy management problem, which was solved by proposing a convex reformulation of the problem in space domain; in this case, *the lack of flexibility is also an unsolved issue*. The findings presented in [21] use a game-theoretic approach to solve the CVEM problems in a decentralized manner, where all the subsystems share a limited amount of information and are able to take some decisions autonomously. On-line implementations were obtained within this approach, where *predicted information is not considered, thus limiting the on-line implementation of the strategy*. In this research, *the inclusion of battery wear and charging acceptance are promising research directions that were not addressed*. Moreover, an exploration of algorithms that converge to a Nash's equilibrium are still an open task in in this study.

Recent research has highlighted the relevance of taking into account the interactions between thermal management systems and energy management systems to improve the energy efficiency in vehicles. For instance, considering the impact in energy consumption of considering power-train and battery thermal conditioning or waste heat recovery systems could lead energy management strategies with improved energy savings. This idea is known as integrated thermal and energy management (ITEM). It can be seen as a specific case of the CVEM problem, where a thermal subsystem is considered in the formulation. In [41], a detailed survey on the state of the art on ITEM systems is presented. Along the same line, [42] formulates the ITEM problem as a nonlinear optimal control problem that is solved using a short horizon fast MPC in combination with a large shrinking horizon MPC approach that obtains nearly optimal solutions.

Considering combined energy and emission management strategies for hybrid vehicles [43] can be considered a case of the CVEM framework. In this case, the interactions between the powertrain, combustion engine and aftertreatment system is considered in order to achieve energy optimal operation that is compliant with emission standards. The recent intentions to introduce zero emission zones in the European union have reactivated the interest in combined energy and emission management strategies.

A distributed optimization approach for CVEM is explored in [22] obtaining both on-line and off-line EMS implementations that are scalable and flexible for a large number of subsystems (including on/off auxiliaries) in the vehicle. This approach uses a dual decomposition to split a large and complex optimal control problem into several simple problems related to the subsystems in the vehicle. These subproblems iteratively share information with a central coordinator in order to achieve an equilibrium that is represented by the optimal solution to the CVEM problem. The off-line formulations of the distributed optimization problem presented in [22] are able to drastically reduce the simulation time compared to classic EMS. However,

this approach *requires a priori information of the driving profile and power consumption*. Furthermore, there are open questions related to the numerical aspects of the algorithms proposed to solve the distributed optimization problem, i.e., the convergence of the algorithms proposed has not been formally proved. On the other hand, the distributed optimization on-line formulation of the CVEM problem *uses finite-time horizon predictions in an MPC fashion to obtain a sub-optimal solution*. A disadvantage of the distributed optimization approach to CVEM is that it solves a nonconvex problem for which is *the global optimality of the solution* is not guaranteed. Moreover, it *requires the subsystems to be modeled by linear and (convex) quadratic models*. This renders the distributed optimization approach [22] *not usable for the applications where nonlinear models are required*. However, particular extensions of the distributed optimization approach that include nonlinear models have already been explored. For instance, in [44], a nonlinear battery ageing model has been introduced to the CVEM problem, while in [45], the inertia of the vehicle is considered as an energy buffer and connected to CVEM. This has shown the relevance of *exploring nonlinear optimal control methods to solve CVEM problems*.

1.3.3. Eco-driving

In the aforementioned approaches, the vehicle velocity (and thereby the power needed to propel the vehicle) is often assumed to be completely given a priori. Still, the vehicle inertia, which is the largest energy buffer in the vehicle, can have a large impact in energy savings and consequently in the extension of the driving range. For instance, in [17] it has been reported that changes in driving behavior could improve the energetic performance of the vehicle by more than 30% for journeys with similar distance and time constraints. These promising improvements in energy efficiency have contributed to the emergence of the eco-driving concept, which aims to increase the energy efficiency of a vehicle by means of a convenient selection of driving strategies; i.e. laws, technological implementations or simply changes in the driver's behavior. The problem of finding velocity profiles *(in isolation from the other subsystems in the vehicle)* that minimize the energy consumed by a vehicle in travelling to a specific destination in a fixed time has been considered for conventional vehicles in [46–48], for hybrid electric vehicles by [49, 50], and for electric vehicles by [51–55].

To solve the eco-driving problem, standard techniques used in optimal control have been adopted. In [56, 57] dynamic programming (DP) has been used. Alternatively, Pontryagin's minimum principle (PMP) has been used in [52, 58, 59] and [51] to solve the optimal control problems presented. The main disadvantage is that PMP only provides a necessary condition for optimality and cannot incorporate state constraints easily. Nevertheless, in [60], PMP is used to obtain analytical solutions to the specific scenarios of the eco-driving problems that can be used for on-line implementation. For instance, in [61] analytical solutions are used on a real-time event-triggered MPC implementation providing high-level driving mode suggestions to the driver.

In [48, 49, 55] static nonlinear optimization techniques are used to solve the

problem in the presence of state constraints. In order to guarantee that these static optimization techniques and the methods based on PMP find global optimal solutions, *it is important to understand the structure of the eco-driving optimal control problem*. Unfortunately, the literature related to this topic is scarce. The noticeable exception is [49], where the continuous-time optimal control problem is approximated to a convex formulation. However, the *possible loss of convexity in the discretisation step* (to arrive at a finite dimensional optimization problem) has not been considered in [49]. Eco-driving solutions have been widely implemented in Eco-Driving Assistance Systems (EDAS). Depending on the method used to influence the driving profile, the implementation of eco-driving solutions can be seen as an advisory system, where the driver receives suggestions to adjust the driving style to save energy consumption [61, 62] or as an adaptive cruise control (ACC) system, where the vehicle controls the velocity [63].

1.3.4. Preview Information

The energy performance for real time implementations of classic EMS and CVEM strategies strongly depends on the quality of the predictions that are used to solve the optimal control problem. In the case of eco-driving, complete information related to the driving profile is not necessary. However, this approach assumes no obstacles in the path, e.g., traffic lights, intersections, vehicles, etc. This implies that the performance of the real time eco-driving solutions can be improved using accurate predictions of the environmental conditions that surround the vehicle. Therefore, several methods to improve the preview information used in real time vehicle energy management applications have been reported in literature.

In [48], traffic information is integrated into the energy management problem as time and space varying velocity constraints that are updated every five minutes by the Freeway Performance Measurement System [64]. Similarly, in [65], the eco-driving problem is solved considering traffic conditions; the authors propose a method to automatically create a velocity corridor from statistical data taken from real operation. This velocity corridor is used to represent varying traffic flow. For both of the previous approaches, the results presented are promising; however, these *methods are mainly applicable in highways* where the influence of vehicles and traffic lights of intersections are not significant for the overall performance.

In the last years, energy management in urban traffic environments has become a relevant research branch. For this case, the preview information is mainly obtained by *predictions based on data from sensors and communication networks*, e.g, vehicle to vehicle (V2V) or vehicle to infrastructure (V2I). Approaches to solve the eco-driving problem for a road segment with several traffic lights have been reported in [66, 67]. In [68, 69] energy optimal adaptive cruise controllers are proposed, this approaches uses sensor information and V2V communication to design energy optimal velocity profiles constrained by the interaction with other vehicles in urban environments.

Most of the cases previously described focus its attention on optimizing the velocity profile *neglecting the influence of other subsystems*. Since, EMS require the power request to be known in advance, obtaining accurate predictions of the

power request is fundamental to obtain relevant energy savings in practice. To this end, the use of stochastic optimal control methods have become a popular approach to take into account the uncertainty present in real traffic conditions for EMS. These strategies are typically obtained using Stochastic Dynamic Programming (SDP) [70], which suffers from scalability problems known as the *"Curse of Dimensionality"*, or Stochastic MPC [71], which could become computationally demanding when the number of subsystems considered in the control problem increases. Nevertheless, the need to account for the presence of uncertainty is still an open topic to improve the implementation capabilities of these EMS.

1.4. Research Questions

In this section, the research questions of this dissertation are stated. The state of the art previously discussed shows that a large portion of the research conducted has been devoted to classic energy management for automotive applications; an other large amount of research has been devoted to to optimize the velocity profiles of the vehicle, i.e., eco-driving. The dynamics that emerge from the integration of additional subsystems into classic EMS has started to be explored in the CVEM framework and it has shown significant improvements in energy efficiency.

Note that the classic EMS can be considered a subset as of CVEM strategies. Moreover, by considering the inertia of the vehicle as an energy buffer, eco-driving can be naturally incorporated in the CVEM framework, which eliminates the strong dependence of classic EMS on a priori information of the driving cycle, i.e., the velocity profile for a known trajectory in specific time interval. Unfortunately, this implies the introduction of models with higher complexity in the CVEM formulation, which requires to extend and design methodologies that are suitable to formulate and solve nonlinear optimal control problems for CVEM. This research needs to also focus on the ideal features of the CVEM framework, i.e., global optimality, scalability and flexibility. Furthermore, anticipation and robustness of the strategies have to be considered to maintain an energy efficient operation during uncertain traffic scenarios. As a consequence, the following research question is posed:

Main Research Question

Can the current eco-driving and CVEM methods be improved by considering the integration of dynamical features of the systems and the uncertainty of real traffic scenarios such that both higher energy savings and an adequate computational performance are obtained?

Sub-questions and Contributions

In this section, the main research question is subdivided in different branches, where specific research sub-questions will be posed. Moreover, the contributions of this thesis will be linked to those sub-questions and briefly discussed.

1

B.1 Integrating dynamical systems of higher complexity in the CVEM problem

The current modeling methodology in the CVEM framework aims to approximate the components as buffer, represented by linear dynamical systems, connected to an energy converter, described as static quadratic nonlinearities [22]. This approach is useful to obtain convex approximations of the CVEM optimal control problem. However, it might introduce large errors if components represented by models with a higher complexity need to be integrated in the CVEM problem, e.g., incorporating eco-driving in the CVEM framework. This yields to the following sub-question.

Research Sub-question 1

What modelling frameworks are suitable to formulate CVEM optimal control problems that consider components represented with models of a higher complexity?

This sub-question is addressed in the following chapters:

- In Chapter 3, the traditional eco-driving optimal control problem formulation is extended to consider the effects of cornering. Specifically, an approximation of the cornering effects that completely relies in the geometry of the road is proposed and validated.
- In Chapter 4, the eco-driving problem formulation presented in Chapter 3 is extended to consider multiple fully autonomous vehicles crossing an intersection. This modeling framework formulates the conflict resolution problem as an optimal control problem, where the objective is to minimize energy consumption of all the vehicles, while avoiding collisions.
- In Chapter 7, a modelling approach based on Port-Hamiltonian systems representations is presented. This physically insightful description provides a systematic approach to formulate a decomposable optimal control problem for CVEM. The advantages of this modeling framework are highlighted in simulations that also validate the approach.
- Chapter 8 extends the current CVEM modelling framework to consider systems with nonlinear dynamics. This is especially useful to integrate eco-driving onto the CVEM formulations.

The use of richer models lead to nonlinear and possibly nonconvex optimal control problem formulations for CVEM. Static optimization approaches are suitable candidates to solve these nonlinear optimal control problems, since these approaches lack the disadvantages of DP and PMP. This brings the following research sub-question.

Research Sub-question 2

What static optimization methods are appropiate to solve the different configurations of eco-driving and nonlinear CVEM optimal control problems?

The contributions linked to this sub-question are described in the following list.

- In Chapter 2, Sequential Quadratic Programming (SQP) with an specific Hessian approximation is used to solve the eco-driving optimal control problem formulation.
- In Chapter 4, sequential mixed-integer quadratic programing is used to solve the energy optimal coordination of fully autonomous vehicles crossing intersections.
- Chapter 5 presents a distributed optimization approach for large-scale CVEM problems based on a Primal-Dual Proximal operator splitting method.
- Chapter 6 uses scenario-based optimization as part of a receding horizon approach that solves the CVEM problem in presence of uncertainties for the future power request.
- In Chapter 8, an SQP with Tikhonov regularization is used in combination with a dual decomposition approach to solve a CVEM formulation that integrates eco-driving.
- An advisory eco-driving system implementation is presented in Chapter 9, where the SQP approach proposed in Chapter 2 is used as part of the shrinking horizon model predictive control implemented to solve the eco-driving problem.

B.2 Higher effciency.

Energy management strategies with the highest possible energy efficiency are global optimal solutions to optimal control problems. Therefore, global optimality is an important feature of the CVEM framework [19]. In general, eco-driving and CVEM optimal control problems formulations are nonconvex. Therefore, there are no guarantees about global optimality of the solutions obtained by static optimization methods. One possible path to overcome this is to use convex relaxations. Unfortunately, this methods sometimes needs strong assumptions on modelling or, simply, cannot be directly applied to some configurations of the optimal control problem problem. This discussion leads to the following sub-question.

Research Sub-question 3

Under which conditions is it possible to provide guarantees for the global optimality of the solutions to the eco-driving and CVEM prolems?

The following contributions answer to this sub-question.

- Chapter 2 shows that the existence of a unique global optimal solution to the eco-driving problem is guaranteed under physically realistic conditions.
- In Chapter 5, the conditions under which the existence of only multiple global solutions to the CVEM problem are presented.

B.3 Scalability and flexibility

The distributed optimization approaches proposed in [22] have reported promising results in terms of numerical performance for off-line applications. These methods make the CVEM flexible and scalable. Unfortunately, the convergence in several of the algorithms proposed has not been guaranteed. Moreover, configuring the parameters of the algorithms to obtain satisfactory performance can be a cumbersome task. This opens the following research subquestion.

Research Sub-question 4

What optimization method with convergence guarantees can lead to a simple implementation of CVEM strategies maintaining an acceptable numerical performance?

This sub-question is addressed in Chapter 5, where a distributed optimization algorithm for nonconvex problems is presented. This algorithm is based on a primal-dual proximal splitting method and has theoretical convergence guarantees. Moreover, it uses a spectral method to automatically select the step-sizes of the distributed optimization algorithm at every iteration, which drastically simplifies its implementation. The scalability and flexibility of this method is demonstrated in a simulation study.

B.4 Anticipation and robustness

Real driving conditions are subject to uncertainty, thereby making the energy management a challenging problem. The limitations in energy savings appear as a consequence of the quality of the predictions in the power request. Energy management strategies need to be robust with respect to uncertainty of the real traffic scenarios. For Eco-driving, achieving acceptable energy savings under real driving conditions imply the necessity to anticipate for traffic lights, intersections and the behavior of other vehicles. Nowadays, the access

to historical data or direct information form other vehicles (V2V) or infrastructure (I2V) provides new opportunities to exploit this information to improve the energy savings in energy management implementations that consider real driving scenarios. These new possibilities introduces anticipation and robustness features to the CVEM framework. Under this perspective the natural research sub-question is the following.

Research Sub-question 5

Considering real driving conditions, what are the improvements in energy savings for eco-driving and CVEM strategies that exploit available preview information, i.e., historical data and communication networks?

The contributions linked to this sub-question are summarized below.

- In Chapter 4, eco-driving is extended to solve a conflict resolution problem for multiple autonomous vehicles crossing an intersection. In this scenario, it is assumed that I2V and V2V communications provide all the information required. The energy savings of this approach with respect human driven vehicles are assessed through numerical simulations.
- In Chapter 6, the CVEM framework is employed in a receding horizon fashion, in which random constraints represent realizations of the uncertain driving conditions. In this chapter, available preview information is exploited in three methods for velocity prediction, i.e., a method based on (average) traffic flow information, a method based on Gaussian process regression, and a method that combines both. The energy savings that these approaches obtain are studied in simulation results.

1.5. Thesis Outline

A graphical representation of the structure of this dissertation is depicted in Fig. 1.5. The thesis is divided in three main parts. Part I encompasses the contributions related to eco-driving strategies. In Part II, CVEM strategies constitute the main focus. In this part, the integration of CVEM and eco-driving is also considered. Finally, Part III presents experimental results for an eco-driving strategy described in Part I. Additionally, conclusions and recommendations of this thesis are presented in Part III. An outline of the chapters contained in each part the thesis is given below.

Part I: Eco-driving

In Chapter 2, the existence of a unique global optimal solution for the eco-driving problem is presented. This result is exploited to formulate a sequential quadratic program that efficiently solves the eco-driving optimal control problem. This eco-driving formulation is extended in Chapter 3 to consider cornering effects in the optimal control problem. The strategies obtained are validated in simulations using

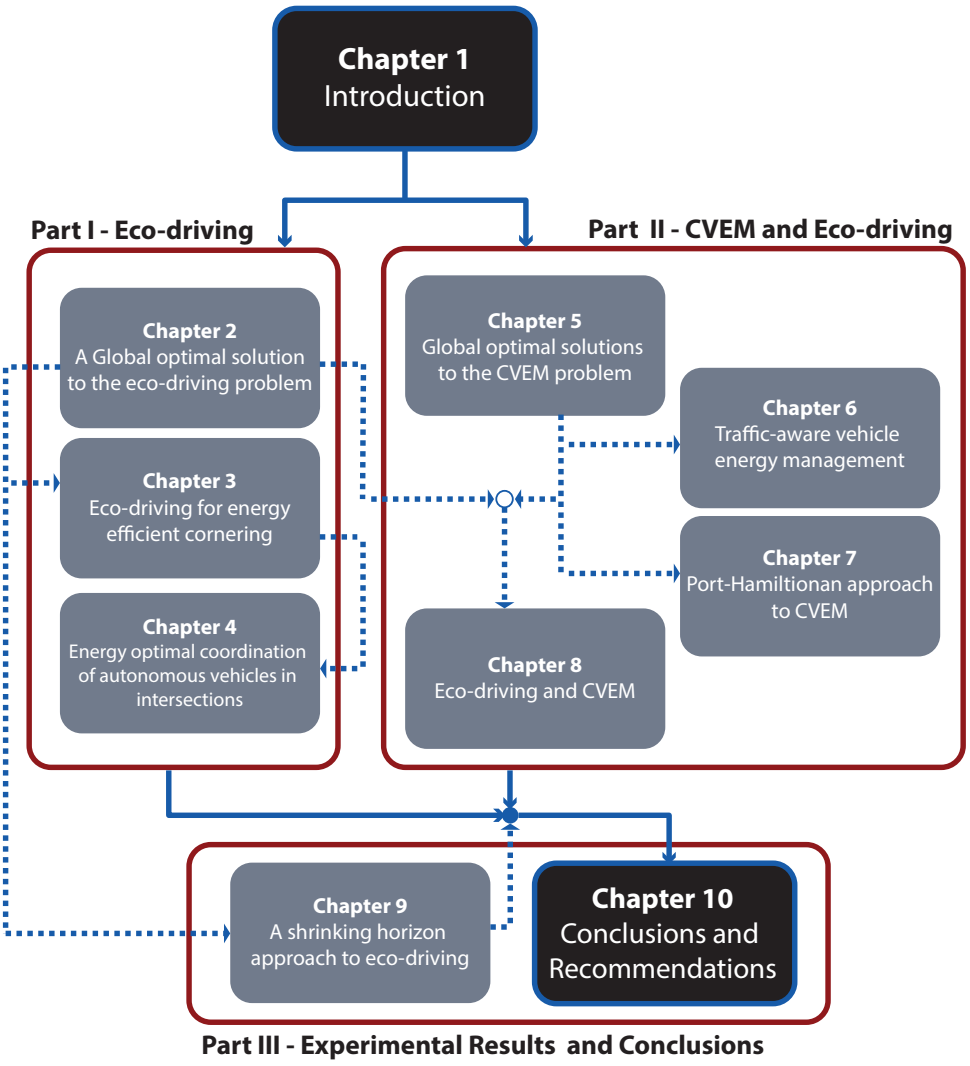

Figure 1.5: Outline of the theis. Arrows indicate "read-before" relations.

a high-fidelity vehicle model. In Chapter 4, the eco-driving formulation presented in Chapter 3 is used as the basis to formulate an energy optimal conflict resolution problem for autonomous vehicles crossing an intersection. The numerical results presented in this chapter show that the optimized coordination of speed profiles for each agent in the intersection has improved energy savings compared to the uncoordinated case.

Part II: CVEM and Eco-driving

Chapter 5 shows that the CVEM problem has only global optimal solutions. Taking advantage of this finding, a distributed optimization algorithm for non-convex problems based on a Primal-Dual operator splitting method is proposed. As a result of splitting the time horizon and separating the components in the power network, the algorithm breaks-down the complexity of the optimization problem to obtain an enhanced numerical performance. Additionally, the implementation of the distributed algorithm is simplified by an adaptive step-size selection approach. In Chapter 6, the uncertainty of real traffic scenarios is considered in the CVEM. The problem is solved using a scenario-based optimization approach and several methods to synthesize uncertainty from available data are explored. An alternative modeling framework based on Port-Hamiltonian representations is presented in Chapter 7. This approach allows the formulation of a physically insightful separable optimal control problem. The modelling framework and problem formulation are validated using numerical simulations. Finally, in Chapter 8 the CVEM framework is extended to integrate eco-driving. The optimal control problem is solved by a combination of sequential quadratic programing and dual decomposition. Numerical results show improved energy savings with respect to a CVEM strategy without eco-driving.

Part III: Experimental Results and Conclusions

In Chapter 9, experimental results from a shrinking horizon approach for eco-driving are presented. This implementation is used to successfully validate the results presented in Chapter 2. Finally, conclusions and recommendations are discussed in Chapter 10.

1

1.6. List of Publications

The contributions discussed in this thesis have been part of the following publications.

P.1 **G. P. Padilla**, C. J. J. Beckers, C. Pelosi and M. C. F. Donkers, *Eco-driving for energy efficient cornering of electric vehicles in urban scenarios*, Proceedings of IFAC World Congress, 2020.

P.2 C. Pelosi, **G. P. Padilla** and M. C .F. Donkers, *Energy optimal coordination of fully autonomous vehicles in urban intersections*, Proceedings of IFAC World Congress, 2020.

P.3 L. A. Wulf, **G. P. Padilla** and M. C. F. Donkers, *Traffic-aware vehicle energy management strategies via scenario-based optimization*, Proceedings of IFAC World Congress, 2020.

P.4 **G. P. Padilla**, J. C. Flores and M. C. F. Donkers, *Port-Hamiltonian approach to complete vehicle energy management: a battery electric vehicle case study*, Proceedings of American Control Conference, 2020.

P.5 **G. P. Padilla**, G. Belgioioso and M. C. F. Donkers, *Global solutions to the complete vehicle energy management problem via forward-backward operator splitting*, Proceedings of IEEE Conference on Decision and Control, 2019.

P.6 **G. P. Padilla**, J. C. Flores and M. C. F. Donkers, *A shrinking horizon approach to eco-driving for electric city buses: implementation and experimental results*, Proceedings of IFAC International Symposium on Advances on Automotive Control, 2019.

P.7 **G. P. Padilla**, S. Weiland and M. C. F. Donkers, *A global optimal solution to the eco-driving problem*, IEEE Control Systems Letters, 2018.

P.8 Z. Khalik, **G. P. Padilla**, T. C. J. Romijn and M. C. F. Donkers, *Vehicle energy management with ecodriving: a sequential quadratic programming approach with dual decomposition*, Proceedings of American Control Conference, 2018.

Part of this thesis has been including in the following unpublished article:

S.1 **G. P. Padilla**, G. Belgioioso and M. C. F. Donkers, *Complete Vehicle Energy Management using AdaptivePrimal-Dual Operator Splitting*, to be submitted for journal publication, 2020.

References

[1] Intergovernmental Panel on Climate Change (IPCC), *Fifth assessment report, climate change 2014: Synthesis report,* (2014).

[2] Climate Action - European Commission, *Reducing CO2 emissions from passenger cars - before 2020,* (2016).

[3] United States Environmental Protection Agency, *Global Greenhouse Gas Emissions Data,* (2016).

[4] J. Seiner, M. Lackner, and W.-Y. Chen, *Energy efficient design of future transportation systems,* in *Handbook of Climate Change Mitigation* (2012).

[5] *How clean are electric cars? | transport & environment,* (2020).

[6] *Global EV Outlook 2020*, Tech. Rep. (International Energy Agency, 2020).

[7] *Global EV Outlook 2017*, Tech. Rep. (International Energy Agency, 2017).

[8] *Electric vehicles in Europe*, Tech. Rep. (European Environment Agency, 2016).

[9] *Electric vehicles in Europe: Gearing up for a new phase?*, Tech. Rep. (McKinsey & Company, 2017).

[10] D. Watzenig and B. Brandstätter, eds., *Comprehensive Energy Management – Eco Routing & Velocity Profiles*, SpringerBriefs in Applied Sciences and Technology (Springer International Publishing, 2017).

[11] H. A. Bonges and A. C. Lusk, *Addressing electric vehicle (ev) sales and range anxiety through parking layout, policy and regulation,* Transportation Research Part A: Policy and Practice (2016).

[12] R. A. Hanifah, S. F. Toha, and S. Ahmad, *Electric vehicle battery modelling and performance comparison in relation to range anxiety,* in *Proc. IEEE International Symposium on Robotics and Intelligent Sensors* (2015).

[13] *Electric Vehicle Battery and Charging Technologies*, Tech. Rep. (ABI Research, 2019).

[14] O. Mohammed, T. Youssef, M. H. Cintuglu, and A. Elsayed, *Chapter 12 - design and simulation issues for secure power networks as resilient smart grid infrastructure,* in *Smart Energy Grid Engineering*, edited by H. A. Gabbar (Academic Press, 2017).

[15] A. Schroeder and T. Traber, *The economics of fast charging infrastructure for electric vehicles,* (2012).

[16] *ALIVE (Advanced High Volume Affordable Lightweighting for Future Electric Vehicles)*, Tech. Rep. (European Commission, 2016).

[17] C. Bingham, C. Walsh, and S. Carroll, *Impact of driving characteristics on electric vehicle energy consumption and range,* IET ITS (2012).

[18] A. Sciarretta, G. D. Nunzio, and L. L. Ojeda, *Optimal Ecodriving Control: Energy-Efficient Driving of Road Vehicles as an Optimal Control Problem,* IEEE Control Systems MAgazine (2015).

[19] J. Kessels, J. H. M. Martens, P. P. J. Van den Bosch, and W. H. A. Hendrix, *Smart vehicle powernet enabling complete vehicle energy management,* in *Proc. IEEE VPP Conference, 2012* (2012).

[20] N. Murgovski, B. Egardt, and M. Nilsson, *Predictive control for complete vehicle energy management*, Tech. Rep. (Swedish Hybrid Vehicle Centre, Sweden, 2015).

[21] H. Chen, *Game-theoretic Solution Concept for Complete Vehicle Energy Management*, Ph.D. thesis, Technische Universiteit Eindhoven (2016).

[22] T. C. J. Romijn, *A Distributed Optimization Approach to Complete Vehicle Energy Management*, Ph.D. thesis, Technische Universiteit Eindhoven (2017).

[23] A. Sciarretta and L. Guzzella, *Control of hybrid electric vehicles,* Control Systems Magazine (2007).

[24] *Model-Based Supervisory Control for Energy Optimization of Hybrid-Electric Vehicles,* in *Control System Applications*, edited by L. Guzzella and A. Sciarretta (2009).

[25] B. d. Jager, T. v. Keulen, and J. Kessels, *Optimal Control of Hybrid Vehicles*, Advances in Industrial Control (2013).

[26] L. Guzzella and A. Sciarretta, *Vehicle Propulsion Systems* (Springer, Berlin, Heidelberg, 2013).

[27] N. Jalil, N. A. Kheir, and M. Salman, *A rule-based energy management strategy for a series hybrid vehicle,* in *Proc. American Control Conference* (1997).

[28] H. Banvait, S. Anwar, and Y. Chen, *A rule-based energy management strategy for Plug-in Hybrid Electric Vehicle (PHEV),* in *Proc. American Control Conference* (2009).

[29] H. Hannoun, D. Diallo, and C. Marchand, *Energy management strategy for a parallel hybrid electric vehicle using fuzzy logic,* in *Proc. International Symposium on Power Electronics, Electrical Drives, Automation and Motion.* (2006).

[30] Z. Chen, C. C. Mi, J. Xu, X. Gong, and C. You, *Energy Management for a Power-Split Plug-in Hybrid Electric Vehicle Based on Dynamic Programming and Neural Networks,* IEEE Transactions on Vehicular Technology (2014).

[31] J. Peng, H. He, and R. Xiong, *Rule based energy management strategy for a series–parallel plug-in hybrid electric bus optimized by dynamic programming,* Applied Energy Clean, Efficient and Affordable Energy for a Sustainable Future (2017).

[32] R. Wang and S. M. Lukic, *Dynamic programming technique in hybrid electric vehicle optimization,* in *Proc. IEEE International Electric Vehicle Conference* (2012).

[33] T. H. Pham, J. T. B. A. Kessels, P. P. J. v. d. Bosch, R. G. M. Huisman, and R. M. P. A. Nevels, *On-line energy and Battery Thermal Management for hybrid electric heavy-duty truck,* in *Proc. American Control Conference* (2013).

[34] S. Ebbesen, P. Elbert, and L. Guzzella, *Battery State-of-Health Perceptive Energy Management for Hybrid Electric Vehicles,* IEEE Transactions on Vehicular Technology (2012).

[35] B. Egardt, N. Murgovski, M. Pourabdollah, and L. J. Mardh, *Electromobility Studies Based on Convex Optimization: Design and Control Issues Regarding Vehicle Electrification,* Control Systems Magazine (2014).

[36] T. Leroy, F. Vidal-Naquet, and P. Tona, *Stochastic Dynamic Programming based Energy Management of HEV's: an Experimental Validation,* Proc. IFAC World Congress (2014).

[37] P. Elbert, M. Widmer, H.-J. Gisler, and C. Onder, *Stochastic dynamic programming for the energy management of a serial hybrid electric bus,* International Journal of Vehicle Design (2015).

[38] G. Paganelli, S. Delprat, T. M. Guerra, J. Rimaux, and J. J. Santin, *Equivalent consumption minimization strategy for parallel hybrid powertrains,* in *Proc. IEEE Vehicular Technology Conference.*

[39] H. Borhan, A. Vahidi, A. M. Phillips, M. L. Kuang, I. V. Kolmanovsky, and S. D. Cairano, *MPC-Based Energy Management of a Power-Split Hybrid Electric Vehicle,* IEEE Transactions on Control Systems Technology (2012).

[40] R. S. Vadamalu and C. Beidl, *Online MPC based PHEV Energy Management using conic interior-point methods,* in *Proc. IEEE Intelligent Vehicles Symposium* (2016).

[41] C. Wei, T. Hofman, E. I. Caarls, and R. van Iperen, *Evolution and classification of energy and thermal management systems in electrified powertrains,* in *Proc. IEEE Vehicle Power and Propulsion Conference* (2019).

[42] Q. Hu, M. R. Amini, H. Wang, I. Kolmanovsky, and J. Sun, *Integrated power and thermal management of connected hevs via multi-horizon mpc,* in *Proc. IEEE American Control Conference* (2020).

[43] J. T. B. A. Kessels, F. P. T. Willems, W. J. Schoot, and P. P. J. van den Bosch, *Integrated energy emission management for hybrid electric truck with scr aftertreatment,* in *IEEE Vehicle Power and Propulsion Conference* (2010).

[44] Z. Khalik, T. C. J. Romijn, M. C. F. Donkers, and S. Weiland, *Effects of Battery Charge Acceptance and Battery Aging in Complete Vehicle Energy Management,* in *Proc. IFAC World Congress* (2017).

[45] D. Chen, Y. Kim, M. Huang, and A. Stefanopoulou, *An iterative and hierarchical approach to co-optimizing the velocity profile and power-split of plug-in hybrid electric vehicles,* in *Proc. American Control Conference* (2020).

[46] D. Maamria, K. Gillet, G. Colin, Y. Chamaillard, and C. Nouillant, *Optimal eco-driving for conventional vehicles: Simulation and experiment,* in *Proc. IFAC World Congress* (2017).

[47] F. Mensing, R. Trigui, and E. Bideaux, *Vehicle trajectory optimization for application in ECO-driving,* in *Proc. IEEE VPP Conference* (2011).

[48] N. J. Kohut, J. K. Hedrick, and F. Borrelli, *Integrating traffic data and model predictive control to improve fuel economy,* in *Proc. Symposium of Control in Trasnportation Systems* (2009).

[49] N. Murgovski, L. Johannesson, X. Hu, B. Egardt, and J. Sjöberg, *Convex relaxations in the optimal control of electrified vehicles,* in *Proc. American Control Conference* (2015).

[50] L. Johannesson, N. Murgovski, E. Jonasson, J. Hellgren, and B. Egardt, *Predictive energy management of hybrid long-haul trucks,* Control Engineering Practice (2015).

[51] N. Petit and A. Sciarretta, *Optimal drive of electric vehicles using an inversion-based trajectory generation approach,* in *Proc. IFAC World Congress* (2011).

[52] W. Dib, A. Chasse, P. Moulin, A. Sciarretta, and G. Corde, *Optimal energy management for an electric vehicle in eco-driving applications,* Control Engineering Practice (2014).

[53] J. Rios-Torres, P. Sauras-Perez, R. Alfaro, J. Taiber, and P. Pisu, *Eco-Driving System for Energy Efficient Driving of an Electric Bus,* SAE International Journal of Passenger Cars - Electronic and Electrical Systems (2015).

[54] A. Lajunen, *Energy-optimal velocity profiles for electric city buses,* in *Proc. IEEE Conference on Automation Science and Engineering, 2013*.

[55] Z. L. Tan, T. Wilhelem, H. Okuda, B. Levedahl, and T. Suzuki, *Computation of energy-optimal velocity profile for electric vehicle considering slope of route,* in *Proc. IEEE/SICE International Symposium on System Integration* (2015).

[56] M. Vašak, M. Baotić, N. Perić, and M. Bago, *Optimal rail route energy management under constraints and fixed arrival time,* in *Proc. IEEE European Control Conference* (2009).

[57] E. Hellström, J. Åslund, and L. Nielsen, *Management of kinetic and electric energy in heavy trucks,* SAE International Journal of Engines (2010).

[58] T. van Keulen, B. de Jager, and M. Steinbuch, *Optimal Trajectories for Vehicles with Energy Recovery Options,* Proc. IFAC World Congress (2001).

[59] M. Henriksson, O. Flärdh, and J. Mårtensson, *Optimal speed trajectory for a heavy duty truck under varying requirements,* in *Proc. IEEE International Conference on Intelligent Transportation Systems* (2016).

[60] A. Sciarretta and A. Vahidi, *Energy-Efficient Driving of Road Vehicles* (Springer International Publishing).

[61] Y. Chen and M. Lazar, *Real-time driving mode advice for eco-driving using mpc,* (2020).

[62] Q. Cheng, L. Nouvelière, and O. Orfila, *A new eco-driving assistance system for a light vehicle: Energy management and speed optimization,* in *Proc. IEEE Intelligent Vehicles Symposium (IV)* (2013).

[63] A. Weissmann, D. Görges, and X. Lin, *Energy-Optimal Adaptive Cruise Control based on Model Predictive Control,* in *Proc. IFAC World Congress* (2017).

[64] *PeMS Data Source,* .

[65] M. Henriksson, O. Flardh, and J. Martensson, *Optimal Speed Trajectories Under Variations in the Driving Corridor,* in *Proc. IFAC World Congress* (Toulouse, 2017).

[66] E. Kural, S. Jones, A. F. Parrilla, and A. Grauers, *Traffic light assistant system for optimized energy consumption in an electric vehicle,* in *Proc. International Conference on Connected Vehicles* (2014).

[67] G. De Nunzio, C. C. de Wit, P. Moulin, and D. Di Domenico, *Eco-driving in urban traffic networks using traffic signals information,* International Journal of Robust and Nonlinear Control (2016).

[68] F. Flehmig, A. Sardari, U. Fischer, and A. Wagner, *Energy optimal Adaptive Cruise Control during following of other vehicles,* in *Proc. IEEE Intelligent Vehicles Symposium* (2015).

[69] L. Bertoni, J. Guanetti, M. Basso, M. Masoero, S. Cetinkunt, and F. Borrelli, *An adaptive cruise control for connected energy-saving electric vehicles,* in *Proc. IFAC World Congress* (2017).

[70] L. Johannesson, M. Asbogard, and B. Egardt, *Assessing the Potential of Predictive Control for Hybrid Vehicle Powertrains Using Stochastic Dynamic Programming,* IEEE Trans on Intell Transportation Syst (2007).

[71] S. Di Cairano, D. Bernardini, A. Bemporad, and I. V. Kolmanovsky, *Stochastic MPC With Learning for Driver-Predictive Vehicle Control and its Application to HEV Energy Managements,* IEEE Trans on Control Syst Techn (2014).

I

Eco-driving

2

A Global Optimal Solution to the Eco-Driving Problem

Eco-driving aims at minimizing the energy consumption of a vehicle by adjusting the vehicle's velocity. This can be formulated as an optimal control problem and this chapter provides a detailed view on the global optimal solution to this problem. A method to reformulate and discretize the problem avoiding the introduction of additional non-convex terms is presented. Furthermore, physically realistic conditions are given that guarantee the existence of the global optimal solution to the eco-driving problem. Subsequently, a sequential quadratic programming algorithm is provided that allows finding the global optimal solution. Finally, two numerical examples are used to illustrate how solutions of the eco-driving problem can be obtained.

This chapter is based on **P.7**.

Improving energy efficiency of vehicles is an important topic of research for the automotive industry. High energy efficiency is important for reducing fuel consumption and meeting emission legislation. Moreover, energy efficiency is also supported by the functional argument of mitigating range anxiety of electric vehicles, i.e., giving a sufficiently large driving range for an electrical vehicle. The problem of reducing the energy consumption of a vehicle over a certain drive cycle can be formulated as an optimal control problem and its solution is often referred to as an energy management strategy. Most of these energy management problems are focused on controlling the power split between the combustion engine and the electric machine of a hybrid electric vehicle [1, 2]. By storing regenerative braking energy and shifting the operating points of the combustion engine, a significant amount of fuel can be saved. A recent trend is to extend this energy management system to incorporate more subsystems of the vehicle [3] or to consider emission constraints in the optimal control problem [4].

In the aforementioned approaches, the vehicle velocity (and thereby the power needed to propel the vehicle) is assumed to be fixed. Nevertheless, the vehicle inertia, which is the largest energy buffer in the vehicle, can have a large impact in energy savings and consequently in the extension of the driving range. For instance, in [5] it has been reported that changes in driving behavior could improve the energetic performance of the vehicle more than 30%. The promising improvements in energy efficiency have contributed to the emergence of the eco-driving concept, which aims to increase the energy efficiency of a vehicle by means of a convenient selection of driving strategies, i.e. legal regulations, technological implementations or simply changes in the driver behavior. Hence, it is clear that eco-driving is a broad concept where government, manufacturers and users participate [6]. The problem of optimizing the velocity profile has been considered for conventional vehicles in [7], for hybrid electric vehicles by [8, 9], and for electric vehicles by [10, 11].

To solve the eco-driving problem, standard techniques used in optimal control have been adopted, see [12] for a detailed overview of the recent literature. In [13, 14], dynamic programming (DP) has been used to find a global solution to this problem. Alternatively, Pontryagin's minimum principle (PMP) has been used in [10, 11, 15, 16]. The main disadvantages PMP are that it only provides a necessary condition for optimality and that incorporating state constraints is not a simple task. Therefore, in [7, 8, 17] static nonlinear optimization techniques are used to solve the problem in the presence of state constraints. It remains unclear from the papers that use static optimization techniques or PMP whether the solutions are, in fact, globally optimal. Unfortunately, the literature related to this topic is scarce. The noticeable exception is [8], where the continuous-time optimal control problem is certified to be convex, which guarantees that the obtained solution is globally optimal. However, [8] does not discuss the possible loss of convexity due to the discretization process. This might occur, as it is demonstrated in this chapter.

This chapter aims to expose a detailed view of the global optimal solution to the eco-driving problem. The results of this chapter can be used to certify optimality of the results presented in the existing literature and in future works. The main con-

tributions presented in this chapter are threefold: Firstly, a method to reformulate and discretize the problem is presented. This is initially done for a simplified case to illustrate the non-convexity of the problem and subsequently extended to the complete eco-driving problem. Secondly, a detailed analysis of the uniqueness of the solution to the reformulated problem is used to obtain a set of mild conditions that guarantee the global optimality of the solution. Thirdly, a sequential quadratic programming (SQP) method is employed to efficiently solve the eco-driving problem. We expect our contribution to be used to certify the global optimality of methods exciting in current literature, e.g., see examples and references in [12], as well as in future works.

The content of this chapter is organized in seven sections. In Section 2.1, the eco-driving problem is formulated as a continuous-time optimal control problem. Section 2.2 discusses issues related to the preservation of convexity properties for different discretization schemes. A reduction and discretization method and a condition to guarantee the the existence of a global solution to the eco-driving problem are presented in Section 2.3. In Section 2.4, a SQP method to efficiently solve the discrete time optimal control problem is proposed. Later, the solution of a numerical eco-driving example is analysed in Section 2.5. Finally, Section 2.6 contains the conclusions of this chapter.

2.1. Continuous-Time Problem Formulation

In this section, a continuous-time formulation of the eco-driving concept as an optimal control problem is provided. Eco-driving aims at obtaining an optimal control force $u(t)$ and velocity profile $v(t)$ that minimizes the integral of the power $P(v,u)$ consumed by a vehicle while traveling during a given time interval $[t_o, t_f]$ over a given trajectory $s(t) \in [s_o, s_f]$ with known geographical characteristics, i.e., with a given road grade $\alpha : [s_o, s_f] \to [-\frac{\pi}{2}, \frac{\pi}{2}]$, where $\alpha(s)$ is the grade at position s; while being subject to longitudinal vehicle dynamics, non-negative velocity bounds $v(t) \in [\underline{v}, \overline{v}]$, and boundary conditions on position and velocity. This can be stated in the form of the following optimal control problem:

$$\min_{s(t),v(t),u(t)} \quad \int_{t_o}^{t_f} P(v(t),u(t))\mathrm{d}t \tag{2.1a}$$

$$\text{subject to} \quad m\frac{\mathrm{d}v}{\mathrm{d}t} = u(t) - f(v(t),s(t)), \tag{2.1b}$$

$$\frac{\mathrm{d}s}{\mathrm{d}t} = v(t), \tag{2.1c}$$

$$s(t_o) = s_o,\ s(t_f) = s_f \tag{2.1d}$$

$$v(t_o) = v_o,\ v(t_f) = v_f \tag{2.1e}$$

$$\underline{v} \le v(t) \le \overline{v}, \tag{2.1f}$$

where (2.1b) represents the longitudinal vehicle dynamics, in which $u(t)$ is the control force and $f(v,s)$ describes the aerodynamic drag, rolling resistance and gravity forces as

$$f(v,s) = \sigma_d v^2 + c_r mg\cos(\alpha(s)) + mg\sin(\alpha(s)), \tag{2.2}$$

In (2.1b) and (2.2), m represents the combined mass of the vehicle and the inertia of the driveline, $g \approx 9.81[m/s^2]$ is the gravitational constant, $c_r > 0$ describes the rolling force coefficient and $\sigma_d = \frac{1}{2} c_d \rho_a A_f$ with $c_d > 0$ is the drag coefficient, in which ρ_a denotes the air density and A_f is the frontal area of the vehicle.

The consumed power $P(v,u)$ can be obtained from different modeling approaches that capture the energy consumption in the powertrain. In this chapter, it is assumed to be a quadratic function of the form

$$P(v,u) = \beta_0 v^2 + \beta_1 vu + \beta_2 u^2, \tag{2.3}$$

for some non-negative parameters β_0, β_1 and β_2. Equation (2.3) is a physically realistic approximation, e.g., for electric motors due to the fact that the friction and Ohmic losses are captured by the terms $\beta_0 v^2$ and $\beta_2 u^2$, respectively. The optimal control problem (2.1) does not consider constraints on the control force $u(t)$ nor constraints on propulsion power $P(v,u)$, as in (2.3). However, the results of this chapter can be extended to include such constraints. Alternatively, constraints on propulsion power can be incorporated by connecting the eco-driving to vehicle energy management, as it was done in [8], and it will be done in Chapter 8, where power constraints of powertrain components are present.

In general, (2.1) is a nonlinear optimal control problem that might have multiple local solutions due to specific features of the vehicle model and road profile, see (2.2). This implies that direct optimization methods or methods based on PMP only provide candidate minima, which might not correspond to the global solution to problem (2.1).

2.2. Convexity in Relation to Discretization

To illustrate that the solution methods for the control problem (2.1) can introduce non-convexity, which might complicate finding the global minimum, a simplified version of problem (2.1) is considered in this section. Using this simplified example, we will illustrate a possible reformulation of the problem as a convex optimal control problem, which implies the existence of a unique solution. Because of the presence of state constraints in (2.1), we will focus on discrete-time approximations of the optimal control, which might by itself introduce non-convexity, even for specific cases where the continuous-time problem (2.1) is convex.

For a simplified version of problem (2.1) used in this section, consider $\beta_0 = 0$, $\beta_1 = 1$ and $\beta_2 = 0$ in (2.3), which corresponds to an electric motor with perfect energy conversion and no friction and Ohmic losses. Constant velocity bounds are also considered. Moreover, assume a flat road, meaning that $\alpha(s) = 0$ so that the rolling friction is constant, i.e. $\cos(\alpha(s)) = 1$, and the gravitational force has no effect on the longitudinal vehicle dynamics as $\sin(\alpha(s)) = 0$. Under these assumptions, (2.1)-(2.3) reduces to

$$\min_{s(t),v(t),u(t)} \quad \int_{t_0}^{t_f} u(t)\, v(t)\, \mathrm{d}t. \tag{2.4a}$$

subject to (2.1c)-(2.1f) and

$$m\frac{\mathrm{d}v}{\mathrm{d}t} = u(t) - \sigma_d v(t)^2 - c_r mg. \tag{2.4b}$$

The above optimization problem is non-convex due to (2.4b), meaning that application of PMP or finite dimensional optimization methods cannot guarantee a global optimal solution. We will show how this problem can be reformulated as a convex optimization problem, where we focus on discrete-time approximations so that static optimization methods can be applied.

2.2.1. Direct Discretization

In order to illustrate that caution should be taken when discretizing the optimal control problem (2.4) with (2.1c)-(2.1f), we show that direct discretization leads to a non-convex optimization problem. In an attempt to assess convexity of (2.4) with (2.1c)-(2.1f), we eliminate $u(t)$ by substituting the equality constraints (2.4b) into the objective function (2.4a), thereby producing an equivalent optimization problem. This procedure is a useful tool to analyse the convexity of the problem in the feasible set, see, e.g., [18], and leads to

$$\min_{s(t),v(t)} \quad \int_{t_\mathrm{o}}^{t_f} m\frac{\mathrm{d}v}{\mathrm{d}t}v(t) + c_r mgv(t) + \sigma_d v(t)^3 \,\mathrm{d}t, \tag{2.5}$$

subject to (2.1c)-(2.1f).

In order to solve (2.5) subject to (2.1c)-(2.1f), using direct optimization methods, we can approximate the integral in the objective function using a forward Euler discretization method at $v_k = v(t_k)$ and $s_k = s(t_k)$, i.e., at instances t_k, $k \in \{0, \dots, N\}$, for some $N \in \mathbb{N}$, where $t_{k+1} > t_k$, $t_0 = t_\mathrm{o}$, $t_N = t_f$ and step size $\tau_k = t_{k+1} - t_k > 0$. This leads to a forward Euler discretization of the objective function in (2.5), given by

$$\textstyle\sum_{k=0}^{N-1} \tau_k \left(m\frac{(v_{k+1}-v_k)}{\tau_k}v_k + \sigma_d v_k^3 + c_r mgv_k \right) \tag{2.6}$$

which can be rewritten as

$$\tfrac{1}{2}m(v_f^2 - v_\mathrm{o}^2) + \sum_{k=0}^{N-1} \tau_k(\sigma_d v_k^3 + c_r mgv_k) - \tfrac{1}{2}m(v_{k+1} - v_k)^2, \tag{2.7}$$

using (2.1e). The last term in this expression is non-convex, which is a direct consequence of the forward Euler discretization. It should be noted that this result is independent of the step size τ_k and a similar conclusion can be drawn from the application of a backward Euler method. This shows the loss of convexity when applying discrete-time approximations of the eco-driving problem (2.1). Higher-order discrete approximations of (2.5) possibly lead to a convex optimization problem, albeit at the cost of increased complexity. Instead, we will here reformulate the optimal control problem (2.5) subject to (2.1c)-(2.1f) in a way that introduction of non-convex terms is avoided, as will be shown below.

2.2.2. Continuous-Time Reformulation

The reformulation of the simplified eco-driving problem is based on the observation that, instead of discretizing the objective function directly, the first two terms in (2.5) can be integrated over the boundary conditions (2.1d) and (2.1e) to obtain

$$\min_{s(t),v(t)} \ \tfrac{1}{2}m(v_f^2 - v_o^2) + c_r m g (s_f - s_0) + \int_{t_o}^{t_f} \sigma_d v(t)^3 \ \mathrm{d}t, \tag{2.8}$$

subject to (2.1c)-(2.1f). The three terms in this objective function describe the change in kinetic and potential energy of the vehicle over the complete trajectory, and the loss due to rolling resistance, respectively. Since v_o, s_o, v_f and s_f are known, these terms do not influence the optimal solution. Interestingly, the remaining term describes the energy losses due to aerodynamic drag. Thus, the reduced expression is discretized using a forward Euler approach, leading to

$$\min_{s_k,v_k} \quad \sum_{k=0}^{N-1} \tau_k \sigma_d v_k^3, \tag{2.9}$$

subject to $s_{k+1} = s_k + \tau_k v_k$, (2.1d)-(2.1f). The resulting discrete objective function (2.9) is convex for $v_k > 0$, which corresponds to the vehicle driving in forward direction.

Hence, this simplified case shows that a direct discretization of the eco-driving can lead to a non-convex optimization problem, while a reformulated problem yields a convex optimization problem after discretization. The ideas in this section will be extended in the next section towards the complete eco-driving problem (2.1) to prove the existence of a unique solution of the optimal control problem.

2.3. A Global Solution to the Eco-Driving Problem

In this section, the ideas presented in Section 2.2 will be applied to problem (2.1), without making the simplifications considered in Section 2.2.2. This allows an equivalent optimization problem of reduced complexity to be formulated, which can be discretized using a forward Euler method without introducing additional non-convex terms. The structure of the reduced discrete-time optimal control problem will be exploited to prove that a unique global optimal solution exists under mild and realistic conditions.

2.3.1. Reduction of the Continuous-Time Problem

Non-convex optimization problems can show multiple local minima, therefore finding a global solution of the problem could be a cumbersome task. Nonconvexity is not only a consequence of a discretization action, it can also be related to other parameters of the nonlinear optimal control problem (2.1). For instance, (2.1a) could be a non-convex objective function, which occurs for particular values of β_0, β_1 and β_2 that make (2.3) a non-convex function. Moreover, a realistic road grade $\alpha(s)$ might also introduce non-convexity in the equality constraint (2.1b). As done in the previous section, an equivalent optimal control problem will be obtained by substituting the equality constraint (2.1b) into the objective function.

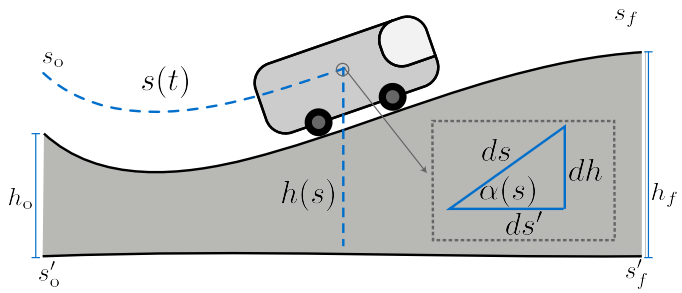

Figure 2.1: Geometry of the road profile.

Adopting the basic ideas presented in Section 2.2, the continuous-time optimal control problem (2.1) is reformulated into a convenient form given by

$$\min_{a(t),s(t),v(t)} \int_{t_o}^{t_f} P(v(t), ma(t) + f(v(t), s(t))) \, \mathrm{d}t \tag{2.10a}$$

subject to (2.1c)-(2.1f) and

$$\frac{\mathrm{d}v}{\mathrm{d}t} = a(t), \tag{2.10b}$$

where $a(t)$ is a new decision variable, which represents the vehicle acceleration, and $f(v,s)$ is given by (2.2). It is important to remark that (2.10a) is obtained from the substitution of (2.1b) into (2.1a), and its integrand is given by

$$\begin{aligned} P(v, ma + f(v,s)) =& \beta_2 (mg\gamma_g(s) + c_d v^2 + c_r mg\gamma_r(s) + ma)^2 \\ &+ \beta_1 v (ma + c_d v^2 + mg\gamma_g(s) + c_r mg\gamma_r(s)) + \beta_0 v^2 \end{aligned} \tag{2.11}$$

in which $\gamma_g(s) = \sin(\alpha(s))$ and $\gamma_r(s) = \cos(\alpha(s))$. The relevance of (2.11) is that it contains information of the longitudinal vehicle dynamics, where the majority of the nonlinearities of the problem are embedded. This information and the structure of the problem (2.10) with (2.1c)-(2.1f) can be exploited to obtain a reduced, yet equivalent, optimal control problem. The first step to achieve this goal is to observe that

$$\gamma_g(s) = \frac{\mathrm{d}h}{\mathrm{d}s} \quad \text{and} \quad \gamma_r(s) = \frac{\mathrm{d}s'}{\mathrm{d}s} \tag{2.12}$$

where $h(s)$ is the given elevation profile and $s'(t)$ can be interpreted as the horizontal projection of $s(t)$. The validity of these expressions can be explained using Fig. 2.1, where the relation between the elevation profile $h(s)$ and the position s can be observed. The geometry in this physical configuration shows that for any specific point in the road, the change in elevation with respect to the displacement is $\frac{\mathrm{d}h}{\mathrm{d}s} = \sin(\alpha(s))$, and $\frac{\mathrm{d}s'}{\mathrm{d}s} = \cos(\alpha(s))$, respectively.

The next step is to remove the terms in the objective function (2.10a) that can be solved in advance and have no contribution to the optimal control problem. In

particular, consider the following terms from (2.10a):

$$\begin{aligned} E_G &= \int_{t_o}^{t_f} \beta_1 m(a + g\gamma_g(s) + c_r g\gamma_r(s))v + 2\beta_2 m\sigma_d v^2 a \, \mathrm{d}t \\ &= \int_{t_o}^{t_f} \beta_1 m\left(v\tfrac{\mathrm{d}v}{\mathrm{d}t} + g\tfrac{\mathrm{d}h}{\mathrm{d}s}\tfrac{\mathrm{d}s}{\mathrm{d}t} + gc_r\tfrac{\mathrm{d}s'}{\mathrm{d}s}\tfrac{\mathrm{d}s}{\mathrm{d}t}\right) + 2\beta_2 m\sigma_d v^2\tfrac{\mathrm{d}v}{\mathrm{d}t} \, \mathrm{d}t \\ &= \tfrac{1}{2}\beta_1 m(v_f^2 - v_o^2) + \beta_1 mg(h_f - h_o) + \beta_1 mgc_r(s_f' - s_o') \\ &\quad + \tfrac{2}{3}\beta_2 m\sigma_d(v_f^3 - v_o^3). \end{aligned} \tag{2.13}$$

The first equality in (2.13) is obtained by substitution of (2.1c), (2.10b) and (2.12), and the second equality by solving the integral over the boundary conditions of the problem. The first two terms shows that the total kinetic and potential energy of the vehicle depend only on the velocities and elevations at the boundaries. In a similar way, the last two terms demonstrate that part of the energy consumed by the drag and rolling forces, respectively, are defined by the velocity and horizontal displacement at the boundaries.

Since the value of (2.13) is given by the boundary conditions of the optimization problem (2.10), it is possible to rewrite (2.10a) as

$$\int_{t_o}^{t_f} P(v, ma + f(v,s)) \, \mathrm{d}t = \int_{t_o}^{t_f} P_R(a,v,s)\mathrm{d}t + E_G, \tag{2.14}$$

where

$$\begin{aligned} P_R(a,s,v) =& \beta_0 v^2 + \beta_1\sigma_d v^3 + 2\beta_2 m^2 ga(\gamma_g(s) + c_r\gamma_r(s)) \\ &+ \beta_2(ma)^2 + \beta_2(mg\gamma_g(s) + \sigma_d v^2 + c_r mg\gamma_r(s))^2. \end{aligned} \tag{2.15}$$

Removing the constant term E_G from the objective function, thereby changing (2.11) to (2.15) in the optimal control problem, does not change its optimal solution.

2.3.2. Unique Solution to the Discrete-Time Optimal Control Problem

The reduced continuous-time optimal control problem obtained in the previous section can be discretized in order to make it solvable using static optimization methods. In this section, it will be shown that the discrete-time problem has a unique solution under realistic conditions and an efficient method to obtain this global minimum will be presented in Section 2.4.

In order to discretize the problem, we consider again a forward Euler discretization method and define $a_k = a(t_k)$, $v_k = v(t_k)$ and $s_k = s(t_k)$ at instances $t_k = k\tau + t_o$,

$k \in \mathcal{K} = \{0, \dots, N\}$, with fixed step size $\tau = \frac{t_f - t_o}{N}$, for some $N \in \mathbb{N}$. This leads to

$$\min_{a_k, s_k, v_k} \quad \sum_{k=0}^{N-1} \tau P_R(a_k, s_k, v_k) \tag{2.16a}$$

$$\text{subject to} \quad s_{k+1} = s_k + \tau v_k, \tag{2.16b}$$

$$v_{k+1} = v_k + \tau a_k, \tag{2.16c}$$

$$s_0 = s_o, \; s_N = s_f, \tag{2.16d}$$

$$v_0 = v_o, \; v_N = v_f, \tag{2.16e}$$

$$\underline{v} \leq v_k \leq \overline{v} \tag{2.16f}$$

The theorem below is the main results of this section and provides conditions under which the optimal control problem (2.16) has a unique global minimum.

Theorem 2.3.1. *Suppose optimization problem* (2.16) *is feasible. if* $\beta_2 > 0$ *and if*

$$g\tau^2\left(\frac{\mathrm{d}\gamma_g(s_k)}{\mathrm{d}s} + c_r \frac{\mathrm{d}\gamma_r(s_k)}{\mathrm{d}s}\right) \neq -1$$

for all $k \in \{0, \dots, N-1\}$*, then optimization problem* (2.16) *has a unique global minimum.*

Proof. The first-order necessary conditions for optimality of (2.16) are given by the so-called Karuhn-Kuhn-Tucker (KKT) conditions, see, e.g, [18]. Instrumental in these KKT conditions is the Lagrangian

$$\begin{aligned} L(a_k, s_k, v_k, \kappa_k, \lambda_k, \mu_k, \nu_k) = &\sum_{k=0}^{N-1} \beta_0 \tau v_k^2 + \beta_1 \tau \sigma_d v_k^3 \\ &+ \beta_2 \tau (m a_k)^2 + \beta_2 \tau (m g \gamma_g(s_k) + \sigma_d v_k^2 + c_r m g \gamma_r(s_k))^2 \\ &+ 2\beta_2 \tau m^2 g a (\gamma_g(s_k) + c_r \gamma_r(s_k)) + \kappa_{k+1}(s_{k+1} - s_k - \tau v_k) \\ &+ \lambda_{k+1}(v_{k+1} - v_k - \tau a_k) + \mu_k(v_k - \overline{v}) + \nu_k(\underline{v} - v_k). \end{aligned} \tag{2.17}$$

Since all constraints are linear, a critical point, or stationary point, of (2.16) is characterized by

$$\frac{\partial L}{\partial a_k} = 2\beta_2 m^2 \tau (a_k + g\gamma_g(s_k) + c_r g \gamma_r(s_k)) - \lambda_{k+1}\tau = 0 \tag{2.18a}$$

$$\begin{aligned} \frac{\partial L}{\partial s_k} = &2\beta_2 \tau m g (m a_k + m g \gamma_g(s_k) + \sigma_d v_k^2 + c_r m g \gamma_r(s_k)) \times \left(\frac{\mathrm{d}\gamma_g(s_k)}{\mathrm{d}s} + c_r \frac{\mathrm{d}\gamma_r(s_k)}{\mathrm{d}s}\right) \\ &+ \kappa_k - \kappa_{k+1} = 0 \end{aligned} \tag{2.18b}$$

$$\begin{aligned} \frac{\partial L}{\partial v_k} = &2\beta_0 \tau v_k + 3\beta_1 \tau \sigma_d v_k^2 + 4\beta_2 \tau \sigma_d v_k \left(m g \gamma_g(s_k) + \sigma_d v_k^2 + c_r m g \gamma_r(s_k)\right) - \tau \kappa_{k+1} \\ &+ \lambda_k - \lambda_{k+1} + (\mu_k - \nu_k) = 0 \end{aligned} \tag{2.18c}$$

and $\frac{\partial L}{\partial \kappa_k}$, $\frac{\partial L}{\partial \lambda_k}$ described by (2.16b) and (2.16c) respectively for some Lagrange multipliers κ_k, λ_k and $\mu_k \geqslant 0$, $\nu_k \geqslant 0$, $k \in \{0, \dots, N\}$, such that

$$\mu_k(v_k - \overline{v}) = 0 \quad \text{and} \quad \nu_k(\underline{v} - v_k) = 0, \tag{2.18d}$$

and κ_0, λ_0, κ_N, and λ_N chosen such a way that (2.16d) and (2.16e) are satisfied. Now rewriting (2.18a) as

$$a_k = \frac{1}{2\beta_2 m^2}\lambda_{k+1} - g\gamma_g(s_k) - c_r g \gamma_r(s_k)), \tag{2.19}$$

and substituting this into (2.18b) yields

$$\kappa_k = \kappa_{k+1} - 2\beta_2 \tau m g \left(\frac{1}{2m\beta_2} \lambda_{k+1} + \sigma_d v_k^2 \right) \left(\frac{\mathrm{d}\gamma_g(s_k)}{\mathrm{d}s} + c_r \frac{\mathrm{d}\gamma_r(s_k)}{\mathrm{d}s} \right). \tag{2.20}$$

Substituting (2.19) into (2.16c) leads to a characterization of a critical point of (2.16), given by

$$\begin{bmatrix} s_{k+1} \\ v_{k+1} \end{bmatrix} = \begin{bmatrix} s_k + \tau v_k \\ v_k - \tau g \phi(s_k) + \frac{\tau}{2\beta_2 m^2} \lambda_{k+1} \end{bmatrix} \tag{2.21a}$$

and

$$\begin{bmatrix} \kappa_k \\ \lambda_k \end{bmatrix} = \begin{bmatrix} 1 & -\tau g \frac{\mathrm{d}\phi}{\mathrm{d}s_k} \\ \tau & 1 \end{bmatrix} \begin{bmatrix} \kappa_{k+1} \\ \lambda_{k+1} \end{bmatrix} + \begin{bmatrix} 0 \\ 1 \end{bmatrix} (v_k - \mu_k) - \tau \Phi(s_k, v_k) \tag{2.21b}$$

with

$$\Phi(s, v) = \begin{bmatrix} 2\beta_2 m g^2 \sigma_d v^2 \frac{\mathrm{d}\phi}{\mathrm{d}s_k} \\ 2\beta_0 v + 3\beta_1 \sigma_d v^2 + 4\beta_2 \sigma_d v \left(\sigma_d v_k^2 + mg\phi(s_k) \right) \end{bmatrix} \tag{2.21c}$$

and $\phi(s) = \gamma_g(s) + c_r \gamma_r(s)$. For this characterization, $\mu_k \geq 0$ and $\nu_k \geq 0$ can always be uniquely chosen so that λ_k has the value needed to ensure $\underline{v} \leq v_k \leq \overline{v}$, while satisfying (2.18d). Furthermore, since the matrix $\begin{bmatrix} 1 & -\tau g \frac{\mathrm{d}\phi}{\mathrm{d}s_k} \\ \tau & 1 \end{bmatrix}$ is full rank for every $k \in \{0, \dots, N-1\}$ by the hypothesis of the theorem, every pair (κ_N, λ_N) leads to a unique trajectory of κ_k and λ_k , meaning that they can be uniquely chosen such that (2.16d) and (2.16e) are satisfied if (2.16) is feasible.

The KKT conditions provide necessary conditions for optimality in the sense that they characterize points that satisfy

$$\nabla F(x)\, d \geqslant 0 \tag{2.22}$$

for all feasible directions d at x. In the above equation $\nabla F(x)$ is the gradient of the objective function (2.16a), where $x = [a_0, \dots, a_{N-1}, s_0, \dots, s_{N-1}, v_0, \dots, v_{N-1}]^\mathsf{T}$, and the feasible directions d at $x \in \mathcal{F}$ are all vectors that satisfy $x + \alpha d \in \mathcal{F}$ for some $\alpha > 0$ and where $\mathcal{F} = \{x |$ (2.16b)–(2.16f)$\}$, which is a compact set. Points satisfying (2.22) can in principle be minima, maxima or saddle points. Because of uniqueness of the solutions to (2.21), the obtained critical point has to be a minimum. Indeed, suppose the critical point would be a maximum or a saddle point, there would exist at least one other x that would satisfy the necessary conditions. In other words, if x is a saddle point or a maximum, it is possible to move away from this x and lower the value of the objective function until the boundary of the feasible set $\mathcal{F}$ would be reached. At this point, we would find another point x that satisfies (2.22). This contradicts the fact that there is only one critical point. Therefore, this unique critical point has to be the global minimum, which completes the proof. □

The result presented in Theorem 2.3.1 is unexpected since the optimization problem (2.16) is non-convex, which often implies the existence of multiple local minima. The existence of a unique global solution to the eco-driving problem (2.16) is important result that eliminates the necessity of using dynamic programming to obtain globally optimal eco-driving strategies.

Remark 2.3.1. *The conditions presented in Theorem 2.3.1 are satisfied for many realistic cases. For instance, $\beta_2 > 0$ is always satisfied if Ohmic losses of the electric motor are considered in the objective function. Moreover, standard road design guidelines, e.g, [19], suggest curvatures that yield $\left|\frac{\mathrm{d}\gamma_g(s_k)}{\mathrm{d}s}\right| \ll 1$ and $\left|\frac{\mathrm{d}\gamma_r(s_k)}{\mathrm{d}s}\right| \ll 1$.*

2.4. Solution to the Eco-Driving Problem

In this section, we will propose an efficient numerical method for solving the optimal control problem (2.16). The solution method we propose uses Sequential Quadratic Programming (SQP). The effectiveness of SQP to solve constrained nonlinear optimization problems is the main reason for the large acceptance of this method. The scent of this approach is to iteratively solve linearly constrained quadratic (QP) sub-problems, that are an approximation of the original problem evaluated in a previous solution, until some convergence criterion is achieved [20]. The uniqueness of the solution guarantees that the SQP algorithm finds the global minimum, provided that the algorithm converges.

Since the objective function in (2.16) is non-convex even after the reformulation and reduction presented in Section 2.3, we employ the results of [21] to formulate a convex QP sub-problem by making an approximation of the Hessian matrix of (2.15), which is given by

$$H = \begin{bmatrix} \frac{\partial^2 P_R}{\partial a^2} & \frac{\partial^2 P_R}{\partial a\,\partial s} & \frac{\partial^2 P_R}{\partial a\,\partial v} \\ \frac{\partial^2 P_R}{\partial a\,\partial s} & \frac{\partial^2 P_R}{\partial s^2} & \frac{\partial^2 P_R}{\partial s\,\partial v} \\ \frac{\partial^2 P_R}{\partial a\,\partial v} & \frac{\partial^2 P_R}{\partial s\,\partial v} & \frac{\partial^2 P_R}{\partial v^2} \end{bmatrix} = \begin{bmatrix} h_{11} & h_{12}(s) & 0 \\ h_{12}(s) & h_{22}(a,s,v) & h_{23}(s,v) \\ 0 & h_{23}(s,v) & h_{33}(s,v) \end{bmatrix}, \tag{2.23}$$

in which we have omitted the arguments of the function $P_R(a,s,v)$ for compactness of notation, and where

$$h_{11} = 2\beta_2 m^2, \tag{2.24a}$$

$$h_{12}(s) = 2\beta_2 m^2 g\left(\frac{\mathrm{d}\gamma_g(s)}{\mathrm{d}s} + c_r \frac{\mathrm{d}\gamma_r(s)}{\mathrm{d}s}\right), \tag{2.24b}$$

$$h_{22}(a,s,v) = 2\beta_2 mg\Big(mg\big(\frac{\mathrm{d}\gamma_g(s)}{\mathrm{d}s} + c_r \frac{\mathrm{d}\gamma_r(s)}{\mathrm{d}s}\big)^2 + (ma + mg\gamma_g(s) + \sigma_d v^2 + mgc_r\gamma_r(s)) \times \big(\frac{\mathrm{d}^2\gamma_g(s)}{\mathrm{d}s^2} + c_r \frac{\mathrm{d}^2\gamma_r(s)}{\mathrm{d}s^2}\big)\Big), \tag{2.24c}$$

$$h_{23}(s,v) = 4mg\beta_2\sigma_d v\big(\frac{\mathrm{d}\gamma_g(s)}{\mathrm{d}s} + c_r \frac{\mathrm{d}\gamma_r(s)}{\mathrm{d}s}\big), \tag{2.24d}$$

$$h_{33}(s,v) = 4\beta_2\sigma_d mg(\gamma_g(s) + c_r\gamma_r(s)) + 2\beta_0 + 6\beta_1\sigma_d v + 12\beta_2\sigma_d^2 v^2. \tag{2.24e}$$

Since $h_{22}(a,s,v)$ and $h_{33}(s,v)$ can become negative, we propose in this chapter to use

$$\widehat{H}(s,v) = \mathrm{diag}\left(2\beta_2 m^2,\ \epsilon_{22},\ \max(h_{33}(s,v), \epsilon_{33})\right), \tag{2.25}$$

as a positive definite approximate Hessian in the SQP algorithm presented below, in which ϵ_{22}, ϵ_{33} are small positive numbers and $h_{33}(s,v)$ is given by (2.24e).

The approximated Hessian matrix allow us to solve the eco-driving problem by sequentially solving the following convex second-order approximation of (2.15) as:

$$\{a_k^{i+1}, s_k^{i+1}, v_k^{i+1}\}_{k\in\mathcal{K}} = \underset{a_k,s_k,v_k}{\operatorname{argmin}} \sum_{k=0}^{N-1} \tau P_{QP}(a_k, s_k, v_k, a_k^i, s_k^i, v_k^i), \tag{2.26}$$

subject to (2.16b)-(2.16f), where

$$P_{QP}(a_k, s_k, v_k, a_k^i, s_k^i, v_k^i) = \frac{1}{2}\begin{bmatrix} a_k \\ s_k \\ v_k \end{bmatrix}^{\mathsf{T}} \widehat{H}(s_k^i, v_k^i)\begin{bmatrix} a_k \\ s_k \\ v_k \end{bmatrix} + \left(\nabla P_R(a_k^i, s_k^i, v_k^i) - \begin{bmatrix} a_k^i \\ s_k^i \\ v_k^i \end{bmatrix}^{T} \widehat{H}(s_k^i, v_k^i)\right)\begin{bmatrix} a_k \\ s_k \\ v_k \end{bmatrix}. \tag{2.27}$$

In (2.27), $\nabla P_R(a_k^i, s_k^i, v_k^i)$ is the gradient of (2.15), and $\widehat{H}(s_k^i, v_k^i)$ the positive definite approximated Hessian matrix given by (2.24), both evaluated at (a_k^i, s_k^i, v_k^i), where i indicates the iteration of the SQP algorithm. Convergence of the proposed SQP approach is guaranteed due to the fact that the Hessian matrix (2.25) satisfies the conditions for convergence presented in [21, Section 3.2]. Hence, the proposed SQP algorithm terminates when the difference of reduced discrete objective function (2.16a) between two successive iterations is lower than a tolerance $\Delta_{Tol} > 0$, i.e.,

$$\left|\sum_{k=0}^{N-1} \tau\big(P_R(a_k^{i+1}, s_k^{i+1}, v_k^{i+1}) - P_R(a_k^i, s_k^i, v_k^i)\big)\right| \leq \Delta_{Tol}.$$

Hence, obtaining the global minimizer to the eco-driving problem (2.16).

2.5. Numerical Examples

In this section, the SQP algorithm proposed in Section 2.4 is used to find the optimal solution of two numerical examples of the eco-driving problem. First, the benchmark problem for electric vehicles presented in [10] is solved. In the second example, conventional and eco-driving profiles are compared for a heavy-duty vehicle in order to show the potential savings obtained from eco-driving concept.

2.5.1. Benchmark Problem for Electric Vehicles

In this example, we revisit the numerical benchmark problem for eco-driving that have been introduced in [10] and uses PMP to solve it. In this case, the input of the longitudinal vehicle dynamics u is describing the percentage of the maximum mechanical torque produced by the electric motor. Moreover, The energy consumption in this model considers a frictionless electric motor, i.e., $\beta_0 = 0$. The effects of the rolling force in the vehicle are assumed to be constant, i.e., $\gamma_r = 1$, while the effects of the gravitational force are described by

$$\gamma(s) = g\gamma_g(s) = p_0 + p_1 s + p_2 s^2 + p_3 s^3. \tag{2.28}$$

It is important to note that the polynomial function $\gamma(s)$ also embeds information related to the road profile used in this example. In Table 2.1, the parameters presented in [10] are translated to the eco-driving formulation proposed in this

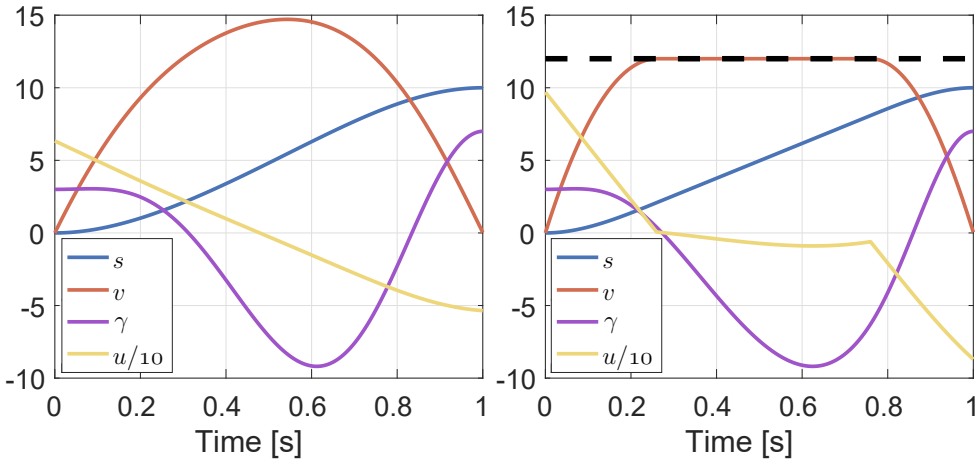

(a) Original formulation.

(b) Including velocity contraints.

Figure 2.2: Global solution to the eco-driving problem [10].

chapter. Since the example of [10] is a numerical example, the parameters in Table 2.1 and the optimal solution do not have a physical interpretation.

The method proposed in Section 2.4 returns an optimal solution that is depicted in Fig. 2.2a. This solution shows the same features reported in [10]. In fact, the final cost obtained using SQP is 1.2295×10^6, which differs only 0.0767% from the results reported in [10], while having a similar computation time. Considering that in this case $\beta_2 > 0$, from Theorem 2.3.1, it is possible to conclude that the solution is a global minimum of the problem. Using the SQP approach presented in this chapter, velocity constraints can be easily added, as shown in Fig. 2.2b, which is not straightforward using the PMP-based approach of [10].

2.5.2. Hybrid Electric Heavy-Duty Vehicle

In this example, a hybrid electric heavy-duty vehicle driving at a constant speed is compared with an eco-driving strategy, where the velocity is allowed to change between given bounds. The settings of the eco-driving problem used in this example are summarized in Table 2.2 and the elevation profile is defined by

$$h(s) = 225\cos\left(\tfrac{3\pi}{21000}s + \tfrac{\pi}{4}\right) + 225 \ [m], \tag{2.29}$$

which is depicted in Fig. 2.3 as a green surface.

p_0:	3	$v(t_o)$:	0	m:	1	t_o:	0
p_1:	0.4	$v(t_f)$:	0	g:	1	t_f:	1
p_2:	-1	$s(t_o)$:	0	c_r:	0.1	τ:	0.001
p_3:	0.1	$s(t_f)$:	10	σ_d:	10^{-3}	$v_0(t)$:	0

Table 2.1: EV parameters in [10].

β_0: 0.292	$v(t_o)$: $70[km/h]$	m: $15950[kg]$	t_o: $0[s]$
β_1: 1.005	$v(t_f)$: $70[km/h]$	g: $9.81[m/s^2]$	t_f: $1080[s]$
β_2: 2.652×10^{-4}	$s(t_o)$: $0[km]$	c_r: 0.1	$\overline{v}$: $80[km/h]$
τ: $5[s]$	$s(t_f)$: $21[km]$	σ_d: 3.1246	$\underline{v}$: $60[km/h]$

Table 2.2: Parameters for the heavy-duty vehicle example.

The constant-speed driving profile is described by a solid line in Fig. 2.3. In this case, the total energy consumed by the vehicle is $3.0719 \times 10^4[kJ]$. On the other hand, the dashed line presented in Fig. 2.3 describes the optimal control force u and velocity profile v obtained as the global solution to the eco-driving optimal control problem studied in this case. It can be noted that the velocity is reduced when the vehicle is moving downhill. This means that potential and kinetic energy are recovered, which implies that the total energy consumption is also reduced. To be more specific, the total energy consumed by the vehicle under this strategy is $2.843 \times 10^4[kJ]$, which is approximately 7.44% lower than the energy consumed by the vehicle driving at constant velocity.

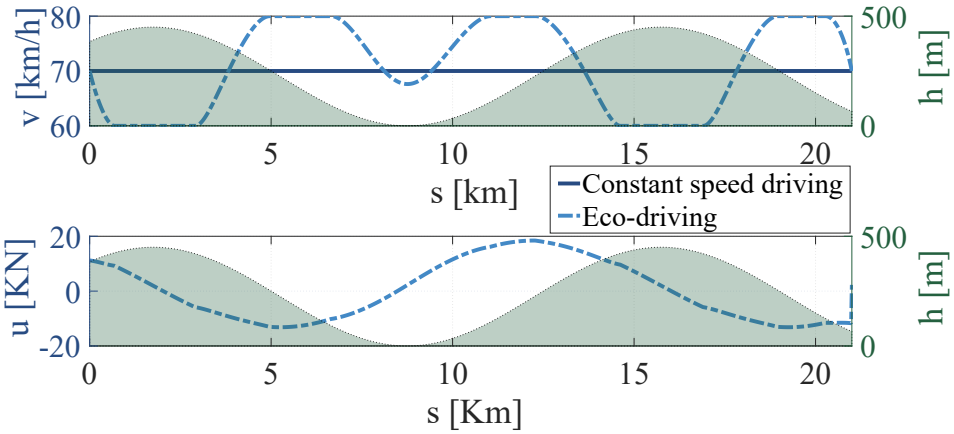

Figure 2.3: Global solution to the eco-driving problem.

2.6. Conclusions

In this chapter, a detailed study has been conducted on the global optimality of the eco-driving optimal control problem. We have proposed to reformulate and discretize the problem and have subsequently derived conditions that guarantee the existence of the global solution to the eco-driving problem. Taking advantage of these results, a SQP algorithm that efficiently solves the eco-driving problem has been proposed. The methodologies and results were illustrated in two numerical examples.

References

[1] B. Egardt, N. Murgovski, M. Pourabdollah, and L. J. Mardh, *Electromobility Studies Based on Convex Optimization: Design and Control Issues Regarding Vehicle Electrification,* IEEE Control Systems Magazine (2014).

[2] J. Kessels, J. H. M. Martens, P. P. J. van den Bosch, and W. H. A. Hendrix, *Smart vehicle powernet enabling complete vehicle energy management,* in *Proc. Vehicle Propulsion & Power Control , 2012* (2012).

[3] T. C. J. Romijn, M. C. F. Donkers, J. T. Kessels, and S. Weiland, *A dual decomposition approach to complete energy management for a heavy-duty vehicle,* in *Proc. IEEE Conference on Decision and Control* (2014).

[4] M. Donkers, J. van Schijndel, W. Heemels, and F. Willems, *Optimal control for integrated emission management in diesel engines,* Control Engineering Practice (2017).

[5] C. Bingham, C. Walsh, and S. Carroll, *Impact of driving characteristics on electric vehicle energy consumption and range,* IET Intelligent Transport Systems (2012).

[6] B. Seraens, *Optimal Control Based Eco-Driving: Theoretical Approach and Practical Applications*, Ph.D. thesis, Katholieke Universiteit Leuven (2012).

[7] N. J. Kohut, J. K. Hedrick, and F. Borrelli, *Integrating traffic data and model predictive control to improve fuel economy,* in *Proc. IFAC World Congress* (2009).

[8] N. Murgovski, L. Johannesson, X. Hu, B. Egardt, and J. Sjöberg, *Convex relaxations in the optimal control of electrified vehicles,* in *Proc. American Control Conference* (2015).

[9] L. Johannesson, N. Murgovski, E. Jonasson, J. Hellgren, and B. Egardt, *Predictive energy management of hybrid long-haul trucks,* Control Engineering Practice (2015).

[10] N. Petit and A. Sciarretta, *Optimal drive of electric vehicles using an inversion-based trajectory generation approach,* in *Proc. IFAC World Congress* (2011).

[11] W. Dib, A. Chasse, P. Moulin, A. Sciarretta, and G. Corde, *Optimal energy management for an electric vehicle in eco-driving applications,* Control Engineering Practice (2014).

[12] A. Sciarretta, G. D. Nunzio, and L. L. Ojeda, *Optimal Ecodriving Control: Energy-Efficient Driving of Road Vehicles as an Optimal Control Problem,* IEEE Control Systems MAgazine (2015).

[13] E. Hellström, J. Åslund, and L. Nielsen, *Management of kinetic and electric energy in heavy trucks,* in *Proc. SAE World Congress and Exhibition* (2010).

[14] E. Ozatay, S. Onori, J. Wollaeger, U. Ozguner, G. Rizzoni, D. Filev, J. Michelini, and S. D. Cairano, *Cloud-Based Velocity Profile Optimization for Everyday Driving: A Dynamic-Programming-Based Solution,* IEEE Transactions on Intelligent Transportation Systems (2014).

[15] E. Ozatay, U. Ozguner, and D. Filev, *Velocity profile optimization of on road vehicles: Pontryagin's Maximum Principle based approach,* Control Eng Pract (2017).

[16] M. A. S. Kamal, M. Mukai, J. Murata, and T. Kawabe, *Ecological Vehicle Control on Roads With Up-Down Slopes,* IEEE Transactions on Intelligent Transportation Systems (2011).

[17] M. Vajedi and N. L. Azad, *Ecological Adaptive Cruise Controller for Plug-In Hybrid Electric Vehicles Using Nonlinear Model Predictive Control,* IEEE Transactions on Intelligent Transportation Systems (2016).

[18] S. P. Boyd and L. Vandenberghe, *Convex optimization, Cambridge University Press New York* (2014).

[19] A. A. of State Highway and T. O. (AASHTO), *A Policy on Geometric Design of Highways and Streets*, Tech. Rep.

[20] J. Nocedal and S. J. Wright, *Numerical Optimization* (Springer, 2006).

[21] P. T. Boggs and J. W. Tolle, *Sequential quadratic programming,* Acta numerica (1995).

3

Eco-Driving for Energy Efficient Cornering of Electric Vehicles in Urban Scenarios

In this chapter, we propose a model for eco-driving that considers cornering effects. The proposed model purely relies on the geometric configuration of the vehicle and road. Consequently, we propose an eco-driving optimal control problem formulation that is suitable for both straight and curved trajectories in urban scenarios. Moreover, it can be applied for vehicles with front wheel drive (FWD) or rear wheel drive (RWD). We use a case study for an electric vehicle executing cornering maneuvers to validate the proposed approach with a high fidelity vehicle model. Results show an approximated improvement of 8% *in energy savings with respect to traditional eco-driving strategies, especially in trajectories with large curvatures.*

This chapter is based on **P.1**.

The capability to extend driving range by reducing power demand demonstrated by eco-driving techniques has positioned these approaches as strong tools alleviate effects of range anxiety, e.g., the promising experimental results that will be presented in Chapter 9. As indicated in the previous chapter of this thesis, eco-driving is a selection of energy efficient driving strategies [1], which can be obtained by solving an optimal control problem (OCP) that aims to find optimized velocity profiles that reduce the total consumption of the vehicle, e.g., see also [2]. This concept has been studied in terms of the energy source of the vehicle, e.g., for conventional vehicles in [3], for hybrid electric vehicles will be presented in Chapter 8, and for electric vehicles by [4]. Eco-driving has also been analyzed in terms of the surrounding operational conditions. For urban scenario cases, [5] has included traffic light information into the eco-driving formulation, [6] uses traffic statistic data to create velocity corridors where solutions the eco-driving OCP lay, and [7] considers the effects of the preceding vehicle in the problem formulation. Interestingly, the literature about eco-driving for urban trajectories where cornering is considered is scarce.

In [8], a high-fidelity model is presented to calculate additional energy losses in the tires during cornering of the vehicle. The results presented in this work have shown that energy losses during cornering maneuvers should not be neglected. Cornering losses become relevant during urban scenarios where the vehicle might follow routes where several turning maneuvers are performed. Often, eco-driving formulations that consider the road curvature include a constraint linked to the centripetal acceleration, which indirectly limits the maximum velocity during cornering, e.g., [9]. In this case, the cornering losses are not directly considered in the formulation. As a result, the solutions obtained are unlikely to be energy optimal during the cornering maneuver. An interesting case is presented in [10], where a dynamical vehicle model is used to describe a simplified model that can be used to formulate an eco-driving OCP. Unfortunately, this description depends on cornering stiffness of the tires, which can show significant variations between vehicles and tire conditions. Other approaches aim to achieve energy efficient cornering by applying energy efficient torque vectoring to the vehicle [11]. Unfortunately, these approaches partially neglect the eco-driving concept by only focusing on the cornering maneuver itself.

In this chapter, we aim to bridge the gap observed in literature by extending the eco-driving OCP formulation presented in the previous chapter to consider cornering effects. In particular, our main contributions are the use of a kinematic bicycle model to approximate the dissipative forces produced during cornering in the longitudinal direction of the vehicle. This model purely depends on the geometry of the road and the vehicle, which makes it suitable to be deployed in real applications where the tire properties are often unknown. Thus, we propose a trajectory dependent model for eco-driving that can be used for vehicles with front wheel drive (FWD) and rear wheel drive (RWD). This allow us to formulate generalized eco-driving OCP that is suitable to be used in urban routes.

The remainder of this chapter is organized as follows. In Section 3.1, the corner-

ing effects are approximated in a low complexity model for eco-driving applications. Section 3.2, proposes an OCP formulation that takes advantages of the modeling choice proposed in this chapter. Later, a case study for an electric vehicle performing a cornering maneuver in an urban intersection is presented in Section 3.3. Here we will validate our approach using a high-fidelity model to calculate losses during cornering and we will highlight the advantages of the proposed approach. Finally, we will draw conclusions in Section 3.4.

3.1. A Trajectory-Dependent Model for Eco-driving

In this section, we provide a general vehicle dynamical model to be used in the eco-driving optimal control problem proposed in this chapter. To this end, we analyze the representations used for straight trajectories, which coincides with traditional models used for eco-driving in the current literature. Later, we propose a generalized description of the dissipative forces for curved trajectories, which are often present in urban scenarios. Finally, we show that the generalized models obtained for curved trajectories can easily describe the dynamics for straight trajectories as well.

The main objective of eco-driving strategies is to obtain energy optimal velocity profiles. In general, the dynamical models considered in traditional eco-driving approaches represent the longitudinal vehicle dynamics by the interaction between the traction force in the longitudinal axis $F_l(t)$ and dissipative forces $F_d(t)$, i.e.,

$$ma = F_l - F_d, \tag{3.1}$$

where m represents the equivalent mass of the vehicle, and $a(t) = \frac{\mathrm{d}v}{\mathrm{d}t}$ is the vehicle acceleration. The definition of $F_d(t)$ in (3.1) can vary depending on the trajectory that the vehicle is describing. Specifically, we consider the cases for straight and curved trajectories below.

3.1.1. Straight Trajectories

A traditional assumption for eco-driving problem formulations is that the vehicle moves along a straight trajectory such that the dissipative force is given by

$$F_d(v,s) = F_{air} + F_{roll+grav} = \sigma_d v^2 + mg(c_r \cos(\alpha(s)) + \sin(\alpha(s))), \tag{3.2}$$

where $v(t)$ represents the vehicle velocity, $s(t)$ describes displacement, $\alpha(s(t))$ is the road grade, g is the gravitational acceleration, $c_r > 0$ is the rolling resistance coefficient, and $\sigma_d = \frac{1}{2} c_d \rho_a A_f$ with the aerodynamical drag coefficient $c_d > 0$, air density ρ_a and frontal area of the vehicle A_f. In the right-hand side of (3.2), the term F_{air} represents the force produced by aerodynamical drag, and the term $F_{roll+grav}$ is the force connected to rolling resistance and gravity. These forces are depicted in Fig. 3.1 for a straight trajectory case. Finally, by defining the total traction force provided by the electric motor $F_u(t)$, we see that

$$F_l = F_u \tag{3.3}$$

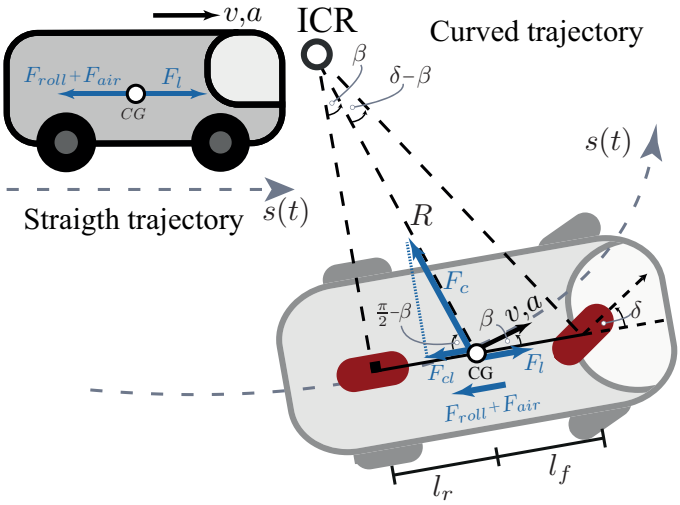

Figure 3.1: Forces on the londitudinal axis for both straight and curved trajectories.

Note that this relationship is independent of the drive configuration of the vehicle, i.e., (3.3) holds for both RWD and FWD configurations.

The assumption of a straight trajectory is widely adopted in literature, see, e.g., [2] and the references therein. It is intuitive to validate this assumption for vehicles driving in highways, where trajectories with large curvature are not often present. However, cornering actions are often needed during a typical urban trajectory. Moreover, the curvatures of these trajectories are significantly higher than in highways, which is translated into a larger energy consumption that should not be neglected, e.g., [8, 10].

3.1.2. Curved Trajectories

In this section we will include cornering effects in the model used for eco-driving OCP in urban scenarios, i.e., assuming curved trajectories. The effect of cornering in terms of energy consumption has been discussed in [8], where a detailed non-linear model has been developed and validated experimentally. This model describes additional tire slip losses during cornering. The results presented in the aforementioned work show that the energy consumed as consequence of cornering can be significant. In this section, we follow a simplified approach to approximate the effects of cornering into a low-complexity model that will be used to formulate the eco-driving OCP in Section 3.2.

Let us consider the curved trajectory observed in Fig. 3.1, which is characterized by a position-dependent curvature function $K(s)$, where the curvature is defined as the reciprocal of the radius $R(s)$, i.e.,

$$K(s) = \frac{1}{R(s)}. \tag{3.4}$$

The radius R is measured from the instantaneous center of rotation (ICR) to the vehicle center of gravity (CG). We assume that the CG shown in Fig. 3.1 is located at a distance l_r from the rear wheel axle and a distance l_f form the front wheel axle. Moreover, the vehicle depicted in Fig. 3.1 has a front wheel steering angle $\delta(s) \in [-\frac{\pi}{2}, \frac{\pi}{2}]$.

In order to analyze the interaction of traction and dissipative forces in this case, we use a kinematic bicycle model. Despite the simplicity of a kinematic bicycle model, it can achieve similar results as a dynamical bicycle model for vehicle control purposes [12]. The bicycle model considers that the two front and rear wheels are respectively lumped into one single front and rear wheel, which in Fig. 3.1 are represented in red color. Even thought the kinematic version of this model is strictly true only for low lateral vehicle accelerations, applying this model to high-velocity corners will result in an over-estimate of the cornering energy, thereby making the model quantitatively conservative. Moreover, we assume vehicles with front-wheels-only steering systems, implying that the rear wheel will be aligned with the longitudinal axis of the vehicle for the entire route. For the sake of simplicity, we assume that the dissipative forces F_{roll} and F_{air} are aligned with the longitudinal axis of the vehicle. Note that the velocity of the vehicle $v(t)$ is tangential to the trajectory and shows an angle $\beta(s(t)) \in [-\frac{\pi}{2}, \frac{\pi}{2}]$ with respect to the longitudinal axis, which is given by

$$\beta(s) = \arcsin\left(l_r K(s)\right). \tag{3.5}$$

The total centripetal force applied at CG and its projection into the longitudinal vehicle axis are given by

$$F_c(v,s) = mv^2 K(s), \tag{3.6}$$

and

$$F_{cl}(v,s) = F_c(v,s)\cos(\tfrac{\pi}{2} - \beta(s(t))) = ml_r v^2 K(s)^2, \tag{3.7}$$

respectively.

An analysis of the forces acting on the longitudinal axis of the vehicle shows that for curved trajectories the total dissipative force in that direction is given by

$$F_d(v,s) = F_{roll+grav} + F_{air} + F_{cl}. \tag{3.8}$$

Note that projection of the centripetal force into the longitudinal axis (3.7) can be physically interpreted as a lumped approximation in the longitudinal direction of the lateral forces generated on the tires during cornering. From (3.2) and (3.7), it is possible to rewrite (3.8) as

$$F_d(v,s) = mg(c_r\cos(\alpha(s)) + \sin(\alpha(s))) + (\sigma_d + ml_r K(s)^2)v^2. \tag{3.9}$$

Unlike the approach in [10], the dissipating force introduced by cornering F_{cl} is an approximation that only depends on the geometric configuration of the vehicle and the road, which comes as a consequence of the use of a kinematic model. In

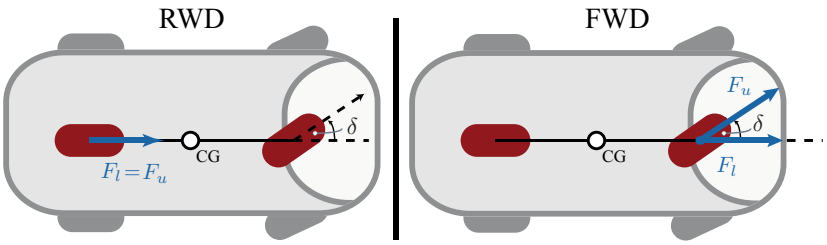

Figure 3.2: Traction force for RWD and FWD configurations.

Section 3.3, we will use a numerical example to show that the obtained approximation, even though it is simple, properly captures the behavior of the vehicle during cornering.

The traction force in the longitudinal direction F_l depends on the drive configuration of the vehicle, i.e., in a RWD configuration the total motor traction force $F_u(t)$ is directly applied directly to the longitudinal direction of the vehicle, while for FWD case only a fraction of $F_u(t)$ is applied in the longitudinal direction. This idea is depicted in Fig. 3.2, where the traction forces for the two drive configurations are shown. It is clear to see that the traction force for a vehicle with RWD can be described by (3.3). On the other hand, the traction force in the longitudinal direction for a FWD vehicle depends on the steering angle as

$$F_l(F_u, s) = F_u \cos(\delta(s)), \tag{3.10}$$

where according to the kinematic bicycle model

$$\delta(s) = \arctan\left(\frac{l_f + l_r}{l_r} \tan(\beta(s))\right). \tag{3.11}$$

After substituting (3.5) into (3.11) and applying a composition of trigonometric and inverse trigonometric functions, the traction force into the longitudinal direction (3.12) can be reformulated as

$$F_l(F_u, s) = \frac{F_u}{\sqrt{1 + \frac{(l_f+l_r)^2 K^2(s)}{1 - l_r^2 K^2(s)}}}. \tag{3.12}$$

The projection of the centripetal force and the traction force in the direction of motion allows us to generalize the longitudinal vehicle dynamics model (3.1) for curved trajectories as

$$ma = F_l(F_u, s) - F_d(v, s), \tag{3.13}$$

where $a(t) = \frac{\mathrm{d}v}{\mathrm{d}t}$ is the acceleration in the tangential direction to the trajectory. Considering that the forces are analyzed in the longitudinal axis of the vehicle, the use of $a(t)$ instead of the longitudinal acceleration $a_l(t)$ in (3.13) is justified by a small angle approximation such that $a_l(t) = a(t)\cos(\beta(s)) \approx a(t)$. Additionally

in (3.13), $F_d(v,s)$ is given by (3.9), and $F_l(F_u,s)$ is described by (3.3) and (3.12) for vehicles with FWD and RWD, respectively. As a final observation, it should be noted that taking $K(s) = 0$ implies that the vehicle moves on a straight trajectory. For this specific case, (3.9) is equivalent to (3.2), which represent the dissipating forces for a straight trajectory. Similarly, for FWD vehicles (3.12) is equivalent to (3.3), which describes the traction force in the longitudinal direction for vehicles driving in straight trajectories. These observations show the generality of the proposed models.

3.2. Optimal Control Problem

A continuous-time optimal control problem (OCP) formulation that represents the eco-driving problem for urban city scenarios is provided in this section. In particular, we will extend the eco-driving formulation proposed in [13] to include the cornering effects captured by the trajectory dependent models presented in the previous section. Additionally, we discuss the differences between the OCP proposed in this chapter and common approaches of eco-driving for cornering available in literature.

3.2.1. Problem Formulation

For a route with given curvature $K(s)$ and road grade $\alpha(s)$, eco-driving aims to minimize the aggregative power $P(v(t),F_u(t))$ over a fixed period of time $[t_o,t_f]$ required by a vehicle driving a trajectory $s(t) \in [s_o,s_f]$, while being subject to position dependent velocity and acceleration bounds $v(t) \in [\underline{v}(s),\overline{v}(s)]$, $a(t) \in [\underline{a}(s),\overline{a}(s)]$, respectively. Moreover, the vehicle longitudinal dynamics and initial final conditions for position and velocity are considered. A mathematical formulation of the eco-driving problem as an OCP is given by

$$\min_{s(t),v(t),a(t),F_u(t)} \quad \int_{t_o}^{t_f} P(v(t),F_u(t))\mathrm{d}t \tag{3.14a}$$

$$\text{subject to} \quad ma(t) = F_l(F_u(t),s(t)) - F_d(v(t),s(t)), \tag{3.14b}$$

$$\frac{\mathrm{d}}{\mathrm{d}t}s(t) = v(t), \tag{3.14c}$$

$$\frac{\mathrm{d}}{\mathrm{d}t}v(t) = a(t), \tag{3.14d}$$

$$s(t_o) = s_o, \quad s(t_f) = s_f \tag{3.14e}$$

$$v(t_o) = v_o, \quad v(t_f) = v_f \tag{3.14f}$$

$$a(t)^2 + v(t)^4K(s(t))^2 \leq (\mu_s g)^2, \tag{3.14g}$$

$$\underline{v}(s(t)) \leq v(t) \leq \overline{v}(s(t)), \tag{3.14h}$$

$$\underline{a}(s(t)) \leq a(t) \leq \overline{a}(s(t)), \tag{3.14i}$$

where the power consumed by the electric motor and driveline at a given time instant is

$$P(v,F_u) = \beta_2F_u^2 + \beta_1vF_u + \beta_0v^2 \tag{3.15}$$

with positive coefficients β_2 to penalize the Ohmic losses, β_1 to describe effective power consumed, and β_0 that penalizes the friction losses in the electric motor. Note

that the power consumption (3.15) considers regenerative braking. The longitudinal vehicle dynamics are described by (3.14b) with the definitions provided for (3.13), the time evolution of acceleration, velocity and position are described by (3.14d) and (3.14c), and boundaries for position of velocity are represented by (3.14e) and (3.14f), respectively. Finally, (3.14g) represents a constraint imposed on the total acceleration of the vehicle, where $\mu_s > 0$ is a friction coefficient dependent on the characteristics of the tires and the road conditions. In order to give a physical justification to (3.14g), let us note that the maximum friction force between the road and tires is given by $F_{fric} = m\mu_s g$. For safety reasons, is required to avoid the vehicle to slip, which implies that the total force applied to the vehicle is lower than the maximum friction force during normal operation, i.e.,

$$(ma(t))^2 + (mv(t)^2 K(s(t)))^2 \leq (m\mu_s g)^2, \tag{3.16}$$

which can be simplified into (3.14g). The first term in the left hand side of (3.16) represents the resultant force applied to the vehicle in the tangential direction of the trajectory, and the second term is the centripetal force. Note that (3.14g) is mainly relevant during cornering. During straight trajectories this constraint is inactive because upper acceleration bound in (3.14i) is expected to satisfy $\overline{a}(s) \leq \mu_s g$.

3.2.2. Effects of Cornering

From the scarce literature about eco-driving approaches that consider cornering effects, it is possible to note that often the OCP formulation includes a constraint linked to the centripetal acceleration of the vehicle, see, e.g., [9], which is similar to (3.14g). This type of hard constraint implicitly imposes a limit to the maximum velocity during cornering. In the approach presented in this chapter, we improve the representation of cornering effects by including those effects in longitudinal vehicle dynamics, i.e., (3.14b). This specific modeling choice can be seen as a soft constraint that highly penalizes the velocity while cornering. To this end, we will use a simplified example that, without losing generality, allows us to observe the effects of cornering in the OCP (3.14).

Let us consider a RWD vehicle, driving in a circular trajectory on a flat road, i.e., $K(s) = \frac{1}{R}$ and $\alpha(s) = 0$. It is possible to find an equivalent formulation fo the OCP (3.14) by substituting (3.14b) into (3.14a) (see , e.g., [14, §4.1.3]), leading to

$$\begin{aligned} &\min_{s(t),v(t),a(t)} \quad \int_{t_o}^{t_f} P(v(t), ma(t) + F_d(v(t), s(t)))\mathrm{d}t \\ &\text{subject to} \qquad \text{(3.14c)-(3.14i)}, \end{aligned} \tag{3.17}$$

in which

$$\begin{aligned} P(v, ma + F_d(v,s)) = \beta_2\big(m(a + gc_r) + (\sigma_d + ml_r K^2)v^2\big)^2 \\ + \beta_1 v\big(m(a + gc_r) + (\sigma_d + ml_r K^2)v^2\big) + \beta_0 v^2. \end{aligned} \tag{3.18}$$

Thus, we can note the the term $ml_r K^2$ drastically penalizes velocity in the new cost function. This penalization, depends quadratically on the road curvature, which implies that the optimal solution might show lower decelerations during cornering maneuvers.

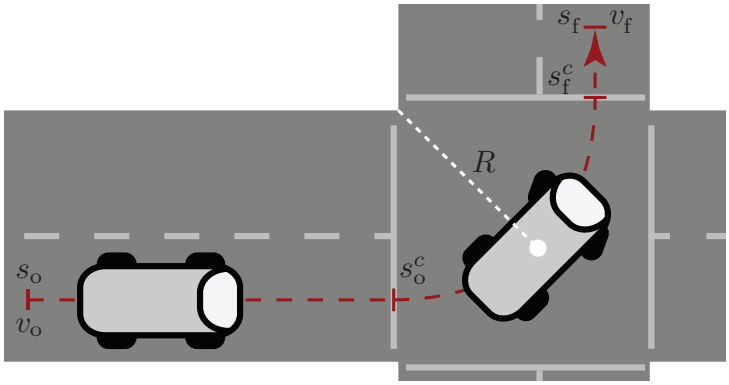

Figure 3.3: Urban intersection considered in the case study.

3.3. Case Study

In this section, we study an electric vehicle executing a cornering maneuver in an urban environment with different curvatures. The advantages of the model and OPC formulation presented in this chapter are highlighted in this example. To this end, we will contrast the results with traditional eco-driving approaches. Moreover, we will show the relevance of the proposed approach using an experimentally validated high-fidelity model to calculate the instantaneous power and total energy consumption produced during the cornering maneuvers analyzed.

Let us consider an electric vehicle with RWD and parameters listed in Table 3.1. The vehicle executes a cornering maneuver on an urban intersection as is depicted in Fig. 3.3, which curvature is defined as

$$K(s) = \begin{cases} \frac{1}{R} & \text{for } s_o^c \leq s \leq s_f^c, \\ 0 & \text{otherwise;} \end{cases} \tag{3.19}$$

where s_o^c is the position where the corner begins and s_f^c is the final corner position. The curvature (3.19), will be specified for three different scenarios that are detailed in Table 3.2.

The OCP (3.14) is formulated using the parameters in Table 3.1. To find the solutions of this OCP, we discretize the problem (3.14) and solve a static optimization problem. It is important to remark that this chapter focuses on the modeling and OPC formulation rather than in the methodology to find the solution. However, the interested reader can follow the methodology detailed in Chapter 2 of this thesis. The optimal solutions to (3.14) are depicted in Fig. 3.4 as velocity and acceleration profiles for each scenario considered in the case study. Note that the vertical lines depicted in both profiles indicate the initial and final positions of the curved section of the trajectory. It can be observed that the vehicle decelerates before entering the curved section of the trajectory. When the vehicle enters the curved section of the trajectory the deceleration rate is reduced and approximately at halfway along the curved section the vehicle begins accelerating. As soon as the vehicle

Table 3.1: Vehicle and OCP parameters

Par.	Value	Units	Par.	Value	Units
m	15000	$[kg]$	σ_d	3.24625	$[Ns^2/m^2]$
c_r	0.007	–	μ_s	0.35	–
β_0	0.292	$[ws^2/m^2]$	β_1	1.005	–
β_2	2.652e-4	$[w/N^2]$	s_0	0	$[m]$
s_f	150	$[m]$	v_0	30	$[m/s]$
v_f	35	$[m/s]$	$\overline{v}$	60	$[m/s]$
$\underline{v}$	0	$[m/s]$	$\overline{a}$	0.2g	$[m/s^2]$
$\underline{a}$	-0.2g	$[m/s^2]$			

Table 3.2: Parameters for different scenarios.

R	s_o^c	s_f^c
12 $[m]$	70 $[m]$	70+$R\pi/2$ $[m]$
14 $[m]$	70 $[m]$	70+$R\pi/2$ $[m]$
17 $[m]$	70 $[m]$	70+$R\pi/2$ $[m]$

leaves the curved section of the trajectory the acceleration is immediately increased. Interestingly, the differences between scenarios considered is clearly observed in the velocity profiles, where at higher curvatures lower velocities are observed in the curved section of the trajectory. This result is expected because velocity is highly penalized for high curvatures in the road. This effect has been discussed in Section 3.2.2.

In order to highlight the advantages of our general approach, we compare the optimal solution to the OCP (3.14) with a traditional eco-driving OCP formulation. Specifically, a traditional OCP considers the constraint (3.14g), but the cornering effects in (3.14b) are neglected. In Fig. 3.5, the optimal velocity and acceleration profiles for traditional and general eco-driving formulations are presented for the specific scenario where $R = 14\,[m]$. Note that the velocity profile of the traditional approach shows constant velocity during the curved section of the road, which also indicates zero acceleration during that section. This is expected since traditional eco-driving strategies avoids changes in acceleration to reduce energy consumption. As a consequence, the vehicle crosses the curved section with the maximum possible velocity, which is defined by constrain (3.14g). On the other hand, the optimal strategy obtained by the general approach proposed in this chapter shows lower velocities during the curved section, which is connected to the velocity being penalized by the curvature of the road. This causes non-zero longitudinal acceleration in the curved section.

The effects of both strategies in terms of power consumption can be observed in in Fig. 3.6, where the instantaneous cumulative power consumption produced

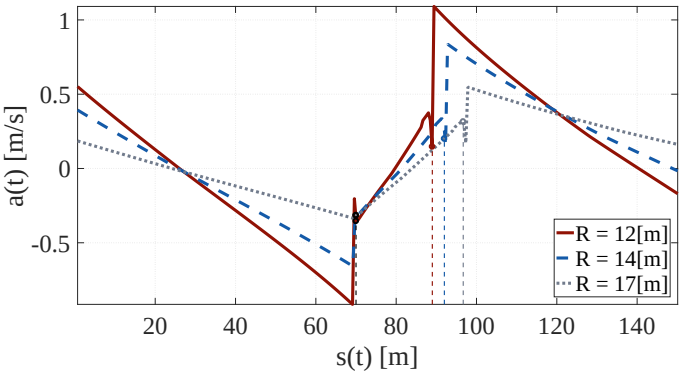

(a) Acceleration profiles.

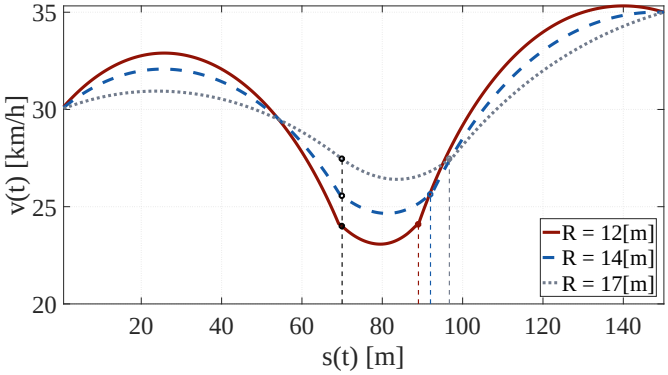

(b) Velocity profiles.

Figure 3.4: Optimal solutions to the OCP (3.14) for different curvatures.

by these two strategies is depicted. Here, we use the experimentally validated high-fidelity model from [8] to calculate the cornering losses, in combination with instantaneous power consumed by the inertia, aerodynamical drag, rolling resistance, and electric machine losses. As expected, the main difference between both strategies are observed in the curved section of the trajectory. For the traditional strategy, the power losses due to cornering and electric machine losses are constant during the curved section, while the general strategy indicates virtually no electric machine losses during the first half of the curved trajectory. This shows that the cornering maneuver obtained form the general strategy is more energy efficient than the traditional counterpart. This observation is reinforced by simulations performed on the rest of the scenarios considered in this case study.

In Fig. 3.7, we present the cumulative energy obtained by using the traditional and general strategies for scenarios with three different curvatures, and in Table 3.3, we summarize the total energy calculated with the high-fidelity model for each case and strategy. The trend observed from these results indicates that the general

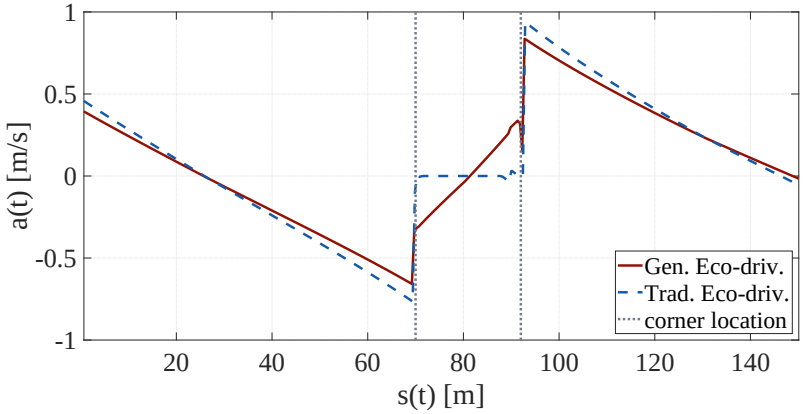

(a) Acceleration profiles.

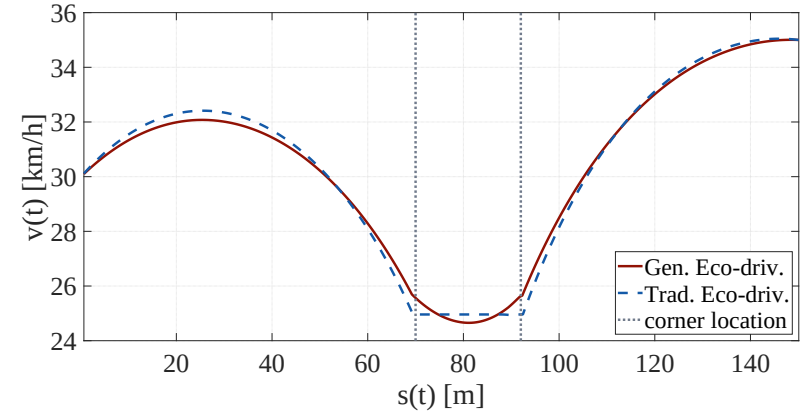

(b) Velocity profiles.

Figure 3.5: Comparison for OCP formulations for cornering scenario with $R = 14\,[m]$.

Table 3.3: Comparison of energy consumption between strategies.

Scenario	**Tot. Energy (Traditional)**	**Tot. Energy (General)**	**Diff. %**
$R = 12\,[m]$	$820.2\,[kJ]$	$757.6\,[kJ]$	8.26
$R = 14\,[m]$	$687.5\,[kJ]$	$658.2\,[kJ]$	4.45
$R = 17\,[m]$	$574.2\,[kJ]$	$573.4\,[kJ]$	0.14

strategy proposed in this chapter is able to improve the energy efficiency of the vehicle for all the considered scenarios. In fact, the proposed eco-driving strategy saves a larger amount of energy for scenarios with larger curvatures, while for roads with small curvature the total consumption of the general strategy tends

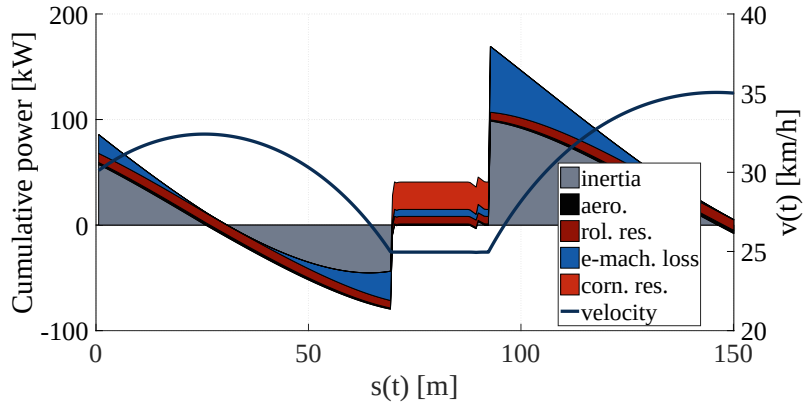

(a) Tradditional eco-driving aprpoach.

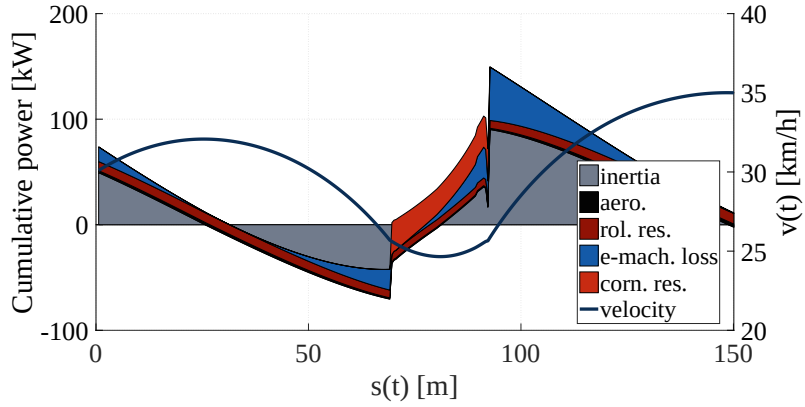

(b) Eco-driving for for general trajectories.

Figure 3.6: Velocity and energy losses for a cornering scenario with $R = 14[m]$.

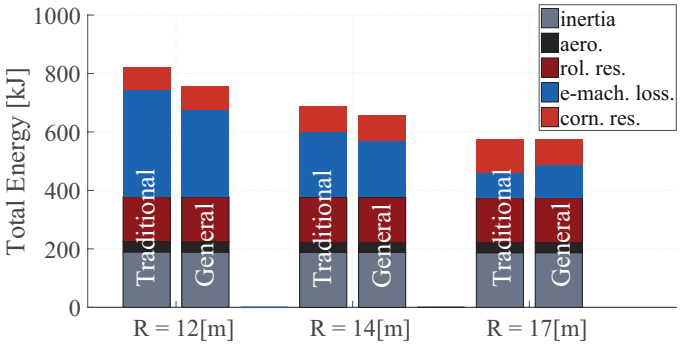

Figure 3.7: Cumulative energy consumption for different scenarios and eco-driving strategies.

to approximate to the traditional approach. This is a consistent result since our OCP formulation resembles traditional eco-driving formulations when roads with no curvature are considered, as has been discussed in Section 3.1.2. Remarkably, in Fig. 3.7, it is possible to see that a higher energy efficiency of the proposed strategy mainly comes from a reduction of the energy losses in the electric machine. This shows that, in general, considering cornering effects in the OCP formulation results into an improved operation of the electric machine instead of a reduction of the losses due to cornering.

3.4. Conclusions

A model that approximates cornering forces into the longitudinal axis of the vehicle has been proposed in this chapter. The simplicity of this model relies on the geometry of the vehicle and the road, making it unnecessary to identify specific tire parameters. Based on this model, we have proposed a general eco-driving optimal control problem formulation that can be used for both straight and curved trajectories. Moreover, it can be used for front wheel drive and rear wheel drive configurations of the vehicle. The advantages of the proposed OCP have been analyzed on a case study, where the use of a high-fidelity model have allowed not only to validate the proposed model and OCP formulation, but also to show the improvements of this approach with respect to traditional approaches found in current literature. The results have shown that the use of the general OCP formulation proposed in this chapter yields to an improvement energy savings for cornering maneuvers in trajectories with large curvatures, which are approximately up to 8% larger than traditional eco-driving strategies.

References

[1] C. Bingham, C. Walsh, and S. Carroll, *Impact of driving characteristics on electric vehicle energy consumption and range,* IET Intelligent Transport Systems (2012).

[2] A. Sciarretta, G. D. Nunzio, and L. L. Ojeda, *Optimal Ecodriving Control: Energy-Efficient Driving of Road Vehicles as an Optimal Control Problem,* IEEE Control Systems MAgazine (2015).

[3] D. Maamria, K. Gillet, G. Colin, Y. Chamaillard, and C. Nouillant, *Optimal ecodriving for conventional vehicles: Simulation and experiment,* in *Proc. IFAC World Congress* (2017).

[4] N. Petit and A. Sciarretta, *Optimal drive of electric vehicles using an inversion-based trajectory generation approach,* in *Proc. IFAC World Congress* (2011).

[5] G. D. Nunzio, C. C. d. Wit, P. Moulin, and D. D. Domenico, *Eco-driving in urban traffic networks using traffic signal information,* in *Proc. Conference on Decision and Control* (2013).

[6] M. Henriksson, O. Flardh, and J. Martensson, *Optimal speed trajectories under variations in the driving corridor,* in *Proc. IFAC World Congress* (2017).

[7] J. Han, A. Sciarretta, L. L. Ojeda, G. De Nunzio, and L. Thibault, *Safe- and eco-driving control for connected and automated electric vehicles using analytical state-constrained optimal solution,* IEEE Transactions on Intelligent Vehicles (2018).

[8] C. Beckers, I. Besselink, and H. Nijmeijer, *Assessing the impact of cornering losses on the energy consumption of electric city buses (in press),* Transp. Res. Part D Transp. Environ. (2020).

[9] P. Polterauer, G. P. Incremona, P. Colancri, and L. d. Re, *A switching nonlinear MPC approach for ecodriving,* in *Proc. American Control Conference* (2019).

[10] Y. Ikezawa, H. Fujimoto, D. Kawano, Y. Goto, Y. Takeda, and K. Sato, *Range extension autonomous driving for electric vehicle based on optimal vehicle velocity profile in consideration of cornering,* IEEE Transactions on Industry Applications (2017).

[11] J. Edrén, M. Jonasson, J. Jerrelind, A. Stensson Trigell, and L. Drugge, *Energy efficient cornering using over-actuation,* Mechatronics (2019).

[12] J. Kong, M. Pfeiffer, G. Schildbach, and F. Borrelli, *Kinematic and dynamic vehicle models for autonomous driving control design,* in *Proc. IEEE Intelligent Vehicles Symposium* (2015).

[13] G. P. Padilla, S. Weiland, and M. C. F. Donkers, *A global optimal solution to the eco-driving problem,* IEEE Control Systems Letters (2018).

[14] S. P. Boyd and L. Vandenberghe, *Convex optimization, Cambridge University Press New York* (2014).

4

Energy Optimal Coordination of Fully Autonomous Vehicles in Urban Intersections

This chapter provides an energy optimal solution to conflict resolutions between autonomous vehicles crossing an urban intersection. The eco-driving formulation presented in Chapter 3 is extended to include conflict resolution constraints in the optimal control problem formulation. The objective is to minimize energy consumption of all the vehicles, while avoiding collisions. A static optimization approach is used to find solutions to the optimal control problem. In particular, a sequential mixed-integer quadratically constrained program is proposed. Simulations results show that the AVs can take advantage of the available information through infrastructure-to-vehicle or vehicle-to-vehicle communication to anticipate the driving scenarios and, consequently, coordinate the intersection crossing order and obtain the optimal velocity profiles that minimize the overall energy consumption at the intersection. The research outcome underlines the benefits of using available information to improve energy savings by anticipation of the driving conditions.

This chapter is based on **P.2**.

Technological developments in the automotive industry have enabled the possibility to create communication networks between the different agents of an urban intersection, e.g., communication infrastructure-to-vehicle (I2V) and vehicle-to-vehicle (V2V). The exploitation of this information leads to new advances in terms of autonomous operation of vehicles, which brings improvements to safety, comfort and energy savings. In fact, electric autonomous vehicles (AV) can play a principal role since they have shown advantages in terms of being environmentally friendly and energy efficient [1–3]. For instance, as shown in [4], fully automated road transport systems will lead to energy consumption reductions of $55\% - 66\%$. In this chapter, we will explore the energy saving that can be achieved in an urban intersection, where fully autonomous vehicles with complete information of the driving scenario are coordinated.

The topic of coordination of vehicles along an intersection has been addressed in the literature from different perspectives. For instance, [5] proposes a decentralized problem formulation where each agent solves a local optimization problem. However, the intersection decision order considers heuristics for priority assignments, which might lead to an energy sub-optimal solution. In [6], a scheduling-based approach is proposed, where the authors focus on the feasibility of a crossing sequence where a supervisory controller acts, when necessary, to maintain safety. Unfortunately, this approach does not guarantee an energy optimal solution. On the other hand, optimal control problem formulations allow the use of explicit performance objectives such as energy efficiency. However, while it is frequently stated that energy minimization is the goal, this target is commonly not explicitly included in the cost function [7–9]. In [10], an economic model predictive control formulation is proposed using an objective function which directly captures both energy consumption and travel time. However, rear-end collision avoidance is not taken into account, i.e., scenarios where multiple vehicles proceed in the same direction after crossing the intersection.

This chapter proposes an approach which aims to fill the gap noticed in the literature by proposing an optimal control problem (OPC) formulation that provides an energy optimal solution to intersection conflict scenarios. Specifically, the eco-driving modelling framework presented in Chapter 2 and Chapter 3 is the basis for the OPC formulation considered in this chapter, where multiple vehicles considered and constraints that consider safety while crossing and leaving the intersection are included. The proposed energy optimal coordination problem is solved using a sequential mixed-integer quadratically constrained program. The energy savings of the proposed approach are highlighted in simulations where the energy optimal coordinated strategies are compared to scenarios with uncoordinated human-driven vehicles crossing the intersection.

The remainder of this chapter is organized as follows. Section 4.1 provides a description of the energy optimal coordination problem and in Section 4.2 the associated optimal control problem is formulated. Simulation results are given in Section 4.3, in which the relevance of energy-optimal vehicle coordination strategies is shown. Finally, conclusions are drawn in section 4.4.

4.1. Problem Framework

In this chapter, the energy optimal coordination of an urban intersection scenario of N_V AVs is solved.Each vehicle $n \in \mathcal{N}_\mathcal{V} := \{1, ..., N_v\}$ follows a pre-defined route such that a collision could occur if no control action is applied. The desired route of each AV is considered to be given in advance, i.e., by using a high-level path planning algorithm, which is outside the scope of this study. Hence, the objective is to control the velocity of each vehicle along its trajectory such that the energy consumption is minimized and the vehicle positions are mutually exclusive, i.e, a control agent will modify the desired velocity profiles of the vehicles in order to let them cross safely while minimizing energy losses.

Specifically, a four-way perpendicular intersection is considered in this analysis. This configuration represents a typical urban intersection and allows to perform analysis on complex intersection scenarios, which will be observed in Section 4.3. Nevertheless, the work carried out in this chapter can be adapted for scenarios with different cross angles and different number of road segments, the second one at the cost of an increase of the number of variables. Finally, all vehicles are considered to be equipped with V2V, V2I communication systems and at most one vehicle per lane is approaching the intersection, i.e., cases with multiple vehicles reaching the intersection from the same direction are not taken into account. This last assumption reduces the problem complexity as it excludes rear-end collisions before the intersection joint, outside the purpose of this work. However, this simplification can be removed effortlessly imposing a minimum distance constraint between vehicles reaching the intersection from the same lane.

4.1.1. Mapping from 2D to 1D

The geometry of the intersection is depicted in Fig. 4.1a, where we define as intersection zone (IZ) the area where two or more routes might intersect, i.e., where a side collision could occur. The IZ is defined by a set of four coordinates $\mathcal{IZ} = \{(x_l^I, y_l^I)\}_{l\in\{1,..,4\}}$ with respect to the absolute Cartesian coordinate system OXY which define the edges of the IZ, where the superindex I refers to $Intersection$. Moreover, the absolute position of the N_v vehicles is defined with respect to OXY and the initial and final conditions on position and velocity are known and defined as $\mathcal{P}_n^{\mathrm{o}} := \{(x_n^{\mathrm{o}}, y_n^{\mathrm{o}})\}_{n\in\mathcal{N}_\mathcal{V}}$, $\mathcal{P}_n^{\mathrm{f}} := \{(x_n^{\mathrm{f}}, y_n^{\mathrm{f}})\}_{n\in\mathcal{N}_\mathcal{V}}$, $\overline{V}_n^{\mathrm{o}}$, $\overline{V}_n^{\mathrm{f}}$, for all $n \in \mathcal{N}_\mathcal{V}$, respectively. The relative position of each vehicle with respect to each other is defined through a $o_n x_n y_n$ coordinate system, coplanar to the absolute one and rigid to the associated vehicle n, for all $n \in \mathcal{N}_\mathcal{V}$. The motion of each AV in the two-dimensional space can be described by the following equations of motion:

$$\frac{\mathrm{d}}{\mathrm{d}s_n} x_n = \cos\theta_n \tag{4.1a}$$

$$\frac{\mathrm{d}}{\mathrm{d}s_n} y_n = \sin\theta_n \tag{4.1b}$$

$$\frac{\mathrm{d}}{\mathrm{d}s_n} \theta_n = K_n \tag{4.1c}$$

where θ_n defines the orientation of the vehicle with respect to the initial configuration, and derivatives are taken with respect to the trajectory s_n (see Fig. 4.1b).

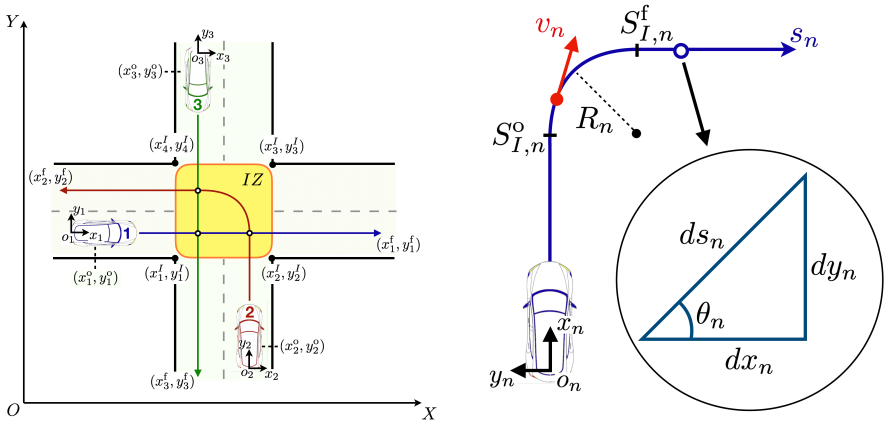

(a) Crossroad schematic & conflict graph definition (b) Vehicle's trajectory definition

Figure 4.1: Intersection and trajectory schemes.

To simplify the analysis and the mathematical formulation that will be detailed in Section 4.2, the trajectory of each vehicle is considered to be straight, however still keeping the curvature information of the vehicle as shown in Fig. 4.2. This formulation allows to simplify the problem into a single dimensional formulation, while still having knowledge of which vehicle is performing a turning maneuver inside the IZ. Finally, in order to define the vehicles and intersection information with respect to an absolute one-dimensional reference system, the information defined for each vehicle n on the respective trajectory s_n are mapped to the absolute coordinate s^* as shown in Fig. 4.2, setting $S^o_1 = S^o_2 = \ldots = S^o_{N_v} = S^o$.

The single dimension coordinate reformulation is justified from the fact that vehicle's trajectories are imposed and cannot be modified and therefore, the tangential velocity, which is the variable desired to be regulated, can be modified just in terms of intensity, i.e., its modulus can be varied but not its direction. Therefore, using a 1D framework will allow to ease the problem formulation, reducing the number of control variables, which will need to be defined just with respect to the single dimensional trajectory coordinate s^*. On the other hand, the price that has to be paid is that 2D trajectory information has to be converted into a single dimension first, which however do not represent a limitation for the application, since the computational time is not substantial.

4.1.2. Conflicting Points

Two vehicles crossing the intersection define a conflicting point (CP) if their trajectory intersects. Therefore, for each vehicle $j \in \mathcal{N}_\mathcal{V}$ we define a set

$$\mathcal{A}^j = \left\{ n \in \mathcal{N}_\mathcal{V} \mid \left\| \begin{bmatrix} x_n(s_1) \\ y_n(s_1) \end{bmatrix} - \begin{bmatrix} x_n(s_2) \\ y_n(s_2) \end{bmatrix} \right\| = 0 \right\}$$

for some $s_1, s_2 \in \mathcal{R}_+$. Moreover, since the CP for vehicle n with vehicle j coincides with the CP of vehicle j with vehicle n, in order to remove redundant CPs, the

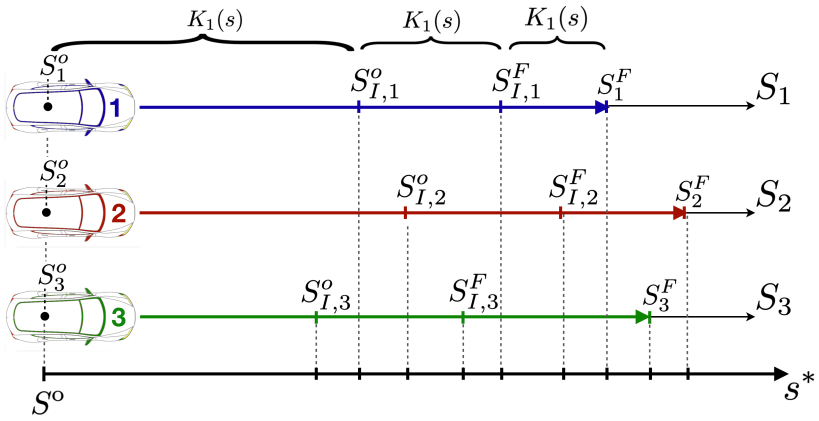

Figure 4.2: Definition of a global one-dimensional reference

conflicting points set is defined as $\mathcal{CP} = \{(i,j) \in \mathcal{N}_\mathcal{V} \times \mathcal{N}_\mathcal{V} : i \in \mathcal{A}^j, \text{with} \quad j > i\}$.

4.2. Optimal Control Problem Formulation

In the previous section, we have presented a representation for the vehicle coordination problem as a one-dimensional motion, in which possible conflicts are represented by conflicting points. This representation will be used to define the energy optimal vehicle coordination problem, which is formulated as an optimal control problem in this section. The problem can be seen as an extension of the eco-driving problem presented in Chapter 3 towards multiple vehicles, while at the same time *i)* including additional constraints representing the avoidance of conflicts on the intersection, *ii)* avoiding rear-end collisions. Note that in this modelling framework energy-losses during cornering are considered.

The objective in the eco-driving problem, as discussed in Chapter 2 and Chapter 3, is to minimize the power $P(t)$ required from a vehicle in order to cover a given distance $S^\mathrm{f} - S^\mathrm{o}$ over a provided time interval $t^\mathrm{f} - t^\mathrm{o}$, knowing the velocity and acceleration bounds $v(t) \in [\underline{v}, \overline{v}]$, $a(t) \in [\underline{a}, \overline{a}]$, respectively, the boundary conditions on position and velocity and subject to longitudinal vehicle dynamics.

4.2.1. Intersection Constraint

As introduced in Section 4.1.2, a conflicting point is defined between each pair of AVs for which the trajectories intersect. Mathematically, if we consider AVs as point masses, in order to prevent collisions between vehicles, the condition $S_i(t) \neq S_j(t)$ has to hold for all $(i,j) \in \mathcal{CP}$ and for all $t \geq 0$. However, since the trajectories of two vehicles can cross only inside the intersection, the constraint needs to be active just when one of the two vehicles resides inside the intersection and can be disregarded if at least one of the two vehicles has already left the intersection zone. Moreover, since each vehicle has a length and a width, the aforementioned constraint does not guarantees safety and, hence, it has to be modified to accommodate for the length

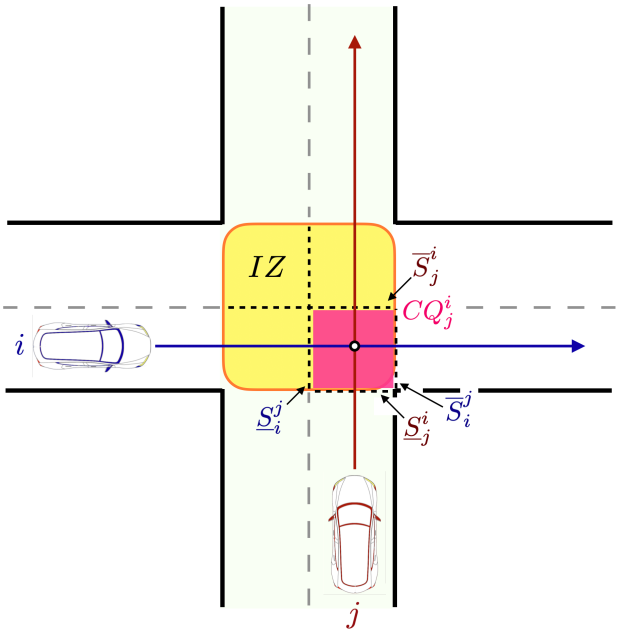

Figure 4.3: Conflicting Quadrant definition

of the vehicles. Thus, we consider to divide the IZ in four quadrants as shown in Fig. 4.3 and we define a conflicting quadrant $CQ_j^i \ \forall (i,j) \in \mathcal{CP}$.

Furthermore, we consider that each vehicle can reside entirely in one quadrant. Therefore, for each pair $(i,j) \in \mathcal{CP}$ we define two bounds $\underline{S}_i^j, \overline{S}_i^j$ which define the beginning and the end respectively of the CQ_j^i for vehicle i and, similarly for vehicle j, $\underline{S}_j^i, \overline{S}_j^i$. In Fig. 4.3 an example is given in order to clarify the concept. Therefore, in order to guarantee a collision free scenario, the constraints have been defined as

$$\overline{S}_j^i \delta_{i,j} \leq s_j \leq \underline{S}_j^i (1 - \delta_{i,j}) + S_j^f \delta_{i,j} \tag{4.2a}$$

for all $(i,j) \in \mathcal{CP}$ and $\underline{S}_i^j \leq s_i(t) \leq \overline{S}_i^j$, where $\delta_{i,j} \in \{0,1\}$ is the intersection decision variable (IDV) which will decide the crossing order between the two vehicles. Specifically, The binary IDV will enforce vehicle j to leave the intersection before vehicle i if $\delta_{i,j} = 1$, or await until vehicle i has exit the intersection if $\delta_{i,j} = 0$.

4.2.2. Rear-End Constraint

In the case where two or more vehicles proceed in the same direction after crossing the intersection, an additional constraint has to be imposed to prevent rear-end collisions. In order to prevent collisions among vehicles i and j, with $i,j \in \mathcal{N}_\mathcal{V}$ and

$i \neq j$. This can be imposed by requiring that either

$$s_{r,i}(t) - s_{r,j}(t) \geq \epsilon \quad \text{if} \quad s_{r,i}(t) > s_{r,j}(t), \text{ for } t \geq t^{\mathrm{f}}_{I,i}, \tag{4.3a}$$

or

$$s_{r,j}(t) - s_{r,i}(t) \geq \epsilon \quad \text{if} \quad s_{r,j}(t) > s_{r,i}(t), \text{ for } t \geq t^{\mathrm{f}}_{I,i}, \tag{4.3b}$$

holds, in which $s_{r,i}(t) = s_i(t) - S^{\mathrm{f}}_{I,i}$ and $s_{r,j}(t) = s_j(t) - S^{\mathrm{f}}_{I,j}$ are the positions of the vehicles measured from exit point of the IZ, $t^{\mathrm{f}}_{I,i}$ being the time instant at which the i-th vehicle exits the IZ and ϵ is a positive constant that guarantees a safety distance among the two vehicles. Note that (4.3) can be expressed as the product between the two inequalities, leading to the following nonconvex quadratic inequality constraint:

$$(s_{r,i}(t) - s_{r,j}(t))^2 \geq \epsilon^2 \tag{4.4}$$

As a remark, (4.4) has to be active only for those vehicle which proceed in the same direction and just when the i-th vehicle exits the intersection. Therefore, (4.4) is required for all $(i,j) \in \mathcal{R}_{\mathcal{E}} = \{(i,j) : s_i(t_i) = s_j(t_j)\}$ for some $t_i, t_j \in \mathbb{R}^+$ and $t_i \geq t^f_{I,i}$.

4.2.3. Dynamical Model

Typically, traditional eco-driving formulations neglect lateral dynamics and only consider longitudinal vehicle dynamics defined by the difference between the traction force in the longitudinal direction $F_u(t)$ and the dissipative forces which, for a vehicle proceeding on a trajectory with no slope, are the aerodynamical drag force F_{air} and rolling resistance F_{roll}. Therefore, the vehicle dynamics are defined by Newton's second law as

$$mu = F_u - \underbrace{\sigma_d v^2}_{F_{air}} - \underbrace{mgc_r}_{F_{roll}} \tag{4.5}$$

where m represents the equivalent mass of the vehicle, and $u(t) = \frac{dv}{dt}$ is the vehicle acceleration. $v(t)$ defines the vehicle velocity, $g \approx 9.81 m/s^2$ is the gravitational acceleration constant, c_r is the rolling force coefficient and $\sigma_d = \frac{1}{2} c_d \rho_a A_f$, with σ_d the drag coefficient, ρ_a the air density and A_f the frontal area of the vehicle. As discussed in Chapter 3, this model is not suitable for cornering maneuvers, since it neglects the effects of the friction force which has a substantial impact on the energy losses. Therefore, along the lines of Chapter 3, we consider the following dynamical model

$$mu = F_u - \sigma_d v^2 - mgc_r - mKv^2 \cos\alpha \tag{4.6}$$

where the last term on the right hand side represents the component of the friction force $\widehat{F}_{fr}$ acting on the longitudinal direction of the vehicle.

In this chapter, a kinematic bicycle model as depicted in Fig. 4.4 is considered, i.e., the velocity vectors at points A and B are aligned with the longitudinal direction of the front and rear wheels, respectively, which is a reasonable assumption for low vehicle motion speed ($\leq 5\ m/s$), [11]. Moreover, we assume rear-wheel traction

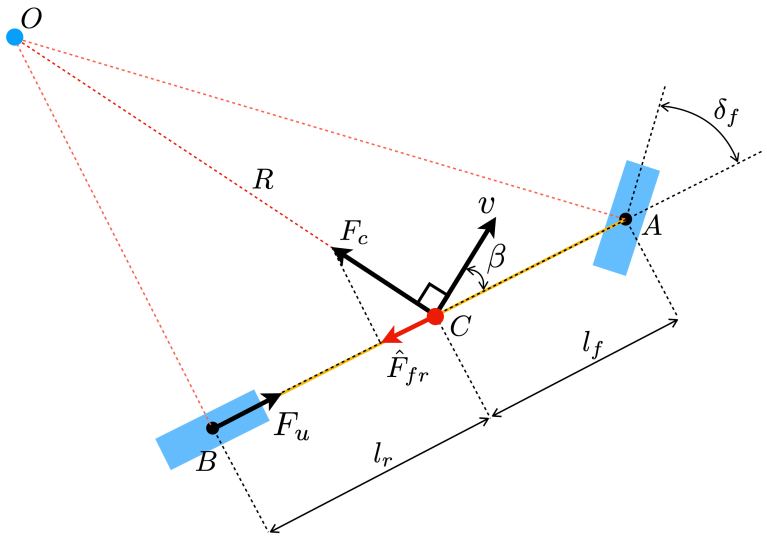

Figure 4.4: Bicycle Model; Kinematics of lateral vehicle motion

vehicles with front-wheels-only steering systems, implying that the rear wheel will be aligned with the longitudinal axis of the vehicle for the entire route. On the other hand, the front wheel is able to change orientation and his steering angle is defined by $\delta_f \in (-\frac{\pi}{2}, \frac{\pi}{2})$. The radius of curvature R is defined from the instantaneous center of rotation O and the center of gravity C. We assume C to be located at a distance l_r, l_f from the rear and front wheel axis, respectively. The friction force supplies the centripetal force F_c which is applied in C, and points toward O as depicted in Fig. 4.4. Note that the velocity vector of the vehicle is tangential to the trajectory and forms an angle β with respect to the longitudinal vehicle axis given by

$$\beta = \arcsin(l_r K) \tag{4.7}$$

Therefore, the component acting on the longitudinal axis of the vehicle can be obtained as

$$\widehat{F}_{fr} = F_c \cos(\tfrac{\pi}{2} - \beta) = m l_r v^2 K^2 \tag{4.8}$$

As a remark, (4.8) can be used also for vehicles with straight trajectories since the term related to friction force will vanish due to his dependency on K.

4.2.4. Cost Function Extension

In Chapter 2 and Chapter 3 the objective of the eco-driving problem is to minimize the power consumption $P(t)$ of a vehicle, which is assumed to be a quadratic function of the form

$$P(v, F_u) = \beta_0 v^2 + \beta_1 v F_u + \beta_2 F_u^2 \tag{4.9}$$

for some non-negative parameters β_0,β_1, and β_2. The quadratic form is a realistic assumption for EVs since it properly captures the losses due to mechanical friction

and Ohmic heating. The dynamical model of the vehicle (4.6) is substituted in (4.9) in order to obtain a simplified yet equivalent formulation. Thus, the cost function for a generic AV becomes:

$$P(v,s,u) = \beta_0 v^2 + \beta_1 \eta(s) v^3 + \beta_2 (mu)^2 + \beta_2 (\eta(s) v^2 + c_r mg)^2 \tag{4.10}$$

with $\eta(s) = \sigma_d + m l_r K(s)^2$.

The goal of our problem is to minimize the global energy consumption of N_v AVs approaching from multiple lanes. We therefore take the cost function of the optimal control problem as the arithmetic sum of the cost function defined for each vehicle, i.e.,

$$P(\{v_n, s_n, u_n\}_{n \in \mathcal{N}_v}) = \sum_{n \in \mathcal{N}_v} P(v_n, s_n, u_n) \tag{4.11}$$

in which every vehicle can have different $\beta_{0,n}$, $\beta_{1,n}$ and $\beta_{2,n}$, according to (4.10).

4.2.5. Cornering Constraint

The introduction of a further restriction while cornering arises from the desire to guarantee safe driving conditions for all the vehicles involved in the intersection control problem. As introduced in Section 4.2.3, in order to make a turn, the centripetal force needs to be applied to the vehicle. However, in order to avoid vehicle's slip, the total force applied to the vehicle must be lower than the maximum friction force during normal operation defined as

$$(mu(t))^2 + m^2 v(t)^4 K(s(t))^2 \leq (m\mu_s g)^2 \tag{4.12}$$

where the terms in the left-hand side of (4.12) represent the resultant force applied to the vehicle in the tangential direction and the centripetal force, respectively, and the term on the right-hand side is the maximum friction force, with $\mu_s > 0$ being the friction coefficient.

4.2.6. Optimal Control Problem

After introducing and motivating all the constraints required for energy optimal coordination of N_v AVs crossing an intersection, we can now formalize this problem as the following optimal control problem:

$$\min_{s_n(t),v_n(t),u_n(t),\delta_{i,j}(t)} \quad \int_{t^o}^{t^f} \sum_{n\in\mathcal{N}_v} P(v_n(t),s_n(t),u_n(t))\mathrm{d}t \tag{4.13a}$$

$$\text{s.t.} \quad \tfrac{\mathrm{d}}{\mathrm{d}t}s(t) = v(t), \qquad \tfrac{\mathrm{d}}{\mathrm{d}t}v(t) = u(t) \tag{4.13b}$$

$$s_n(t^{\mathrm{o}}) = S_n^{\mathrm{o}}, \qquad s_n(t^{\mathrm{f}}) \geq S_n^{\mathrm{f}} \tag{4.13c}$$

$$v_n(t^{\mathrm{o}}) = V_n^{\mathrm{o}}, \qquad v_n(t^{\mathrm{f}}) = V_n^{\mathrm{f}} \tag{4.13d}$$

$$\underline{v}_n \leq v_n(t) \leq \overline{v}_n \tag{4.13e}$$

$$\underline{u}_n \leq u_n(t) \leq \overline{u}_n \tag{4.13f}$$

$$u_n(t)^2 + v_n(t)^4 K_n^2 \leq (\mu_{s,n} g)^2 \text{ for all } S_{I,n}^{\mathrm{o}} \leq s_n(t) \leq S_{I,n}^{\mathrm{f}} \tag{4.13g}$$

$$\overline{S}_j^i \delta_{i,j}(t) \leq s_j(t) \leq \underline{S}_j^i [1-\delta_{i,j}(t)] + S_j^{\mathrm{f}} \delta_{i,j}(t), \text{ for all } (i,j) \in \mathcal{CP} \text{ and } \underline{S}_i^j \leq s_i(t) \leq \overline{S}_i^j \tag{4.13h}$$

$$(s_i(t) - s_j(t) - S_{I,i}^{\mathrm{f}} + S_{I,j}^{\mathrm{f}})^2 \geq \epsilon^2, \text{ for all } (i,j) \in \mathcal{R}_{\mathcal{E}} \text{ and } s_i(t) \geq S_{I,i}^{\mathrm{f}} \tag{4.13i}$$

where (4.13a) is defined as in (4.11), the time evolution of velocity and position are defined by (4.13b), (4.13c) and (4.13d) define initial and final conditions on position and velocity, respectively, and boundary conditions on velocity and acceleration are defined by (4.13e) and (4.13f), respectively. Equation (4.13g) defines a constraint imposed on the overall acceleration of the vehicle which has been obtained from (4.12). As a remark, (4.13g) becomes inactive when the vehicle is proceeding on a straight trajectory ($K_n = 0$), since it is assumed that $\overline{u} \leq \mu_s g$. Finally, (4.13h) define the intersection constraint and (4.13i) prevents rear-end collisions. As a last remark, notice that in order to not force the crossing order between vehicles proceeding toward the same direction, the condition on the final position in (4.13c) has to be imposed in terms of inequality constraint.

4.2.7. Solution Method

The optimal control problem (4.13) belongs to the nonlinear mixed-integer programming category of problems, since (4.13g) is nonlinear and because the control inputs of the problem, $u_n(t)$ and $\delta_{i,j}(t)$, are continuous and discrete, respectively. In order to solve the optimal control problem using a static optimization technique, (4.13) has been discretized at times $t_k = k\tau + t_0$, $k \in \mathcal{K} = \{0,\ldots,K-1\}$ with time step $\tau = \frac{t_f - t_0}{K}$ using a forward Euler discretization method. Since the objective function (4.13a) is nonconvex and the constraint (4.13g) is nonlinear, the discrete-time optimal control problem can be seen as a mixed-integer nonconvex nonlinear programming problem.

A common approach to solving nonlinear programs is the use of sequential quadratic programming (SQP) algorithms. For instance in [12], a modified SQP method that can deal with mixed-integer nonconvex formulations. The algorithm is stabilized by a trust region method and uses Broyden–Fletcher–Goldfarb–Shanno (BFGS) updates to approximate the hessians of the functions. In this chapter, we

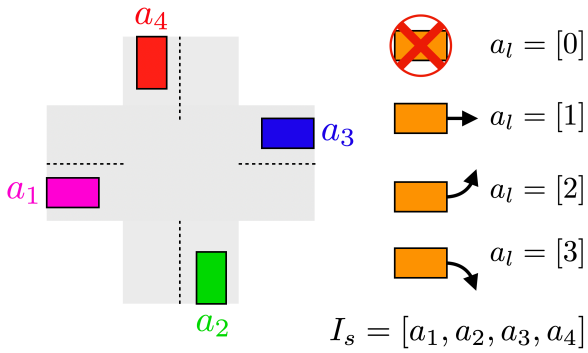

Figure 4.5: Intersection Scenario (I_s) Definition

follow a similar idea by formulating a sequential mixed-integer quadratically constrained quadratic programming approach. Specifically, we sequentially solve a mixed integer quadratic program with quadratic constraints (MIQCQP), taking advantage of the MIQCQP routines of the commercial solver CPLEX [13]. This MIQCQP is obtained from linearized version of the constraint (4.13g) and a second-order convex approximation of the cost function (4.13a).

It should be mentioned that we proposed this sequential mixed-integer quadratically constraint program as pragmatic and easily implementable approach to assess the benefits of the optimal control problem formulation discussed in this chapter. Although we are unable to provide more insight about its convergence properties, we observed an stable behavior for the extensive numerical simulations we performed, i.e., (at least locally) an optimal solution was always obtained.

4.3. Simulation Study

In this section, several simulations are reported in order to show the benefits of relying the energy optimal coordinated strategy proposed in this chapter. First, we compare how uncoordinated human-driven vehicles (HDVs) and coordinated AVs resolve intersection conflicts and show the benefits in terms of energy and time savings. Subsequently, a comparison between different intersections configurations is made in order to present additional remarks on the proposed control problem studied in this chapter.

4.3.1. Coordinated AVs strategies versus uncoordinated HDVs

In order to show the benefits that coordinated strategies for AVs can exhibit in terms of energy savings and reduced travel time, a comparison has been made between two equal intersection scenarios, one considering coordinated AVs and the other with HDVs. For this analysis, we consider a four-way intersection scenario where vehicles follow V_l predefined trajectories a_l with $l \in \{1,...,4\}$ to cross the intersection. The trajectories a_l are enumerated considering their starting point in an anti-clockwise manner starting at the left, as depicted in Fig. 4.5. Moreover,

Table 4.1: Additioal energy savings of the coordinated AVs compared to HVDV, time required by all HDVs to cross the intersection and coordinated AVs crossing order

Cases	Additional energy savings for AVs $[\%]$	Required crossing time for HDVs $[s]$	AVs intersection crossing order
1	6.6	27.4	$V_4 - V_1 - V_2$
2	16.2	29.7	$V_1 - V_4 - V_2$
3	11.2	23.6	$V_4 - V_1 - V_2$
4	10.8	23.6	$V_1 - V_4 - V_2$
5	14.4	22.6	$V_4 - V_2 - V_1$

in order to indicate the trajectory of each vehicle, as seen in Fig. 4.5, for each $l \in \{1, ..., 4\}$ we have

$$a_l = \begin{cases} 0 & \text{if there is no vehicle entering,} \\ 1 & \text{if a vehicle aims to cross the intersection in a straigth trajectory,} \\ 2 & \text{if the vehicle plans a left turn,} \\ 3 & \text{if the vehicle plans a right turn,} \end{cases} \tag{4.14}$$

such that the Intersection Scenario (I_s) is defined as the vector $I_s = [a_1, a_2, a_3, a_4]$.

The intersection scenario $I_s = [1, 2, 0, 1]$ depicted in Fig. 4.6 (bottom-left corner) is considered for this analysis, where we study 5 cases with different initial and final conditions for the involved vehicles. All the cases of this scenario are solved for both the coordinated AVs and for he HDVs. For the HDVs, the crossing order is predefined by traffic laws. For instance, the road code (in Europe) defines that in the event of potential trajectory intersection between vehicles right of way priority is applied, i.e., the vehicles whose right side is free can enter the intersection, and at most one vehicle at a time can reside in the intersection. Therefore, for the considered intersection the scenario I_s, the vehicles V_1 and V_4 need to stop before the intersection while vehicle V_2 crosses first. Later, the vehicle V_1 crosses followed by vehicle V_4. For the sake of simplicity, describe the intersection crossing order for HDVs is as $V_2 - V_1 - V_4$. It should be mentioned that velocity profiles for the turning V_2, which does not stop at the intersection, was defined using a third order polynomial model proposed in [14]. This model provides stochastic speed profiles of free-flowing left and right turning vehicles. On the other hand, for the HDVs V_1 and V_4 that follow a straight trajectories with a stop before the intersection, the acceleration and deceleration profiles are described a a quadratic and an exponential functions, respectively. These descriptions are obtained from the models proposed in [15, Table 6].

Table 4.1 summarizes the results of the comparison between AVs and HDVs for the proposed I_s with the different initial and final condition cases. This table presents the additional energy savings obtained by the coordinated AVs with respect to to the HDVs, total time time required by the HDVs to cross the intersection

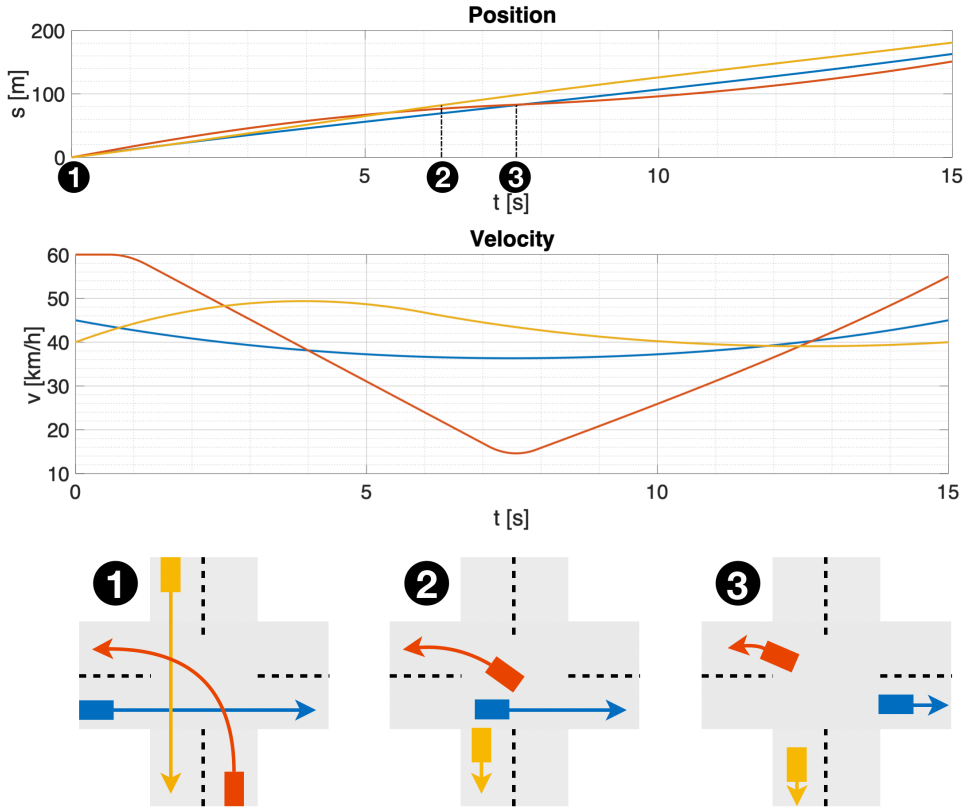

Figure 4.6: Position, velocity profiles & order resolution of $I_S = [1, 2, 0, 1]$

and cover their trajectories, and the coordinated crossing order of the coordinated AVs. The results show that the energy savings achieved by the coordinated AVs can be up to 16.2% more than the HDVs. Moreover, note that, contrary to the HDVs, the crossing order of the AVs is not predetermined and changes from case to case. Since crossing order for HDVs is pre-defined by the traffic rules, it often leads to inefficient solutions in terms of time and energy consumption. This results highlights the role of coordination to achieve a reduced energy consumption in the intersection. Table 4.1 also shows the time required in the different cases from the HDVs to reach the respective final destinations. Note that for the coordinated AVs this time is fixed a priori, which for this analysis has been chosen as $15[s]$. As we can observe, AVs can be approximately be up to 2 times faster than HDVs resolving the crossing conflict, which shows the advantage of using coordinated strategies to reduce the waiting times at intersections.

Table 4.2: Total energy consumption, computational time and number of iterations for Different Intersection scenarios (I_s)

I_s	Energy consumption $[MW]$	Computational time $[s]$	Number of iterations
$[3,0,0,0]$	5.26	1.52	5
$[1,1,0,0]$	7.07	5.56	3
$[1,2,0,0]$	7.91	15.8	6
$[2,2,0,0]$	9.64	94.01	33
$[1,0,0,2]$	8.71	15.4	2
$[1,0,0,3]$	8.95	10.24	5
$[1,1,0,2]$	11.6	176.59	6
$[1,2,0,1]$	10.8	19.71	7
$[1,1,1,1]$	14.3	24.3	5

4.3.2. Mutiple scenarios for Coordinated AVs

In this section, we discuss the differences between multiple scenarios where coordinated AVs are crossing an intersection. We will make emphasis in the features of the optimal velocity profiles and priority crossing order obtained for scenarios that differ on the predefined trajectories and the number of AVs approaching the intersection. To do so, let us compare the bottom-left corner of Fig. 4.6 with the bottom-left corner of Fig. 4.7. As can be seen, in both scenarios two vehicles follow a straight trajectory while a third one makes a left turn. However, the vehicles arrival directions are different. The initial and final conditions for vehicles coming from the same direction are equal. As can be noticed comparing the position plots between the two cases (Fig. 4.6-4.7 top), the distances covered from the vehicles vary in order to obtain the optimal solution for the different cases. Moreover, it can be noticed that even though the vehicles are coming from the same direction in both cases, the different trajectories affect the intersection resolution order in the two scenarios (Fig. 4.6-4.7 bottom). It should be mentioned that even though the two scenarios are similar to each other, the computational time differs significantly. Solving the scenario depicted in in Fig. 4.6 takes approximately $20[s]$, while fot the case in Fig. 4.7 the required computational time is $120[s]$. This difference in the computational performance is explained by higher complexity of of the last case, where rear-end collision avoidance constraints are considered in the optimal control problem formulation.

To be more specific, note that (4.13) is solved as a sequential mixed-integer quadratically constrained program, in which successive quadratic approximations of the nonlinear mixed-integer programs are solved. In the case of Fig. 4.6, the quadratic constraint (4.13i) is inactive, while for Fig. 4.7, the quadratic constraint (4.13i) is active between vehicle V_4 and V_1 since they aim to proceed towards the same direction. This leads to a significantly higher computational complexity. Lastly, in order to give a deeper understanding on how the solutions will change

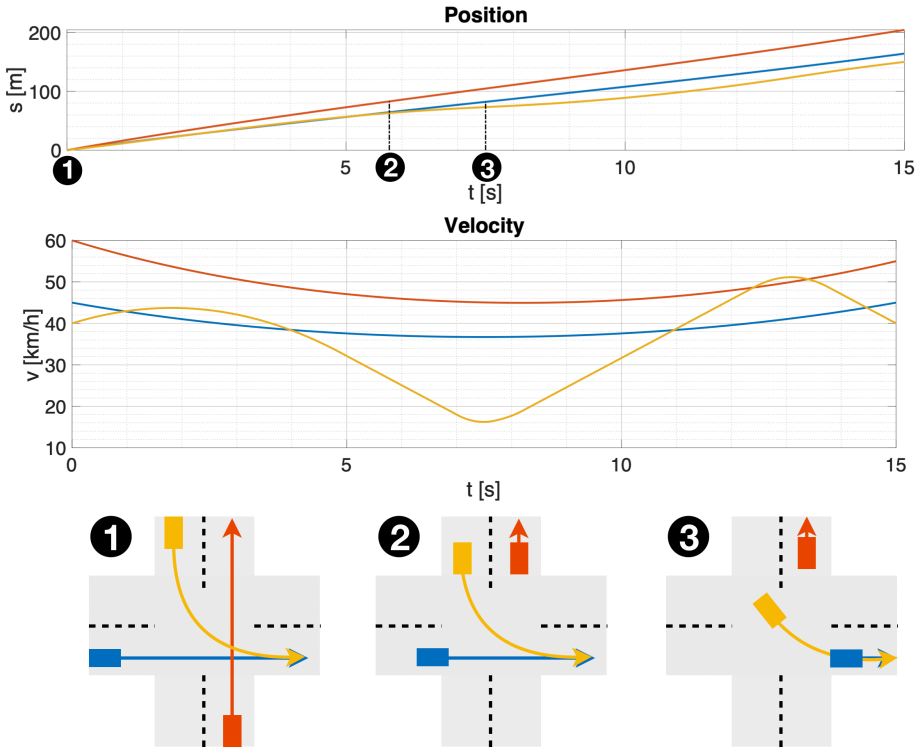

Figure 4.7: Position, velocity profiles & order resolution of $I_S = [1, 1, 0, 2]$

depending on the scenarios and the differences in computational performance, Table 4.2 reports the total energy consumption of the vehicles crossing the intersection, the time required to compute the solution and the number of iterations to achieve convergence for different intersection scenarios (I_s) defined accordingly to Fig. 4.5 as previously explained.

4.4. Conclusions

In this chapter, we have proposed and optimal control problem formulation to find energy optimal coordination strategies for AVs crossing an intersection. The proposed optimal control problem has been obtained as an extension of the eco-driving problem presented in Chapter 2 and Chapter 3 to consider multiple vehicles crossing an intersection. For each vehicle, the proposed formulation, aims to obtain the velocity profiles and the priority crossing order that minimize the aggregated energy consumption subject to safety constraints. The combinatorial nature of the energy optimal conflict resolution problem has been handled using a sequential mixed integer program. Simulation results have shown that coordinated autonomous vehicles can reduce energy consumption to approximately 16.2% compared to human driven vehicles with lack of coordination.

References

[1] G. Xu, C. Zheng, Y. Zhang, K. Xu, and J. Liang, *Energy Efficiency of Electric Vehicles – Energy Saving and Optimal Control Technologies* (IntechOpen, 2015).

[2] A. Grauers, S. Sarasini, and M. Karlstrom, *Why electromobility and what is it?* in *Sytems Perspective on Electromobility* (Chalmers University of Technology, 2012).

[3] T. Litman, *Autonomous Vehicle Implementation Predictions: Implications for Transport Planning* (Victoria transport institute, 2019).

[4] L. Tate, S. Hochgreb, J. Hall, and M. Bassett, *Energy efficiency of autonomous car powertrain,* SAE International (2018).

[5] G. R. Campos, P. Falcone, and J. Sjoberg, *Traffic safety at intersections: a priority based approach for cooperative collision avoidance,* in *Proc. International Symp Future Active Safety Technology* (2015).

[6] A. Colombo and D. D. Vecchio, *Least restrictive supervisors for intersection collision avoidance: A scheduling approach,* IEEE Trans Autom Control (2015).

[7] G. R. de Campos, P. Falcone, H. Wymeersch, R. Hult, and J. Sjoberg, *Cooperative receading horizon conflict resolution at traffic intersections,* in *Proc. Conference Decision and Control* (2014).

[8] G. R. de Campos, P. Falcone, and H. Wymeersch, *An approximate solution to the optimal coordination problem for autonomousvehicles at intersections,* in *Proc. American Control Conference* (2015).

[9] Y. J. Zhang, A. A. Malikopoulos, , and C. G. Cassandras, *Optimal control and coordination of connected and automated vehicles at urban traffic intersections,* in *Proc. American Control Conference* (2016).

[10] R. Hult, M. Zanon, S. Gros, and P. Falcone, *Energy-optimal coordination of autonomous vehicles at intersections,* in *Proc. European Control Conference* (2018).

[11] R. Rajamani, *Vehicle Dynamics and Control* (Springer, 2012).

[12] O. Exler and K. Schittkowski, *A trust region SQP algorithm for mixed-integer nonlinear programming,* (2007).

[13] *ILOG CPLEX optimization studio, MIQCP: mixed integer programs with quadratic terms in the constraints,* (2020).

[14] A. Wolfermann, W. K. Alhajyaseen, and H. Nakamura, *Modeling speed profiles of turning vehicles at signalized intersections,* in *Proc. International Conference on Road Safety and Simulation* (2011).

[15] A. K. Maurya and P. S. Bokare, *Acceleration-deceleration behavious of various vehicle types,* in *Proc. World Conference on Transport Research* (2016).

II

CVEM and Eco-driving

5

Global Solutions to the Complete Vehicle Energy Management Problem via Primal-Dual Operator Splitting

Complete Vehicle energy Management (CVEM) aims to minimize the energy consumption of all subsystems in a vehicle. We consider the case where the subsystems consist of energy buffers with linear dynamics and/or energy converters with quadratic power losses. In this chapter, we show the existence of only global solutions for the CVEM OCP and propose a reformulation of this problem such that it can be decomposed in terms of components and time intervals, so that it can be solved using a Primal Dual Proximal splitting algorithm for non-convex optimization problems. Moreover, we propose the use of a spectral method to automatically select the step-sizes of the distributed optimization algorithm at every iteration. It is shown that the regularization properties of this algorithm allow solving CVEM cases that were difficult using other approaches as dual decomposition. Finally, we present a case study for a parallel-hybrid vehicle where we illustrate the features of our method and highlight its numerical performance.

Parts of this chapter have been published in **P.5** and **S.1**.

The automotive industry has been largely involved in research that aims at finding efficient operation through a coordinated split of power flows among the powertrain components to provide the required power to the wheels, i.e., energy management strategies. Besides the energy savings, energy management strategies can bring additional advantages. For instance, for hybrid vehicles, an energy efficiency operation leads to lower emissions, while the main motivation to improve efficiency of electric vehicles is that it will extend the range of the vehicle and thereby mitigating range anxiety and enabling acceptance of electrified vehicles by the users [1], [2]. An energy management strategy (EMS) is the solution to an optimal control problem (OCP), for which, modelling frameworks and solution methods have been studied in [3–6]. As discussed in Chapter 1, a recent trend in this research area is to consider all the energy consumers inside the vehicle and this concept is known as Complete Vehicle Energy Management (CVEM) [7]. CVEM requires the OCP to be scalable, as it requires a larger number of subsystems to be connected to the power network compared to earlier solutions for EMS.

The difficulties that appear as a consequence of using classic EMS methods to solve the CVEM problem have been mentioned in [7]. For instance, dynamic programming can provide global optimal solutions to CVEM problems. However, scalability becomes an issue due to the "curse of dimensionality" inherent to dynamic programming. Similarly, state constraints, which are normally present in the CVEM problem, make Pontryagin's maximum principle approaches difficult to be used for this application. As a consequence, static optimization techniques have emerged as tractable approaches to tackle the CVEM problem, see, e.g., [8, 9]. In particular, [10] has incorporated the control of auxiliary systems into the EMS and [11] has used convex relaxations to guarantee optimality of the solution. However, due to the use of centralized optimization methods, those approaches are not flexible in the sense that subsystems cannot be easily added or removed. Similarly, [12, 13] uses convex formulations that consider non-linear losses to study in detail the numerical performance of the static optimization algorithms used in predictive control for energy management strategies. In [12], a solver based on alternating direction method of multipliers (ADMM) is used to solve energy management problems with horizons up to 1000 time steps. Remarkably, the solution times obtained are 3 orders of magnitude less than the commercial solvers used as benchmark. An extension to this ADMM solver is presented in [14] to solve energy management problems that consider on/off engine decisions. The research presented in [15] uses a game-theoretic approach to solve the CVEM problems in a decentralized manner, where all the subsystems share a limited amount of information and are able to take some decisions autonomously. Unfortunately, global optimality of the centralized OCP is not guaranteed in this case.

A static distributed optimization approach for CVEM is presented in [16, 17]. The method proposed in these papers are scalable and flexible. The main idea is to use dual decomposition to split the original OCP into several simpler problems related to interconnected subsystems. As a result, the computation time is drastically reduced and adding and/or removing subsystems becomes easy. However,

several open questions exist related to numerical aspects of the algorithms proposed to solve the distributed optimization problem. For instance, [16] proposes a second-order dual update for which the convergence of the algorithm has not been formally proven. Additionally, the approach requires the introduction of the concept of "sum of losses" to describe separable optimal control problems that are suitable for dual decomposition. Unfortunately, this artifact can be difficult to adapt to some configurations of the CVEM OCP. In [16], the subsystems are described with linear dynamics and quadratic energy conversion models. In cases where some of the components present an energy conversion model is almost linear, the distributed optimization approaches become ill conditioned, causing the algorithm to have difficulties to converge.

In [18], we have presented an alternative version of this work, where we proposed a static optimization algorithm based on Forward-Backward splitting methods. In this contribution, we claimed the existence of only global solutions to the CVEM problem, however, we did not formally prove this important result. Additionally, the proposed methodology allows only parallelization of the optimization problem in terms of the subsystems considered in the power network, which limits the scalability of the optimization problem when large time horizon lengths are considered in the formulation.

In this chapter, we design an efficient algorithm with convergence guarantee for the CVEM problem, based on the Primal Dual (PD) Proximal operator splitting method [19]. We show that the non-convex CVEM problem only has global optimal solutions. Then, by taking advantage of the globality of the solutions, we apply the PD splitting method to the CVEM problem to obtain a distributed static optimization algorithm. The convergence of the proposed algorithm relies on a recent result on non-convex optimization problems [19]. Remarkably, the method we propose introduces regularization that prevents ill-conditioning of the optimization problem. This means that convergence is possible even if linear models and quadratic models are mixed to describe the power consumption of the vehicle subsystems. We also extend the parallelization capabilities of this method by introducing the possibility to split the time horizon into several time intervals. Breaking the complexity of the problem allow us to find global optimal solutions for large scale CVEM problems. Finally, we use spectral methods [20] to propose an adaptive step-size selection approach for the optimization algorithm that drastically simplifies its implementation.

The chapter is organized as follows. In Section 5.1, we present the general CVEM problem as a non-convex OCP, and we show that it has only global solutions. Additionally, the CVEM problem is cast into a numerically well-behaved formulation that is suitable for splitting in terms of components and time intervals. In Section 5.2, we reformulate the optimization problem as a saddle-point problem, whose solution can be written as finding the zero of a certain set-valued operator. Consequently, a Primal-Dual splitting method is used to design a distributed optimization algorithm with adaptive step-size selection. In Section 5.3, we illustrate the algorithm on a case study for a parallel-hybrid vehicle to highlight the features of our method. Finally, we draw conclusions in Section 5.4.

Nomenclature

$\mathbb{R}$ denotes the set of real numbers, $\mathbb{R}_+$ the set of non-negative real numbers, and $\overline{\mathbb{R}} := \mathbb{R} \cup \{+\infty\}$ the set of extended real numbers. For $a, b \in \mathbb{R}$, a significant strict inequality that is denoted by $a \ll b$ implies that a is much less than b. The matrices $\mathbf{0}$ and $\mathbf{1}$ denote matrices with all elements equal to 0 and 1, respectively, and the matrix $\mathbf{I}$ denotes the identity matrix. To improve clarity, we sometimes add the dimension of these matrices as subscript. Furthermore, $\mathrm{diag}(A_1, \cdots, A_N)$ denotes a block-diagonal matrix with matrices $A_1, \cdots, A_N$ on the diagonal. Given N vectors $x_1, \ldots, x_N \in \mathbb{R}^n$, we denote $\mathrm{col}(\{x_i\}_{i\in\{1,\ldots,N\}}) = [x_1^\mathsf{T}, \ldots, x_N^\mathsf{T}]^\mathsf{T}$. The short hand notation $\{x_{p,q}\}$ is used to denote $\{x_{p,q}\}_{p\in\mathcal{P},q\in\mathcal{Q}}$.

Given a set $\mathcal{S} \subseteq \mathbb{R}^n$, the mapping $\iota_S : \mathbb{R}^n \to \{0, +\infty\}$ denotes the indicator function satisfying $\iota_S(x) = 0$ if $x \in S$ and $\iota_S(x) = \infty$ if $x \notin S$, and set-valued mapping $\mathrm{N}_S : \mathbb{R}^n \rightrightarrows \mathbb{R}^n$ denotes the normal cone operator satisfying $\mathrm{N}_S(x) = \{v \in \mathbb{R}^n \mid \sup_{z\in S} v^\mathsf{T}(z - x) \leq 0\}$ if $x \in S$ and $\mathrm{N}_S(x) = \emptyset$ if $x \notin S$. The mapping $\mathrm{proj}_S : \mathbb{R}^n \to S$ for a closed set $S \subseteq \mathbb{R}^n$ denotes the projection onto S, i.e., $\mathrm{proj}_S(x) = \mathrm{argmin}_{y\in S} \|y - x\|^2$, where $\|\cdot\|$ is the usual euclidean norm in $\mathbb{R}^n$.

For a function $\psi : \mathbb{R}^n \to \overline{\mathbb{R}}$ with $\mathrm{dom}(\psi) := \{x \in \mathbb{R}^n \mid \psi(x) < \infty\}$, the subdifferential set-valued mapping $\partial\psi : \mathrm{dom}(\psi) \rightrightarrows \mathbb{R}^n$ is defined as $\partial\psi(x) := \{v \in \mathbb{R}^n \mid \psi(z) \geq \psi(x) + v^\mathsf{T}(z - x)$ for all $z \in \mathrm{dom}(\psi)\}$. In case ψ is continuously differentiable, the subgradient is equal to its gradient, i.e., $\partial\psi(x) = \nabla\psi(x)$.

5.1. CVEM as Optimal Control Problem

In this section, we first discuss a mathematical description of a power network model for CVEM. Later, we will formulate the discrete-time OCP for CVEM, which will turn out to be non-convex, and we will show that all the solutions to this non-convex OCP are global optimal solutions. Finally, we will propose convenient equivalent formulations of the problem that will be exploited in Section 5.2 to find an optimization algorithm based on operator splitting techniques.

5.1.1. Power Network Model for CVEM

The CVEM problem aims to minimize the energy consumption for a network of subsystems $m \in \mathcal{M} := \{1, \ldots, M\}$, where M is the total number of subsystems. These subsystems are composed of a combination of an energy converter, possibly with an energy buffer. For instance, considering a battery, the capacity of storing energy is modeled as an energy buffer, while the power losses produced during the transformation of chemical energy into electrical energy in the battery are represented by an energy converter.

A power network for CVEM is schematically depicted in Fig. 5.1. We assume that the network topology is such that the energy buffers are always connected to energy converters by the power input $u_{m,k}$. Furthermore, the converters are connected to each other according to a specific topology via the network nodes $j \in \mathcal{J} := \{1, \ldots, J\}$, where J is the total number of nodes in the network. In this case, power outputs $y_{m,k}$ and inputs $u_{m,k}$ of the converters could be directly connected to a network node. Every node $j \in \mathcal{J}$ can have a known exogenous load signal $v_{j,k}$

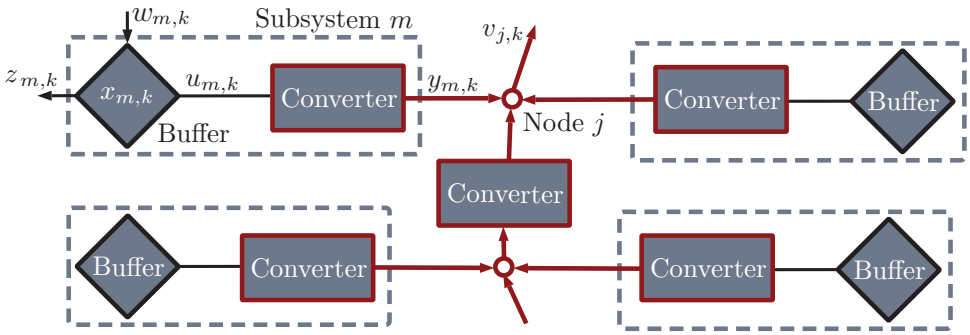

Figure 5.1: Power network for CVEM.

given for each time instant k.

Note that, the power network has a tree structure topology, which means that every subsystem is connected to only one node, and two consecutive nodes are always bridged by an individual power converter. Moreover, only converters can be connected directly to a network node. These simple principles observed in in Fig. 5.1 are the fundamental blocks that can be found in more complicated network topologies. A formal description of these ideas are presented in the following section as part of the modelling and OCP formulation proposed in this chapter.

5

5.1.2. Optimal Control Problem

The CVEM problem is an OCP that aims to minimize the total aggregated energy consumption of the components over a time horizon $\mathcal{K} := \{0, 1, \dots, K-1\}$, while considering the interaction of all the components interconnected in the power network. Thus, the OCP is given by

$$\min_{\{y_{m,k}, u_{m,k}, x_{m,k}, z_{m,k}\}} \sum_{k \in \mathcal{K}} \sum_{m \in \mathcal{M}} a_m y_{m,k} + b_m u_{m,k}, \tag{5.1a}$$

where for every subsystem $m \in \mathcal{M}$ the (scalar) outputs of the converter are denoted as $y_{m,k} \in \mathbb{R}$, $u_{m,k} \in \mathbb{R}$ are the (scalar) inputs, $x_{m,k} \in \mathbb{R}^{n_{xm}}$ are the states and $z_{m,k} \in \mathbb{R}^{n_{zm}}$ are the outputs of the energy buffer, while $a_m \in \mathbb{R}_+$ and $b_m \in \mathbb{R}$ are coefficients to define the cost function. A typical objective in CVEM is to minimize the fuel consumption, in which case assume the subsystem $m = 1$ corresponds to the combustion engine and $u_{1,k}$ denotes the chemical fuel power flow at time $k \in \mathcal{K}$. In this case, only $b_1 = 1$, while all other a_m and b_m are zero.

The cost function in (5.1a) is to be minimized subject to a quadratic equality constraint that describes the input-output behavior of each converter, i.e.,

$$y_{m,k} = \tfrac{1}{2} q_{2,m} u_{m,k}^2 + q_{1,m} u_{m,k} + q_{0,m}, \tag{5.1b}$$

where $q_{0,m} \in \mathbb{R}$, $q_{1,m} \in \mathbb{R}$ and (positive) $q_{2,m} \in \mathbb{R}_+$ are efficiency coefficients of the

converter $m \in \mathcal{M}$, and subject to the linear system dynamics of the energy buffer

$$x_{m,k+1} = A_m x_{m,k} + B_m u_{m,k} + E w_{m,k}, \tag{5.1c}$$
$$z_{m,k} = C_m x_{m,k} + D_m u_{m,k} + F w_{m,k}, \tag{5.1d}$$

that needs to hold for all $k \in \mathcal{K}$ and for all $m \in \mathcal{M}$, with appropriate matrices. In (5.1c) and (5.1d), $w_{m,k} \in \mathbb{R}^{n_{wm}}$ are known state and output disturbances for the energy buffer. Moreover, the initial state $x_{m,0}$ of the storage device is assumed to be given and its inputs and outputs are subject to

$$\underline{u}_m \leq u_{m,k} \leq \overline{u}_m, \tag{5.1e}$$
$$\underline{z}_m \leq z_{m,k} \leq \overline{z}_m, \tag{5.1f}$$

where for all $m \in \mathcal{M}$ the given input and output bounds are respectively $\underline{u}_m, \overline{u}_m \in \mathbb{R}$ and $\underline{z}_m, \overline{z}_m \in \mathbb{R}^{n_{zm}}$. Note that the inequalities in (5.1e) and (5.1f) are interpreted elementwise. In [16], it has been shown that quadratic static models for energy converters and linear dynamical models for buffers are an adequate approximation to describe typical components in CVEM.

The interaction between the subsystems in the power network is given by the power balance at each node $j \in \mathcal{J}$. We distinguish between energy conserving nodes, given by

$$\sum_{m \in \mathcal{M}} c_{j,m} y_{m,k} + d_{j,m} u_{m,k} + v_{j,k} = 0, \tag{5.1g}$$

for $j \in \mathcal{J}_c = \{1, 2, \ldots, J_c\}$ and energy dissipating nodes

$$\sum_{m \in \mathcal{M}} c_{j,m} y_{m,k} + d_{j,m} u_{m,k} + v_{j,k} \leq 0, \tag{5.1h}$$

for $j \in \mathcal{J}_d = \{J_c + 1, J_c + 2, \ldots, J\}$. Here, $\mathcal{J}_c \cap \mathcal{J}_d = \varnothing$ and $\mathcal{J}_c \cup \mathcal{J}_d = \mathcal{J}$. In these expressions, $c_{j,m}$ is 1 if the correspondent power signal $y_{m,k}$ is connected to the node j and 0 otherwise. The constant $d_{j,m}$ is -1 if the respective power signal $u_{m,k}$, flows into node j,it is 1 if the power flows out of node j, and 0 if the respective signal is not connected to the node. It should be noted that dissipating nodes (5.1h) exist, e.g., because mechanical braking can be modeled as a power dissipation in a node. Finally, the following assumption on the network topology is considered in this chapter.

Assumption 5.1.1. *For all the nodes $j \in \mathcal{J}$, the tree structure topology of the power network satisfies the following conditions:*

(A1) For all $m \in \mathcal{M}$, $c_{j,m} = 1$ implies $d_{j,m} = 0$ for the same $j \in \mathcal{J}$.

(A2) For all $m \in \mathcal{M}$, $d_{j,m} \in \{-1, 1\}$ implies $c_{j,m} = 0$ for the same $j \in \mathcal{J}$.

(A3) For at least one $m \in \mathcal{M}$, $c_{j,m} = 1$. □

This assumption formalizes the main features of the power network described in the previous section, i.e, every subsystem is connected to only one node, two consecutive nodes are always bridged by an individual power converter, and only converters are connected directly to a network node. Moreover, Assumption 5.1.1 implies that the network topology can represented by a full row rank matrix, this is an important implication that will will be discussed in Section 5.1.5.

5.1.3. Global Solutions to the Nonconvex CVEM Problem

The OCP (5.1) is non-convex due to (5.1b). This might cause that solvers get stuck in a local minimum. In this section, we show that all (local) solutions to (5.1) are global solutions under very mild conditions.

To show this, we relax the equality constraint (5.1b) to an inequality constraint, i.e.,

$$\tfrac{1}{2}q_{2,m}u_{m,k}^2 + q_{1,m}u_{m,k} + q_{0,m} - y_{m,k} \leq 0 \tag{5.1b'}$$

for $m \in \mathcal{M}$ and $k \in \mathcal{K}$, allowing us to define a relaxed OCP

$$\begin{aligned} \min_{\{y_{m,k},u_{m,k},x_{m,k},z_{m,k}\}} \quad & \textstyle\sum_{k\in\mathcal{K}} \sum_{m\in\mathcal{M}} a_m y_{m,k} + b_m u_{m,k} \\ \text{s.t.} \quad & (5.1b'), (5.1c)–(5.1h). \end{aligned} \tag{5.2}$$

The discrete-time OCP (5.2) is convex, thus every locally minimal solution to (5.2) is globally minimal. The optimal value of the original problem (5.1) and of the convex relaxation (5.2) satisfies

$$p^{CR} \leq p^{NC}, \tag{5.3}$$

where p^{CR} and p^{NC} denote the optimal value of the convex relaxation (5.2) and the non-convex OCP (5.1) respectively, because the convex relaxation has a larger feasible set due to (5.1b').

The next theorem shows that for this particular OCP and its relaxation, it holds that, $p^{\text{CR}} = p^{\text{NC}}$ and that (5.2) always has a solution that satisfies (5.1b') with equality, thus it satisfies (5.1b) and solves (5.1).

Theorem 5.1.1. *Assume that the bounds $\underline{u}_m$, $\overline{u}_m$, $\underline{z}_m$ and $\overline{z}$ for all $m \in \mathcal{M}$ are finite and that there exists at least one feasible point $\{u_{m,k}, z_{m,k}, x_{m,k}, y_{m,k}\}$ for (5.2) with strict inequalities (5.1b'), (5.1e) and (5.1f). Then, an optimal solution to (5.2) exists that satisfies (5.1b') with equality, $p^{CR} = p^{NC}$, and (5.1) only has global optimal solutions.*

Proof. The fact that the bounds $\underline{u}_m$ and $\overline{u}_m$ are finite for all $m \in \mathcal{M}$ means that the optimal solution to the convex relaxation is finite, while a feasible point exists for (5.2) with strict inequalities (5.1b') and (5.1e), means that strong duality holds (due to Slater's constraint qualification [21, §5.2.3]).

We will now use strong duality to show that (5.2) always has a solution that satisfies (5.1b') with equality. The dual problem of (5.2) is given by

$$\begin{aligned} \max_{\{\kappa_{m,k},\mu_{m,k}\}} \min_{\{\omega_{m,k}\}} & \sum_{k\in\mathcal{K}} \sum_{m\in\mathcal{M}} L_{m.k}(\omega_{m,k}, \kappa_{m,k}) + \sum_{j\in\mathcal{J}} \mu_{j,k}(c_{j,m}y_{m,k} + d_{j,m}u_{m,k} + v_{j,k}) \\ & + \iota_{\Omega}(\{\omega_{m,k}\}, \{\kappa_{m,k}\}, \{\mu_{j,k}\}), \end{aligned} \tag{5.4}$$

with $\omega_{m,k} = \mathrm{col}(u_{m,k}, x_{m,k}, z_{m,k})$ and

$$L_{m,k}(\omega, \kappa) = a_m y + b_m u + \kappa(q_{2,m}u^2 + q_{1,m}u + q_{0,m} - y). \tag{5.5}$$

In (5.4), ι_Ω is the indicator function of the set

$$\Omega := \{\{\omega_{m,k}\}, \{\kappa_{m,k}\}, \{\mu_{j,k}\} \mid (5.1c)\text{-}(5.1f),\ \kappa_{m,k} \geq 0 \text{ and } \mu_{j,k} \geq 0 \text{ are satisfied } \forall\ m \in \mathcal{M}\ \forall\ j \in \mathcal{J}_d\}. \tag{5.6}$$

The stationary conditions with respect to $y_{m,k}$ (one of the necessary conditions for optimality) are given by

$$a_m - \kappa_{m,k} + \sum_{j \in \mathcal{J}} \mu_{j,k} c_{j,m} = 0. \tag{5.7}$$

Substituting (5.7) into (5.5) yields that $y_{m,k}$ disappears for the Lagrangian function in (5.4). Therefore, any $y_{m,k}$ satisfying (5.1b') leads to the same optimal value, meaning that $y_{m,k}$ can be freely chosen so that (5.1b') is satisfied with equality. Since the relaxed OCP (5.2) only has global solutions, and some of the global optimal solutions are feasible for (5.1), we have that $p^{CR} = p^{NC}$ and (5.1) only has global optimal solutions. □

5.1.4. An Equivalent Formulation of the CVEM OPC

In this subsection, we will reformulate the OCP (5.1) into an equivalent form. This new formulation introduces a set of useful features that will be later exploited by the optimization algorithm presented in Section 5.2. The reformulation of (5.1) considers five main steps that are described and justified as follows:

1. Substitution of the quadratic equality constraint (5.1b) into (5.1a), (5.1g), (5.1h). This substitution aims to reduce the number of decision variables by the elimination of $y_{m,k}$ from the OCP.

2. Conversion of the inequality constraint (5.1h) into an equality constraint using slack variables $s_{j,k}$, with $j \in \mathcal{J}$ and $k \in \mathcal{K}$, of which some are constrained to zero. This allows for a unified treatment of (5.1g) and (5.1h) in the form of (5.8e), where (5.1g) is satisfied due to (5.8f). This simplifies formulation of the algorithm that will be proposed in Section 5.2.

3. Introduction of quadratic penalty terms associated to the equality constraints (5.1g) and (5.1h). This is done without removing these constraints. The resulting Lagrangian function of the OCP can be seen as an augmented Lagrangian function. The advantage of this formulation is that it introduces regularization to the optimization procedure, thereby improving the convergence properties of the algorithm [22, §3.2.1, §4.2].

4. Splitting of the time horizon to provide additional degrees of freedom to the distributed optimization algorithm proposed in Section 5.2. To this end, the horizon $\mathcal{K}$ is divided into L time intervals $\mathcal{K}_\ell := \{K_{\ell-1}, \dots, K_\ell - 1\}$ for all $\ell \in \mathcal{L} := \{1, \dots, L\}$, with $K_0 = 0$ and $K_L = K$. This yields that $\mathcal{K} = \bigcup_{\ell \in \mathcal{L}} \mathcal{K}_\ell$. To arrive at a separable OPC, we introduce the auxiliary variables $\widetilde{x}_{m,K_{\ell-1}}$ that allows rewriting (5.1c) as (5.8b) and (5.8c). The auxiliary variable $\widetilde{x}_{m,K_{\ell-1}}$ is both the initial condition for the interval $\mathcal{K}_\ell$ and the final condition of the previous interval, i.e., (5.8d). Also, (5.8d) is added to the cost function (5.8a) as a quadratic penalty.

5. Introduction of a vanishing penalty $\nu_{\ell,m}(\cdot) \in \mathbb{R}$ that appears in response to the existence of multiple global solutions in the OCP. This additional term in the cost function aims to guide the optimization algorithm to a region where an optimal solution with desired features might exists. The penalty term is non-permanent and it will be chosen so that vanishes after some iterations of the algorithm, which implies that the solutions of the original OCP are not modified.

The equivalent OCP obtained as a result of the previous steps is given by

$$\min_{\{u_{m,k}, x_{m,k}, z_{m,k}, s_{j,k}, \widetilde{x}_{m,K_{\ell-1}}\}} \sum_{\ell \in \mathcal{L}} \sum_{k \in \mathcal{K}_\ell} \Bigg(\sum_{m \in \mathcal{M}} \big(p_m(u_{m,k}) + \nu_m(u_{m,k}, x_{m,k}, z_{m,k})\big) + \sum_{j \in \mathcal{J}} \frac{\sigma_j}{2} \Big(\sum_{m \in \mathcal{M}} r_{j,m}(u_{m,k}) + \tfrac{1}{2} s_{j,k}^2 \Big)^2 \Bigg) + \sum_{\ell \in \mathcal{L}} \sum_{m \in \mathcal{M}} \frac{\rho_m}{2} \| x_{m,K_{\ell-1}} - \widetilde{x}_{m,K_{\ell-1}} \|^2 \tag{5.8a}$$

s.t. (5.1d), (5.1e), (5.1f),

$$x_{m,k+1} = A_m x_{m,k} + B_m u_{m,k} + E w_{m,k}, \quad \text{for all } k \in \mathcal{K} \setminus \{K_0, \dots, K_{L-1}\} \text{ and } m \in \mathcal{M}, \tag{5.8b}$$

$$x_{m,K_{\ell-1}+1} = A_m \widetilde{x}_{m,K_{\ell-1}} + B_m u_{m,K_{\ell-1}} + E w_{m,K_{\ell-1}}, \quad \text{for all } \ell \in \mathcal{L} \text{ and } m \in \mathcal{M}, \tag{5.8c}$$

$$x_{m,K_{\ell-1}} - \widetilde{x}_{m,K_{\ell-1}} = 0, \quad \text{for all } \ell \in \mathcal{L} \text{ and } m \in \mathcal{M}, \tag{5.8d}$$

$$\sum_{m \in \mathcal{M}} r_{j,m}(u_{m,k}) + \tfrac{1}{2} s_{j,k}^2 = 0, \quad \text{for all } \ell \in \mathcal{L} \text{ and } j \in \mathcal{J}, \tag{5.8e}$$

$$s_{j,k} = 0, \quad \text{for all } \ell \in \mathcal{L} \text{ and } j \in \mathcal{J}_c; \tag{5.8f}$$

where $\sigma_{\ell,j} \in \mathbb{R}_+$ are coefficients that weight the penalty terms in (5.8a). Furthermore,

$$p_m(u) = a_m\big(\tfrac{1}{2} q_{2,m} u^2 + q_{1,m} u + q_{0,m}\big) + b_m u, \tag{5.9}$$

$$r_{j,m}(u) = c_{j,m}\big(\tfrac{1}{2} q_{2,m} u^2 + q_{1,m} u + q_{0,m}\big) + d_{j,m} u + v_j. \tag{5.10}$$

It should be noted that constraint (5.8f) acts only on the energy conserving nodes $\mathcal{J}_c$, which means that the equality constraint (5.1g) is embedded in (5.8e) for this formulation.

5.1.5. Reformulation as a Static Optimization Problem

n this subsection, we will rewrite the OCP (5.8) into a static optimization problem that is suitable to be solved with the operator splitting technique presented in Section 5.2. To reformulate the OCP (5.8) as a static optimization problem, we define the following vectors

$$\mathbf{u}_{\ell,m} = \operatorname{col}(\{u_{m,k}\}_{k\in\mathcal{K}_\ell}) \in \mathbb{R}^{K_\ell}, \tag{5.11a}$$
$$\mathbf{x}_{\ell,m} = \operatorname{col}(\widetilde{x}_{m,K_{\ell-1}}, \{x_{\ell,m,k+1}\}_{k\in\mathcal{K}_\ell}) \in \mathbb{R}^{(K_\ell+1)n_{xm}}, \tag{5.11b}$$
$$\mathbf{z}_{\ell,m} = \operatorname{col}(\{z_{m,k}\}_{k\in\mathcal{K}_\ell}) \in \mathbb{R}^{K_\ell n_{zm}}, \tag{5.11c}$$
$$\mathbf{w}_{\ell,m} = \operatorname{col}(\{w_{m,k}\}_{k\in\mathcal{K}_\ell}) \in \mathbb{R}^{K_\ell n_{wm}}, \tag{5.11d}$$
$$\mathbf{s}_{\ell,j} = \operatorname{col}(\{s_{j,k}\}_{k\in\mathcal{K}_\ell}) \in \mathbb{R}^{K}, \tag{5.11e}$$
$$\mathbf{v}_{\ell,j} = \operatorname{col}(\{v_{j,k}\}_{k\in\mathcal{K}_\ell}) \in \mathbb{R}^{K}, \tag{5.11f}$$

for all $\ell \in \mathcal{L}$, $m \in \mathcal{M}$ and $j \in \mathcal{J}$. This notation allows us to write (5.8b), (5.8c) and (5.1d) in compact form as

$$\Gamma_{\ell,A_m}\mathbf{x}_{\ell,m} + \Gamma_{\ell,B_m}\mathbf{u}_{\ell,m} + \Gamma_{\ell,E_m}\mathbf{w}_{\ell,m} = \mathbf{0} \tag{5.12a}$$
$$-\mathbf{z}_{\ell,m} + \Gamma_{\ell,C_m}\mathbf{x}_{\ell,m} + \Gamma_{\ell,D_m}\mathbf{u}_{\ell,m} + \Gamma_{\ell,F_m}\mathbf{w}_{\ell,m} = \mathbf{0} \tag{5.12b}$$

with matrices

$$\Gamma_{\ell,A_m} = \begin{bmatrix} A_m & -\mathbf{I}_{n_{xm}} & & \\ & \ddots & \ddots & \\ & & A_m & -\mathbf{I}_{n_{xm}} \end{bmatrix} \in \mathbb{R}^{K_\ell n_{xm}\times(K_\ell+1)n_{xm}}, \tag{5.13a}$$
$$\Gamma_{\ell,B_m} = \mathbf{I}_{K_\ell} \otimes B_m, \tag{5.13b}$$
$$\Gamma_{\ell,E_m} = \mathbf{I}_{K_\ell} \otimes E_m, \tag{5.13c}$$
$$\Gamma_{\ell,C_m} = \begin{bmatrix} \mathbf{I}_{K_\ell} \otimes C_m & \mathbf{0}_{K_\ell n_{zm}\times n_{xm}} \end{bmatrix}, \tag{5.13d}$$
$$\Gamma_{\ell,D_m} = \mathbf{I}_{K_\ell} \otimes D_m, \tag{5.13e}$$
$$\Gamma_{\ell,F_m} = \mathbf{I}_{K_\ell} \otimes F_m. \tag{5.13f}$$

The bounds (5.1e), (5.1f) are rewritten as

$$\mathbf{1}\underline{u}_m \le \mathbf{u}_{\ell,m} \le \mathbf{1}\overline{u}_m, \tag{5.14a}$$
$$\mathbf{1} \otimes \underline{z}_m \le \mathbf{z}_{\ell,m} \le \mathbf{1} \otimes \overline{z}_m, \tag{5.14b}$$

and, for all $m \in \mathcal{M}$, the initial conditions are given by

$$\mathbf{x}_{0,m} = x_{m,0}. \tag{5.15}$$

The linking constraints (5.8d) are given by

$$\Xi^f_{\ell-1,m}\mathbf{x}_{m,\ell-1} - \Xi^o_{\ell,m}\mathbf{x}_{\ell,m} = \mathbf{0}, \tag{5.16}$$

for all $m \in \mathcal{M}$ and $\ell \in \mathcal{L}$, with selection matrices

$$\begin{aligned} \Xi^o_{m,\ell} &= \begin{bmatrix} \mathbf{I}_{n_{xm}} & \mathbf{0}_{n_{xm}\times K_\ell n_{xm}} \end{bmatrix}, \\ \Xi^f_{m,\ell} &= \begin{bmatrix} \mathbf{0}_{n_{xm}\times K_\ell n_{xm}} & \mathbf{I}_{n_{xm}} \end{bmatrix}, \\ \Xi^f_{0,m} &= \mathbf{I}_{n_{xm}}; \end{aligned} \tag{5.17}$$

Note that for the sake of simplicity, we have not considered final state conditions in the OPC formulation (5.1) and consequently in the equivalent formulations. However, note that they can be easily introduced by adding a constraint of the form $\Xi^f_{m,L}\mathbf{x}_{L,m} = x_{m,K}$.

Now, by exploiting (5.11) - (5.14), we rewrite the discrete-time OCP (5.8) as the following static optimization problem

$$\min_{\{\mathbf{u}_{\ell,m},\mathbf{x}_{\ell,m},\mathbf{z}_{\ell,m},\mathbf{s}_{\ell,j}\}} \sum_{\ell\in\mathcal{L}}\Bigg(\sum_{m\in\mathcal{M}}\Big(P_{\ell,m}(\mathbf{u}_{\ell,m}) + \boldsymbol{\nu}_{\ell,m}(\mathbf{u}_{\ell,m},\mathbf{x}_{\ell,m},\mathbf{z}_{\ell,m}) + \tfrac{\rho_{\ell,m}}{2}\|\Xi^f_{\ell-1,m}\mathbf{x}_{\ell-1,m} - \Xi^o_{\ell,m}\mathbf{x}_{\ell,m}\|_2^2\Big) + \sum_{j\in\mathcal{J}_c}\frac{\sigma_{\ell,j}}{2}\Big\|\sum_{m\in\mathcal{M}} R_{\ell,m,j}(\mathbf{u}_{\ell,m}) + \tfrac{1}{2}\mathbf{s}^2_{\ell,j}\Big\|_2^2\Bigg) \tag{5.18a}$$

$$\text{s.t.}\quad \Xi^f_{\ell-1,m}\mathbf{x}_{\ell-1,m} - \Xi^o_{\ell,m}\mathbf{x}_{\ell,m} = \mathbf{0}, \qquad \text{for all } m\in\mathcal{M} \text{ and } \ell\in\mathcal{L}, \tag{5.18b}$$

$$\sum_{m\in\mathcal{M}} R_{\ell,m,j}(\mathbf{u}_{\ell,m}) + \tfrac{1}{2}\mathbf{s}^2_{\ell,j} = \mathbf{0}, \qquad \text{for all } j\in\mathcal{J} \text{ and } \ell\in\mathcal{L}, \tag{5.18c}$$

$$\mathbf{s}_{\ell,j} = \mathbf{0}, \qquad \text{for all } j\in\mathcal{J}_c \text{ and } \ell\in\mathcal{L}, \tag{5.18d}$$

$$\{\mathbf{u}_{\ell,m},\mathbf{x}_{\ell,m},\mathbf{z}_{\ell,m}\}\in\boldsymbol{\Omega}_{\ell,m}, \qquad \text{for all } m\in\mathcal{M} \text{ and } \ell\in\mathcal{L}; \tag{5.18e}$$

where

$$P_{\ell,m}(\mathbf{u}) = \mathbf{1}_K^T(a_m\mathbf{y}_{\ell,m}(\mathbf{u}) + b_m\mathbf{u}), \tag{5.19a}$$

$$R_{\ell,m,j}(\mathbf{u}) = c_{j,m}\boldsymbol{\zeta}_{\ell,m}(\mathbf{u}) + d_{j,m}\mathbf{u} + \mathbf{v}_{\ell,j}, \tag{5.19b}$$

and

$$\boldsymbol{\Omega}_{\ell,m} = \{\{\mathbf{u}_{\ell,m},\mathbf{x}_{\ell,m},\mathbf{z}_{\ell,m}\} \mid \text{satisfy (5.12) and (5.14)}\}, \tag{5.19c}$$

in which

$$\mathbf{y}_{\ell,m}(\mathbf{u}) = \big(\tfrac{1}{2}q_{2,m}\mathrm{diag}(\mathbf{u}) + q_{1,m}\mathbf{1}_{K_\ell}\big)\mathbf{u} + q_{0,m}\mathbf{1}_{K_\ell}. \tag{5.20}$$

This convenient reformulation shows a non-convex static optimization problem that will be used to design a parallelizable algorithm to solve the CVEM problem (5.1), based on the PD operator splitting method [19, Algorithm1.1].To this end, the static optimization problem (5.18) should satisfy some regularity conditions or constraint qualification (CQ). For a complete survey of CQ for non-linear programming see [23, 24]. In the following lemma, we present conditions to guarantee that (5.8) satisfies a linear independence CQ (LICQ) under some mild conditions.

Lemma 5.1.1. *The feasible set of the discrete optimal control problem* (5.8) *satisfies LICQ, if the following conditions hold:*

(I) For all $m\in\mathcal{M}$ *the bounds on* $u_{\ell,m,k}$ *in* (5.1e) *satisfy*

$$\underline{u}_m > -\frac{q_{1,m}}{q_{2,m}} \qquad \text{or} \qquad \overline{u}_m < -\frac{q_{1,m}}{q_{2,m}}. \tag{5.21a}$$

(II) The optimal input powers $u^*_{m,k}$ satisfy

$$\underline{u}_m < u^*_{m,k} < \overline{u}_m, \tag{5.21b}$$

for all $\ell \in \mathcal{L}$, $k \in \mathcal{K}_\ell$ and at least one $m \in \mathcal{M}_j \subseteq \mathcal{M}$, where $\mathcal{M}_j$ is the set of subsystems that interact at the node $j \in \mathcal{J}$.

Proof. We will show that the optimization problem (5.8) satisfies LICQ, if the conditions in the lemma are satisfied. This means that the KKT conditions hold at the critical points of the optimization problem. For this, let us define the vector $\mathbf{u} = \mathrm{col}(\{\mathbf{u}_{\ell,m}\})$ and $\mathbf{x}_0$, $\mathbf{x}$, $\mathbf{z}$, $\mathbf{w}$, $\mathbf{s}$, $\mathbf{v}$ in a similar manner. Additionally, consider the matrix $\mathbf{\Gamma}_A = \mathrm{diag}(\{\Gamma_{\ell,A_m}\})$ and $\mathbf{\Gamma}_B$ to $\mathbf{\Gamma}_F$ in the same way. Furthermore, we define

$$\mathbf{\Theta}_2 = \mathrm{diag}(\{\mathbf{1}_{K_\ell} c_{j,m} q_{2,m}\}), \tag{5.22a}$$
$$\mathbf{\Theta}_1 = \mathrm{diag}(\{\mathbf{1}_{K_\ell} (c_{j,m} q_{1,m} + d_{j,m})\}), \tag{5.22b}$$
$$\mathbf{\Theta}_0 = \mathrm{diag}(\{\mathbf{1}_{K_\ell} c_{j,m} q_{0,m}\}), \tag{5.22c}$$
$$\mathbf{\Xi} = \begin{bmatrix} -\mathbf{\Xi}^o_1 & & & \\ \mathbf{\Xi}^f_1 & -\mathbf{\Xi}^o_2 & & \\ & \ddots & \ddots & \\ & & \mathbf{\Xi}^f_{L-1} & -\mathbf{\Xi}^o_L \end{bmatrix}, \tag{5.22d}$$
$$\mathbf{\Xi_0} = \begin{bmatrix} \mathbf{\Xi}^f_0 \\ \mathbf{0} \end{bmatrix}, \tag{5.22e}$$

with block diagonal matrices $\mathbf{\Xi}^f_\ell = \mathrm{diag}(\{\Xi^f_{\ell,m}\}_{m\in\mathcal{M}})$ and $\mathbf{\Xi}^o_\ell = \mathrm{diag}(\{\Xi^o_{\ell,m}\}_{m\in\mathcal{M}})$. Without loss of generality, for this analysis, we will consider the absence of constraints on the final states. Herewith, the active constraints of the static optimization problem (5.18) can be written as

$$\mathbf{\Gamma}_A\mathbf{x} + \mathbf{\Gamma}_B\mathbf{u} + \mathbf{\Gamma}_E\mathbf{w} = \mathbf{0} \tag{5.23a}$$
$$-\mathbf{Z} + \mathbf{\Gamma}_C\mathbf{x} + \mathbf{\Gamma}_D\mathbf{u} + \mathbf{\Gamma}_F\mathbf{w} = \mathbf{0} \tag{5.23b}$$
$$\mathbf{\Xi}_0\mathbf{x}_0 + \mathbf{\Xi}\mathbf{x} = \mathbf{0} \tag{5.23c}$$
$$\mathbf{x}_0 - \mathrm{col}(\{x_{m,0}\}) = \mathbf{0} \tag{5.23d}$$
$$\tfrac{1}{2}\mathbf{\Theta}_2\mathrm{diag}(\mathbf{u})\mathbf{u} + \mathbf{\Theta}_1\mathbf{u} + \Theta_0 + \tfrac{1}{2}\mathrm{diag}(\mathbf{s})\mathbf{s} + \mathbf{v} = \mathbf{0} \tag{5.23e}$$
$$\overline{\boldsymbol{\phi}}_{\mathbf{u}}\big(\mathbf{u} - \mathrm{col}(\{\mathbf{1}_{K_\ell}\overline{u}_m\})\big) = \mathbf{0} \tag{5.23f}$$
$$\underline{\boldsymbol{\phi}}_{\mathbf{u}}\big(-\mathbf{u} + \mathrm{col}(\{\mathbf{1}_{K_\ell}\underline{u}_m\})\big) = \mathbf{0}, \tag{5.23g}$$
$$\overline{\boldsymbol{\phi}}_{\mathbf{z}}\big(\mathbf{z} - \mathrm{col}(\{\mathbf{1}_{K_\ell} \otimes \overline{z}_m\})\big) = \mathbf{0}, \tag{5.23h}$$
$$\underline{\boldsymbol{\phi}}_{\mathbf{z}}\big(-\mathbf{z} + \mathrm{col}(\{\mathbf{1}_{K_\ell} \otimes \underline{z}_m\})\big) = \mathbf{0}, \tag{5.23i}$$

where the matrices $\overline{\boldsymbol{\phi}}_{\mathbf{u}}$ and $\overline{\boldsymbol{\phi}}_{\mathbf{z}}$ select the active upper bounds, while the active lower bounds are linked to the matrices $\underline{\boldsymbol{\phi}}_{\mathbf{u}}$ and $\underline{\boldsymbol{\phi}}_{\mathbf{z}}$. These matrices have rows with

single non-zero entries to indicate an active constraints. The gradient of (5.23) with respect to decision variables $\{\mathbf{u}, \mathbf{x}_0, \mathbf{x}, \mathbf{z}, \mathbf{s}\}$ reads as

$$\begin{bmatrix} \boldsymbol{\Gamma}_B & \boldsymbol{\Gamma}_A & \mathbf{0} & \mathbf{0} \\ \boldsymbol{\Gamma}_D & \boldsymbol{\Gamma}_C & \mathbf{I} & \mathbf{0} \\ \mathbf{0} & \boldsymbol{\Xi} & \mathbf{0} & \mathbf{0} \\ \boldsymbol{\Theta}_2 \mathrm{diag}(\mathbf{u}) + \boldsymbol{\Theta}_1 & \mathbf{0} & \mathbf{0} & \mathrm{diag}(\mathbf{s}) \\ \overline{\boldsymbol{\phi}}_{\mathbf{u}} & \mathbf{0} & \mathbf{0} & \mathbf{0} \\ -\underline{\boldsymbol{\phi}}_{\mathbf{u}} & \mathbf{0} & \mathbf{0} & \mathbf{0} \\ \mathbf{0} & \mathbf{0} & \overline{\boldsymbol{\phi}}_{\mathbf{z}} & \mathbf{0} \\ \mathbf{0} & \mathbf{0} & -\underline{\boldsymbol{\phi}}_{\mathbf{z}} & \mathbf{0} \end{bmatrix} \tag{5.24}$$

If (5.24) is full row rank, the static optimization problem (5.18) satisfy LICQ. To describe the conditions that guarantee linear independent rows in (5.24), we will assume a worst case scenario, where all the network constraints are active (i.e., $\mathbf{s} = \mathbf{0}$). Initially, we only consider the case where the inequalities that describe the bounds on $\mathbf{u}$ are inactive, i.e., $\boldsymbol{\phi}_{\mathbf{u}}$ and $\boldsymbol{\phi}_{\mathbf{z}}$ disappear from (5.24). In this scenario, equation (5.24) is full row rank if $\boldsymbol{\Theta}_2 \mathrm{diag}(\mathbf{u}) + \boldsymbol{\Theta}_1 \neq 0$, which is equivalent to

$$c_{j,m}(q_{2,m} u_{\ell,m,k} + q_{1,m}) + d_{j,m} \neq 0 \tag{5.25}$$

for all $k \in \mathcal{K}_\ell$ and $m \in \mathcal{M}$, $j \in \mathcal{J}$ and $\ell \in \mathcal{L}$. It follows from Assumption (5.1.1) that 5.25 can be reduced to

$$q_{2,m} u_{\ell,m,k} + q_{1,m} \neq 0, \tag{5.26}$$

which holds if condition (I) of this lemma is satisfied.

For the case, where active inequality bound constraints exist, equation (5.24) has linearly independent rows if the following matrix has full row rank

$$\begin{bmatrix} \Theta_2 \mathrm{diag}(\mathbf{u}) + \boldsymbol{\Theta}_1 \\ \overline{\boldsymbol{\phi}}_{\mathbf{u}} \\ -\underline{\boldsymbol{\phi}}_{\mathbf{u}} \end{bmatrix}. \tag{5.27}$$

This occurs if condition (I) of this lemma is satisfied and if all the subsystems interacting at each node $j \in \mathcal{J}$ are not simultaneously operating on its power bounds. Note that, for a given node j in the network and discrete-time instant k, condition (II) of this lemma guarantees that al least one subsystem does not operate on its bounds. Consequently, if conditions (I) and (II) in of this lemma hold, the complete Jacobian of the feasible set (5.23) has linearly independent rows and the optimization problem (5.8) satisfies LICQ. This completes the proof. □

Condition (I) to guarantee LICQ of optimization problem (5.18) presented in this lemma can be tested a priori via a simple inspection of the power bounds for all the subsystems. For realistic applications, it typically holds that $|q_{2,m}| \ll |q_{1,m}|$, which suggests that (5.21a) is a mild condition. On the other hand, condition (II) can be

verified a posteriori. This condition is satisfied for many real scenarios cases, and in practice, this condition does not limit the performance of optimization algorithm proposed in Section 5.2.2. The satisfaction of LICQ by the optimization problem (5.18) indicates that its critical points are regular. The result presented in Lemma 5.1.1 and the equivalence of the discrete-time optimal control problems (5.1) and the static optimization problem (5.18) will be exploited in the following section to show that the static optimization algorithm, proposed in this chapter, obtains global minimizers of the OCP (5.1). The aforementioned equivalence between the formulations (5.1) and (5.18) is presented in the following lemma.

Lemma 5.1.2. *The optimization problems* (5.1) *and* (5.18) *have the same necessary conditions for optimality and the same global minimizers if the vanishing penalty satisfies*

$$v_{\ell,m}(u_{\ell,m,k}, x_{\ell,m,k}, z_{\ell,m,k}) = 0. \tag{5.28}$$

for all $\ell \in \mathcal{L}$, $m \in \mathcal{M}$ *and* $k \in \mathcal{K}_\ell$.

Proof. Since the static optimization problem (5.18) is an equivalent formulation of the discrete-time OCP (5.8), it remains to demonstrate that the steps made to reformulate (5.1) into (5.8) do not modify the original set of minimizers. The elimination and introduction of decision variables detailed in step 1) and step 4), respectively, are justified in [21, §4.1.3]. The introduction of slack variables and quadratic penalties for the augmented Lagrangian formulation detailed in steps 2),3) and 4), respectively, are supported by [21, §4.1.3], [22, §3.2.1, §3.3.2]. Moreover, if (5.28) holds, the cost function of the formulations (5.1) and (5.8) are equivalent. Hence, the set of minimizers of (5.1),(5.8) and (5.18) are the same. Finally, from Theorem 5.1.1 we conclude that the minimizers of (5.18) are global, because the minimizers of (5.1) are global. □

This result indicates that the vanishing penalty $v_{\ell,m}$ does not modify the OCP if (5.28) is satisfied. The optimization algorithm presented in Section 5.2.2, uses the vanishing penalty term to steer its iterations towards a solution with some desired features. Since, this penalty is designed to disappear after certain number of iterations, the results of Lemma 5.1.2 can be used to show that the aforementioned optimization algorithm obtains solutions to the original OCP (5.1).

5.2. A primal-dual algorithm for CVEM

In the previous section, we showed that the CVEM problem (5.1) only has global solutions, thus solvers cannot get stuck in local minima. Moreover, it was demonstrated that (5.18) is an equivalent formulation to (5.1). In this section, we will take advantage of the previous results to propose a method to solve the static optimization CVEM problem (5.18) using an operator splitting approach.

5.2.1. Saddle-point Problem and KKT Conditions

Operator splitting methods [25, §26] and [26, 27] can be used to find zeros of (set-valued) mappings. In constrained optimization theory, these splitting methods are

used to find the points that satisfy the KKT conditions of a saddle-point problem. In particular, constraints (5.18e) will be embedded in the optimization problem using indicator functions, which will yield to non-smooth non-convex saddle-point problem. In doing so, the KKT conditions of the static optimization problem (5.18) can be represented as a set-valued mapping, which is shown in this subsection, so that (candidate) minimizers can be found using operator splitting methods.

To formulate the aforementioned saddle-point problem in compact form, we define the vector of primal variables

$$\boldsymbol{\chi} = \mathrm{col}(\{\boldsymbol{\omega}_\ell, \mathbf{s}_\ell\}_{\ell\in\mathcal{L}}), \tag{5.29}$$

where $\mathbf{s}_\ell = \mathrm{col}(\{\mathbf{s}_{\ell,j}\}_{j\in J})$ and

$$\boldsymbol{\omega}_\ell = \mathrm{col}(\{\boldsymbol{\omega}_{\ell,m}\}_{m\in\mathcal{M}}), \tag{5.30a}$$

with

$$\boldsymbol{\omega}_{\ell,m} = \mathrm{col}(\mathbf{u}_{\ell,m}, \mathbf{x}_{\ell,m}, \mathbf{z}_{\ell,m}). \tag{5.30b}$$

Additionally, the vector of dual variables is defined as

$$\boldsymbol{\psi} = \mathrm{col}(\{\boldsymbol{\lambda}_\ell, \boldsymbol{\mu}_\ell\}_{\ell\in\mathcal{L}}), \tag{5.31}$$

with $\boldsymbol{\lambda}_\ell = \mathrm{col}(\{\boldsymbol{\lambda}_{\ell,j}\}_{j\in J})$ and $\boldsymbol{\mu}_\ell = \mathrm{col}(\{\boldsymbol{\mu}_{\ell,m}\}_{m\in\mathcal{M}})$ where $\boldsymbol{\lambda}_{\ell,j} \in \mathbb{R}^{K_\ell}$ and $\boldsymbol{\mu}_{\ell,m} \in \mathbb{R}^{n_x m}$ are Lagrange multipliers. Herewith, we cast the static optimization problem (5.18) as the following saddle-point problem

$$\max_{\boldsymbol{\psi}} \min_{\boldsymbol{\chi}} \quad \mathbf{H}(\boldsymbol{\chi}) + \mathbf{Q}(\boldsymbol{\chi}, \boldsymbol{\psi}) \tag{5.32}$$

with a non-smooth convex function

$$\mathbf{H}(\boldsymbol{\chi}) = \sum_{\ell\in\mathcal{L}} \left(\sum_{m\in\mathcal{M}} \iota_{\Omega_{\ell,m}}(\boldsymbol{\omega}_{\ell,m}) + \sum_{j\in\mathcal{J}_c} \iota_{\{\mathbf{0}\}}(\mathbf{s}_{\ell,j}) \right), \tag{5.33}$$

where $\iota_{\{\mathbf{0}\}}(\cdot)$ and $\iota_{\Omega_{\ell,m}}(\cdot)$ are the indicator functions corresponding to (5.18d) and (5.18e), respectively. Moreover,

$$\begin{aligned}\mathbf{Q}(\boldsymbol{\chi}, \boldsymbol{\psi}) = \sum_{\ell\in\mathcal{L}} \Bigg(& \sum_{m\in\mathcal{M}} P_{\ell,m}(\mathbf{u}_{\ell,m}) + \boldsymbol{\nu}_{\ell,m}(\mathbf{u}_{\ell,m}, \mathbf{x}_{\ell,m}, \mathbf{z}_{\ell,m}) \\ & + \sum_{j\in\mathcal{J}} \Big(\tfrac{\sigma_{\ell,j}}{2} \Big\| \sum_{m\in\mathcal{M}} R_{\ell,m,j}(\mathbf{u}_{\ell,m}) + \tfrac{1}{2}\mathbf{s}_{\ell,j}^2 \Big\|_2^2 + \boldsymbol{\lambda}_{\ell,j}^\top \Big(\sum_{m\in\mathcal{M}} R_{\ell,m,j}(\mathbf{u}_{\ell,m}) + \tfrac{1}{2}\mathbf{s}_{\ell,j}^2 \Big) \Big) \Bigg) \\ & + \sum_{\ell\in\mathcal{L}} \Bigg(\sum_{m\in\mathcal{M}} \tfrac{\rho_{\ell,m}}{2} \| \Xi_{\ell-1,m}^f \mathbf{x}_{\ell-1,m} - \Xi_{\ell,m}^o \mathbf{x}_{\ell,m} \|_2^2 + \boldsymbol{\mu}_{\ell,m}^\top \big(\Xi_{\ell-1,m}^f \mathbf{x}_{\ell-1,m} - \Xi_{\ell,m}^o \mathbf{x}_{\ell,m} \big) \Bigg),\end{aligned} \tag{5.34}$$

is a differentiable function. The specific design of the non-smooth cost function of (5.32) is connected to the splitting algorithm that will be presented in Section 5.2.2. Namely, the linear part of the feasible set is expressed as indicator functions while the non-linear and possibly non-convex part of the problem (5.18) is embedded in the continuously differentiable function (5.34). The linear part of the feasible set is also separable for every $\ell \in \mathcal{L}$ and $m \in \mathcal{M}$, which will make the algorithm parallelizable.

The KKT conditions of the static optimization problem (5.18) are the same KKT conditions of the saddle-point problem (5.32) and can be expressed in compact form as $\mathbf{0} \in \partial\mathbf{H}(\boldsymbol{\chi}) + \nabla\mathbf{Q}(\boldsymbol{\chi}, \boldsymbol{\psi})$, with

$$\partial\mathbf{H}(\boldsymbol{\chi}) = \begin{bmatrix} \operatorname{col}(\{\mathrm{N}_{\Omega_{\ell,m}}(\boldsymbol{\omega}_{\ell,m})\}) \\ \operatorname{col}(\{\mathrm{N}_{\{\mathbf{0}\}}(\mathbf{s}_{\ell,j})\}_{\ell\in\mathcal{L},j\in\mathcal{J}_c}) \\ \mathbf{0} \\ \mathbf{0} \\ \mathbf{0} \end{bmatrix}, \tag{5.35a}$$

$$\begin{aligned} \nabla\mathbf{Q}(\boldsymbol{\chi}, \boldsymbol{\psi}) &= \begin{bmatrix} \nabla_{\boldsymbol{\chi}}\mathbf{Q} \\ -\nabla_{\boldsymbol{\psi}}\mathbf{Q} \end{bmatrix} \\ &= \begin{bmatrix} \operatorname{col}(\{\mathbf{F}_{\ell,m}(\mathbf{u}_\ell, \mathbf{u}_{\ell,m}, \mathbf{x}_{\ell-1,m}, \mathbf{x}_\ell, \mathbf{x}_{\ell+1,m}, \mathbf{z}_{\ell,m}, \mathbf{s}_{\ell,j}, \boldsymbol{\lambda}_\ell, \boldsymbol{\mu}_{\ell-1,m}, \boldsymbol{\mu}_{\ell,m})\}) \\ \operatorname{col}(\{\mathbf{G}_{\ell,j}(\mathbf{u}_\ell, \mathbf{s}_{\ell,j}, \boldsymbol{\lambda}_{\ell,j})\}_{\ell\in\mathcal{L},j\in\mathcal{J}_c}) \\ \operatorname{col}(\{\mathbf{G}_{\ell,j}(\mathbf{u}_\ell, \mathbf{s}_{\ell,j}, \boldsymbol{\lambda}_{\ell,j})\}_{\ell\in\mathcal{L},j\in\mathcal{J}_d}) \\ \operatorname{col}(\{-\Lambda_{\ell,j}(\mathbf{u}_\ell, \mathbf{s}_{\ell,j})\}) \\ \operatorname{col}(\{-\Upsilon_{\ell,m}(\mathbf{x}_{\ell-1,m}, \mathbf{x}_{\ell,m})\}) \end{bmatrix}; \end{aligned} \tag{5.35b}$$

where

$$\begin{aligned} \mathbf{F}_{\ell,m}(\mathbf{u}_\ell, \mathbf{u}_{\ell,m}, \mathbf{x}_{\ell-1,m}, \mathbf{x}_\ell, \mathbf{x}_{\ell+1,m}, \mathbf{z}_{\ell,m}, \mathbf{s}_{\ell,j}, \boldsymbol{\lambda}_\ell, \boldsymbol{\mu}_{\ell-1,m}, \boldsymbol{\mu}_{\ell,m}) &= \nabla\boldsymbol{\nu}(\mathbf{u}_{\ell,m}, \mathbf{x}_{\ell,m}, \mathbf{z}_{\ell,m}) \\ &+ \begin{bmatrix} \nabla P_{\ell,m}(\mathbf{u}_{\ell,m}) + \sum_{j\in\mathcal{J}_c} \nabla R_{\ell,m}(\mathbf{u}_{\ell,m})\big(\boldsymbol{\lambda}_{\ell,j} + \sigma_{\ell,j}\Lambda_{\ell,j}(\mathbf{u}_\ell, \mathbf{s}_{\ell,j})\big) \\ \Phi_{\ell,m}(\mathbf{x}_{\ell-1,m}, \mathbf{x}_{\ell,m}, \mathbf{x}_{\ell,m}, \boldsymbol{\mu}_{\ell,m}, \boldsymbol{\mu}_{\ell+1,m}) \\ \mathbf{0} \end{bmatrix} \end{aligned} \tag{5.36a}$$

$$\mathbf{G}_{\ell,j}(\mathbf{u}_\ell, \mathbf{s}_{\ell,j}, \boldsymbol{\lambda}_{\ell,j}) = \operatorname{diag}(\mathbf{s}_{\ell,j})\big(\boldsymbol{\lambda}_{\ell,j} + \sigma_{\ell,j}\Lambda_{\ell,j}(\mathbf{u}_\ell, \mathbf{s}_{\ell,j})\big), \tag{5.36b}$$

$$\Lambda_{\ell,j}(\mathbf{u}_\ell, \mathbf{s}_{\ell,j}) = \sum_{m\in\mathcal{M}} R_{\ell,m}(\mathbf{u}_{\ell,m}) + \tfrac{1}{2}\mathbf{s}_{\ell,j}^2, \tag{5.36c}$$

$$\Upsilon_{\ell,m}(\mathbf{x}_{\ell-1,m}, \mathbf{x}_{\ell,m}) = \Xi^f_{\ell-1,m}\mathbf{x}_{\ell-1,m} - \Xi^o_{\ell,m}\mathbf{x}_{\ell,m} \tag{5.36d}$$

in which

$$\nabla P_{\ell,m}(\mathbf{u}) = a_m \mathbf{1}_{K_\ell} \nabla \mathbf{y}_{\ell,}(\mathbf{u}) + b_m \mathbf{1}_{K_\ell}, \tag{5.37a}$$

$$\nabla R_{\ell,m}(\mathbf{u}) = c_{j,m} \nabla \mathbf{y}_{\ell,m}(\mathbf{u}) + d_{j,m} \mathbf{I}_{K_\ell}, \tag{5.37b}$$

$$\nabla \mathbf{y}_m(\mathbf{u}) = q_{2,m} \mathrm{diag}(\mathbf{u}) + q_{1,m} \mathbf{1}_{K_\ell}, \tag{5.37c}$$

$$\begin{aligned} \Phi_{\ell,m}(\widehat{\mathbf{x}}, \mathbf{x}, \widetilde{\mathbf{x}}, \boldsymbol{\mu}, \widetilde{\boldsymbol{\mu}}) = &- (\Xi^o_{\ell,m})^\top \big(\boldsymbol{\mu} + \rho_{\ell,m} \Upsilon_{\ell,m}(\widehat{\mathbf{x}}, \mathbf{x})\big) \\ &+ (\Xi^f_{\ell+1,m})^\top \big(\widetilde{\boldsymbol{\mu}} + \rho_{\ell+1,m} \Upsilon_{\ell+1,m}(\mathbf{x}, \widetilde{\mathbf{x}})\big) \end{aligned} \tag{5.37d}$$

and $\nabla \boldsymbol{\nu}(\boldsymbol{\omega}_\ell)$ is the gradient of the vanishing penalty function.

In (5.35), we characterized the KKT conditions related to the static optimization problem (5.18). Under certain regularity conditions, the points $\{\boldsymbol{\chi}^*, \boldsymbol{\psi}^*\}$ satisfying $\mathbf{0} \in \partial \mathbf{H}(\boldsymbol{\chi}^*) + \nabla \mathbf{Q}(\boldsymbol{\chi}^*, \boldsymbol{\psi}^*)$ provide candidate minima of the optimization problem (5.18), see [22, §3.3.1] and [28] for a detailed discussion on this topic. In the theorem below, we formally state that $\mathbf{0} \in \partial \mathbf{H}(\boldsymbol{\chi}^*) + \nabla \mathbf{Q}(\boldsymbol{\chi}^*, \boldsymbol{\psi}^*)$ leads to global minimizers to the discrete OCP (5.1).

Theorem 5.2.1. *Suppose that the conditions of Lemma 5.1.1 and Lemma 5.1.2 are satisfied, and the feasible sets $\Omega_{\ell,m}$ for all $m \in \mathcal{M}$ and $\ell \in \mathcal{L}$ are compact. Then, globally optimal solutions $\{u^*_{m,k}, x^*_{m,k}, z^*_{m,k}, y^*_{m,k}\}$ to the discrete-time optimal control problem (5.1) can be obtained from points $\{\boldsymbol{\chi}^*, \boldsymbol{\psi}^*\}$ satisfying $\mathbf{0} \in \partial \mathbf{H}(\boldsymbol{\chi}^*) + \nabla \mathbf{Q}(\boldsymbol{\chi}^*, \boldsymbol{\psi}^*)$.*

Proof. From Lemma 5.1.1, we observe that if condition (5.21) is satisfied, the static optimization problem (5.18) satisfies LICQ. Furthermore, note that finite bounds on $u_{m,k}$ in (5.1e) imply that sets $\Omega_{\ell,m}$ are compact for all $m \in \mathcal{M}$ and $\ell \in \mathcal{L}$. Then, from [22, §3.3.1] the points $\{\boldsymbol{\chi}^*, \boldsymbol{\psi}^*\}$ satisfying the KKT conditions $\mathbf{0} \in \partial \mathbf{H}(\boldsymbol{\chi}^*) + \nabla \mathbf{Q}(\boldsymbol{\chi}^*, \boldsymbol{\psi}^*)$ are critical points of optimization problem (5.18). The primal part $\boldsymbol{\chi}^*$ of those critical points can be used to recover a solution $\{u^*_{\ell,m,k}, x^*_{\ell,m,k}, z^*_{\ell,m,k}, s^*_{\ell,j,k}\}$ of OCP (5.8). Finally, as a consequence of the equivalence of the formulations (5.1), (5.8) and (5.18) shown in Lemma 5.1.2, we can conclude that the globally optimal solution $\{u^*_{m,k}, x^*_{m,k}, z^*_{m,k}, y^*_{m,k}\}$ to OCP (5.1) can be obtained from critical points $\{\boldsymbol{\chi}^*, \boldsymbol{\psi}^*\}$. □

5.2.2. A Primal-Dual Proximal Splitting Algorithm

In this section, we use the Primal-Dual (PD) proximal splitting method presented in [19, Algorithm 1.1], which will be used to find points $\mathrm{col}(\boldsymbol{\chi}^*, \boldsymbol{\psi}^*)$ satisfying $\mathbf{0} \in \partial \mathbf{H}(\boldsymbol{\chi}^*) + \nabla \mathbf{Q}(\boldsymbol{\chi}^*, \boldsymbol{\psi}^*)$, thereby finding global minimizers of the optimal control problem (OCP) in (5.1). It should be noted that for convex optimization problems, this PD splitting leads to the widely used Chambolle–Pock method [29, 30] , while recent extensions of the PD splitting method show its application to solve non-convex problems [31], [32].

To solve the non-convex and non-smooth saddle point problem (5.32), we apply the primal-dual splitting method presented in [19]. This leads to the following

iteration that is described in compact form as

$$\boldsymbol{\chi}^{i+1} = (\mathbf{I} + \boldsymbol{\alpha}^i \partial \mathbf{H})^{-1}(\boldsymbol{\chi}^i - \boldsymbol{\alpha}^i \nabla_{\boldsymbol{\chi}} \mathbf{Q}(\boldsymbol{\chi}^i, \boldsymbol{\psi}^i)), \tag{5.38a}$$

$$\widehat{\boldsymbol{\chi}}^{i+1} = \boldsymbol{\chi}^{i+1} + \boldsymbol{\beta}(\boldsymbol{\chi}^{i+1} - \boldsymbol{\chi}^i), \tag{5.38b}$$

$$\boldsymbol{\psi}^{i+1} = \boldsymbol{\psi}^i + \boldsymbol{\gamma}^i \nabla_{\boldsymbol{\psi}} \mathbf{Q}(\widehat{\boldsymbol{\chi}}^{i+1}, \boldsymbol{\psi}^i)); \tag{5.38c}$$

where the superscript $i \in \{1, 2, ...\}$ denotes the i-th iteration. The diagonal matrices with positive entries $\boldsymbol{\alpha}$ and $\boldsymbol{\gamma}$ indicate the primal and dual step sizes of the algorithm, respectively. Moreover, $\boldsymbol{\beta}$ is a diagonal matrix with positive entries that represents the over-relaxation factor. Note that (5.38) is a modified Gauss-Seidel iteration with three steps that, respectively, represent the primal updates, the over-relaxation step, the dual updates. The modification introduced by the over-relaxation step aims to accelerate the convergence of the algorithm. In (5.38a), the term $(\mathbf{I} + \boldsymbol{\alpha}\partial\mathbf{H})^{-1}$ is a monotone operator since the sub-differential $\partial\mathbf{H}$ contains only normal cones of convex sets. The resolvent of this monotone operator is as a projection, i.e., see [33, Example 23.4] for more details. Interestingly, this projection can be efficiently implemented as a constrained least squares problems. Additionally, it should be noted from (5.35) that both, the gradient $\nabla\mathbf{Q}$ as well as subdifferential $\partial\mathbf{H}$, are highly structured. This allows for a parallelizable approach that is fully detailed in Algorithm 1, which employs Algorithm 1a and Algorithm 1b.

The three steps presented in (5.38) are also explicitly detailed in Algorithm 1. Note that **STEP 1** and **STEP 3** are linked to Algorithm 1a and Algorithm 1b, which aim to automatically select step-sizes and regularization factors at every iteration. This is motivated by the high level of parallelization of Algorithm 1, which implies that a large set of step-sizes need to be chosen. Manually selecting the step-sizes so as to obtain good performance, is a nontrivial process that is often done manually.

Algorithm 1: Primal-Dual Splitting

Initialization
For all $\ell \in \mathcal{L}$:

- Select the positive scalar step-sizes $\alpha^0_{u_{\ell,m}}$, $\alpha^0_{x_{\ell,m}}$, $\alpha^0_{z_{\ell,m}}$ for all $m \in \mathcal{M}$ such that
$$\boldsymbol{\alpha}^0_{\omega_{\ell,m}} = \mathrm{diag}(\alpha^0_{u_{\ell,m}}\mathbf{I}_{K_\ell}, \alpha^0_{x_{\ell,m}}\mathbf{I}_{n_{xm}(K_\ell+1)}, \alpha^0_{z_{\ell,m}}\mathbf{I}_{n_{zm}K_\ell});$$
$\alpha^0_{s_{\ell,j}}$ for all $J \in \mathcal{J}_d$, $\gamma^0_{\lambda_{\ell,j}}$ for all $J \in \mathcal{J}$ and $\gamma^0_{\mu_{\ell,m}}$ for all $m \in \mathcal{M}$.
- Select the positive scalar over-relaxation factors $\beta_{u_{\ell,m}}$, $\beta_{x_{\ell,m}}$, $\beta_{z_{\ell,m}}$ for all $m \in \mathcal{M}$ such that
$$\boldsymbol{\beta}_{\omega_{\ell,m}} = \mathrm{diag}(\beta_{u_{\ell,m}}\mathbf{I}_{K_\ell}, \beta_{x_{\ell,m}}\mathbf{I}_{n_{xm}(K_\ell+1)}, \beta_{z_{\ell,m}}\mathbf{I}_{n_{zm}K_\ell});$$
and $\beta_{s_{\ell,j}}$ for all $J \in \mathcal{J}_d$.
- Select the positive scalar regularization factors $\sigma^0_{\ell,j}$, $\varsigma_{\ell,j}$ for all $j \in \mathcal{J}_d$ and $\rho^0_{\ell,m}$, $\varrho_{\ell,m}$ for all $m \in \mathcal{M}$.
- Set initial values for $\boldsymbol{\omega}^0_{\ell,m} \in \Omega_{\ell,m}$ for all $m \in \mathcal{M}$, $\mathbf{s}^0_{\ell,j} \in \mathbb{R}^{K_\ell}$ for all $j \in \mathcal{J}_d$, $\mathbf{s}^i_{\ell,j} = \mathbf{0}_{K_\ell \times 1}$ for all $j \in \mathcal{J}_c$ and $i \in \mathbb{N}$, $\boldsymbol{\lambda}^0_{\ell,j} \in \mathbb{R}^{K_\ell}$ for all $j \in \mathcal{J}$, $\boldsymbol{\mu}_{\ell,m} \in R^{n_{xm}}$ for all $m \in \mathcal{M}$.

Iterate until convergence:

STEP 1: Primal update. For all $\ell \in \mathcal{L}$,

if $i > 1$ then go to Algorithm 1a

$$\boldsymbol{\omega}^{i+1}_{\ell,m} = \mathrm{proj}_{\Omega_{\ell,m}}\left(\boldsymbol{\omega}^i_{\ell,m} - \boldsymbol{\alpha}^i_{\omega_{\ell,m}}\mathbf{F}_{\ell,m}(\mathbf{u}^i_\ell, \mathbf{u}^i_{\ell,m}, \mathbf{x}^i_{\ell-1,m}, \mathbf{x}^i_\ell, \mathbf{x}^i_{\ell+1,m}, \mathbf{z}^i_{\ell,m}, \mathbf{s}^i_{\ell,j}, \boldsymbol{\lambda}^i_\ell, \boldsymbol{\mu}^i_{\ell-1,m}, \boldsymbol{\mu}^i_{\ell,m})\right),$$
for all $m \in \mathcal{M}$

$$\mathbf{s}^{i+1}_{\ell,j} = \mathbf{s}^i_{\ell,j} - \alpha^i_{s_{\ell,j}}\mathbf{G}_{\ell,j}(\mathbf{u}^i_\ell, \mathbf{s}^i_{\ell,j}, \boldsymbol{\lambda}^i_{\ell,j}), \text{ for all } \; j \in \mathcal{J}_d$$

STEP 2: Over-relaxation. For all $\ell \in \mathcal{L}$,

$$\widehat{\boldsymbol{\omega}}^{i+1}_{\ell,m} = \boldsymbol{\omega}^{i+1}_{\ell,m} + \boldsymbol{\beta}_{\omega_{\ell,m}}(\boldsymbol{\omega}^{i+1}_{\ell,m} - \boldsymbol{\omega}^i_{\ell,m}), \quad \text{for all } m \in \mathcal{M}$$

$$\widehat{\mathbf{s}}^{i+1}_{\ell,j} = \mathbf{s}^{i+1}_{\ell,j} + \beta_{s_{\ell,j}}(\mathbf{s}^{i+1}_{\ell,j} - \mathbf{s}^i_{\ell,j}), \qquad \text{for all } \; j \in \mathcal{J}_d$$

STEP 3 : Dual update. For all $\ell \in \mathcal{L}$,

if $i > 1$ then go to Algorithm 1b

$$\boldsymbol{\lambda}^{i+1}_{\ell,j} = \boldsymbol{\lambda}^i_{\ell,j} + \gamma^i_{\lambda_{\ell,j}}\boldsymbol{\Lambda}_{\ell,j}(\widehat{\mathbf{u}}^{i+1}_\ell, \widehat{\mathbf{s}}^{i+1}_{\ell,j}), \quad \text{for all } \; j \in \mathcal{J}$$

$$\boldsymbol{\mu}^{i+1}_{\ell,m} = \boldsymbol{\mu}^i_{\ell,m} + \gamma^i_{\mu_{\ell,m}}\boldsymbol{\Upsilon}_{\ell,m}(\widehat{\mathbf{x}}^{i+1}_{\ell,m}, \widehat{\mathbf{x}}^{i+1}_{\ell+1,m}), \text{ for all } m \in \mathcal{M}$$

Algorithm 1a: Selection of primal step-sizes.

For all $m \in \mathcal{M}$:

$$\Delta\boldsymbol{\omega}^i_{\ell,m} = \boldsymbol{\omega}^i_{\ell,m} - \boldsymbol{\omega}^{i-1}_{\ell,m}$$

$$\Delta\mathbf{F}^i_{\ell,m} = \mathbf{F}_{\ell,m}(\mathbf{u}^i_\ell, \mathbf{u}^i_{\ell,m}, \mathbf{x}^i_{\ell-1,m}, \mathbf{x}^i_\ell, \mathbf{x}^i_{\ell+1,m}, \mathbf{z}^i_{\ell,m}, \mathbf{s}^i_{\ell,j}, \boldsymbol{\lambda}^i_\ell, \boldsymbol{\mu}^i_{\ell-1,m}, \boldsymbol{\mu}^i_{\ell,m}) - \mathbf{F}_{\ell,m}(\mathbf{u}^{i+1}_\ell, \mathbf{u}^{i-1}_{\ell,m}, \mathbf{x}^{i-1}_{\ell-1,m}, \mathbf{x}^{i-1}_\ell, \mathbf{x}^{i-1}_{\ell+1,m}, \mathbf{z}^{i-1}_{\ell,m}, \mathbf{s}^{i-1}_{\ell,j}, \boldsymbol{\lambda}^{i-1}_\ell, \boldsymbol{\mu}^i_{\ell-1,m}, \boldsymbol{\mu}^{i-1}_{\ell,m})$$

$$\Xi_u = \left[\, \mathbf{I}_{K_\ell} \; \mathbf{0} \; \mathbf{0} \,\right]$$

Compute $\alpha^i_{u_{\ell,m}}$ using Algorithm 2 with inputs $\Xi_u\Delta\boldsymbol{\omega}^i_{\ell,m}$ and $\Xi_u\Delta\mathbf{F}^i_{\ell,m}$)

$$\Xi_x = \left[\, \mathbf{0} \; \mathbf{I}_{n_{xm}(K_\ell+1)} \; \mathbf{0} \,\right]$$

Compute $\alpha^i_{x_{\ell,m}}$ using Algorithm 2 with inputs $\Xi_x\Delta\boldsymbol{\omega}^i_{\ell,m}$ and $\Xi_x\Delta\mathbf{F}^i_{\ell,m}$

$$\Xi_z = \left[\, \mathbf{0} \; \mathbf{0} \; \mathbf{I}_{n_{zm}K_\ell} \,\right]$$

Compute $\alpha^i_{z_{\ell,m}}$ using Algorithm 2 with inputs $\Xi_z\Delta\boldsymbol{\omega}^i_{\ell,m}$ and $\Xi_z\Delta\mathbf{F}^i_{\ell,m}$

$$\boldsymbol{\alpha}^i_{\omega_{\ell,m}} = \mathrm{diag}(\alpha^i_{u_{\ell,m}}\mathbf{I}_{K_\ell}, \alpha^i_{x_{\ell,m}}\mathbf{I}_{n_{xm}(K_\ell+1)}, \alpha^i_{z_{\ell,m}}\mathbf{I}_{n_{zm}K_\ell})$$

For all $j \in \mathcal{J}_d$:

$$\Delta\mathbf{s}^i_{\ell,j} = \mathbf{s}^i_{\ell,j} - \mathbf{s}^{i-1}_{\ell,j}$$

$$\Delta\mathbf{G}^i_{\ell,j} = \mathbf{G}_{\ell,j}(\mathbf{u}^i_\ell, \mathbf{s}^i_{\ell,j}, \boldsymbol{\lambda}^i_{\ell,j}) - \mathbf{G}_{\ell,j}(\mathbf{u}^{i-1}_\ell, \mathbf{s}^{i-1}_{\ell,j}, \boldsymbol{\lambda}^{i-1}_{\ell,j})$$

Compute $\alpha^i_{s_{\ell,j}}$ using Algorithm 2 with inputs $\Delta\mathbf{s}^i_{\ell,j}$ and $\Delta\mathbf{G}^i_{\ell,j}$

Algorithm 1b: Selection of dual step-sizes and regularization factors.

For all $j \in \mathcal{J}$:

$$\Delta\boldsymbol{\lambda}^i_{\ell,j} = \boldsymbol{\lambda}^i_{\ell,j} - \boldsymbol{\lambda}^{i-1}_{\ell,j}$$

$$\Delta\boldsymbol{\Lambda}^i_{\ell,j} = \Lambda_{\ell,j}(\widehat{\mathbf{u}}^{i+1}_\ell, \widehat{\mathbf{s}}^{i+1}_{\ell,j}) - \Lambda_{\ell,j}(\widehat{\mathbf{u}}^i_\ell, \widehat{\mathbf{s}}^i_{\ell,j})$$

Compute $\gamma^i_{\lambda_{\ell,j}}$ using Algorithm 2 with inputs $\Delta\boldsymbol{\lambda}^i_{\ell,j}$ and $\Delta\boldsymbol{\Lambda}^i_{\ell,j}$

$$\sigma^i_{\ell,j} = \varsigma_{\ell,j}\gamma^i_{\lambda_{\ell,j}}$$

For all $m \in \mathcal{M}$:

$$\Delta\boldsymbol{\mu}^i_{\ell,m} = \boldsymbol{\mu}^i_{\ell,m} - \boldsymbol{\mu}^{i-1}_{\ell,m}$$

$$\Delta\boldsymbol{\Upsilon}^i_{\ell,m} = \boldsymbol{\Upsilon}_{\ell,m}(\widehat{\mathbf{x}}^{i+1}_{\ell,m}, \widehat{\mathbf{x}}^{i+1}_{\ell+1,m}) - \boldsymbol{\Upsilon}_{\ell,m}(\widehat{\mathbf{x}}^i_{\ell,m}, \widehat{\mathbf{x}}^i_{\ell+1,m})$$

Compute $\gamma^i_{\mu_{\ell,m}}$ using Algorithm 2 with inputs $\Delta\boldsymbol{\mu}^i_{\ell,m}$ and $\Delta\boldsymbol{\Upsilon}^i_{\ell,m}$

$$\rho^i_{\ell,m} = \varrho_{\ell,m}\gamma^i_{\mu_{\ell,m}}$$

Essentially, Algorithm 1a and Algorithm 1b feed information from the current and past iterations to Algorithm 2, which is in charge of calculating the optimal step-sizes. We will postpone the discussion of Algorithm 2 for following section. However, it is important to remark the adaptive nature of this scheme, which provides step-sizes at every iteration that depend on the previous evolution of the iterations. Additionally, it should be noted that an adaptive selection of over-relaxation factors is not considered in our methodology. However, in Section 5.2.4 we will provide guidance to manually choose this factors.

In [18], a forward backward splitting algorithm to find solutions of problem (5.1) was presented. This algorithm does not have an over-relaxation step and the primal and primal variables are updated in parallel. On the contrary, Algorithm 1 shows a Gauss-Seidel type of iteration. Moreover, Algorithm 1 uses horizon splitting to increase the scalability the method. Finally, the algorithm presented in [18], considers fixed step-sizes, which makes the tuning process of the algorithm a time-consuming task. Algorithm 1, considers step-sizes that are selected at every iteration, which from a practical viewpoint, improves the numerical performance and reduces the complexity of implementing the algorithm. Interestingly, the optimization algorithm presented in [18] can be retrieved by selecting -1 for the diagonal entries of the matrix $\boldsymbol{\beta}$ in (5.38).

In [19, Theorem 4.2], weak convergence of the algorithm to a critical point is provided under some rules for step-length selection. Unfortunately, convergence rates under over-relaxation of Algorithm 1 can not be obtained since the non-smooth function $\mathbf{H}(\chi)$, that describes the linear feasible set of (5.18), is not strongly convex (see [19, Theorem 4.4]).

5.2.3. Adaptive Step-size Selection

The amount of parameters to tune in Algorithm 1 grows proportionally with the number of parallel iterations that the setting of algorithm considers. Moreover, the performance of the algorithm depends directly on these parameters. This could make the tuning process of Algorithm 1 a cumbersome task, i.e., if several subsystems are considered in the network and/or when a long time horizon is split in many smaller intervals.

In this section, we aim to reduce the complexity of selecting step-sizes and regularization factors for the distributed optimization algorithm proposed in the previous section by the use of a spectral method commonly known as Barzilai-Borwein (BB) methods. In [20], a complete review of of the BB method for large scale unconstrained optimization methods is presented. In fact, this method is directly linked to the class of optimization techniques known as Spectral Gradient methods, e.g, [34]. Recently, it has also been adopted in the context of forward backward splitting algorithms [35]. However, to our understanding, this work is the first to present the an adaptive BB method in connection with a primal-dual algorithm for a non-convex constrained optimization problem. The main idea behind the adaptive step-size selection use information from the current and previous iteration to calculate the next "optimal" step-size. Note, that this optimality of the step-size assumes that the iterations of the algorithm belong to a quadratic approximation of the smooth func-

tion $\mathbf{Q}(\boldsymbol{\chi}, \boldsymbol{\psi})$. For a concise but insightful explanation of this concept the readers can refer to [35, §4.1]. Moreover, we need to remark that our step-size selection algorithm is a minor modification of the methodology described in [35, §4.1]. The adaptive step-size method proposed in this chapter is presented in the following algorithm.

Algorithm 2: Adaptive step-size selection

Inputs:
$\Delta\boldsymbol{\xi}^i$, $\Delta\Gamma^i$
Output:
Step-size τ^i
Initialization:
Set the upper step-size bound $\overline{\tau} > 0$ and lower step-size bound $\underline{\tau} > 0$.

Find

$$\tau_s^i = \frac{(\Delta\boldsymbol{\xi}^i)^\top(\Delta\boldsymbol{\xi}^i)}{(\Delta\boldsymbol{\xi}^i)^\top(\Delta\Gamma^i)}, \qquad \tau_m^i = \frac{(\Delta\boldsymbol{\xi}^i)^\top(\Delta\Gamma^i)}{(\Delta\Gamma^i)^\top(\Delta\Gamma^i)},$$

$$\tau_p^i = \begin{cases} \tau_m^i & \text{if } \tau_m^i > 2\tau_s^i, \\ \tau_s^i - \frac{1}{2}\tau_m^i, & \text{otherwise,} \end{cases}$$

$$\tau^i = \begin{cases} \tau_p^i & \text{if } \underline{\tau} \leq \tau_p^i \leq \overline{\tau} \\ \tau^{i-1} & \text{otherwise.} \end{cases}$$

The first step in Algorithm 2 is to calculate a large step-size τ_s^i, and small step-size τ_m^i, that are know as the steepest descent step-size and the minimum residual step-size, respectively. The steepest descent step-size aims to generate a sufficient reduction of the cost in the next iteration, while the minimum residual step-size tries to obtain a favorable descending direction. In the second step of Algorithm 2, a selection between the two possible step sizes is performed. This is achieved using the adaptive rule presented in [36]. The final step of the algorithm is to guarantees that the step-sizes remain within the predefined bounds. This is an important step since the optimization problem is non-convex, which implies that the step-sizes could become negative. In case that the bounds are violated, the last valid step-size is used.

5.2.4. Implementation Remarks

Even though Algorithm 2 updates the step-sizes automatically, still the bounds on these step-sizes need to be specified. Consequently, some manual tuning is needed although the number of bounds is much smaller than the number of step-sizes (which can change for every iteration). Therefore, we provide a set of heuristics

rules to set-up the Algorithm 1 and Algorithm 2. These rules have been obtained from experience after extensive simulations. As mentioned before, the parameters that need to be tunned are the upper and lower bounds for the step-sizes in Algorithm 2 and the regularization factors in Algorithm 1. In most of the cases, it is enough set only two sets of common upper and lower step-size bounds, i.e., step-size bounds primal variables and step-size bounds for dual variables. Moreover, the lower bounds for both groups can be the same with a value that is almost zero. On the other hand, the upper bound for the group of primal variables could often be set approximately four orders of magnitude higher to the upper bound for the group of dual variables.

As observed in Algorithm 1b, the selection of regularization factors is automated by linking them to the dual step-sizes with the coefficients $\varsigma_{\ell,j}$, $\varrho_{\ell,m}$. Often, satisfactory results can be obtained by choosing

$$\varsigma_{\ell,j} = \varrho_{\ell,m} = \delta, \tag{5.39}$$

for all $\ell \in \mathcal{L}$, $m \in \mathcal{M}$ and $j \in \mathcal{J}$, with $\delta < 20$. Our methodology does not consider the selection of over-relaxation factors. In fact, from simulations we have observed that its effect in the numerical performance of the algorithm can overruled by the adaptive step selection. Nevertheless, choosing small over-relaxation steps can marginally improve the number of iterations than the algorithm takes to converge.

In case that a vanishing penalty is required, it is often convenient to an introduce an attenuation coefficient that is inversely proportional to the number of iterations. Moreover, to satisfy the condition of Lemma 5.1.2, the vanishing penalty take a zero value after a certain number of iterations. We provide an example of this design guidelines in Section 5.3.4. Finally, it is important to remark that these guidelines have obtained after numerically conditioning the optimization problem (5.18) , i.e., scaling the problem such that all primal variables at a similar order of magnitude.

5.3. Numerical Results

In this section, we present a detailed numerical analysis of the proposed solution approach to the CVEM problem. Using the methods presented in Section 5.2 to solve the CVEM problem for a parallel-hybrid vehicle will allow us to highlight the advantages of our approach with respect to a commercial solver in terms of the optimal solutions obtained, computation time and scalability. We will also highlight the existence of only global solutions and demonstrate how to steer the iterations of Algorithm 1 to find optimal solutions with specific features. Moreover, we will explore the scalability capabilities of the algorithm to solve a problem using a large horizon, which enable us to observe the links of between level of parallelization, computation time and number of iterations.

5.3.1. CVEM for a Parallel-hybrid Vehicle

For the simulation study presented below, we consider a CVEM OCP for a parallel-hybrid electric vehicle that consists of an internal combustion engine (ICE), an electric machine (EM), a high-voltage battery (HVB), a mechanical compressor

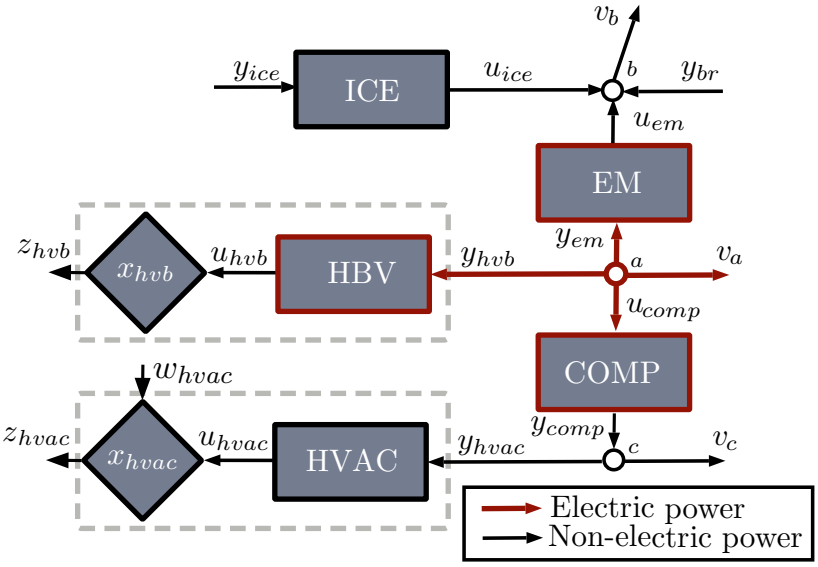

Figure 5.2: Power network topology for a parallel-hybrid vehicle.

(COMP) and a heat ventilation and air conditioning (HVAC) system. For notational convenience, we use the set $\mathcal{M} = \{\text{ice, em, hvb, comp, hvac}\}$, instead of $\mathcal{M} = \{1, 2, 3, 4, 5\}$, and the set $\mathcal{J} = \{\text{a, b, c}\}$, instead of $\mathcal{J} = \{1, 2, 3\}$. Note that this case study considers components that often are considered the main energy consumers in a vehicle. The power network for this configuration is presented in Fig. 5.2. There exist tree nodes $\mathcal{J}$ that describe the mechanical and electrical power balance in the vehicle. These nodes are bridged by the EM and the COMP, which act as power converters to transform power between the electrical and mechanical domains. The power network also contains exogenous signals that represent the power consumed by auxiliary subsystems $v_{a,k} = 1.5[kW]$ and the traction power request $v_{b,k} = y_{req,k}$, which is presented in Fig. 5.3. Note that node c does not have any external disturbance, i.e., $v_{c,k} = 0[kW]$. The presence of the mechanical braking power $y_{br,k} \leq 0$ in node b implies that it is a dissipative node, thus $\mathcal{J}_c = \{a, c\}$ and $\mathcal{J}_d = \{b\}$. By selecting, $c_{c,comp} = d_{b,ice} = d_{a,em} = -1$, $c_{a,hvb} = c_{b,em} = c_{c,hvac} = d_{a,comp} = 1$ and all other coefficients as zero, the power network is described by

$$\begin{aligned} y_{hvb,k} + y_{em,k} + u_{comp} + v_{a,k} &= 0, \\ -u_{ice,k} - u_{em,k} + v_{b,k} = -y_{br,k} &\leq 0, \\ y_{hvac,k} - y_{comp,k} + v_{c,k} &= 0. \end{aligned} \tag{5.40}$$

Considering a sampling time of $5[s]$ and a discrete-time horizon $K = \{1, \ldots, 216\}$, the time span for this example is about $18[min]$. Initially, we will consider a single time interval $\mathcal{L} = \{1\}$, which implies $\mathcal{K} = \mathcal{K}_1$. For the sake of simplicity, we will omit

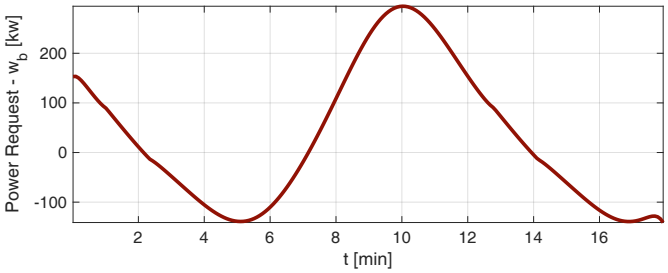

Figure 5.3: Power request.

the subindex ℓ in the notation. Under this considerations, the discrete-time buffers are described by $A_m = B_m = C_m = D_m = Em = F_m = 0$ for all $m \in \{\text{ice, em, comp}\}$. The HBV has been modelled using an equivalent circuit approach, where we consider the charging current to be positive. In this case, we have $A_{hvb} = 1$, $B_{hvb} = 0.1102$, $C_{hvb} = 0.2$, $D_{hvb} = E_{hvb} = F_{hvb} = 0$, with initial and final conditions respectively given by $x_{hvb,0} = x_{hvb,K} = 264.29$, which correspond to initial and final states of charge $z_{hvb,0} = z_{hvb,K} = 52.86[\%]$. The COMP and the HVAC are part of a data-driven model that uses a Hammerstein-Weiner structure with a quadratic and an affine inputs, and an affine output. This model has a dependency on the environment temperature that, in this case, is assumed to be constant $T_{amb} = 5[^\circ C]$. The specific structure of this data-driven model was adapted to the CVEM framework by considering the quadratic input non-linearity as the COMP subsystem, while the HVAC is represented by a discrete-time dynamical system described by

$$
\begin{aligned}
A_{hvac} &= \begin{bmatrix} 0.0080 & 10.6807 & 0.0361 \\ 0.0007 & 0.9898 & 0.0005 \\ -0.0002 & 0.0017 & 0.9990 \end{bmatrix}, & B_{hvac} &= \begin{bmatrix} 0.9260 \\ 0.0972 \\ 0.2354 \end{bmatrix}, \\
C_{hvac} &= \begin{bmatrix} 0.0373 & -0.4035 & -0.0118 \end{bmatrix}, & D_{hvac} &= 0.0075, \\
E_{hvac} &= \operatorname{diag}(1,\ 1,\ 1,\ 0), & F_{hvac} &= \begin{bmatrix} 0 & 0 & 0 & 1 \end{bmatrix},
\end{aligned} \tag{5.41}
$$

with an external disturbance $w_{hvac,k} = [4.4851 \quad 0.4096 \quad -0.0052 \quad 2.6499]^\top$ for all $k \in \mathcal{K}$ and initial condition $x_{hvac,0} = [-305 \quad -24.5 \quad -1342]^\top$, which corresponds to and intital cabin temperature $z_{hvac,0} \approx 17[^\circ C]$. The considered case study aims to minimize the energy consumed by the ICE, which corresponds to $a_{ice} = 1$ while the other a_m and all b_m are zero. Finally, the parameters that describe the power converters are given in Table 5.1, while the input and output bounds of the dynamical systems are detailed in Table 5.2.

Finally, it should be noted that the simplicity of the power request presented in Fig. 5.3 allows us to highlight the main functionalities of our optimization algorithm. Later, we will propose a more challenging and longer power request that will be used to discuss the performance of our methods, specially highlighting its capabilities to deal with large scale CVEM problems.

Table 5.1: Parameters for the power converters.

m	$q_{m,2}$	$q_{m,1}$	$q_{m,0}$
ice	0	1	0
em	2×10^{-5}	2.52	19
hvb	1.67×10^{-3}	1	0
comp	1.78×10^{-2}	−0.93	0.43
hvac	0	1	0

Table 5.2: Input and output bounds.

m	$\underline{u}_m\ [kW]$	$\overline{u}_m\ [kW]$	$\underline{z}_m$	$\overline{z}_m$
ice	0	310	-	-
em	−210	210	-	-
hvb	−92.4	92.4	-	-
comp	0	15	33.33[%]	100[%]
hvac	−15	15	$16.8[^\circ C]$	$19[^\circ C]$

5

5.3.2. Multiple Global Optimal Solutions

The OCP discussed in this case study has been solved using the following four approaches:

- **PD:** Algorithm 1 with static step-sizes presented in Table 5.3. Specifically, we neglect the adaptive step-size selection in this approach by ignoring the calls to Algorithm 1a ans Algorithm 1b. Thus, the initial step-sizes remain unmodified for all the iterations of Algorithm 1.
- **Ad-PD-1, Ad-PD-2:** Algorithm 1 in combination with the adaptive step-size selection scheme described by Algorithm 1. The configuration for this two approaches follows the guidelines presented in Section 5.2.4 to obtain the parameters given in Table 5.4. Moreover, we consider the step-sizes, over-relaxation and regularization factors presented in Table 5.3 as the initial parameters in these approaches.
- **CPLEX:** Commercial solver CPLEX [37] that solves a convexified version of the OCP, where the equality constraints in (5.40) are relaxed into inequalities. This convexification allows to formulate the CVEM problem as a quadratically constrained linear program that can be directly solved by CPLEX. Note that the convex relaxation considered here is a consequence of Theorem 5.1.1 and guarantees that the solutions given by this approach attain the global cost. However, the convex relaxation can lead to solutions that are not physically realizable, which will discussed in the following paragraphs.

The existence of multiple global solutions can be observed in the in Fig. 5.4, where the solutions obtained by the different approaches are presented. The differences between the solutions are specially notorious in the time instants where breaking power y_{br} is different from zero. The way in which power can be dissipated

Table 5.3: Step-sizes, over-relaxation and regularization factors for PD.

$\alpha_{u_{ice}} = 300$	$\beta_{u_{ice}} = 10^{-8}$	$\gamma_a = 10^{-3}$
$\alpha_{u_{em}} = 10$	$\beta_{u_{em}} = 10^{-8}$	$\gamma_b = 10^{-4}$
$\alpha_{u_{hvb}} = 100$	$\beta_{u_{hvb}} = 10^{-8}$	$\gamma_c = 10^{-3}$
$\alpha_{u_{comp}} = 10$	$\beta_{u_{comp}} = 10^{-8}$	$\sigma_a = 10^{-2}$
$\alpha_{u_{hvac}} = 30$	$\beta_{u_{hvac}} = 10^{-8}$	$\sigma_b = 10^{-3}$
$\alpha_{s_b} = 2$	$\beta_{s_b} = 10^{-8}$	$\sigma_c = 10^{-2}$

Table 5.4: Step-size bounds and regularization coeffcients for Ad-PD-1 and Ad-PD-2.

	Ad-PD-1	Ad-PD-2
Primal $\overline{\tau}$	100	150
Primal $\underline{\tau}$	10^{-8}	10^{-8}
Dual $\overline{\tau}$	10^{-2}	7.5×10^{-3}
Dual $\underline{\tau}$	10^{-8}	10^{-8}
δ	15	16

is not unique. As a consequence, the multiplicity of solutions appears naturally here and is propagated to all the other power profiles. Note that the OPC of this case study and its optimal solutions satisfy the conditions of Lemma 5.1.1, thus, from Theorem 5.2.1 we can conclude that the obtained solutions are global. In fact, the optimal cost obtained by all the approaches is $9.97[L/100\ km]$. This is also consistent with the ICE input power depicted in Fig. 5.4, where all the approaches obtain the same power profile.

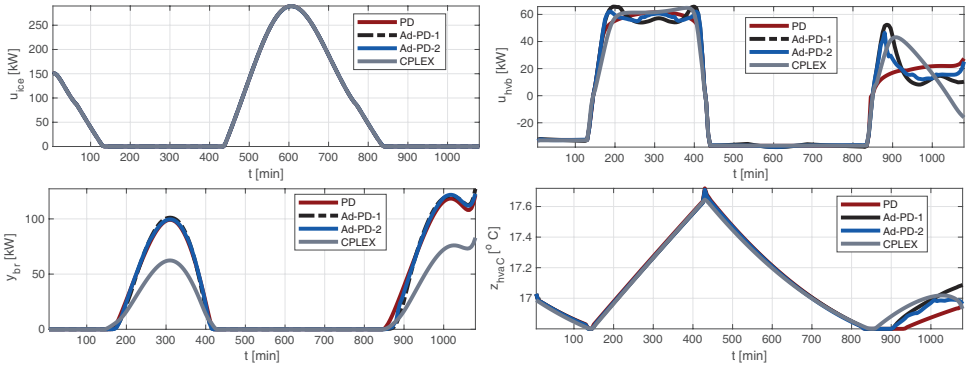

Figure 5.4: Multiple global optimal solutions: Input power profiles for the ICE and the HVB, braking power and cabin temperature.

In Fig. 5.5, the power balance at node a is presented. Here, it can be noted that the solution obtained by CPLEX does not satisfy the power balance with equality. This is a consequence of the convex relaxation used in this approach, where the network equalities were changed into inequalities. Although the solution obtained by CPLEX has the correct global cost and the ICE power profile is the same as

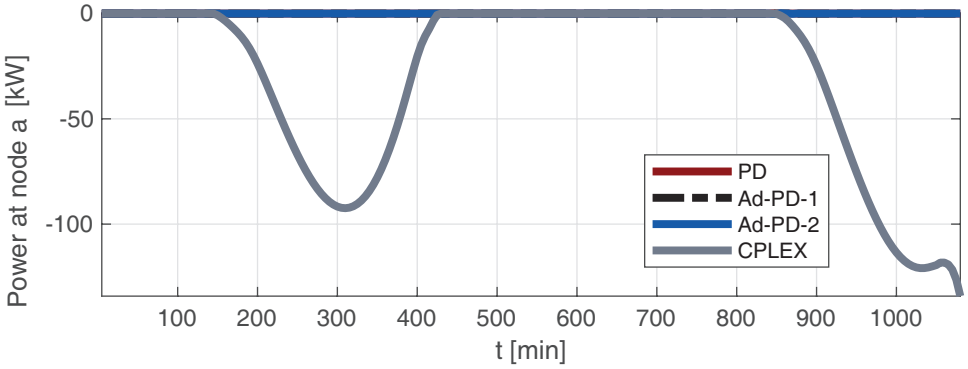

Figure 5.5: Optimal power at the electrical node a for the different solution approaches. The CPLEX approach does not satisfy the power balance with equality.

the other approaches, we cannot guarantee that the power profiles for the rest of subsystems are physically realizable.

5.3.3. Effects of the Adaptive Step-size Selection

The use of the adaptive step-size selection described in Algorithm 2 directly simplifies in the implementation of Algorithm 1. This can be observed from the number of parameters selected to implement the approach PD and the adaptive approaches Ad-PD-1 and Ad-PD-2. In particular, from Table 5.3 and Table 5.4, we observe that PD needs to select 18 parameters Ad-PD-1 and Ad-PD-2 only need to choose 5 parameters. Moreover, if the time horizon is split in more intervals, the number of parameters needed in PD will drastically increase while for Ad-PD-1 and Ad-PD-2 this number will remain the same.

An additional advantage of the adaptive implementations is that, for most of the cases, they could achieve a better numerical performance than implementations with static step-sizes. This is observed in Fig. 5.6, where the convergence of the approaches PD, Ad-PD-1 and Ad-PD-2 is given in terms of the evolution of the merit function

$$\varphi = \sum_{k\in\mathcal{K}} u_{ice,k} + \left\| y_{hvb,k} + y_{em,k} + u_{comp} + v_{a,k} \right\|^2 + \left\| -u_{ice,k} - u_{em,k} + v_{b,k} - y_{br,k} \right\| + \left\| y_{hvac,k} - y_{comp,k} + v_{c,k} \right\| \tag{5.42}$$

with respect to the number of iterations. The convergence of PD algorithm is smooth compared AD-PD-1 and AD-PD-2. However, PD is takes a significant number of additional iterations to converge. This is also observed in Table 5.5, where the computation time of Ad-PD-1 and Ad-PD-2 is approximately one order of magnitude lower than the convergence time for PD. These results do not necesarily imply that using the adaptive step-size selection presented Algorithm 2 automatically leads to a better performance. However, in this analysis we highlight that the use of Algorithm 2 could simplify the implementation of the optimization method described

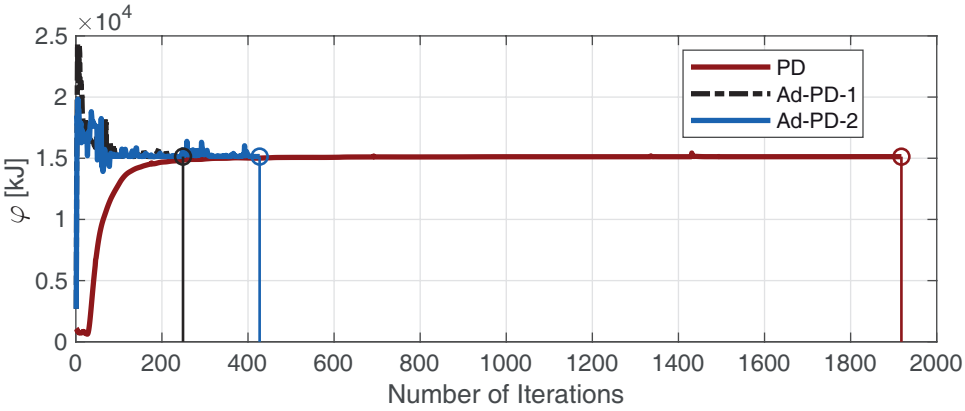

Figure 5.6: Convergence of the approches PD, Ad-PD-1 and Ad-PD-2 using to merit function φ. The approahes with adaptive step-sizes need less iterations to converge.

Table 5.5: Convergence results in therms of cost, number of iterations and computation time for the approaches PD, Ad-PD-1 and Ad-PD-2.

	Cost [l/100 km]	Iterations	Time [s]
PD	9.97	1918	246.9
Ad-PD-1	9.97	249	30.11
Ad-PD-2	9.97	427	49.90

in Algorithm 1, by reducing the number of tuning parameters, and achieve good performance.

5.3.4. Selection of Optimal Solutions

In practice, some specific solutions can be preferred among the set of all possible global solutions of the CVEM OCP. For instance, a smooth power profile for the HVB could be beneficial for reducing battery aging. This motivates the necessity of a tool to steer the iterations of Algorithm 1 towards a desired solution. This tool is the vanishing penalty function introduced in Section 5.1.4. To illustrate this concept, we will use the guidelines given in Section 5.2.4 to define the following vanishing penalty function

$$\boldsymbol{\nu}(\mathbf{u}_{hvb}^{i}) = \begin{cases} \frac{1}{i}\boldsymbol{\vartheta}(\mathbf{u}_{hvb}^{i}), & \text{if } i \leq 150; \\ 0, & \text{otherwise,} \end{cases} \tag{5.43}$$

where i represents the i-th iteration of the algorithm and $\vartheta(\cdot)$ is a function that captures specific features in the desired solution. For our analysis, we will use the following cases:

- **ℓ1-norm**: Considering $\vartheta(\mathbf{u}_{hvb}) = 0.5\,\|\mathbf{u}_{hvb}\|_1$, the vanishing penalty function (5.43) stimulates the existence of peaks in the HVB power profile.

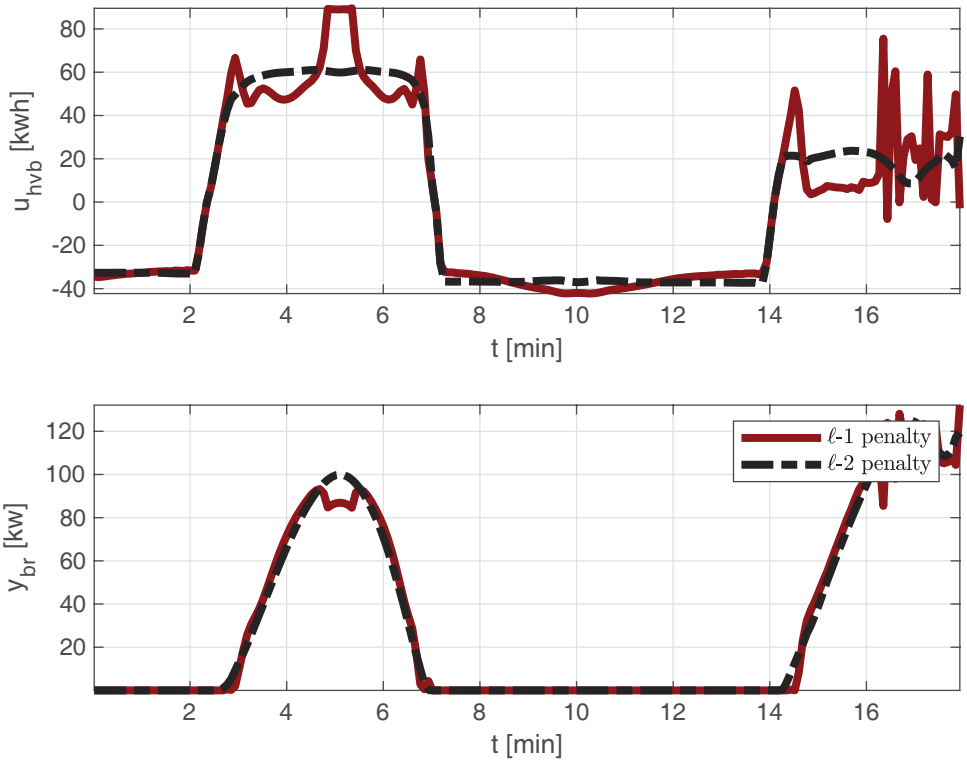

Figure 5.7: Selection of solutions using vanishing penalties. The $\ell 1$-norm case depicts a power profiles with larger peaks while $\ell 2$-norm case shows a smooth power profiles.

- **$\ell 2$-norm:** Considering $\vartheta(\mathbf{u}_{hvb}) = 2.5 \|\mathbf{u}_{hvb}\|_2^2$, a smooth power profile in the HVB is expected.

Note that (5.43) systematically reduces its magnitude with each iteration until it completely vanishes. At this point, we recover the original optimization problem (5.1) and the current iteration of algorithm might be close enough to the domain of attraction of the desired solution, thus converging to it. The solutions for the two vanishing penalties considered in this analysis are depicted in Fig. 5.7, where the expected properties for the $\ell 1$-norm and $\ell 2$-norm cases are observed in the HVB power profile. Interestingly, the penalties also have similar effects on power profiles, e.g., the braking power.

5.3.5. Horizon Splitting

In this section, we will illustrate the functionality of the horizon splitting feature introduced in Section 5.1.4. Although splitting the horizon directly affects the numerical performance of the method proposed in this chapter, we will leave this discussion Section 5.3.6. We split the discrete-time horizon into $L = 3$ intervals of similar length such that $\mathcal{K} = \bigcup_{\ell \in \mathcal{L}} \mathcal{K}_\ell$ with $\mathcal{L} = \{1, 2, 3\}$. For more details, refer to

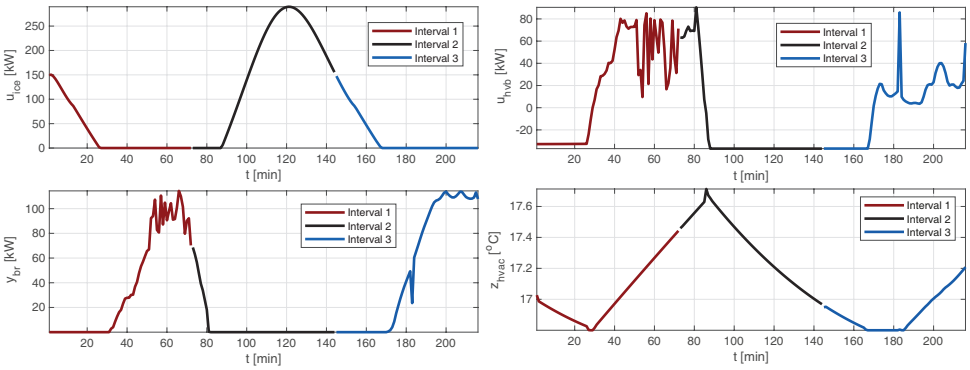

Figure 5.8: Horizon splitting: Input power profiles for the ICE and the HVB, braking power and cabin temperature for 3 time intervals.

step 4 in Section 5.1.4. We consider the settings of Ad-PD-1 presented in Table 5.4 to solve the OPC described under this configuration and ist solutions are depicted in Fig. 5.8. Here, the optimal power and temperature profiles show smooth transitions between the time intervals. As expected, the global optimal cost obtained is $9.77[L/100km]$, which is equal to the cost reported in Section 5.3.2 for the formulation that considers a single time interval. This is also consistent with the optimal ICE power profile depicted in Fig. 5.8, which shows virtually the same curve presented in Fig. 5.4. The multiplicity of global solutions is also noted by comparing the HVB power, the braking power the cabin temperature shown in Fig. 5.8 with the profiles presented in Fig. 5.4.

5.3.6. Scalability and Numerical Performance

The main focus of the analysis presented in this section is the scalability of the methods presented in this chapter. In particular, we will compare the scalability of the approaches Ad-PD-1 and CPLEX. To this end, we will consider a realistic power request with large time horizon to solve the parallel-hybrid vehicle CVEM problem described in Section 5.3.1. This will also allow us to discuss the numerical performance of the implementation Ad-PD-1 under different horizon splitting configurations.

In Fig. 5.9, the power request considered in this analysis is depicted. This power request has been obtained from a real driving cycle that describes a vehicle travelling form Rotterdam to Strasbourg and it contains 23808 data points sampled at $1[s]$. It should be noted that the dynamical representations of the HVB and the HVAC have been discretized with a sampling time of $1[s]$ to be compatible with the power request considered in this analysis. We will compare the computation time of Ad-PD-1 with a single time interval, i.e. $L = 1$, with respect to CPLEX for for different horizon lengths K.

The results depicted in Fig. 5.10 indicate that the computation time of CPLEX has a polynomial growth while Ad-PD-1 shows a linear tendency. Interestingly, CPLEX was not able to provide solutions for horizons lager than $320[s]$, as it is

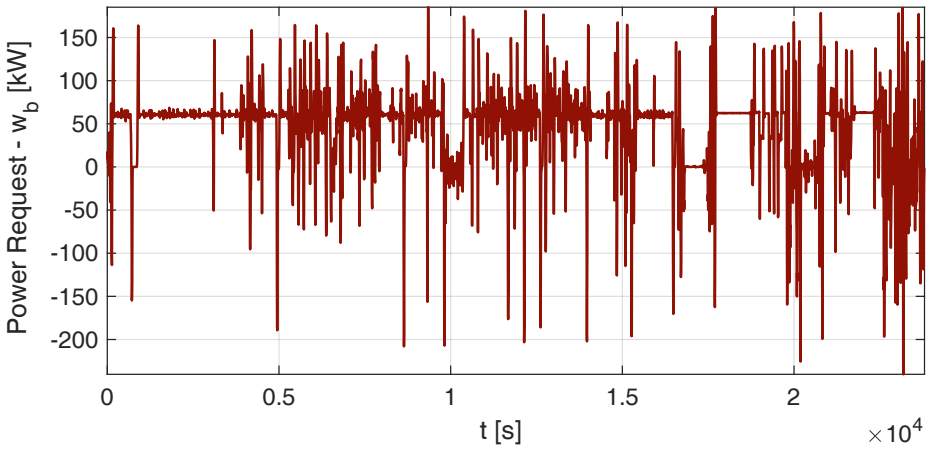

Figure 5.9: Power request considered for scalability and numerical performance analysis. The power request is a 6.6 hours profile obtained from a vehicle travelling from Rotterdam to Strasbourg.

Table 5.6: Computational performace: CPLEX vs. Ad-PD-1

	CPLEX		Ad-PD-1	
K [s]	Cost	Time [s]	Cost	Time [s]
60	11.45	111.45	14	
120	11.26	4	11.26	25
180	14.58	12	14.60	24
240	12.32	52	12.35	27
300	11.17	107	11.17	55
320	10.94	200	10.95	58
360	-	-	10.66	79

presented in Table 5.6. This limitation is due to memory usage. Specifically, in this example, we use the quadratically constrained quadratic programming solver from CPLEX [37], which consumes a large amount of memory to encode the complete set of quadratic power network constraints. On the contrary, Ad-PD-1 solves a sequence of coordinated smaller sub-problems for each subsystem, which is favorable in terms of memory use. Moreover, these sub-problems are constrained least squares programs with highly structured linear feasible sets, which can be solved very efficiently.

In Table 5.7, we complete the scalability analysis of Ad-PD-1 for the rest of the power request cycle considered in this example. Observe that this approach exhibits a linear trend in the computation time with respect to the horizon length for horizons bellow $10000[s]$. Moreover, it should be noted that for horizon lengths larger than $1000[s]$, the reported performance was achieved by splitting the time horizon into several intervals. It is important to remark that in this analysis, we

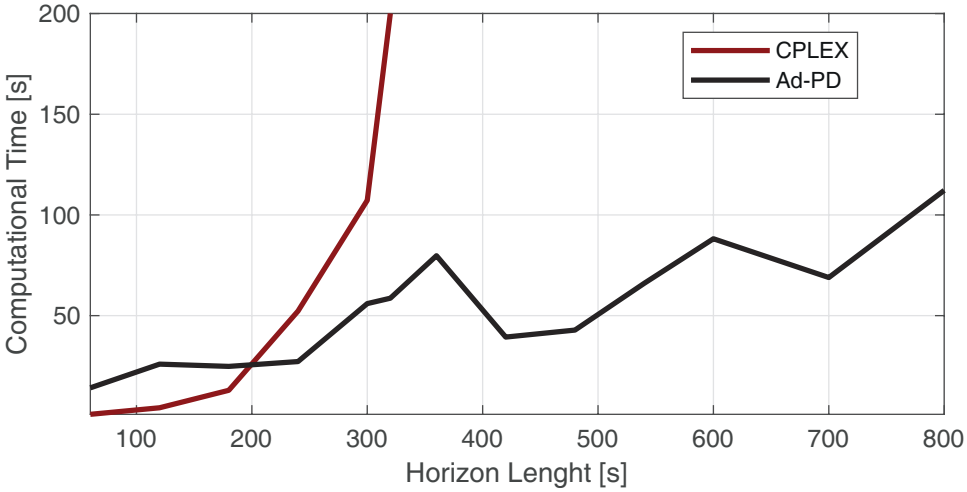

Figure 5.10: Computational perfrmance: CPLEX vs. Ad-PD.

have solved a large scale CVEM problem over a time horizon of approximately $7[h]$. The large-scale optimization problem has more than 4×10^5 decision variables and was solved using a basic desktop computer. This clearly illustrates the advantage of splitting the time horizon.

Splitting the horizon into several intervals helps to break-down the complexity of the optimization problem into several simpler sub-problems. Algorithm 1 was designed to obtain highly structured coordinated sub-problems, which bring as consequence improvement in the numerical performance of the algorithm. However, finding the ideal number of splitting intervals is non-trivial. A large number of intervals implies a large number of sub-problems and the coordination among them could become a bottleneck in Algorithm 1.

We will illustrate this idea by fixing the horizon length at $3000[s]$ and solving the CVEM problem with a different number of time splitting intervals. In Fig. 5.11, we present the results in terms of computation time and number of iterations. Note that the number of iterations tend to increase proportionally to the number of intervals used. However, this tendency is not observed for the computation time. From Fig. 5.11, we observe that the ideal splitting has 3 or 4 intervals. For the cases with one and two intervals, a higher computation time is observed although the number of iterations is lower. This is expected since the sub-problems are larger for those cases, therefore, consuming more computation time. On the other hand, for the cases with a number of intervals larger than 5, the number of iterations and also the computation time are larger. In those cases, the sub-problems are smaller but the coordination between a larger number of sub-problems takes more iterations and consequently the computation time also increases. The previous results show the advantage of decomposing the time horizon for large scale CVEM problems. However, the choice of the number of splitting intervals should be made with caution.

Table 5.7: Scalability of Ad-PD-1

K [s]	Cost	Time [s]	Iterations	Intervals
360	10.66	79	541	1
420	10.29	39	198	1
480	10.04	42	174	1
540	9.85	66	229	1
600	9.74	88	278	1
700	9.46	68	172	1
800	9.07	112	213	1
1000	9.82	108	243	3
2000	9.22	267	234	3
3000	9.06	592	212	3
6000	8.74	2100	185	3
10000	8.85	2867	384	10
23808	9.03	30126	1807	30

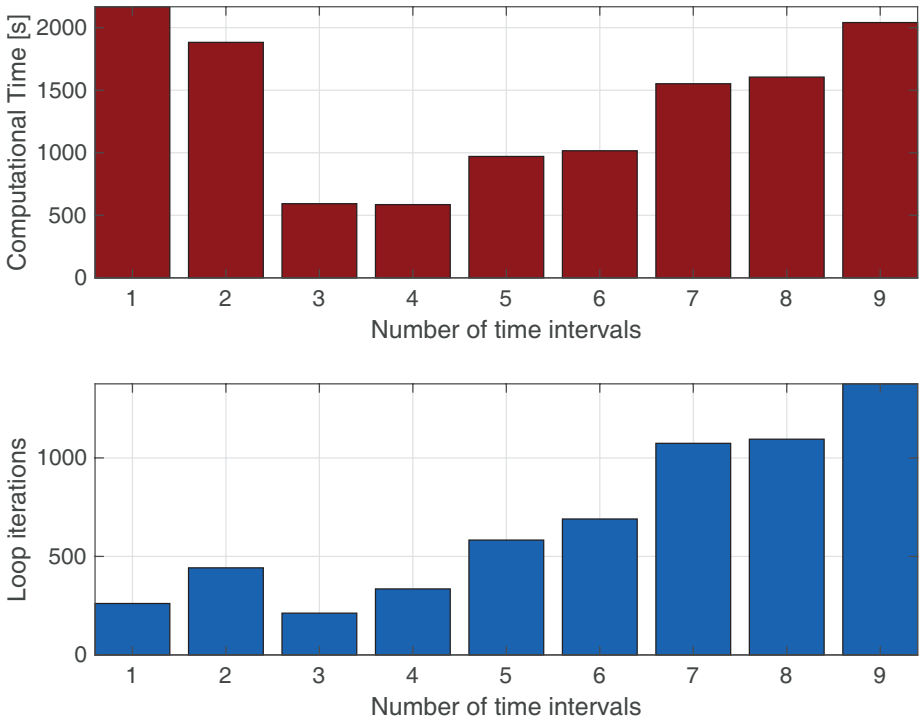

Figure 5.11: Computational perfrmance of Ad-PD-1 for different number of time intervals with K=3000[s].

5.4. Conclusions

In this chapter, we have developed scalable and flexible optimization methods for solving non-convex CVEM problem. By analyzing the inherent structure of OCP, we have proved that the non-convex CVEM problem only has global optimal solutions under mild conditions. We exploited this result in order to propose a reformulation of the CVEM problem that is separable in terms of interconnected subsystems and time intervals. The proposed formulation has been addressed using Primal Dual Splitting method to obtain a distributed optimization algorithm. The proposed algorithm breaks down the complexity of the problem into several simpler highly structured coordinated sub-problems, which has brought as consequence an improved scalability and computation time compared to the early work presented in [18]. Spectral methods have been be used to automatically select the step-sizes of the optimization algorithm at every iteration, which has not only simplified the implementation process but it also has provided a reduced computation time for convergence of the algorithm.

The regularization properties of our formulation allowed us to solve a CVEM problem for a parallel-hybrid vehicle case study that presents almost linear power losses, which was cumbersome with approaches like dual decomposition. Furthermore, we solved the CVEM for large horizon to demonstrate the scalability of the algorithm and its numerical performance. Specifically, this method as been able to solve the CVEM problem approximately 3 times faster than the CPLEX implementation and it has solved the problem with a 100 times larger time horizon. The results obtained have demonstrated that the methodology presented in this work can be used to solve large scale CVEM problems. Moreover, since we have provided guarantees for the global optimality of solutions obtained by the algorithm, this methodology could be used to create benchmarks for CVEM strategies without the necessity of rely to dynamic programing approaches.

References

[1] *Global EV Outlook 2017*, Tech. Rep. (International Energy Agency, 2017).

[2] *Electric vehicles in Europe*, Tech. Rep. (European Environment Agency, 2016).

[3] A. Sciarretta and L. Guzzella, *Control of hybrid electric vehicles,* Control Systems Magazine (2007).

[4] B. d. Jager, T. v. Keulen, and J. Kessels, *Optimal Control of Hybrid Vehicles*, Advances in Industrial Control (2013).

[5] L. Guzzella and A. Sciarretta, *Vehicle Propulsion Systems* (Springer, Berlin, Heidelberg, 2013).

[6] *Model-Based Supervisory Control for Energy Optimization of Hybrid-Electric Vehicles,* in *Control System Applications*, edited by L. Guzzella and A. Sciarretta (2009).

[7] J. Kessels, J. H. M. Martens, P. P. J. Van den Bosch, and W. H. A. Hendrix, *Smart vehicle powernet enabling complete vehicle energy management,* in *Proc. Vehicle Power and Propulsion Conference* (2012).

[8] S. Marinkov, N. Murgovski, and B. de Jager, *Convex modeling and optimization of a vehicle powertrain equipped with a generator–turbine throttle unit,* IEEE Trans. Control Syst. Tech. (2017).

[9] X. Hu, S. J. Moura, N. Murgovski, B. Egardt, and D. Cao, *Integrated optimization of battery sizing, charging, and power management in plug-in hybrid electric vehicles,* IEEE Trans. Control Syst. Tech. (2016).

[10] E. Feru, N. Murgovski, B. de Jager, and F. Willems, *Supervisory control of a heavy-duty diesel engine with an electrified waste heat recovery system,* Control Engineering Practice (2016).

[11] N. Murgovski, L. Johannesson, X. Hu, B. Egardt, and J. Sjöberg, *Convex relaxations in the optimal control of electrified vehicles,* in *Proc. American Control Conference* (IEEE, 2015).

[12] S. East and M. Cannon, *Energy management in plug-in hybrid electric vehicles: Convex optimization algorithms for model predictive control,* IEEE Transactions on Control Systems Technology , 1 (2019).

[13] S. East and M. Cannon, *Optimal power allocation in battery/supercapacitor electric vehicles using convex optimization,* IEEE Transactions on Vehicular Technology (2020), 10.1109/TVT.2020.3023186.

[14] S. East and M. Cannon, *Fast optimal energy management with engine on/off decisions for plug-in hybrid electric vehicles,* IEEE Control Systems Letters (2019).

[15] K. D. Nguyen, E. Bideaux, M. T. Pham, and P. Le Brusq, *Game theoretic approach for electrified auxiliary management in high voltage network of hev/phev,* in *Proc. IEEE International Electric Vehicle Conference* (2014) pp. 1–8.

[16] T. C. J. Romijn, M. C. F. Donkers, J. T. B. A. Kessels, and S. Weiland, *A distributed optimization approach for complete vehicle energy management,* IEEE Transactions on Control Systems Technology (2018).

[17] T. Romijn, M. Donkers, J. Kessels, and S. Weiland, *Real-time distributed economic model predictive control for complete vehicle energy management,* Energies (2017).

[18] G. P. Padilla, G. Belgioioso, and M. C. F. Donkers, *Global solutions to the complete vehicle energy management problem via forward-backward operator splitting,* in *Proc. IEEE Conference on Decision and Control* (2019).

[19] C. Clason, S. Mazurenko, and T. Valkonen, *Primal–dual proximal splitting and generalized conjugation in non-smooth non-convex optimization,* Applied Mathematics & Optimization (2020).

[20] R. Fletcher, *On the barzilai-borwein method,* in *Proc. Optimization and control with applications* (Springer US, 2005).

[21] S. P. Boyd and L. Vandenberghe, *Convex optimization* (Cambridge University Press, 2004).

[22] D. P. Bertsekas, *Nonlinear Programming* (Athena Scientific, 1999).

[23] D. W. Peterson, *A Review of Constraint Qualifications in Finite-Dimensional Spaces,* SIAM Review (1973).

[24] J. V. Burke, *Constraint qualifications for nonlinear programming - Numerical Optimization. Course Notes, AMath/Math 516,* (2012).

[25] H. H. Bauschke, P. L. Combettes, *et al.*, *Convex analysis and monotone operator theory in Hilbert spaces*, Vol. 2011 (Springer, 2017).

[26] E. K. Ryu and S. Boyd, *A Primer on Monotone Operator Methods,* Appl. Comput. Math. (2016).

[27] A. Lenoir and P. Mahey, *A survey on operator splitting and decomposition of convex programs,* RAIRO - Operations Research (2017).

[28] F. J. Gould and J. W. Tolle, *A Necessary and Sufficient Qualification for Constrained Optimization,* SIAM Journal on Applied Mathematics (1971).

[29] A. Chambolle and T. Pock, *A first-order primal-dual algorithm for convex problems with applications to imaging,* Journal of Mathematical Imaging and Vision (2011).

[30] A. Chambolle and T. Pock, *On the ergodic convergence rates of a first-order primal–dual algorithm,* Mathematical Programming (2016).

[31] C. Clason and T. Valkonen, *Primal-dual extragradient methods for nonlinear nonsmooth PDE-constrained optimization,* SIAM Journal on Optimization (2017).

[32] C. Clason, S. Mazurenko, and T. Valkonen, *Acceleration and global convergence of a first-order primal-dual method for nonconvex problems,* SIAM Journal on Optimization (2019).

[33] H. Bauschke and P. Combettes, *Convex analysis and monotone operator theory in Hilbert spaces* (Springer Science+Business Media, 2016).

[34] S. J. Wright, R. D. Nowak, and M. A. T. Figueiredo, *Sparse reconstruction by separable approximation,* IEEE Transactions on Signal Processing (2009).

[35] T. Goldstein, C. Studer, and R. Baraniuk, *A field guide to forward-backward splitting with a FASTA implementation,* (2014).

[36] B. Zhou, L. Gao, and Y.-H. Dai, *Gradient methods with adaptive step-sizes,* Computational Optimization and Applications (2006).

[37] IBM Corp: IBM ILOG CPLEX V12.1, *User's Manual for CPLEX (2009)*.

6

Traffic-Aware Vehicle Energy Management Strategies via Scenario-Based Optimization

This chapter explores the development of traffic-aware energy management strategies by means of scenario-based optimization. This is motivated by that fact that real driving conditions are subject to uncertainty, thereby making the real-time optimization of the energy consumption of a vehicle to be a challenging problem. In order to deal with this situation, we employ the current framework of complete vehicle energy management in a receding horizon fashion, in which we consider random constraints representing realizations of exogenous signals, i.e., the uncertain driving conditions. Additionally, we study three methods for velocity prediction, i.e., a method based on (average) traffic flow information, a method based on Gaussian process regression, and a method that combines both. The proposed strategy is tested with real traffic data using a case study of the power split in a series-hybrid electric vehicle. The behavior of the battery, control inputs and fuel consumption generated with the resulting strategies are compared against the optimal solution from offline optimization and a receding horizon strategy with perfect prediction of the future, For the considered case, the use of a Gaussian process regression and the traffic speed achieves near optimal fuel consumption.

This chapter is based on **P.3**.

Energy management strategies (EMS) typically require the driving cycle to be known a priori. Unfortunately, the driving cycle is affected by the presence of uncertain driving conditions, e.g., traffic congestion, varying speed limits and different driving styles. Therefore, limiting the performance of real-time implementations of energy management strategies. Alternatively, stochastic optimal control methods provide noticeable extensions for Traffic-aware Energy Management Strategies (TaEMS), i.e., strategies that take into account the uncertainty present in real traffic conditions. These strategies are typically obtained using Stochastic Dynamic Programming (SDP) [1], which suffers from scalability problems known as *"Curse of Dimensionality"*, or Stochastic MPC [2], which could become computationally demanding when the number of subsystems considered in the control problem increases. Nevertheless, the need to account for the presence of uncertainty is still an open topic to improve the implementation capabilities of these EMS.

In this chapter, we use the recent developments of scenario-based optimization [3–5] to extend the CVEM framework presented in Chapter 5 of this thesis. This aims to achieve a tractable method for traffic-aware complete vehicle energy management, in which an intuitive tradeoff can be made between computational complexity and robustness depending on the number of scenarios considered. Furthermore, the proposed method has the potential of using distributed optimization techniques to improve its implementation capabilities (although this will not be addressed in this chapter). In addition, we propose the use of Gaussian Processes Regression for this TaEMS to generate multiple predictions of the future driving situations, i.e., sample random scenarios, which are combined with traffic flow information to provide long-term speed predictions.

This chapter is organized as follows: In Section 6.1, the general vehicle energy management problem formulation is presented and extended as an uncertain optimal control problem. A description of the prediction methods for traffic-aware vehicle energy management is included in Section 6.2. Section 6.3 presents the case study considered in this chapter and the simulation results obtained are detailed in Section 6.4. Finally, conclusions are presented in Section 6.5.

6.1. Traffic-Aware Vehicle Energy Management

In this section, we present the mathematical formulation describing the optimal control problem arising from the CVEM framework in a receding horizon fashion. Additionally, an extension of the resulting Receding-Horizon Optimal Control Problem (RHOCP) in the context of scenario-based optimization is introduced to account for uncertain factors affecting a vehicle, i.e., the uncertain power request caused by, e.g., unknown driving conditions.

6.1.1. Receding Horizon Optimal Control Problem

In general, the CVEM problem aims to define the optimal energy flows between the subsystems in the power network of a vehicle over a prediction horizon $k \in \mathcal{K} =$

$\{0, 1, \dots, K-1\}$ given the measurements at time step $t \in \mathbb{N}$ represented by

$$\min_{\{u_{m,k|t}, y_{m,k|t}, x_{m,k|t}\}} \sum_{m\in\mathcal{M}} \sum_{k\in\mathcal{K}} a_{m,k} y_{m,k|t} + b_{m,k} u_{m,k|t} \tag{6.1a}$$

where $x_{m,k|t} \in \mathbb{R}^{n_m}$ are the states, $u_{m,k|t} \in \mathbb{R}$ are scalar inputs and $y_{m,k|t} \in \mathbb{R}$ are scalar outputs of the converter of subsystem $m \in \mathcal{M} = \{1, \dots, M\}$, and the coefficients $a_{m,k} \in \mathbb{R}_{+0}$, $b_{m,k} \in \mathbb{R}$ define the desired cost metric based on the energy consumed by each subsystem at time instant $k + t$. For instance, setting all coefficients to zero apart from $a_{1,k}$ and assuming that $m = 1$ corresponds to the combustion engine results in a fuel consumption minimization, where $y_{1,k|t}$ represents the chemical fuel power flow and $a_{1,k}$ can be either a constant or variable coefficient, e.g., sampling time. Note that the subscript $[\cdot]_{\cdot|t}$ will be dropped for clarity of the notation as the terms $\{u, y, x, w\}$ throughout this chapter define predictions at time $k + t$ given information of time $t \in \mathbb{N}$ and $k \in \mathcal{K}$.

The minimization of (6.1a) is subject to a set of constraints describing the behavior of the vehicle's power network and the exchanges of power in it (Fig. 6.1a shows a general network structure). First, we consider quadratic equality constraints that define the input-output behavior of the converter in each subsystem

$$y_{m,k} = \tfrac{1}{2}\gamma_{2,m} u_{m,k}^2 + \gamma_{1,m} u_{m,k} + \gamma_{0,m} \tag{6.1b}$$

with $\gamma_{2,m} \in \mathbb{R}_+$, $\gamma_{1,m} \in \mathbb{R}$ and $\gamma_{0,m} \in \mathbb{R}$ being coefficients that define the efficiency of converter $m \in \mathcal{M}$. Furthermore, the network presents different states that are being controlled, imposing constraints based on the linear system dynamics of the energy buffers

$$x_{m,k+1} = A_{m,k} x_{m,k} + B_{m,k} u_{m,k} \tag{6.1c}$$

with $\gamma_{2,m} \in \mathbb{R}_+$, $\gamma_{1,m} \in \mathbb{R}$ and $\gamma_{0,m} \in \mathbb{R}$ being coefficients that define the efficiency of converter $m \in \mathcal{M}$. Furthermore, the network presents different states that are being controlled, imposing constraints based on the linear system dynamics of the energy buffers

$$x_{m,k+1} = A_{m,k} x_{m,k} + B_{m,k} u_{m,k} \tag{6.1d}$$

in which $x_{m,k} \in \mathbb{R}^{n_m}$ and $u_{m,k} \in \mathbb{R}$ denote the predicted states and inputs, respectively, of subsystem $m \in \mathcal{M}$, and where the initial states $x_{m,0}$ are known. The admissible states and inputs are subject to constraints, i.e.,

$$x_{m,k} \in \mathcal{X}_m \quad \text{and} \quad u_{m,k} \in \mathcal{U}_m \tag{6.1e}$$

Moreover, the interconnections of subsystems are described by $\mathcal{J} = \{1, \dots, J\}$ nodes and no direct interactions between them are considered, i.e., each subsystem can be connected only to a node, resulting in the power balances

$$g_j(y_{m,k}, u_{m,k}, w_{j,k}) \leq 0 \tag{6.1f}$$

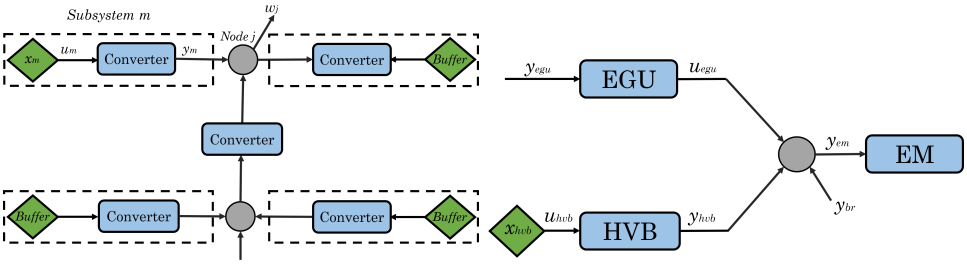

(a) Power network structure (b) Powertrain topology

Figure 6.1: CVEM diagrams.

for all $j \in \mathcal{J}$ and $k \in \mathcal{K}$, in which:

$$g_j(y_{m,k}, u_{m,k}, w_{j,k}) = \sum_{m \in \mathcal{M}} c_{j,m} y_{m,k} + d_{j,m} u_{m,k} + w_{j,k} \tag{6.1g}$$

In (6.1f), $w_{j,k}$ are exogenous signals acting on each node, e.g., the power request from the driver or the auxiliaries. Generally for EMS, it is assumed that these exogenous signals are known in advance or can be perfectly predicted. However, this might not be always true, as they are generated by the environment or external factors, e.g., the driver. Therefore, we can consider that these unknown exogenous signals have a stochastic nature, turning the CVEM problem (6.1) into a Stochastic RHOCP. Even though different methods can be used to solve this problem, we make use of the scenario approach [3] to solve the resulting uncertain RHOCP in a computationally advantageous way as presented in the remainder of this section (Detailed information on the CVEM framework can be found in Chapter 5).

6.1.2. Stochastic RHOCP

Before presenting the scenario approach, let us consider a stochastic extensions to problem (6.1) accounting for the unknown exogenous signals $w_{j,k}$ in nodes $j \in \mathcal{J}$. In particular, we can post the resulting CVEM problem as the following chance-constrained RHOCP

$$\min_{\{u_{m,k}, y_{m,k}, x_{m,k}\}} \sum_{m \in \mathcal{M}} \sum_{k \in \mathcal{K}} a_{m,k} y_{m,k} + b_{m,k} u_{m,k} \tag{6.2a}$$

subject to (6.1b) - (6.1e), and

$$Pr\{g_j(y_{m,k}, u_{m,k}, w_{j,k}) \leq 0\} \geq 1 - \epsilon_j \tag{6.2b}$$

where the parameters ϵ_j are acceptable infeasibility levels and the functions g_j are defined as in (6.1f). Here, the need to guarantee that the chance-constraints (6.2b) will hold for any realization of $w_{j,k}$ becomes a major restriction, since the distributions of these exogenous signals might be unknown and, even if they are known, the solution could be more conservative and lead to an undesired performance.

6.1.3. Scenario-Based Traffic-Aware Energy Management

In order to deal with the characteristics of the chance-constrained formulation in the previous section, we make use of the scenario approach [3] instead. This methodology for data-driven optimization aims to solve the resulting chance-constrained RHOCP by means of a deterministic approximation that considers only a finite number of realizations of the unknown exogenous signals $w_{j,k}$, where taking more samples into account increases the chances of satisfying (6.1f), thereby providing a tuning knob to balance robustness versus performance of the scenario solution. This allows to achieve a computationally tractable problem when multiple subsystems are considered, in comparison to classic stochastic EMS based on SDP [1]. With this in mind, the power balances (6.2b) in problem (6.2) can be replaced by a deterministic set of randomly sampled constraints (scenarios), leading to what we refer to as scenario-based TaEMS.

Now, following the scenario approach and the results in [4, 5], we introduce some definitions and assumptions required for the scenario-based RHOCP:

1. The uncertainties $w_{j,k}$ of each node are contained in a single variable $w_k = [w_{1,k}, \dots, w_{J,k}]^\intercal$ which is a random variable with (maybe unknown) probability measure *Pr* and support set $\mathcal{W}$.

2. A sequence of variables $\{w_0^{[\iota]}, \dots, w_{K-1}^{[\iota]}\}$, where $\iota \in \mathcal{I}$ is the $\iota - th$ realization of the uncertainty w_k over the prediction horizon defining the scenario $w^{[\iota]}$.

3. Enough independent and identically distributed (i.i.d.) samples $w^{[\iota]}$ can be obtained at every time instant, giving a set of scenarios $\mathcal{I} = \{1, \dots, I\}$.

4. The scenario-based RHOCP problem has a feasible solution for every $w^{[\iota]}$.

With this definitions, the resulting scenario-based TaEMS problem is given by

$$\min_{\{u_{m,k}, y_{m,k}, x_{m,k}\}} \sum_{m \in \mathcal{M}} \sum_{k \in \mathcal{K}} a_{m,k} y_{m,k} + b_{m,k} u_{m,k} \tag{6.3a}$$

subject to

$$y_{m,k} = \tfrac{1}{2}\gamma_{2,m} u_{m,k}^2 + \gamma_{1,m} u_{m,k} + \gamma_{0,m} \tag{6.3b}$$

$$x_{m,k+1} = A_{m,k} x_{m,k} + B_{m,k} u_{m,k} \tag{6.3c}$$

$$x_{m,k} \in \mathcal{X}_m, \quad u_{m,k} \in \mathcal{U}_m \tag{6.3d}$$

and

$$g_j(y_{m,k}, u_{m,k}, w_{j,k}^{[\iota]}) \leq 0, \tag{6.3e}$$

for all $\iota \in \mathcal{I}$ and $j \in \mathcal{J}$, and $k \in \mathcal{K}$, $m \in \mathcal{M}$.

It is important to remark that assumption 4 which is linked to [5, Assumption 5], seems to be restrictive for our application. In practice, the infeasibility of the constraints implies that the vehicle cannot provide enough power to satisfy the power balance at some time instant. This might lead to reduced drivability / user comfort and not to problems with vehicle safety. Moreover, as it is also discussed in [5], the

feedback action is expected correct this in the future iterations of the receding horizon control. A possible approach to enforce feasibility during the implementation of this approach is to relax the inequality (6.3e) as

$$g_j(y_{m,k}, u_{m,k}, w_{j,k}^{[\iota]}) \leq \epsilon,$$

where $\epsilon \geq 0$ is an auxiliary decision variable that is penalized in the cost function (6.3a).

From (6.3), we make use of the results in [4] to address the selection of the number of scenarios required for a particular feasibility level. To this end, let us define the probability of constraint violation

$$V_{j,k}(y_{m,k}^*, u_{m,k}^*) = Pr\{g_j(y_{m,k}^*, u_{m,k}^*, w_{j,k}^{[\iota]}) > 0\} \tag{6.4}$$

where $u_{m,k}^*$, $y_{m,k}^*$ refer to the scenario solution. It has been shown in [3] and [4] that $V_{j,k}(y_{m,k}^*, u_{m,k}^*)$ is bounded by a Beta distribution $\mathbf{B}(\rho_j, I - \rho_j + 1)$, such that

$$Pr^I\{V_{j,k}(y_{m,k}^*, u_{m,k}^*) > \epsilon_j\} \leq \mathbf{B}(\rho_j, I - \rho_j + 1) \tag{6.5}$$

where ρ_j is the support rank of the constraint in node j and Pr^I is the $I-th$ product of Pr for the sampled scenarios. Here, we make use of the results in [4] instead of considering the number of decision variables as in the classic scenario approach presented in [3]. This is favorable as only a reduced number of the decision variables in problem (6.3) is affected by (6.3e) at every step on the prediction horizon k regardless of the number of sampled scenarios.

From this formulation, we aim to find the minimum number of samples required to satisfy the original chance constraint, as the more samples are drawn, the more conservative the solution becomes. Nevertheless, given that new samples are drawn at each time step, we consider a bound on the expected violation probability $\mathbb{E}^I[V_{j,k}(y_{m,k|t}^*, u_{m,k|t}^*)] \leq \epsilon_j$, which leads to a sample size of $\epsilon_j \leq \rho_j/(I+1)$. This result follows from the integration of (6.5), which can be interpreted as the probability that the $I+1$ sample becomes a support constraint, i.e., the solution obtained with the scenarios $\mathcal{I}$ does not satisfy the power balances $g_j(\cdot) \leq 0$ (see [3–5] for further details and proofs).

6.2. Scenario Generators

In order to make predictions of the unknown traffic conditions, and thus the exogenous signals $w_{j,k}$, we present the three velocity prediction methods used in this work, e.g., predictions based on GPS/eHorizon data, predictions using a Gaussian Process Regression (GPR) model, and a mixed generator that combines both the GPS and the GPR model.

6.2.1. GPS / eHorizon Methods

First, we consider that the vehicle has access to traffic information through a Global Positioning System (GPS) or an electronic horizon (eHorizon), which are devises

available in today's vehicles. Here, the average traffic speed is calculated based on the traffic flow through a particular section of the road as follows:

$$v_{avg,tw}^{\eta} = \frac{1}{P_\eta} \sum_{p=1}^{P_\eta} v_{tw}^{p},$$

where η are the road sections and P_η is number of vehicles passing through a particular road section during a time window, e.g., an update frequency between 1 to 5 minutes, as is usually done in mapping and traffic management systems [6, 7]. Here, the generation of speed predictions assumes that the vehicle will follow the latest traffic speed recorded depending on the road section where it is located.

6.2.2. Gaussian Process Regression

Since the average traffic speed only provides a deterministic estimate of the traffic situation, a probabilistic model to forecast the future speed of the vehicle is proposed in this section. In particular, we propose to use a Gaussian Process Regression model [8]. The selection of this non-parametric model is motivated by the remarkable prediction capabilities achieved with machine learning methods in [9–11] and, at the same time, its particular ability to provide a direct measure for the uncertainty of the predictions. For our application, the GPR model is employed as a predictor for a Nonlinear Auto-Regressive Model (NAR-GP), which results in regressing a function $\mathbf{z}_k = \mathbf{f}(\mathbf{q}_k) + \mathbf{e}_k$ with a feature vector $\mathbf{q}_k = \{v_{k-p}, \dots, v_k\}$ that predicts the future speed $\mathbf{z}_k = \{v_{k+1}\}$. Additionally, $\mathbf{e}_k \sim \mathcal{N}(0, \sigma_n^2)$ is a noise term acting on the output of the function and $\mathbf{f} \sim \mathcal{GP}(\mu, ker)$ is a GPR defined with a prior distribution with $\mu = 0$, a kernel function ker, e.g., squared exponential, Matérn, etc, and a set of hyper-parameters Θ. Furthermore, the definition of these hyper-parameters is done by minimizing the negative log-likelihood function on training data $\mathbf{D} = \{(q_n, z_n) \mid n = \{1, \dots, N\}\}$, see [8] for further details.

Once the NAR-GP is fully defined, we obtain a model that allows us to generate random samples from the posterior distribution, such that

$$v_{k+1} \sim Pr(z_*|\mathbf{D}, q_*) = \mathcal{N}(\overline{f}_{post}, ker_{post} + \sigma_n^2; \Theta) \tag{6.6a}$$

in which

$$\overline{f}_{\text{post}} = ker^{\intercal}(q_*)(ker + \sigma_n^2\mathbf{I})^{-1}\mathbf{z} \tag{6.6b}$$

$$ker_{\text{post}} = ker(q_*, q_*) - ker^{\intercal}(q_*)(ker + \sigma_n^2\mathbf{I})^{-1}ker(q_*) \tag{6.6c}$$

with $\mathbf{z}$ the output training data, $\mathbf{I}$ the identity matrix and points q_*, z_* referring to a test input and output, respectively. For this method, we consider a *naive* approach to generate the predictions over the horizon $\mathcal{K}$, neglecting the propagation of uncertainty to simplify the process and avoid intractable predictions with large speed changes.

Although predicting over multiple time steps ahead with the NAR-GP results in predictions at uncertain inputs, i.e., regressing the prediction of v_{k+1} that is a

random variable, we only consider a *naive* approach to generate the predictions over the prediction horizon $\mathcal{K}$, since it simplifies the prediction process and avoids large speed changes which might result in intractable predictions.

6.2.3. Mixed Generator Approach

Given that long prediction horizons lead to a better performance of the EMS [12], a combination of the velocity prediction methods is considered in this work in order to exploit the benefits of each method, e.g., account for the uncertainty in a short-term and preserve the preview of the traffic situation given by the average traffic speed. This combination is motivated by the fact that most of the maneuvers in car following or traffic situations require a very short time (see [10] and references therein) and the possible mismatch between the traffic speed and the individual speed profiles. At the same time, it is known that machine learning methods tend to incur in large prediction errors when the prediction horizon length increases, as these methods are not able to account for long-term traffic dependencies [11]. In fact, most of the methods present in the literature are restricted to predictions of 10 seconds in the future and, therefore, the integration of external information could lead to substantial fuel savings while generating more robust solutions against the actions of the driver.

6.3. Case Study Description

In this section, we present a case study is based on a series hybrid vehicle. The relative simplicity of this will allow us to evaluate the potential of the proposed TaEMS formulation. We will start by presenting the RHOCP formulation, followed by the selection of the sample size and the explanation of the power request determination.

6.3.1. Receding Horizon Optimal Control Problem

The case study in this chapter considers a series-hybrid electric vehicle (SHEV), which powertrain topology is represented as the network of energy buffers depicted in Fig. 6.1b with $m = \{egu, hvb, em\}$. In this figure, EGU stands for Engine/Generator Unit, with y_{egu} being the fuel consumption and u_{egu} the power supplied by the EGU to the power network. Furthermore, u_{hvb} and y_{hvb} define the electric power coming from the High-Voltage Battery (HVB) and x_{hvb} represents the stored energy in the battery. Besides this subsystems, the Electric Motor (EM) provides y_{em}, which represents the (unknown) power request defined by the driver. Note that y_{em} propels the vehicle when being positive and brakes the vehicle when being a negative value.

The node interconnecting the elements in the network defines a power balance as in (6.1f), where the parameters $c_{hvb} = 1$, $d_{egu} = -1$ and $c_{em} = 1$ are specified according to the flow direction of the power for each subsystem and all the others are set to zero. On top of this, an external braking signal y_{br} is introduced to account for the mechanical braking that dissipates the excess of energy in the powertrain and $x_{hvb,0} = x_{hvb,K}$ is included in (6.3d). According to the problem

Table 6.1: Powertain model coefficients

EGU		
$\gamma_{2,egu} = 2 \cdot 10^{-5}$	$\gamma_{1,egu} = 2.52$	$\gamma_{0,egu} = 19$
$\overline{u}_{egu} = 210$ [kW]	$\underline{u}_{egu} = 0$ [kW]	
HVB		
$\gamma_{2,hvb} = 1.671 \cdot 10^{-3}$	$\gamma_{1,hvb} = -1$	$\gamma_{0,hvb} = 0$
$\overline{u}_{hvb} = 92.4$ [kW]	$\underline{u}_{hvb} = -92.4$ [kW]	$x_{hvb,0} = 11988$ [kJ]
$\overline{x}_{hbv} = 22680$ [kJ]	$\underline{x}_{hbv} = 7560$ [kJ]	$x_{hvb,K} = 11988$ [kJ]

formulation in Section 6.1.1, the task of reducing the fuel consumed by the SHEV is described by the cost function (6.1a) with $a_{egu,k} = \tau_k$ and all the remaining parameters $a_{m,k} = b_{m,k} = 0$, as they do not contribute to the objective of the problem and where τ_k is the sampling interval along the prediction horizon $\mathcal{K}$. In this case, $y_{em,k}$ is considered to be an uncertain consequence of the driver actions and only the power request $y_{em,0}$ is known at the current time step t, which is a realistic assumption given the on-board sensors in today's vehicles. Furthermore, Table 6.1 presents the parameters defining the powertrain in this case study.

By substituting (6.3b) for the EGU in (6.3a) and considering the case study's parameters, the problem can be reformulated as a Quadratically Constrained Quadratic Program (QCQP) which can be efficiently solved with specialized solvers, e.g., CPLEX [13], resulting in

$$\min_{\{u_{m,k}\}} \sum_{k \in K} \tau_k \left(\tfrac{1}{2} \gamma_{2,egu} u_{egu,k}^2 + \gamma_{1,egu} u_{egu,k} + \gamma_{0,egu} \right) \tag{6.7a}$$

subject to

$$\underbrace{\tfrac{1}{2} \gamma_{2,hvb} u_{hvb,k}^2 + \gamma_{1,hvb} u_{hvb,k} - u_{egu,k}}_{g_{qcqp}} + \gamma_{0_{hvb}} \leq -y_{em,k}^{[\iota]} \tag{6.7b}$$

for all $\iota \in \mathcal{I}$ and

$$\Phi x_{hvb,0} - \Gamma \mathbf{u}_{hvb} \in \mathcal{X}_{hvb} \tag{6.7c}$$

$$u_{m,k} \in \mathcal{U}_m \tag{6.7d}$$

with $k \in \mathcal{K}$, $m \in \{egu, hvb\}$ and $\mathbf{u}_{hvb} = [u_{hvb,0}, \dots, u_{hvb,K-1}]^\top$. Note that (6.7c) is obtained by substituting (6.3c), for the HVB, in (6.3e). This eliminates the state variables through a prediction model as is generally done in linear MPC formulations. Note that this problem is convex since $\gamma_{2,m} > 0$, leading to a direct definition of the sample size for the scenario-based RHOCP.

6.3.2. Sample Size for Scenario-based RHOCP

Since the power balance (6.7b) is present for every prediction of time $k + t$, given information at time t, the problem has K scenario constraints and affect only the

particular inputs at that stage in horizon $\mathcal{K}$. Therefore, it is straightforward to define the support rank of the scenario constraint and specify the required sample size. In this case, the support rank of (6.7b) is calculated as in [4] and given by $\rho = d - \mathcal{L} = 2$, leading to an expected violation probability $\mathbb{E}^I[V_{j,k}(u^*_{m,k})] \leq \frac{2}{I+1}$, where $V_{j,k}(u^*_{m,k}) = Pr\{g_{qcqp} + (\gamma_{0_{hvb}} + y^{[\iota]}_{em,k}) > 0\}$. In this case study, we have defined a sample size of $I = 119$ implying a theoretical bound of $\epsilon \leq 2/120 \approx 1.66\%$. This percentage can be interpreted as the times when the vehicle will not provide enough power to follow the commands of the driver.

6.3.3. Power Request Definition

Given that the scenario generators forecast possible velocity profiles $\{v_1, \dots, v_{K+1}\}$, the power request is considered as the mechanical power $y_{em,k} = v_k u_{em,k}$, where a power limit $\overline{y}_{em} = \overline{u}_{egu} + \overline{y}_{hvb}$ is defined and the traction force $u_{em,k}$ required to follow each profile is calculated using an inverted vehicle dynamics model, given by:

$$y_{em,k} = \frac{v_k}{\sigma_u}\left(\frac{v_{k+1}-v_k}{\tau_k} + \sigma_v v_k^2 + \sigma_r + g\sin(\theta(s_k))\right) \tag{6.8}$$

where $\sigma_r = gc_r$, $\sigma_u = \frac{1}{m}$, $\sigma_v = \frac{1}{2m}c_d\rho_a A_f$ and θ define the rolling resistance, inverse of the mass, aerodynamic drag and the road slope, respectively. The definition and values of these coefficients for the vehicle in this case study can be found in Table 6.2 and a flat road is considered, i.e., $\theta = 0$.

6.4. Simulation Results

In order to analyse the performance of the scenario generators and the TaEMS for the power split problem, we first describe the particular characteristics considered in the simulations and, subsequently, we present results obtained with each method. Here, the solutions of the TaEMSs are compared to the optimal performance given by an offline benchmark and an online solution with perfect prediction of the future driving cycle. Additionally, we assess the benefits of hybridization under uncertain predictions by including the fuel consumption that would be generated if the power request was only covered by the EGU.

For this case study, we used the traffic data set from the *Mobile Century* field experiment [7], which was a project carried out over a 16 km section of the Interstate 880 highway in California to evaluate the use of GPS-enabled smartphones for accurate traffic information systems. The data was recorded from 10:00 to 18:00 and includes a traffic congestion event around 10:30 from where the driving cycles to evaluate the proposed TaEMS are taken (the reader is referred to [7] for further information and descriptions of the data used).

For implementation, we use a moving average filter with a Gaussian window to smooth intractable speed changes present in the predictions from the traffic speed or large noise realizations in the NAR-GP samples.

Table 6.2: Vehicle coefficients

Parameter	symbol	Value
Frontal drag area	A_f	7.5400 $[m^2]$
Drag coefficient	c_d	0.7
Rolling resistance	c_r	0.007
Air density	ρ_a	1.1840
Mass	m	15950 [kg]
Gravitational acceleration	g	9.81 $[m/s^2]$

6.4.1. GPS / eHorizon Method

In order to replicate the information supplied by a GPS, we have divided the road in 100 segments and have considered a time window $tw = 300$ seconds according to the update frequency in [7]. We consider that the vehicle has access to the average speed relative to the current time relative to the driving cycle, e.g., at 10:43 a.m. the information obtained at 10:40 a.m. is known and an update is available at 10:45 a.m.

6.4.2. Gaussian Process Regression

For this probabilistic velocity prediction method, the training data **D** was composed by real driving cycles taken from the *Mobile Century* data set starting before 10:30 a.m., and the HWFET, LA92 short and EPA standard driving cycles in order to provide more dynamic data to the model. Furthermore, the kernel function used in this work is the *Matérn*$\frac{5}{2}$ function, see, e.g., [8]. This selection was motivated by the fact that the real driving cycles present long braking patterns, which were not properly captured when using a squared exponential function due to its smoothness characteristics. Additionally, the total number of lags in the NAR-GP was set to 5, since it was observed that longer dependencies did not provide a substantial improvement of the predictions.

As an example, the mean predictions generated with the NAR-GP for Test Cycle 1 are shown in Fig. 6.2, where the top plot presents the prediction accuracy with different prediction horizons and the trajectories for 10 seconds of prediction are shown in the bottom plot. As it can be seen, when the predictions are made for short periods of time, e.g., 10 seconds, 95% of the errors are smaller than 1 m/s, which is acceptable for the development of energy management strategies. Nevertheless, these errors present an increasing trend when generating a velocity forecast for longer horizon lengths, as only short term correlations are captured from the training data and translated to the predictions while no information of the upcoming traffic is provided to the NAR-GP. Besides this, the NAR-GP occasionally generates wrong braking predictions, e.g., predictions around second 1100, but such errors are mitigated by the presence of multiple random samples that result in a more cautious use of the battery.

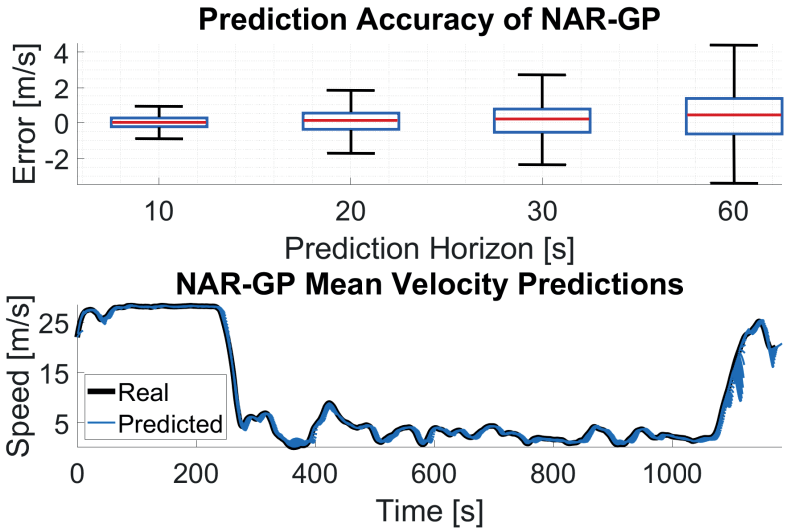

Figure 6.2: NAR-GP predictions for Test Cycle 1. Top: Error of the predicted mean vs. prediction horizon length. Bottom: Predicted mean speed with $K = 10$ seconds.

6

6.4.3. Prediction Horizon Length

In order to establish an appropriate length of the prediction horizon, the fuel consumption obtained with the GPS and the NAR-GP predictions were evaluated. Table 6.3 presents the fuel consumption with a perfect prediction, the scenario solution with the NAR-GP and the average traffic speed (GPS), where the offline benchmark and the EGU-only case (i.e., not using the battery) give the range of possible savings. It can be seen that a longer prediction horizon results in a lower consumption since it allows a larger deviation from the final state constraint imposed in the problem. For Test Cycle 1 and Test Cycle 2, the GPS captures the braking pattern accurately, leading to an appropriate use of the battery compared to the NAR-GP, where the battery is mainly used after the charging event due to prediction errors, see Fig. 6.3. Regarding the third test, the GPS incurs in a higher consumption with longer predictions, while the NAR-GP leads to better fuel economy. This is due to a softer deceleration that deviates from the traffic flow and, as seen in the perfect prediction case, reduces the advantage of a long horizon compared to the other tests.

6.4.4. Mixed Scenario Generator

As shown before, the NAR-GP is capable of producing accurate predictions when a short horizon is specified but fails to anticipate longer braking events, causing a higher fuel consumption. For this reason, and as a reference point with the literature, a horizon length of 10 seconds was selected to generate random speed profiles. After these predictions are made, the average traffic speed is used to complete the remaining part of the prediction horizon assuming that the driver

Table 6.3: Impact of prediction horizon on fuel consumption for the individual methods

Method	Horizon Length [seconds]	Fuel Consumption per Test Cycle [l]/100[km]			Relative Fuel Consumption Increase [%]		
		1	2	3	1	2	3
Offline	-	21.104	24.666	20.310	-	-	-
EGU-only	-	23.390	26.222	21.978	10.83	6.31	8.21
Perfect Prediction	20	22.101	25.689	20.872	4.72	4.15	4.79
	30	21.759	25.327	20.625	3.10	2.68	3.76
	60	21.166	24.748	20.362	0.29	0.33	1.20
	120	21.121	24.684	20.322	0.08	0.07	0.97
NAR−GP	20	22.951	25.731	21.282	8.75	4.32	4.79
	30	22.795	25.482	21.074	8.01	3.31	3.76
	60	22.312	25.353	20.553	5.72	2.79	1.20
	120	22.006	25.160	20.506	4.27	2.00	0.97
GPS	20	22.718	25.836	20.973	7.65	4.74	3.26
	30	22.444	25.459	20.889	6.35	3.21	2.85
	60	22.084	25.003	20.618	4.64	1.37	1.52
	120	21.702	24.947	20.766	2.83	1.14	2.25

follows the GPS after 10 seconds in order to keep the preview of the future traffic conditions and provide more freedom for the usage of the battery.

Finally, since longer horizons have a large impact in the computation time due to the increment of constraints and decision variables in the RHOCP, we incorporate the variable step-size approach proposed in [12] since, as indicated by the authors, coarser predictions of the future have minor impacts in the fuel savings while noticeably reducing the computation complexity of the problem. We consider $(\tau_1, \dots, \tau_K) = (1, 1, 2, 4, 6, 8, 10, 12, 16, 20, 40)$ as the step-size sequence used to generate long-term predictions, where the specific sequence follows the suggestion in [12], such that the total length of the predictions is 120 seconds.

The resulting fuel savings obtained with the mixed scenario generator are reported in Table 6.4, where we present the fuel consumed with 'full mixed' scenario generator (i.e., with constant step sizes $\tau_k = 1$ for all $k \in \mathcal{K}$), the 'variable mixed'

Table 6.4: Fuel consumption of TaEMS with mixed scenarios and GPS information

Method	Fuel Consumption per Test Cycle [l]/100[km]			Relative Fuel Consumption Increase [%]		
	1	2	3	1	2	3
Full Mixed	21.674	24.851	20.804	2.70	0.75	2.44
Variable Mixed	21.852	25.109	21.247	3.54	1.79	4.62
Variable GPS	22.220	25.423	21.136	5.29	3.06	4.07

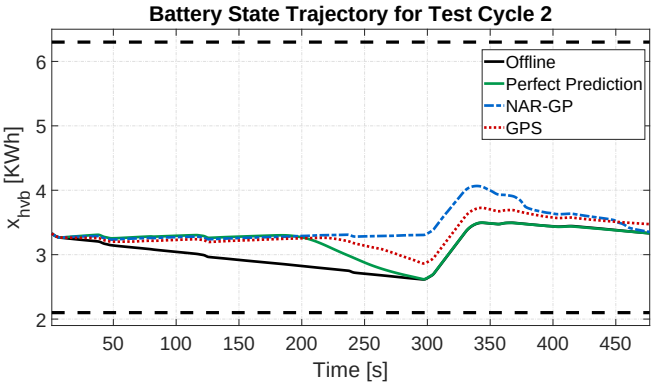

Figure 6.3: Trajectory of the energy stored in the battery for Test Cycle 2 (battery limits are shown as dashed lines)

scenario generator (i.e., with variable step sizes, as explained above) and applying the same variable step size sequence only to the average traffic speed, i.e., 'variable GPS'. Here, the last column presents the increment of fuel consumption relative to the optimal savings of the offline benchmark. Moreover, the state trajectory and the signals acting on the powertrain node in Test Cycle 2 are shown in Fig. 6.4.

From Table 6.4, it can be seen that the proposed TaEMS provides a slight improvement when the full predictions of the mixed scenario generator are considered in comparison to the GPS-based predictions. Nevertheless, the main advantage is observed when the decision variables are reduced by means of the variable sequence τ_k. In this case, we see that the fuel savings decreased as shown in [12] but the incorporation of multiple predictions leads to a better fuel economy, consuming only 0.75% more than the optimal solution in Test Cycle 2 when full predictions are used and 1.79% with the sampling sequence τ_k. On the other hand, the negative effect of faulty predictions is also visible, as the consumption increases due to the mismatch of the long-term predictions in Test Cycle 3.

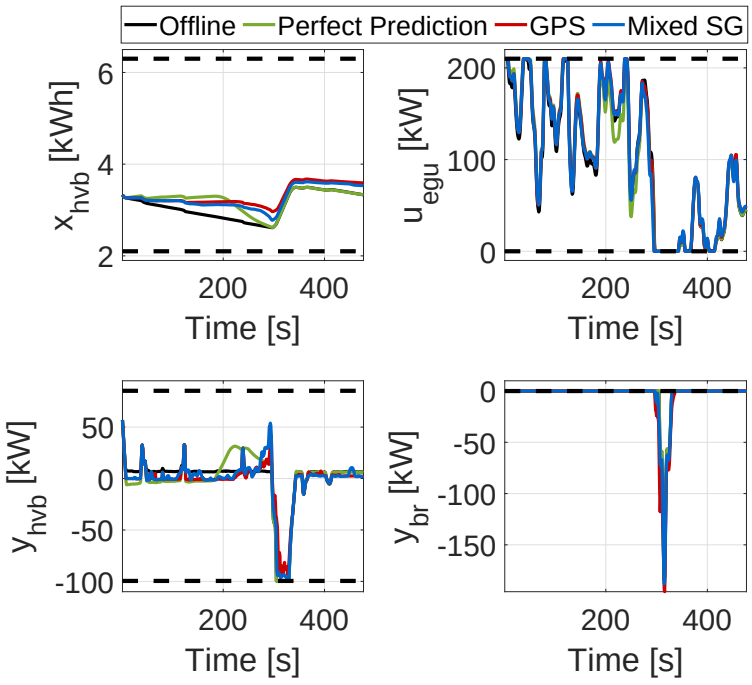

Figure 6.4: State trajectory and node signals from the TaEMSs using sequence τ_k in Test Cycle 2 (dashed lines: limits).

6.5. Conclusions

In this chapter, a traffic-aware energy management strategy that accounts for uncertain driving conditions has been developed. This strategy is based on the solution to a scenario-based optimal control problem used in a receding horizon fashion. The scenario-based approach reduces the probability of running out of energy during a driving mission. Different alternatives to include traffic information for the generation of scenarios have been explored, achieving a deviation of 0.75% from the optimal consumption with a suitable mix of the available information and 1.79% using variable step-size predictions. Nevertheless, the need of accurate traffic data becomes an essential factor for this TaEMS, however, such quality of information was provided by the traffic behavior in the highway situation considered.

References

[1] L. Johannesson, M. Asbogard, and B. Egardt, *Assessing the Potential of Predictive Control for Hybrid Vehicle Powertrains Using Stochastic Dynamic Programming,* IEEE Trans on Intell Transportation Syst (2007).

[2] S. Di Cairano, D. Bernardini, A. Bemporad, and I. V. Kolmanovsky, *Stochastic*

MPC With Learning for Driver-Predictive Vehicle Control and its Application to HEV Energy Managements, IEEE Trans on Control Syst Techn (2014).

[3] M. C. Campi and S. Garatti, *Introduction to the Scenario Approach, Volume 26 of MOS-SIAM Series on Optimization* (SIAM, 2018).

[4] G. Schildbach, L. Fagiano, and M. Morari, *Randomized Solutions to Convex Programs with Multiple Chance Constraints,* SIAM Journal on Optimization (2013).

[5] G. Schildbach, L. Fagiano, C. Frei, and M. Morari, *The scenario approach for stochastic model predictive control with bounds on closed-loop constraint violations,* Automatica (2014).

[6] HERE Global B.V, *HERE real-time traffic,* (2020), online; accessed 28-04-2020.

[7] J. Herrera, D. Work, R. Herring, X. Ban, Q. Jacobson, and A. Bayen, *Evaluation of traffic data obtained via gps-enabled mobile phones: The mobile century field experiment,* Transportation Research Part C: Emerging Technologies (2010).

[8] C. E. Rasmussen and C. K. I. Williams, *Gaussian Processes for Machine Learning* (The MIT Press, 2006).

[9] C. Sun, X. Hu, S. Moura, and F. Sun, *Velocity predictors for predictive energy management in hybrid electric vehicles,* IEEE Trans on Control Syst Techn (2015).

[10] S. Lefèvre, C. Sun, R. Bajcsy, and C. Laugier, *Comparison of parametric and non-parametric approaches for vehicle speed prediction,* in *Proc. American Control Conference* (2014).

[11] K. Liu, Z. Asher, X. Gong, M. Huang, and I. Kolmanovsky, *Vehicle Velocity Prediction and Energy Management Strategy Part 1: Deterministic and Stochastic Vehicle Velocity Prediction Using Machine Learning,* SAE Technical Paper (2019).

[12] T. Romijn, M. Donkers, J. Kessels, and S. Weiland, *Real-time distributed economic model predictive control for complete vehicle energy management,* Energies (2017).

[13] *IBM ILOG CPLEX V12.9 Users Manual for CPLEX* (2019).

7

A Port-Hamiltonian Approach to Complete Vehicle Energy Management: A Battery Electric Vehicle Case Study

In this chapter, we present a modelling approach to vehicle energy management based on Port-Hamiltonian systems representations. We consider a network of interconnected port-Hamiltonian systems that describes the powertrain components and auxiliaries in the vehicle. This description is suitable to obtain a systematic approach to formulate a decomposable optimal control problem for Complete Vehicle Energy Management. A physically insightful cost function that describes the total energy consumption of the vehicle is proposed in terms of internal energy and losses of each system connected to the network. Taking advantage of the modularity of the proposed formulation, we use a distributed optimization algorithm to find solutions to the energy management problem. To illustrate this modelling methodology, we consider a case study in which the energy consumption of a battery electric vehicle is optimized.

This chapter is based on **P.4**.

In the current literature related to vehicle energy management, the modelling and the optimal control problem (OCP) formulation are mainly obtained by applying power-based approaches like [1–3] or the one presented in Chapter 5. The main idea of these approaches is to describe the behavior of the interconnected subsystems in a network, in terms of power interactions. In other words, each subsystem is represented by an energy buffer connected to a power converter. The buffer stores energy and it is modeled as a linear dynamical system, which often resembles an integrator. The power converter represents energy consumption and is modeled as a static non-linear function, normally approximated to a quadratic function using measurements.

However, power-based approaches are difficult to use when the optimization variables cannot be easily described in terms of power. For instance, in Chapter 8 and in [4] attempts are made to unify CVEM and eco-driving (finding energy optimal velocity profiles). In this case, velocity becomes a decision variable and describing it in terms of power is a non-trivial task. Other disadvantage of power-based approaches is that it is difficult to constrain physical variables that describe power in the model. For instance, imposing constraints on the battery power do not necessarily imply that the solution of the OCP is physically realizable. Power in the battery is described as the product of voltage and current, thus an optimal solution that satisfies power constraints not necessarily satisfies the bounds on voltage and current. Additionally, power-based approaches do not always allow for an intuitive formulation of decomposable OCP, which are useful when distributed optimization techniques are applied to approximate solutions. For instance, in [2] the concept of 'sum of losses' is introduced to formulate a separable OCP for CVEM. Unfortunately, this concept is not always simple to apply.

In this chapter, we propose an alternative modelling framework based on interconnected port-Hamiltonian (pH) systems, e.g. see [5, 6] and references therein, aiming to overcome the previously discussed limitations of power-based approaches. In this modelling approach, each subsystem is represented as a dissipative dynamical system that inherently describes energy losses and changes of internal energy in the subsystem. The main contributions of this work are twofold. First, we propose to use pH representations to model networks for CVEM applications, thus unifying the power-based concepts of energy buffers and power converters in a single dynamical model, i.e., in terms of internal energy and losses. Second, a systematic approach is proposed to formulate a decomposable OCP for CVEM, which is useful when distributed static optimization techniques are considered to solve the CVEM OPC.

The remainder of this chapter is organized as follows. In Section 7.1, we briefly introduce the pH modelling theoretical background and use these concepts to model CVEM networks. In Section 7.2, we take advantage of the pH modelling approach to formulate decomposable OCP for CVEM. The pH methodology for CVEM is applied to a case study of a battery electric vehicle presented in Section 7.3. Finally, the conclusions are drawn in Section 7.4.

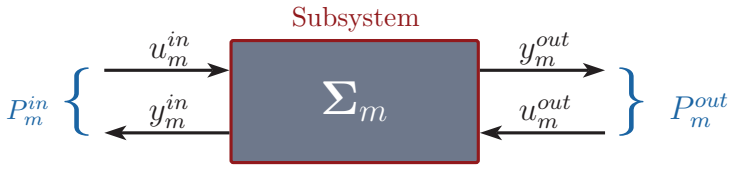

Figure 7.1: Port-Hamiltonian subsystem Σ_m

7.1. Port-Hamiltonian Modelling for CVEM

The main objective of this section is to present the pH modelling framework for energy management applications. Specifically, we adapt the pH framework to the holistic philosophy of CVEM presented in [7]. To achieve this, we briefly discuss the main concepts of pH representations. Later, the main features of networks of interconnected subsystems for CVEM are translated into a compatible description with pH models.

7.1.1. Port-Hamiltonian Representation

From a modelling perspective, a pH representation is a port-based modelling approach that considers a pair of conjugated variables in each port, whose product represents power. This has been depicted in Fig. 7.1, where a generic graphical representation of a two-port pH system is presented. Although in literature, there is a large number of possible pH representations, in this chapter we will only focus on linear input-state-output models with a direct feedthrough term.

Consider a linear subsystem $m \in \mathcal{M} := \{1, \dots, M\}$, where M is the total number of interconnected subsystems in the network. The internal energy of the m subsystem is expressed as a quadratic function given by

$$\mathcal{H}_m(x_m) = \tfrac{1}{2} x_m^\top Q_m x_m, \tag{7.1}$$

where $x_m \in \mathbb{R}^n$ represents the state vector and $Q_m \in \mathbb{R}^{n\times n}$ is a symmetric positive semi-definite matrix, which is called energy matrix. This energy function is used in an input-state-output with feedthrough term pH representation [6],[5, §4] of the m subsystem, and is given by

$$\frac{\mathrm{d}x_m}{\mathrm{d}t} = \big(J_m - R_m\big) Q_m x_m + B_m u_m \tag{7.2a}$$

$$y_m = (B_m + 2P_m)^\top Q_m x_m + (M_m + S_m) u_m \tag{7.2b}$$

where $u_m \in \mathbb{R}^2$ and $y_m \in \mathbb{R}^2$ are the system input and output, respectively, given by

$$u_m = \begin{bmatrix} u_m^{\text{in}} \\ u_m^{\text{out}} \end{bmatrix} \quad \text{and} \quad y_m = \begin{bmatrix} y_m^{\text{in}} \\ y_m^{\text{out}} \end{bmatrix}. \tag{7.3}$$

In (7.2), $J_m \in \mathbb{R}^{n\times n}$ is a skew symmetric matrix known as the interconnection matrix, and $R_m \in \mathbb{R}^{n\times n}$ is a positive semidefinite matrix known as dissipation matrix.

The port-Hamiltonian model (7.2) satisfies the following power balance equation [5, §4]

$$\frac{\partial \mathcal{H}_m}{\partial t}(x_m) = -\begin{bmatrix} x_m \\ u_m \end{bmatrix}^\top L_m \begin{bmatrix} x_m \\ u_m \end{bmatrix} + y_m^\top u_m. \tag{7.4}$$

in which

$$L_m := \begin{bmatrix} Q_m R_m Q_m & Q_m P_m \\ \mathcal{P}_m^\top Q_m & S_m \end{bmatrix}. \tag{7.5}$$

In case that $L_m \succeq 0$, passivity of the system is guaranteed [8, §7.1]. Furthermore, an energy balance can be described by reorganizing and integrating both sides of (7.4) over the interval $[t_0,\ t_f]$, hence obtaining

$$\Delta E_m = E_m^{\text{in}} + E_m^{\text{out}} = \Delta \mathcal{H}_m + \mathcal{L}_m \tag{7.6}$$

with

$$\Delta E_m = \int_{t_0}^{t_f} y_m^\top u_m \, \mathrm{d}t = \underbrace{\int_{t_0}^{t_f} y_m^{\text{in}} u_m^{\text{in}} \, \mathrm{d}t + \int_{t_0}^{t_f} y_m^{\text{out}} u_m^{\text{out}} \, \mathrm{d}t}_{E_m^{\text{in}} + E_m^{\text{out}}} \tag{7.7a}$$

$$\Delta \mathcal{H}_m = \mathcal{H}_m(x_m(t_f)) - \mathcal{H}_m(x_m(t_0)) \tag{7.7b}$$

$$\mathcal{L}_m = \int_{t_0}^{t_f} \begin{bmatrix} x_m \\ u_m \end{bmatrix}^\top L_m \begin{bmatrix} x_m \\ u_m \end{bmatrix} \mathrm{d}t \tag{7.7c}$$

where ΔE_m represents the net supplied energy to the m subsystem, $\Delta \mathcal{H}_m$ is the change on internal energy and $\mathcal{L}_m$ describes the total energy losses. Moreover, let us define the set of source subsystems

$$\mathcal{S} := \{m \in \mathcal{M} \,|\, E_m^{\text{in}} = 0\}, \tag{7.8a}$$

the set of consumers

$$\mathcal{C} := \mathcal{M} \setminus \mathcal{S}, \tag{7.8b}$$

and the set of terminal subsystems

$$\mathcal{T} := \{m \in \mathcal{M} \,|\, E_m^{\text{out}} = 0\}. \tag{7.8c}$$

A physical example of a source subsystem, which only has an output port, is chemical energy stored in a battery. On the other hand, mechanical brake is a physical example of a terminal system, which has only an input port.

7.1.2. Port-based Network Topology

Interconnections of pH systems have been studied in [9], where a methodology has been proposed to describe networks of pH systems with the final goal to perform stability analysis. Although in this chapter, we consider some ideas from the

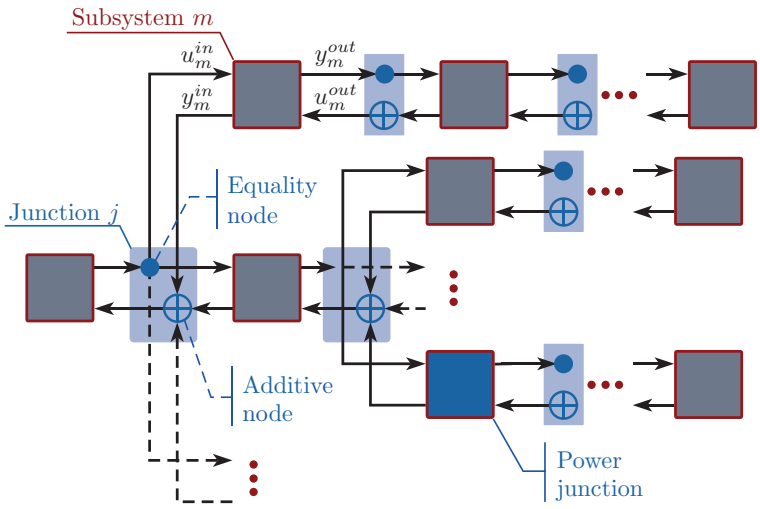

Figure 7.2: Port-based topology for interconnected port-Hamiltonian systems

work presented in [9], we will deviate from this approach to propose a specialized description of network topologies that capture specific features found in CVEM applications.

A tree structure port-based network topology is presented in Fig. 7.2, where each subsystem $m \in \mathcal{M}$ is depicted by a gray square. The interconnection between subsystems takes place through junctions $j \in \mathcal{J} := \{1, \dots, J\}$, where $J \in \mathbb{N}$ is the total number junctions in the network. These junctions are power preserving interconnections that are described in terms of the conjugated input output variables as follows

$$\sum_{m \in \mathcal{M}} a_{j,m} u_m^{\text{in}} y_m^{\text{in}} + b_{j,m} u_m^{\text{out}} y_m^{\text{out}} = 0, \qquad \text{for all } j \in \mathcal{J}, \tag{7.9}$$

where $a_{j,m} = 1$ if the input port of subsystem m is connected to junction j, and $a_{j,m} = 0$ otherwise. Similarly, $b_{j,m} = 1$ if the output port of subsystem m is connected to junction j, and $b_{j,m} = 0$ otherwise.

In CVEM networks, there is a type of junction that can be decomposed into an additive node and an equality node. A physical interpretation of these type of nodes is observed in electrical interconnections between subsystems, e.g., Kirchhoff's law of currents can be seen as an additive node, while Kirchhoff's law of voltages as an equality node. Let us define the set of all the decomposable junctions in the network $\mathcal{J}_n := \{1, \dots, J_n\}$, where $J_n \leq J$ is the total number of these type of junctions in the network. Thus, the power preserving equation (7.9) can be rewritten as

$$\sum_{m \in \mathcal{M}} [a_{j,m} \; 0] u_m + [0 \; b_{j,m}] y_m = 0, \tag{7.10a}$$

$$[a_{j,m} \; 0] y_m - [0 \; b_{j,m}] u_m = 0 \text{ for all } m \in \mathcal{M}, \tag{7.10b}$$

for all $j \in \mathcal{J}_n$. Note that (7.10a) and (7.10b) are referred as additive node and an equality nodes, respectively.

Another type of power preserving interconnections observed in CVEM networks are power junctions. The power junction artifact introduced in this framework obeys the necessity to resemble the functionality of DC-DC converters in CVEM networks. It is well known that DC-DC converters can be represented as non-linear pH systems, e.g., see [10]. In fact, from steady-state approximations of the models proposed in [10], under the assumption that the DC-DC converter is lossless, it is possible to prove that DC-DC converters satisfy (7.9). In order to keep consistent notation, we rewrite (7.9) as

$$\sum_{m\in\mathcal{M}} y_m^\top \begin{bmatrix} a_{j,m} & 0 \\ 0 & b_{j,m} \end{bmatrix} u_m = 0, \tag{7.11}$$

for all $j \in \mathcal{J}_p$; with $\mathcal{J}_p := \{J_n + 1, \dots, J\}$ the set of all power junctions in the network.

7.2. Optimal Control Problem for pH CVEM

In this section, we first provide a general formulation for a continuous-time optimal control problem (OCP) for the pH CVEM modelling approach described in the previous section. Subsequently, we propose a physically insightful cost function that enables decomposability of the proposed pH OCP for CVEM. Finally, we present a discrete-time OCP for pH CVEM.

The main objective of CVEM is to minimize the total energy consumed by a network of interconnected subsystems over a fixed time interval, subject to the dynamical behavior of each subsystem and bounds on the respective inputs, outputs and states. From a mathematical perspective, this goal can be described as an OCP. Hence, a general formulation of the pH OCP for CVEM is given by

$$\min_{\{x_m,u_m,y_m\}_{m\in\mathcal{M}}} \quad \mathscr{J}\left(\{x_m,u_m,y_m\}_{m\in\mathcal{M}}\right) \tag{7.12a}$$

subject to: (7.2), (7.10), (7.11),

$$\underline{x}_m \le x_m \le \overline{x}_m, \tag{7.12b}$$

$$\underline{u}_m \le u_m \le \overline{u}_m, \tag{7.12c}$$

$$\underline{y}_m \le y_m \le \overline{y}_m, \tag{7.12d}$$

for all $m \in \mathcal{M}$ and all $t \in [t_0, t_f]$. Note that (7.12a) represents a general cost function that aims to describe the total energy consumed by the subsystems in the network. We propose a physically insightful and decomposable cost function for the OCP (7.12) below.

7.2.1. Power Consumption in pH CVEM

The physical interpretation provided by pH models in terms of internal energy and energy losses of the subsystems can be exploited to formulate a sensible description of the energy consumed in the network. In particular, we could aim to maximize the

internal energy in each source subsystem, which implies minimizing consumption, i.e., see (7.7b). This can be described by (7.12) if the cost function is defined as

$$\mathscr{J}\left(\{x_m, u_m, y_m\}_{m\in\mathcal{M}}\right) = \sum_{m\in\mathcal{S}} -\Delta\mathcal{H}_m(x_m, u_m, y_m). \tag{7.13}$$

Note that the minus sign in (7.13) is necessary because (7.12) is defined as a minimization problem.

Interestingly, by decomposing the cost function (7.13) it is possible to obtain an equivalent expression that can be interpreted as minimizing the aggregated internal energy of all the consumers and the energy losses of all the subsystems. In order to see this, let us recall that power preserving interconnections are considered for all the junctions $j \in \mathcal{J}$ in the network. Therefore, by integrating (7.9) for a given time interval we obtain the following energy balance

$$\sum_{m\in\mathcal{M}} a_{j,m}E_m^{\text{in}} + b_{j,m}E_m^{\text{out}} = 0, \tag{7.14}$$

for all $j \in \mathcal{J}$. Hence, it is possible to follow a recursive procedure where we substitute (7.6) into (7.13) to obtain the partially expanded function

$$\mathscr{J} = \sum_{m\in\mathcal{S}} \mathcal{L}_m - E_m^{\text{out}} = \sum_{m\in\mathcal{S}} \mathcal{L}_m - b_{m,j}E_m^{\text{out}}, \tag{7.15a}$$

for some node $j \in \mathcal{J}$ where the subsystem m is connected. By substituting (7.14) into (7.15a), and subsequently (7.6) in the the resultant expression we obtain

$$\begin{aligned}\mathscr{J} &= \sum_{m\in\mathcal{S}} \left(\mathcal{L}_m + \sum_{n\in\mathcal{C}} a_{n,j}E_n^{\text{in}}\right) \\ &= \sum_{m\in\mathcal{S}} \left(\mathcal{L}_m + \sum_{n\in\mathcal{C}} a_{n,j}\left(\Delta\mathcal{H}_n + \mathcal{L}_n - E_n^{\text{out}}\right)\right).\end{aligned} \tag{7.15b}$$

The recursive expansion of this cost function ends with terminal subsystems in each branch of the tree network. Hence, the complete expansion of (7.13) is given by

$$\mathscr{J} = \sum_{m\in\mathcal{M}} \mathcal{L}_m + \sum_{n\in\mathcal{C}} \Delta\mathcal{H}_n, \tag{7.16}$$

which implies that maximization of internal energy is equivalent to minimizing the losses of all subsystems and the internal energy of only the consumers in the network. These results not only show the importance of pH formulations to obtain physically insightful interpretations of cost functions, but also open the door to obtain possible equivalent cost functions that could be beneficial for specific solution methods used to solve the CVEM OCP (7.12), e.g., see [2] and the optimization method presented in Chapter 5.

7.2.2. Discretization

The use of static optimization techniques to approximate solutions of (7.12) in a finite-time horizon requires the discretization of this OCP. It is important to remark that we are aware that there are no conclusive results about preservation of the discrete-time energy balance equation under interconnection of discrete-time pH systems. Although promising results can be found in literature, e.g., [11, 12], we will neglect this issue in this work.

To arrive at a discrete-time OCP, (7.12) is discretized at times $t_k = k\delta_t + t_0$, $k \in \mathcal{K} = \{0, \dots, K-1\}$, with time step $\delta_t = \frac{t_f - t_0}{K}$ for some $K \in \mathbb{N}$ using the forward Euler discretization method. This leads to

$$\min_{\substack{\{x_{m,k}, u_{m,k}, y_{m,k}\}_{m\in\mathcal{M},} \\ k\in\mathcal{K}}} \sum_{m\in\mathcal{M}} e_m \Delta\widehat{\mathcal{H}}_m + \widehat{\mathcal{L}}_m \tag{7.17a}$$

subject to the discrete-time dynamical model

$$x_{m,k+1} = (I + \delta_t\big(J_m - R_m\big)Q_m)x_{m,k} + \delta_t B_m u_{m,k}, \tag{7.17b}$$

$$y_{m,k} = (B_m + 2P_m)^\top Q_m x_{m,k} + (M_m + S_m)u_{m,k}, \tag{7.17c}$$

discrete-time versions of (7.10), (7.11), and $\{x_{m,k}, u_{m,k}, y_{m,k}\} \in \Omega_m$ for all $m \in \mathcal{M}$ and $k \in \mathcal{K}$, where

$$\Omega_m := \{x_{m,k} \in \mathbb{R}^n, y_{m,k} \in \mathbb{R}^2, u_{m,k} \in \mathbb{R}^2 \mid \text{(7.12b), (7.12c) and (7.12d) hold}\}. \tag{7.17d}$$

Note that (7.17a) is an equivalent formulation of the cost function (7.16), where $e_m = 1$ if $m \in \mathcal{C}$ and $e_m = 0$ otherwise. This indicates that the cost function (7.17a) penalizes changes of internal energy only for the set of energy consumers. The discretized versions of internal energy and losses are given respectively by

$$\Delta\widehat{\mathcal{H}}_m = \tfrac{1}{2}x_{m,K}^\top Q_m x_{m,K} - \tfrac{1}{2}x_{m,0}^\top Q_m x_{m,0}, \tag{7.18a}$$

$$\widehat{\mathcal{L}}_m = \delta_t \sum_{k\in\mathcal{K}} \begin{bmatrix} x_{m,k} \\ u_{m,k} \end{bmatrix}^\top L_m \begin{bmatrix} x_{m,k} \\ u_{m,k} \end{bmatrix}. \tag{7.18b}$$

The advantage of the pH framework exposed in this chapter lays in the possibility to formulate decomposable problems by expanding the cost function in terms of internal energy and losses of the subsystem in the network. Therefore, distributed static optimization techniques can be easily adapted to find solutions of the discrete OCP (7.17).

7.3. Case Study: Battery Electric Vehicle

The pH CVEM framework described in Section 7.1 and the associated OCP of Section 7.2 are illustrated in a case study presented in this section. We consider a Battery Electric Vehicle (BEV), whose topology is depicted in Fig. 7.3. A high-voltage battery (HVB) is connected via a DC-DC converter to an electric machine (EM). The mechanical part in this driveline yields a power balance between the requested

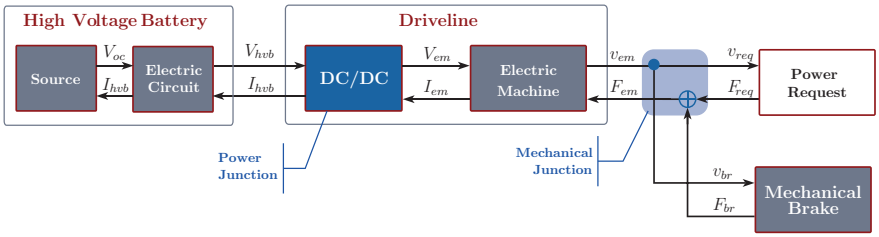

Figure 7.3: CVEM port-based configuration for a battery electric vehicle.

propulsion power and the mechanical braking power. Even though this configuration is simple, it allows to illustrate the proposed modelling approach for CVEM and the solution method. Moreover, it should be noted that this case study considers electrical, mechanical and thermal subsystems. This highlights the flexibility of the pH CVEM approach to preserve the physical variables linked to each physical domain.

In the remainder of this section, we provide details for modelling the topology presented in Fig. 7.3 and formulate an OCP for CVEM. Later, we discuss the connections between power-based and pH OCP formulations highlighting the advantages of the approach proposed in this chapter. Finally, simulations results for this case study are presented and analyzed.

7.3.1. Modelling

In the topology presented in Fig. 7.3, it is possible to observe the physical conjugated variables that describe the power preserving interconnection between subsystems. We will use these variables to define the input-output ports for each subsystem. Additionally, the pH models for the subsystems will be obtained from first-principle models and described in terms of the pH representation given in Section 7.1.1.

The set $\mathcal{M}$ is the set of interconnected subsystems for the BEV considered in this case. For the sake of readability, we use $\mathcal{M} = \{vs, ec, em, br, req\}$ instead of a enumerated set to denote battery voltage source, battery electric circuit, electric machine, mechanical brake and power request, respectively. Note that vs is a source subsystem, while br and req are terminal subsystems. Similarly, $\mathcal{J}_n = \{1\}$ represents the mechanical node in the topology, while $\mathcal{J}_p = \{2\}$ is the power junction of the network, which corresponds to the DC-DC converter.

High-Voltage Battery

We consider an equivalent circuit model with constant open circuit voltage V_{oc} and internal resistance R_{hvb} in this chapter. The voltage and current in the terminals are denoted as V_{hvb} and I_{hvb}, respectively. The pH formulation of the HVB is constituted of subsystems vs and ec, which represent an ideal lossless voltage source and the internal resistance of the battery, respectively. The input and output ports and the

states of the aforementioned subsystems are defined as

$$u_{vs} = \begin{bmatrix} 0 \\ -I_{hvb} \end{bmatrix}, \quad y_{vs} = \begin{bmatrix} 0 \\ V_{oc} \end{bmatrix}, u_{ec} = \begin{bmatrix} V_{oc} \\ I_{hvb} \end{bmatrix}, \quad x_{ec} = \text{SoC}, \quad y_{ec} = \begin{bmatrix} I_{hvb} \\ -V_{hvb} \end{bmatrix}, \tag{7.19a}$$

where SoC denotes the HVB state-of-charge. Note that these definitions indicate that the interconnection between the voltage source vs and the electric circuit ec is power preserving, i.e., $y_{vs}^{\text{out}} u_{vs}^{\text{out}} + y_{ec}^{\text{in}} u_{ec}^{\text{in}} = 0$. Therefore, the pH models of the subsystems in the HVB are given by

$$Q_{ec} = J_{ec} = R_{ec} = 0,\ P_{ec} = \begin{bmatrix} 0 & 0 \end{bmatrix},\ B_{ec} = \begin{bmatrix} 0 & -\frac{1}{q_{hvb}} \end{bmatrix} \quad M_{ec} = \begin{bmatrix} 0 & 1 \\ -1 & 0 \end{bmatrix},\ S_{ec} = \begin{bmatrix} 0 & 0 \\ 0 & R_{hvb} \end{bmatrix}, \tag{7.19b}$$

where q_{hvb} denotes the HVB capacity. Numerical values for the parameters associated to the HVB are given in Table 7.1.

Electric Machine

The HVB is connected to an EM through an ideal DC-DC convertor represented by junction $\mathcal{J}_p$. The pH formulation for the EM is defined using

$$u_{em} = \begin{bmatrix} V_{em} \\ F_{em} \end{bmatrix},\ x_{em} = \begin{bmatrix} LI_{em} \\ \frac{g_r}{r_w} I_m v_{em} \end{bmatrix},\ y_{em} = \begin{bmatrix} I_{em} \\ -v_{em} \end{bmatrix}, \tag{7.20a}$$

where V_{em}, I_{em} denotes the voltage and current in the EM, respectively; F_{em} is the propulsion force and v_{em} the longitudinal velocity. Additionally, the positive constants L, I_m, r_w and g_r denote the electric inductance, moment of inertia, wheel radius and total gear ratio, respectively. These definitions allow the pH model of the EM to be defined using

$$Q_{em} = \begin{bmatrix} \frac{1}{L} & 0 \\ 0 & \frac{1}{I_m} \end{bmatrix}, \quad J_{em} = \begin{bmatrix} 0 & \frac{\kappa_V + \kappa_\tau}{2} \\ -\frac{\kappa_V + \kappa_\tau}{2} & 0 \end{bmatrix}, \quad P_{em} = M_{em} = S_{em} = \begin{bmatrix} 0 & 0 \\ 0 & 0 \end{bmatrix},$$
$$B_{em} = \begin{bmatrix} 1 & 0 \\ 0 & -\frac{r_w}{g_r} \end{bmatrix}, \quad R_{em} = \begin{bmatrix} R_e & \frac{\kappa_V - \kappa_\tau}{2} \\ \frac{\kappa_V - \kappa_\tau}{2} & \beta \end{bmatrix}, \tag{7.20b}$$

Table 7.1: High-Voltage Battery (HVB) parameters

Variable	Value	Definition	Observations
V_{oc}	658	open circuit voltage	$[V]$
R_{hvb}	0.33	series resistance	$[\Omega]$
q_{hvb}	180	capacity of the battery	$[Ah]$
$\underline{I}_{hvb}$	-800	minimum current	$[A]$
$\overline{I}_{hvb}$	800	maximum current	$[A]$
$\underline{V}_{hvb}$	400	minimum voltage	$[V]$
$\overline{V}_{hvb}$	1000	maximum voltage	$[V]$

Table 7.2: Driveline parameters

Variable	Value	Definition	Observations
R_e	1	equivalent resistance	$[\Omega]$
L	2	equivalent inductance	$[H]$
I_e	99.68	equivalent axle inertia	$[kg\ m^2]$
β	1.1e-03	friction coefficient (rotational)	$[Nm\ s/rad)]$
κ_τ	4.2175	torque constant	$[Nm/A]$
κ_V	4.27	back-electromotive constant	$[Vs/rad]$
r_w	0.5715	wheel radius	$[m]$
g_r	6.1	gear ratio	$[-]$
$\underline{I}_{em}$	-600	minimum current	$[A]$
$\overline{I}_{em}$	600	maximum current	$[A]$
$\underline{V}_{em}$	0	minimum voltage	$[V]$
$\overline{V}_{em}$	1000	maximum voltage	$[V]$

where R_e, κ_V, κ_τ and β are positive constants that denote the equivalent electric resistance, back-electromotive constant, torque constant and damping coefficient, respectively. In Table 7.2, numerical values of the driveline parameters used for this case study are presented.

Mechanical Brake

The function of this subsystem is to dissipate all the power provided to it. It is considered as a terminal subsystem and its ports are defined as

$$u_{br} = \begin{bmatrix} v_{br} \\ 0 \end{bmatrix},\ y_{br} = \begin{bmatrix} F_{br} \\ 0 \end{bmatrix}, \tag{7.21}$$

where $F_{br} \geq 0$ is the mechanical braking force and v_{br} denotes the longitudinal velocity of the vehicle. Note that a complete description of the subsystem is not necessary because we are only interested in its consumption. Thus, the terms that describe internal energy and losses for the mechanical brake subsystem in the cost function (7.16) can be replaced by the total energy consumed by the subsystem, i.e.,

$$\Delta\mathcal{H}_{br} + \mathcal{L}_{br} = \int_{t_0}^{t_f} y_{brk}^{\mathsf{T}} u_{br} \mathrm{d}t. \tag{7.22}$$

Power Request

This subsystem describes the power required by the vehicle to travel a certain period of time with a given longitudinal velocity profile v_{req} and traction force F_{req}. It is considered a terminal subsystem, whose ports are defined as

$$u_{req} = \begin{bmatrix} v_{req} \\ 0 \end{bmatrix},\ y_{req} = \begin{bmatrix} F_{req} \\ 0 \end{bmatrix}. \tag{7.23}$$

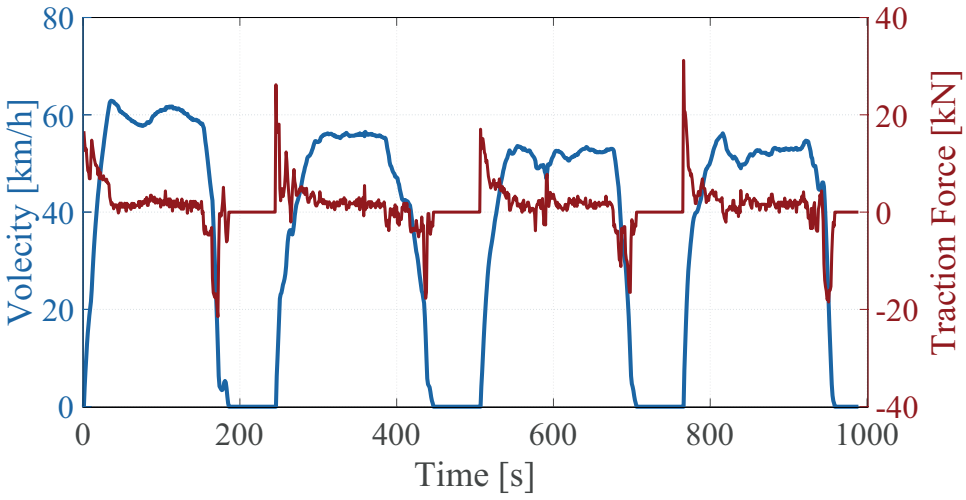

Figure 7.4: Requested traction force and longitudinal velocity.

The requested force and velocity profiles used in this case study are shown in Fig. 7.4. In this case, a complete description of the subsystem is not provided, because its behavior is already given. However, to preserve consistency in the cost function formulation (7.16), the terms that describe internal energy and losses are replaced by the total power consumed by the subsystem, i.e.,

$$\Delta\mathcal{H}_{req} + \mathcal{L}_{req} = \int_{t_0}^{t_f} y_{req}^{\top} u_{req} \mathrm{d}t. \tag{7.24}$$

Interconnections

The set $\mathcal{J} = \mathcal{J}_n \cup \mathcal{J}_p = \{1, 2\}$ contains the two junctions in network topology depicted in Fig. 7.3. This junctions are described by

$$b_{em,1} = a_{br,1} = a_{req,1} = 1, \tag{7.25a}$$
$$b_{ec,2} = a_{em,2} = 1, \tag{7.25b}$$

and zero for the remaining coefficients.

7.3.2. Optimal Control Problem

After describing pH representations for all the subsystems and its interconnections, the procedure to formulate a CVEM OCP for this case study is reduced to a simple substitution. In particular, a continuous-time CVEM OCP for this case study is obtained by substituting (7.19)-(7.25) into (7.12) and (7.16). Similarly, substituting (7.19)-(7.25) into (7.17) and (7.18) generates a discrete-time OCP.

Interestingly, for this case study it is also possible to find and equivalent OCP using a power-based approach. For instance, let us consider the modelling framework

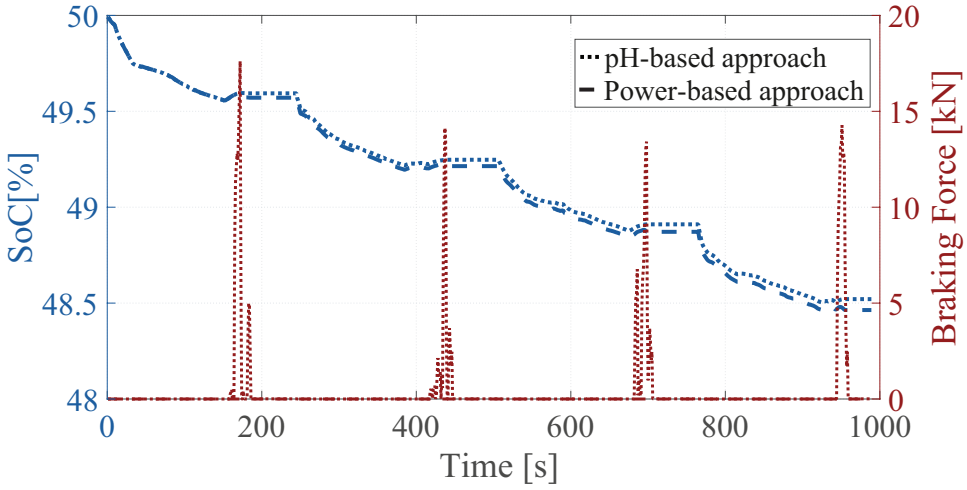

Figure 7.5: State of charge and braking force.

presented in Chapter 5. In this approach, the source subsystem is represented as a linear system that describes the accumulation of energy, and the conversion of power in all subsystems is defined by a quadratic function of the form

$$P_{out} = \tfrac{1}{2}\gamma_2 P_{in}^2 + \gamma_1 P_{in} + \gamma_0, \tag{7.26}$$

where P_{out}, P_{in} represent the power in the input and output ports of the subsystem, respectively. To illustrate the connection between the power-based approach in Chapter 5 with the pH framework proposed in this chapter, let us consider the EM model described by (7.2) and (7.20) in steady state. After some algebraic manipulations and by defining $P_{out} = V_{em} I_{em}$ and $P_{in} = F_{em} v_{em}$, it is possible to obtain

$$\gamma_2 = \frac{R_e r_w^2}{\kappa_V^2 g_r^2 v_{em}^2}, \qquad \gamma_1 = \frac{2R_e\beta}{\kappa_V^2} + \frac{\kappa_\tau}{\kappa_V}, \qquad \gamma_0 = \left(\frac{R_e\beta^2}{\kappa_V^2} + \frac{\kappa_\tau\beta}{\kappa_V}\right)\frac{g_r^2}{r_w^2} v_{em}^2. \tag{7.27}$$

Hence, considering that the longitudinal velocity v_{em} is given, (7.26) describes only a static relation between input and output powers. Performing a similar procedure in the rest of the subsystems of this example allows us to obtain an equivalent OCP that has power in the input-output ports of the subsystems as decision variables.

The advantage of this formulation is that if static optimization methods are used to obtain solutions, the number of decision variables is lower than in the port-based case. However, this framework fails to describe problems of higher complexity and extensions are needed. For instance, Chapter 8 will present and attempt to extend the modelling framework described in Chapter 5 to unify the optimization of velocity profiles, i.e., eco-driving, and CVEM for the subsystems of a vehicle. Using the pH framework for CVEM presented in this chapter, the integration of eco-driving and CVEM is natural. In fact, it is equivalent to include the longitudinal vehicle dynamics as an additional subsystem in the port-based network.

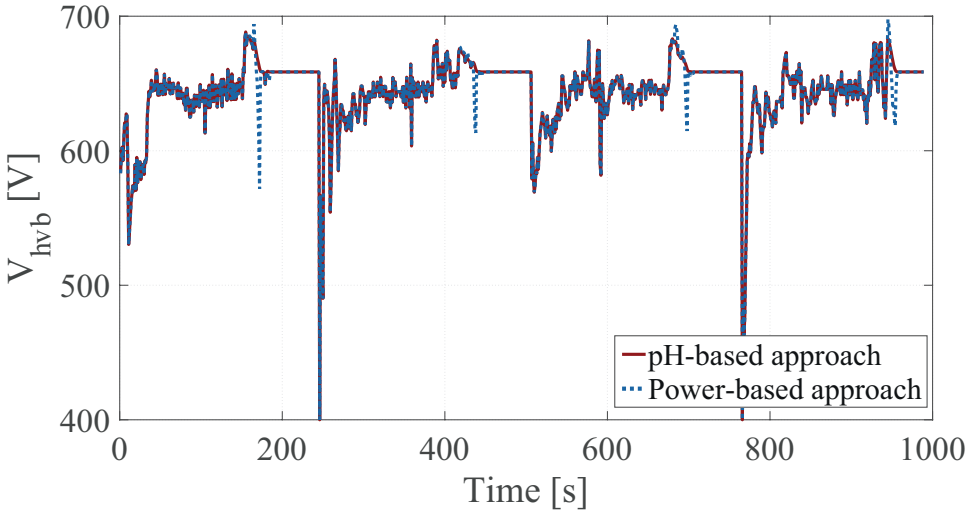

Figure 7.6: Battery voltage.

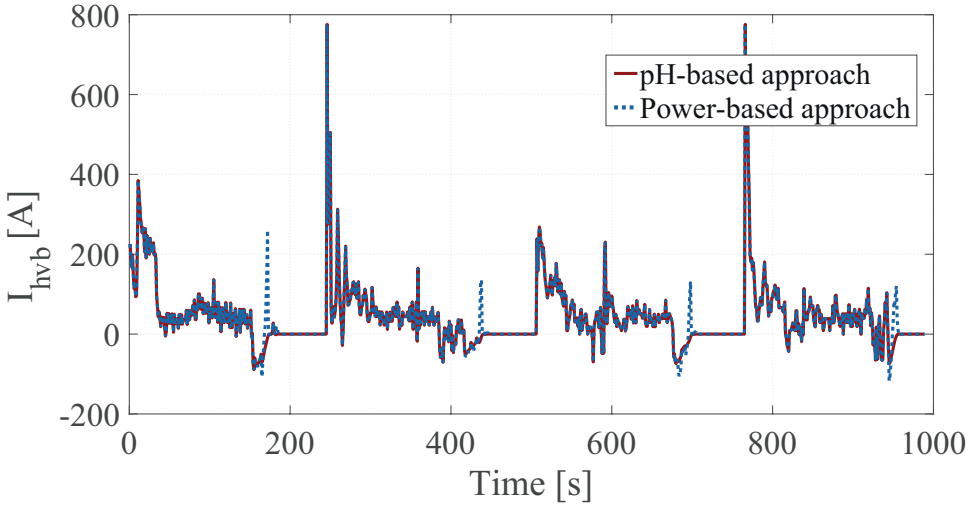

Figure 7.7: Battery current.

7.3.3. Simulation Results

We use the approach presented in Chapter 5 to find a solution to the discrete-time OCP obtained from the substitution of (7.19)-(7.25) into (7.17) and (7.18). In this case, we use a sampling time $\delta_t = 1[s]$ and a horizon of length $K = 990$. The results obtained using the pH-based approach described in this chapter are compared to a power-based benchmark where all the mechanical braking power is zero, which means that the energy produced by deceleration of the vehicle is completely stored

in the HVB. In Fig. 7.5, the SoC and the mechanical braking force can be observed as function of time for both the power-based approach as well as the pH-based approach. The final SoC corresponding to the optimal solution is 0.0717% higher than the benchmark solution, which implies energy savings of 4.896% for the given power request. Interestingly, the optimal solution still requires some mechanical braking. This clearly shows that the optimal solution selects efficient operational points for the subsystems, instead of only trying to recover as much mechanical energy as possible.

Physical insight about the HVB operation for both cases can be observed in Fig. 7.6 and Fig. 7.7, where the behavior of battery voltage and current, is respectively depicted for both approaches. Note that regions where the voltage in the battery terminals increases correspond to negative currents in the HVB. This implies charging the battery, which is also observed in Fig. 7.5. An advantage of the pH CVEM framework proposed in this chapter is that it is possible to give independent treatment to each conjugated variable in the port of the subsystems, i.e., setting independent constraints to each variable. For this study case, the constrains on the voltage and current of the HVB aim to capture the charge acceptance phenomenon in the battery. This is not directly possible in power-based approaches because voltage and current are combined as power in a single decision variable. Along the same lines, it should be mentioned that the pH-based approach allows only positive voltages in the electric machine (EM). If this constraint is neglected, the pH-based approach obtains the same solution as the power-based approach. This causes the differences in the solutions reported for this case study. This also shows that power based approaches could provide solutions that are no physically realizable.

7.4. Conclusions

We have proposed a systematic modelling approach to describe CVEM networks in terms of interconnected pH systems representations. This is an alternative to power-based approaches for CVEM and has allowed us to unify the concepts of energy storage and losses directly in the dynamical models of the subsystems. We have highlighted the relevance of the pH framework in terms of formulation of a physically insightful decomposable OCP. Moreover, the extra freedom obtained by describing power in terms of conjugated variables has opened the door to include additional physical phenomena as constraints in the OCP. Numerical simulations of a case study for a battery electric vehicle have shown that the pH-based approach to CVEM presented in this chapter improves the energy savings approximately 4.9% with respect to the power-based approach used in the case study. Moreover, it has been observed that power-based approaches could provide solutions that are not physically realizable.

References

[1] S. Onori, L. Serrao, and G. Rizzoni, *Hybrid electric vehicles: Energy management strategies* (Springer, 2016).

[2] T. C. J. Romijn, M. C. F. Donkers, J. T. B. A. Kessels, and S. Weiland, *A Distributed Optimization Approach for Complete Vehicle Energy Management,* IEEE Transactions on Control Systems Technology (2018).

[3] N. Murgovski, L. Johannesson, and J. Sjöberg, *Convex modeling of energy buffers in power control applications,* in *Proc. IFAC Workshop on Engine and Powertrain Control* (2012).

[4] N. Murgovski, L. Johannesson, X. Hu, B. Egardt, and J. Sjöberg, *Convex relaxations in the optimal control of electrified vehicles,* in *Proc. American Control Conf* (2015).

[5] A. van der Schaft and D. Jeltsema, *Port-Hamiltonian Systems Theory: An Introductory Overview* (now Publishers Inc., 2014).

[6] A. van der Schaft, *Interconnections of input-output Hamiltonian systems with dissipation,* Johann Bernoulli Institute for Mathematics and Computer Science (2016).

[7] J. T. B. A. Kessels, J. H. M. Martens, P. P. J. van den Bosch, and W. H. A. Hendrix, *Smart vehicle powernet enabling complete vehicle energy management,* Proc. Vehicle Propulsion & Power Control (2012).

[8] V. Duindam, A. Macchelli, S. Stramigioli, and H. Bruyninckx, *Modeling and Control of Complex Physical Systems: The Port-Hamiltonian Approach* (Springer Berlin Heidelberg, 2009).

[9] A. van der Schaft, *Interconnections of input-output hamiltonian systems with dissipation,* (2016).

[10] O. D. M. Giraldo, A. G. Ruiz, I. O. Velázquez, and G. R. E. Pérez, *Passivity-based control for battery charging/discharging applications by using a buck-boost DC-DC converter,* in *Proc. IEEE Green Technologies Conference* (2018).

[11] E. Celledoni and E. H. Hoiseth, *Energy-Preserving and Passivity-Consistent Numerical Discretization of Port-Hamiltonian Systems,* IEEE Transactions on Automatic Control (2017).

[12] Y. Yalcin, G. Sümer, and K. S., *Discrete-time modeling of Hamiltonian systems,* Turkish Journal of Electrical Engineering & Computer Sciences (2013).

8

Complete Vehicle Energy Management and Eco-driving

In this chapter, we integrate the eco-driving problem into the Complete Vehicle Energy Management (CVEM) framework. To this end, we solve the eco-driving problem using a Sequential Quadratic Programming (SQP) algorithm with Thikhonov regularization. We will further show that the SQP algorithm can be embedded in a distributed optimization approach, allowing it to be used for Complete Vehicle Energy Management (CVEM), incorporating optimal control of the vehicle's auxiliary systems, in combination with eco-driving. We consider two case studies for the eco-driving problem. The first case study concerns the optimal control of a Full-Electric Vehicle, which has one control input and two states and is solved with the SQP algorithm. The second case study lays a foundation for CVEM with eco-driving, where we will solve an energy management problem with eco-driving for a Series-Hybrid Electric Vehicle, which has three control inputs and three states, using the aforementioned SQP algorithm and dual decomposition.

This chapter is based on **P.8**.

Hybrid electric vehicles offer the potential to reduce fuel consumption of a vehicle by adding an electric motor with a high-voltage battery to the powertrain. This allows braking energy to be recuperated and allows the combustion engine to work at a more efficient operating point. In energy management, supervisory control is used to determine the optimal power flow between the electric machine and the combustion engine. A recent trend is to extend the energy management problem to incorporate more auxiliary devices, such as a refrigerated semitrailer or a climate control system [1], engine thermal management [2], battery thermal management [3], battery ageing [4, 5]. Integrating all the vehicle energy consumers into the energy management problem is referred to as Complete Vehicle Energy Management (CVEM) in [6]. The rationale behind this is that the auxiliaries also consume a considerable amount of energy. However, in all these vehicle energy management problems, the vehicle speed is assumed to be given, while most of the power generated by the powertrain is used for propelling the vehicle. Therefore, optimizing the speed of a vehicle over a certain trajectory, thereby allowing for an optimal conversion of potential energy from the road profile into kinetic energy of the vehicle, can lead to a considerable energy consumption reduction. In this chapter, we refer to this latter problem as the eco-driving problem.

In Vehicle Energy Management (VEM), global optimal solutions are typically achieved using Dynamic Programming (DP) [7], see e.g., [8]. However, DP has the inherent disadvantage that the computational burden increases with the number of states. Optimization methods based on the Pontryagin's Maximum Principle (PMP), see, e.g., [4, 9] can handle computational complexity of multi-state energy management problems. In PMP, the problem is reduced to solving a two-point boundary value problem, which can be difficult to solve in the presence of state constraints. Static optimization methods guarantee a global optimal solution for convex approximations of the energy management problems, e.g., [10]. To increase scalability of the static optimization problem to allow for a large number of auxiliary systems, distributed optimization approaches have been proposed in [1, 11] for complete vehicle energy management. Using a dual decomposition, a large optimal control problem is split up into several smaller optimal control problems. A disadvantage of the convex optimization approach to vehicle energy management of [1, 11] is that it requires the powertrain components to be described by (convex) quadratic models. This renders the distributed optimization approach not usable for the eco-driving problem, as the longitudinal vehicle dynamics is nonlinear. However, a particular extension of the distributed optimization approach of [1, 11] towards a nonlinear battery ageing model has been made in [5], showing its ability to handle nonlinear convex models as well.

Some of the above mentioned optimization methods have been applied to the eco-driving problem, e.g. PMP in [12, 13], DP in [14, 15], and static optimization in [16]. The approaches based on PMP and DP suffer from their inherent difficulties, i.e., incorporating state constraints in PMP and more dynamics in DP, while the approach based on (convex) static optimization [16] applies an Euler discretization to a continuous time optimal control problem. As the problem is formulated as

a second-order cone program, some of the powertrain components can only be modeled using (piecewise) linear functions. Furthermore, convexity might be lost after applying the Euler discretization, as it was shown in Chapter 2.

In this chapter, we will propose to solve the nonlinear (and possibly nonconvex) eco-driving problem using an alternative static optimization approach to the one presented in Chapter 2, which will be later easily extended to consider the CVEM framework. To handle the nonlinearity and nonconvexity of the resulting optimal control problem, we employ a Sequential Quadratic programming (SQP) algorithm [17, 18]. The SQP algorithm is similar in nature to the algorithm in [19], where the hessians are approximated to accelerate convergence, however we take advantage of the problem structure and further eliminate the state variables as is often done in MPC. Furthermore, we will show that the presented SQP algorithm can be embedded in the distributed optimization approach of [1, 11], allowing it to be used for complete vehicle energy management, incorporating optimal control of the vehicle's auxiliary systems, in combination with eco-driving. We will benchmark our solution strategy on a Full Electric Vehicle (FEV) problem presented in [13], which solves the problem using PMP, and solve the problem using SQP. We show the advantage of SQP over the PMP approach used in [13], as state constraints can be very easily added in our proposed approach. Furthermore, we demonstrate the combined eco-driving problem with the powersplit control of a series hybrid powertrain, as was also considered in [16].

The outline of this chapter is as follows. Section 8.1 gives the problem formulation used in this chapter for the eco-driving problem. Section 8.2 presents the sequential quadratic programming algorithm. Section 8.3 considers the CVEM with eco-driving problem for the SEHV case study. In Section 8.4, we will show the results for the FEV benchmark case study and the series-hybrid electric vehicle case study. Finally, conclusions are drawn in Section 8.5.

8.1. Eco-driving Problem formulation

In this section, we formulate the eco-driving problem. Moreover, we will propose a discrete-time formulation of the problem and we will show that this leads to a nonconvex optimization problem. We define the eco-driving problem as minimizing traction power over a certain trajectory:

$$\min_{v(t),s(t),u(t)} \int_{t_0}^{t_f} P_{\text{trac}}(v(t),u(t))\mathrm{d}t, \tag{8.1a}$$

where v is speed, u is the mechanical force, t_0 and t_f are the initial and final time respectively. In this chapter, we assume

$$P_{\text{trac}}(v,u) = \tfrac{1}{2}\gamma_2 u^2 + \gamma_1 uv + \tfrac{1}{2}\gamma_0 v^2, \tag{8.1b}$$

where γ_2, γ_1 and γ_0 are parameters. The model (8.1b) is a reasonable model for electric motors, because v^2 is related to friction losses and u^2 is related to dynamic losses of the traction motor. The objective function in (8.1a) is minimized subject

to (8.1b) and the longitudinal dynamics of the vehicle, given by

$$\begin{cases} \frac{\mathrm{d}v(t)}{\mathrm{d}t} &= \sigma_u u(t) - \sigma_v v(t)^2 - \sigma_r - g\sin(\alpha(s(t))), \\ \frac{\mathrm{d}s(t)}{\mathrm{d}t} &= v(t), \end{cases} \tag{8.1c}$$

for $t \in [t_0, t_f]$, and to lower and upper bounds on v and u, i.e.,

$$\underline{v}(t) \leq v(t) \leq \overline{v}(t), \quad \underline{u}(t) \leq u(t) \leq \overline{u}(t), \tag{8.1d}$$

for $t \in [t_0, t_f]$, and $v(t_0)$, $s(t_0)$, $v(t_f)$ and $s(t_f)$ given. In (8.1c), α is the road slope, $\sigma_r = gc_r$, $\sigma_u = \frac{1}{m}$ and $\sigma_v = \frac{1}{2m} c_d \rho_a A_f$. The coefficients m, g, c_d, ρ_a, A_f and c_r are the vehicle's mass, gravitational acceleration, aerodynamic drag coefficient, air density, frontal drag area and rolling resistance coefficient respectively.

To arrive at a finite dimensional optimization problem, we discretize (8.1) using a forward Euler discretization, and arrive at a discrete-time nonlinear optimal control problem of the form:

$$\min_{x_k, u_k} \sum_{k \in \mathcal{K}} \tfrac{1}{2} \begin{bmatrix} x_k \\ u_k \end{bmatrix}^\top H_k \begin{bmatrix} x_k \\ u_k \end{bmatrix} + F_k^\top \begin{bmatrix} x_k \\ u_k \end{bmatrix}, \tag{8.2a}$$

subject to state dynamics,

$$x_{k+1} = f(x_k, u_k), \tag{8.2b}$$

and state constraints and input constraints,

$$\underline{x}_k \leq x_k \leq \overline{x}_k, \qquad \underline{u}_k \leq u_k \leq \overline{u}_k, \tag{8.2c}$$

for $k \in \mathcal{K} = \{0, 1, \ldots, K-1\}$, where $K = \frac{t_f - t_0}{\tau}$ is the optimization horizon with x_0, x_K given and $\tau > 0$, which is chosen such that $\tau t_f \in \mathbb{N}$, is the step size. To arrive at a discrete-time approximation of (8.1), we choose

$$x_k = \begin{bmatrix} v_k \\ s_k \end{bmatrix}, \quad H_k = \tau \begin{bmatrix} \gamma_0 & 0 & \gamma_1 \\ 0 & 0 & 0 \\ \gamma_1 & 0 & \gamma_2 \end{bmatrix}, \quad F_k = \begin{bmatrix} 0 \\ 0 \\ 0 \end{bmatrix}, \tag{8.3a}$$

and

$$f(x_k, u_k) = \begin{bmatrix} v_k + \tau\left(\sigma_u u_k - \sigma_v v_k^2 - \sigma_r - g\sin(\alpha(s_k))\right) \\ s_k + \tau v_k \end{bmatrix}. \tag{8.3b}$$

An electric machine, represented by (8.1b), typically has a close to linear input-output behavior, such that $\gamma_1 \approx 1$, $\gamma_0 \ll 1$ and $\gamma_2 \ll 1$, as the power losses are small generally. This might cause (8.2) with (8.3) to be a nonconvex optimization problem, i.e., $H_k \not\succeq 0$. However, (8.2) may still be convex in the feasible domain, i.e., where the constraints (8.2b) - (8.2c) are satisfied. In Chapter 2, it is shown that due to the discretization step to arrive at (8.2), the discretized problem is nonconvex even in the feasible domain for any sampling time $\tau > 0$. Even though this nonconvexity of the discretized problem, a global solution can be expected due to the results presented in Chapter 2.

8.2. SQP Approach to Eco-driving

In this section, we will present a Sequential Quadratic Programming (SQP) algorithm to solve the nonlinear optimal control problem (8.2). SQP aims at solving a nonlinear optimization problem by sequentially solving linearly constrained quadratic programs (LCQP), which are formed, e.g., by approximating the objective function with a quadratic equation and linearizing the constraints. In the SQP algorithm that we will present below, we take advantage of the fact that the states are expressed as functions of the input, by linearizing the state equations and substituting these into the objective function and constraints, and arrive at a static optimization problem.

8.2.1. Sequential Quadratic Programming Algorithm

In this section, we will present an algorithm to solve (8.2) based on SQP and prove that solving the SQP algorithm yields a solution to (8.2), provided that the solution converges. In particular, we will solve (8.2) by recursively solving

$$\{x_k^{i+1}, u_k^{i+1}\}_{k\in\mathcal{K}} = \underset{x_k,u_k}{\operatorname{argmin}} \sum_{k\in\mathcal{K}} \tfrac{1}{2}\begin{bmatrix} x_k - x_k^i \\ u_k - u_k^i \end{bmatrix}^\top R_k \begin{bmatrix} x_k - x_k^i \\ u_k - u_k^i \end{bmatrix} + \left(H_k \begin{bmatrix} x_k^i \\ u_k^i \end{bmatrix} + F_k\right)^\top \begin{bmatrix} x_k \\ u_k \end{bmatrix}, \quad (8.4a)$$

subject to linearized state dynamics,

$$x_{k+1} = f(x_k^i, u_k^i) + \nabla f(x_k^i, u_k^i) \begin{bmatrix} x_k - x_k^i \\ u_k - u_k^i \end{bmatrix}, \quad (8.4b)$$

and state constraints and input constraints,

$$\underline{x}_k \le x_k \le \overline{x}_k, \quad \underline{u}_k \le u_k \le \overline{u}_k, \quad (8.4c)$$

for all $k \in \mathcal{K}$ and $i \in \mathbb{N}$, and for given x_0, x_K as well as some suitably well chosen $\{x_k^0, u_k^0\}_{k\in\mathcal{K}}$, such that a feasible solution exists for the next iteration of the SQP subproblem (8.4). Thus, we have formed the SQP subproblem (8.4) by linearizing the state equations (8.2b), and linearizing the objective function (8.2a) and adding an $R_k \succeq 0$ to ensure a convex objective function in (8.4a), which can be regarded as a proximal or Thikonov regularization. The matrix R_k can be chosen to warrant that the SQP subproblem (8.4) is strictly convex in its control variables $\{u_k\}_{k\in\mathcal{K}}$ and converges. We note that by choosing $R_k = H_k$, the SQP objective function (8.4a) becomes exactly the original objective function (8.2a). The SQP algorithm can be terminated when, e.g.,

$$|J^{i+1} - J^i| \le \Delta_{\text{tol}}, \quad (8.5a)$$

in which Δ_{tol} is a certain specified tolerance, and

$$J^i = \sum_{k\in\mathcal{K}} \tfrac{1}{2}\begin{bmatrix} x_k^i \\ u_k^i \end{bmatrix}^\top H_k \begin{bmatrix} x_k^i \\ u_k^i \end{bmatrix} + F_k^\top \begin{bmatrix} x_k^i \\ u_k^i \end{bmatrix} + \nu \sum_{k\in\mathcal{K}} |x_{k+1}^i - f(x_k^i, u_k^i)| \quad (8.5b)$$

is the optimal cost at iteration i, which can be considered as a merit function for the SQP approach (8.4). In (8.5b) $\nu \geq 0$ is chosen such that infeasible solutions to the SQP subproblem (8.4) at iteration i return a higher cost than optimal feasible solutions. Note that in this SQP approach, we allow infeasible solutions at iteration i, and as the algorithm converges, i.e., $|J^{i+1} - J^i| \to 0$, feasibility is obtained in the limit. Also note that as the state and input constraints (8.4c) are automatically satisfied with a solution to the SQP (8.4), and thus there is no contribution from these inequality constraints to the merit function (8.5b).

We can prove that when the SQP problem has converged, i.e. $x_k^{i+1} = x_k^i$ and $u_k^{i+1} = u_k^i$ for all $k \in \mathcal{K}$, the first-order necessary conditions for optimality, i.e., the so-called Karush-Kuhn-Tucker (KKT) conditions [20], for (8.4) are identical to the KKT conditions of (8.2). The KKT conditions use the notion of a Lagrangian, which for (8.2) is given by,

$$\begin{aligned} L(\{x_k, u_k, \lambda_k, \mu_k\}) = &\sum_{k\in\mathcal{K}} \tfrac{1}{2}\begin{bmatrix} x_k \\ u_k \end{bmatrix}^\top H_k \begin{bmatrix} x_k \\ u_k \end{bmatrix} + F_k \begin{bmatrix} x_k \\ u_k \end{bmatrix} \\ &+ \sum_{k\in\mathcal{K}} \mu_{k+1}^\top \big(x_{k+1} - f(x_k, u_k)\big) + \lambda_k^\top h(x_k, u_k), \end{aligned} \tag{8.6}$$

where $h(x,u) = \begin{bmatrix} (x-\overline{x})^\top & (\underline{x}-x)^\top & (u-\overline{u})^\top & (\underline{u}-u)^\top \end{bmatrix}^\top$. For a local optimal solution $\{x_k^*, u_k^*\}_{k\in\mathcal{K}}$, there exist $\{\lambda_k^*, \mu_k^*\}_{k\in\mathcal{K}}$ that satisfy stationarity of the Lagrangian, i.e.,

$$H_k \begin{bmatrix} x_k^* \\ u_k^* \end{bmatrix} + F_k + \begin{bmatrix} \mu_k^* \\ 0 \end{bmatrix} - \nabla f(x_k^*, u_k^*)^\top \mu_{k+1}^* + \nabla h(x_k^*, u_k^*)^\top \lambda_k^* = 0, \tag{8.7a}$$

and primal feasibility and complementarity slackness of the constraints, i.e.,

$$x_{k+1}^* - f(x_k^*, u_k^*) = 0 \tag{8.7b}$$

$$0 \leq \lambda_k^* \perp -h(x_k^*, u_k^*) \geq 0, \tag{8.7c}$$

where the notation $0 \leq a \perp b \geq 0$ indicates $a, b \geq 0$, $a^\top b = 0$. Similarly, the necessary conditions for optimality of (8.4) are given by a stationarity condition, i.e.,

$$R_k \begin{bmatrix} x_k^* - x_k^i \\ u_k^* - u_k^i \end{bmatrix} + H_k \begin{bmatrix} x_k^i \\ u_k^i \end{bmatrix} + F_k + \begin{bmatrix} \mu_k^* \\ 0 \end{bmatrix} - \nabla f(x_k^i, u_k^i)^\top \mu_{k+1}^* + \nabla h(x_k^*, u_k^*)^\top \lambda_k^* = 0, \tag{8.8a}$$

and primal feasibility and complementary slackness of the constraints, i.e.,

$$x_{k+1}^* - f(x_k^i, u_k^i) + \nabla f(x_k^i, u_k^i) \begin{bmatrix} x_k^* - x_k^i \\ u_k^* - u_k^i \end{bmatrix} = 0, \tag{8.8b}$$

$$0 \leq \lambda_k^* \perp -h(x_k^*, u_k^*) \geq 0. \tag{8.8c}$$

We observe that when $x_k^* = x_k^{i+1} = x_k^i$ and $u_k^* = u_k^{i+1} = u_k^i$ the KKT conditions (8.8) and (8.7) are equal. Thus, we can find (local) solutions of (8.2) by solving the SQP (8.4), provided that the iterates converge, in the sense that $x_k^{i+1} \to x_k^i$ and $u_k^{i+1} \to u_k^i$ for all $k \in \mathcal{K}$ when $i \to \infty$.

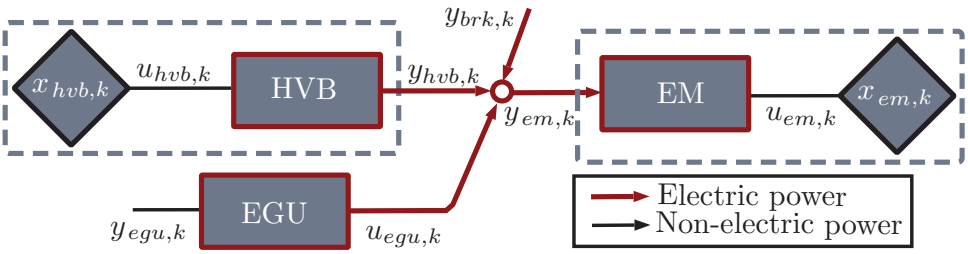

Figure 8.1: Topology.

It should be mentioned that the main difference with the approach presented in Chapter 2 lies in the OCP formulation for the eco-driving problem. In Chapter 2, the eco-driving problem is reformulated to eliminate only the non-linear dynamics by substituting them in the cost. As consequence, the OCP has already a linear feasible set, thus, avoiding the linearization of the feasible set performed in the approach presented in this section. Although both approaches obtain similar numerical performance, the approach presented in this chapter allows a more intuitive extension to the CVEM problem with eco-driving, since it preserves quadratic forms in the cost function.

8.3. Complete Vehicle Energy Management with Eco-driving

As a case study for Complete Vehicle Energy Management (CVEM) with eco-driving, we consider a series-hybrid electric vehicle, consisting of an electric motor (EM), engine-generator unit (EGU) and a high-voltage battery (HVB). The topology is shown in Fig. 8.1, in which y_{egu} and u_{egu} denote the ICE's fuel and mechanical power, respectively, y_{hvb} and u_{hvb} the battery's electrical and stored chemical power, y_{brk} is an artificial braking power exerted at the interconnection of the subsystems, u_{em} and y_{em} the EM's mechanical force and electrical power, respectively, x_{hvb} denotes the battery state of energy and $x_{em} = \left[\begin{smallmatrix} v \\ s \end{smallmatrix}\right]$, denotes the states speed v and distance traveled s of the vehicle. In this case, the main goal is to minimize fuel consumption, given by

$$\sum_{k \in \mathcal{K}} \tau y_{egu,k}, \tag{8.9a}$$

subject to the dynamics and input-output behavior of the converters in Fig 8.1, and the power balance at interconnection of the subsystems, i.e.,

$$y_{em,k} - u_{egu,k} - y_{hvb,k} = y_{brk} \leq 0, \tag{8.9b}$$

for all $k \in \mathcal{K}$. We use the constraint (8.9b) and energy balance constraint of the HVB, i.e.,

$$\sum_{k\in\mathcal{K}} \tau u_{hvb} = x_{hvb,K} - x_{hvb,0} = 0 \tag{8.9c}$$

to rewrite (8.9a) as a 'sum of losses', i.e.,

$$\tau \sum_{k\in\mathcal{K}} y_{egu,k} - u_{egu,k} + u_{hvb,k} - y_{hvb,k} + y_{em,k} - y_{brk,k}. \tag{8.9d}$$

By substituting (8.9b) and (8.9c) into (8.9d), we retrieve the original objective function (8.9a). In this section, we solve the CVEM problem by formulating it as a convex SQP problem and then apply dual decomposition as presented in [1].

8.3.1. Optimal Control Problem

The objective is to minimize fuel consumption, for which we use the equivalent fuel consumption (8.9d), which may be written as

$$\min_{u_{m,k}, y_{m,k}} \sum_{m\in\mathcal{M}} \sum_{k\in\mathcal{K}} a_m u_{m,k} + b_m y_{m,k} \tag{8.10a}$$

where $u_{m,k} \in \mathbb{R}$ and $y_{m,k} \in \mathbb{R}$ are the (scalar) inputs and outputs of the converter in subsystem $m \in \mathcal{M} = \{em, egu, hvb\}$ at time instant $k \in \mathcal{K}$. The optimization problem (8.10a) is to be solved subject to an equality constraint describing the quadratic input-output behavior of each converter, i.e.,

$$y_{m,k} = \tfrac{1}{2}\begin{bmatrix} x_{m,k} \\ u_{m,k} \end{bmatrix}^{\mathsf{T}} H_m \begin{bmatrix} x_{m,k} \\ u_{m,k} \end{bmatrix} + F_m^{\mathsf{T}} \begin{bmatrix} x_{m,k} \\ u_{m,k} \end{bmatrix} + e_m \tag{8.10b}$$

for all $k \in \mathcal{K}$, $m \in \mathcal{M}$, and subject to the system dynamics of the states in subsystem $m \in \mathcal{M}$, i.e.,

$$x_{m,k+1} = f_m(x_{m,k}, u_{m,k}) \tag{8.10c}$$

for all $k \in \mathcal{K}$ where the initial state $x_{m,0}$ and final state $x_{m,K}$ of the energy storage device are assumed to be given, and the input $u_{m,k}$ is subject to linear inequality constraints, i.e.,

$$\underline{u}_{m,k} \leq u_{m,k} \leq \overline{u}_{m,k}, \tag{8.10d}$$

for all $k \in \mathcal{K}$, $m \in \mathcal{M}$ and the state $x_{m,k}$ is subject to linear inequality constraints, i.e.,

$$\underline{x}_{m,k} \leq x_{m,k} \leq \overline{x}_{m,k}, \tag{8.10e}$$

for all $k \in \mathcal{K}$ and $m \in \mathcal{M}$. Finally, the optimization problem is solved subject to a linear inequality constraint describing the interconnection of the subsystems given by (8.9b), which we write as

$$\sum_{m\in\mathcal{M}} c_m u_{m,k} + d_m y_{m,k} = y_{brk,k} \leq 0, \tag{8.10f}$$

for all $k \in \mathcal{K}$, where $c_m, d_m \in \mathbb{R}$. Note that we have left out the term $-y_{brk,k}$ in (8.10a), as $y_{brk,k}$ for all $k \in \mathcal{K}$ is already given by the inequality (8.10f), which renders $y_{brk,k}$ as an implicit decision variable. To have that (8.10a) corresponds to (8.9d), we choose

$$a_{egu} = b_{hvb} = -\tau, \qquad a_{hvb} = b_{egu} = b_{em} = \tau, \qquad a_{em} = 0, \tag{8.11a}$$

and to have that (8.10f) corresponds to (8.9b), we choose

$$c_{egu} = d_{hvb} = -1, \qquad d_{em} = 1, \qquad c_{hvb} = c_{em} = d_{egu} = 0. \tag{8.11b}$$

Finally, we assume in this chapter that the coefficients for the input-output behavior of the converters in (8.10b) are given by

$$\begin{aligned} H_{em} &= \begin{bmatrix} \gamma_{em,0} & 0 & \gamma_{em,1} \\ 0 & 0 & 0 \\ \gamma_{em,1} & 0 & \gamma_{em,2} \end{bmatrix}, & F_{em} &= \begin{bmatrix} 0 \\ 0 \\ 0 \end{bmatrix}, & e_{em} &= 0, \\ H_{hvb} &= \begin{bmatrix} 0 & 0 \\ 0 & \gamma_{hvb,2} \end{bmatrix}, & F_{hvb} &= \begin{bmatrix} 0 \\ \gamma_{hvb,1} \end{bmatrix}, & e_{hvb} &= \gamma_{hvb,0}, \\ H_{egu} &= \gamma_{egu,2}, & F_{egu} &= \gamma_{egu,1}, & e_{egu} &= \gamma_{egu,0}, \end{aligned} \tag{8.11c}$$

for some parameters γ_{m_2}, γ_{m_1}, γ_{m_0}, $m \in \mathcal{M}$, the state dynamics for the EM are given by

$$f(x_{em,k}, u_{em,k}) = \begin{bmatrix} v_k + \tau\left(\sigma_u u_{em,k} - \sigma_v v_k^2 - \sigma_r - g\sin(\alpha(s_k))\right) \\ s_k + \tau v_k \end{bmatrix}, \tag{8.11d}$$

and the battery state of energy is given by

$$f_{hvb}(x_{hvb,k}, u_{hvb,k}) = x_{hvb,k} - \tau u_{hvb,k}. \tag{8.11e}$$

8.3.2. SQP Formulation

To form a convex SQP formulation, we propose to relax the (nonconvex) quadratic input-output behavior of the converters (8.10b) to a convex quadratic approximation by linearizing (8.10b) around $[(x_{m,k}^i)^\top \ (u_{m,k}^i)^\top]^\top$ and adding a convex quadratic part, i.e.,

$$y_{m,k} \approx \tfrac{1}{2}\left(\begin{bmatrix} x_k \\ u_k \end{bmatrix} - \begin{bmatrix} x_k^i \\ u_k^i \end{bmatrix}\right)^\top R_m \left(\begin{bmatrix} x_k \\ u_k \end{bmatrix} - \begin{bmatrix} x_k^i \\ u_k^i \end{bmatrix}\right) + \left(H_m \begin{bmatrix} x_k^i \\ u_k^i \end{bmatrix} + F_m\right)^\top \begin{bmatrix} x_k \\ u_k \end{bmatrix} + e_m, \tag{8.12}$$

for all $k \in \mathcal{K}$ and $m \in \mathcal{M}$, where the matrix $R_m \succeq 0$ is chosen such that (8.12) is convex. We note that the approximation error disappears when $x_{m,k} \to x_{m,k}^i$, $u_{m,k} \to u_{m,k}^i$, and by choosing $R_m = H_m$, we retrieve the original quadratic equation (8.10b). By substituting (8.12) into (8.10a) and (8.10f) and linearizing the dynamics (8.10c), we arrive at the convex SQP subproblem

$$\begin{aligned} \{x_{m,k}^{i+1}, u_{m,k}^{i+1}\}_{k\in\mathcal{K}, m\in\mathcal{M}} = \underset{x_{m,k}, u_{m,k}}{\operatorname{argmin}} \sum_{m\in\mathcal{M}} \sum_{k\in\mathcal{K}} & \tfrac{1}{2} b_m \left(\begin{bmatrix} x_k \\ u_k \end{bmatrix} - \begin{bmatrix} x_k^i \\ u_k^i \end{bmatrix}\right)^\top R_m \left(\begin{bmatrix} x_k \\ u_k \end{bmatrix} - \begin{bmatrix} x_k^i \\ u_k^i \end{bmatrix}\right) \\ & + \left(b_m H_m \begin{bmatrix} x_k^i \\ u_k^i \end{bmatrix} + b_m F_m + \begin{bmatrix} 0 \\ a_m \end{bmatrix}\right)^\top \begin{bmatrix} x_k \\ u_k \end{bmatrix} + b_m e_m, \end{aligned} \tag{8.13a}$$

subject to the linearized state dynamics, i.e.,

$$x_{m,k+1} - f_m(x^i_{m,k}, u^i_{m,k}) - \nabla f_m(x^i_{m,k}, u^i_{m,k})\left(\begin{bmatrix} x_k \\ u_k \end{bmatrix} - \begin{bmatrix} x^i_k \\ u^i_k \end{bmatrix}\right) = 0, \tag{8.13b}$$

for all $k \in \mathcal{K}$, $m \in \mathcal{M}$, and subject to linear inequality constraints, i.e.,

$$\underline{x}_{m,k} \leq x_{m,k} \leq \overline{x}_{m,k}, \qquad \underline{u}_{m,k} \leq u_{m,k} \leq \overline{u}_{m,k} \tag{8.13c}$$

for all $k \in \mathcal{K}$, $m \in \mathcal{M}$, and further subject to the convex quadratic inequality constraint specifying the interconnection of the subsystems

$$\sum_{m\in\mathcal{M}} \tfrac{1}{2} d_m \left(\begin{bmatrix} x_k \\ u_k \end{bmatrix} - \begin{bmatrix} x^i_k \\ u^i_k \end{bmatrix}\right)^\top R_m \left(\begin{bmatrix} x_k \\ u_k \end{bmatrix} - \begin{bmatrix} x^i_k \\ u^i_k \end{bmatrix}\right) + \left(d_m H_m \begin{bmatrix} x^i_k \\ u^i_k \end{bmatrix} + d_m F_m + \begin{bmatrix} 0 \\ c_m \end{bmatrix}\right)^\top \begin{bmatrix} x_k \\ u_k \end{bmatrix} + d_m e_m \leq 0, \tag{8.13d}$$

for all $m \in \mathcal{M}$.

8.3.3. Dual Decomposition

Note that (8.13a) subject to (8.13b) and (8.13c) is entirely separable, and the only complicating constraint is (8.13d), which is the constraint that acts on all components $m \in \mathcal{M}$. Therefore, we propose to decompose (8.13) via dual decomposition by augmenting the objective function with the constraint (8.13d), which results in the so-called 'partial Lagrangian':

$$\begin{aligned} L(\{x_{m,k}, u_{m,k}, \lambda_k\}) = \sum_{k\in\mathcal{K}} \sum_{m\in\mathcal{M}} & \tfrac{1}{2} \left(\begin{bmatrix} x_k \\ u_k \end{bmatrix} - \begin{bmatrix} x^i_k \\ u^i_k \end{bmatrix}\right)^\top \widehat{R}_{m,k} \left(\begin{bmatrix} x_k \\ u_k \end{bmatrix} - \begin{bmatrix} x^i_k \\ u^i_k \end{bmatrix}\right) \\ & + \left(\widehat{H}_{m,k} \begin{bmatrix} x^i_k \\ u^i_k \end{bmatrix} + \widehat{F}_{m,k}\right)^\top \begin{bmatrix} x_k \\ u_k \end{bmatrix} + \widehat{E}_{m,k}, \end{aligned} \tag{8.14a}$$

in which,

$$\begin{aligned} \widehat{R}_{m,k} &= (b_m + d_m \lambda_k) R_m, \\ \widehat{H}_{m,k} &= (b_m + d_m \lambda_k) H_m, \\ \widehat{F}_{m,k} &= (b_m + d_m \lambda_k) F_m + (a_m + c_m \lambda_k) \begin{bmatrix} 0 \\ 1 \end{bmatrix}, \\ \widehat{E}_{m,k} &= (b_m + d_m \lambda_k) e_m, \end{aligned} \tag{8.14b}$$

where $\lambda_k \geq 0 \in \mathbb{R}^N$ is a Lagrange multiplier. The partial Lagrange dual function is then given by

$$g(\{\lambda_k\}) = \min_{x_{m,k}, u_{m,k}} L(\{x_{m,k}, u_{m,k}, \lambda_k\}) = \sum_{m\in\mathcal{M}} g_m(\{\lambda_k\}) + \widehat{E}_{m,k}, \tag{8.15a}$$

subject to (8.13b)-(8.13d), with

$$g_m(\{\lambda_k\}) = \min_{x_{m,k}, u_{m,k}} \sum_{k\in\mathcal{K}} \tfrac{1}{2} \left(\begin{bmatrix} x_k \\ u_k \end{bmatrix} - \begin{bmatrix} x^i_k \\ u^i_k \end{bmatrix}\right)^\top \widehat{R}_{m,k} \left(\begin{bmatrix} x_k \\ u_k \end{bmatrix} - \begin{bmatrix} x^i_k \\ u^i_k \end{bmatrix}\right) + \left(\widehat{H}_{m,k} \begin{bmatrix} x^i_k \\ u^i_k \end{bmatrix} + \widehat{F}_{m,k}\right)^\top \begin{bmatrix} x_k \\ u_k \end{bmatrix}, \tag{8.15b}$$

subject to (8.13b) and (8.13c), the dual problem for each component. Note that for the components whose dynamics $f_m(x_{m,k}, u_{m,k})$ are linear and $R_m = H_m$ yields a convex dual problem (8.15b), SQP is not needed to solve the dual problem, as they can be solved as a QP problem. Typically, g_{egu} and g_{hvb} are both QP problems and g_{em} is an SQP problem that can be solved through the approach given in Section 8.3. However, it may still be beneficial to apply regularization to the other components, since it may improve convergence properties, as we will show in Section 8.4. The dual problem is given by

$$\max_{\lambda_k} g(\{\lambda_k\}) = d^*, \tag{8.16}$$

subject to (8.13b) and (8.13c), where d^* is defined as the dual optimal solution. The dual problem (8.16) gives a lower bound on the primal optimal value p^* of problem (8.13), i.e.,

$$d^* \leq p^*. \tag{8.17}$$

The dual problem equals the primal problem, i.e. $d^* = p^*$, if problem (8.13) is convex and the constraints satisfy Slater's constraint qualifications[20]. As we have formed a convex SQP subproblem (8.13) and assume that the Slater's constraint qualifications are satisfied for this problem formulation, we have that $d^* = p^*$ in our SQP and dual decomposition approach. We maximize the dual problem (8.16) with a steepest ascend method, i.e.,

$$\lambda_k^{i+1} = \max\{0, \lambda_k^i + \rho_k\big(\sum_{m\in\mathcal{M}} c_m u_{m,k}^{i+1} + d_m y_{m,k}^{i+1}\big)\}, \tag{8.18}$$

for all $k \in \mathcal{K}$, where $\rho_k \geq 0$ is chosen small enough such that the dual problem converges. A proof of converge of the dual decomposition(without SQP) is given in [11], however, in our approach, note that in 1 iteration, we solve both the SQP subproblem (8.13) as well as update the Lagrangian multiplier λ_k for all $k \in \mathcal{K}$. This may violate the proof given in [11], although we have found that as long as R_m for all $m \in \mathcal{M}$ are well chosen, this is the fastest way to let the dual problem converge. Furthermore, in [11], a more complex update rule is proposed to maximize the dual problem (8.16), which may further improve convergence. The dual problem (8.16) is terminated similarly to the SQP (8.4), i.e, it is terminated under the condition that

$$|J^{i+1} - J^i| \leq \Delta_{\text{tol}}, \tag{8.19a}$$

in which Δ_{tol} is a certain specified tolerance, and

$$\begin{aligned} J^i = &\sum_{k\in\mathcal{K}} \tau y_{egu,k} + \nu_1 \sum_{k\in\mathcal{K}} \max\{0, \sum_{m\in\mathcal{M}} c_m u_{m,k}^i + d_m y_{m,k}^i\} \\ &+ \nu_2 \sum_{m\in\mathcal{M}} \sum_{k\in\mathcal{K}} |x_{m,k+1}^i - f(x_{m,k}^i, u_{m,k}^i)|, \end{aligned} \tag{8.19b}$$

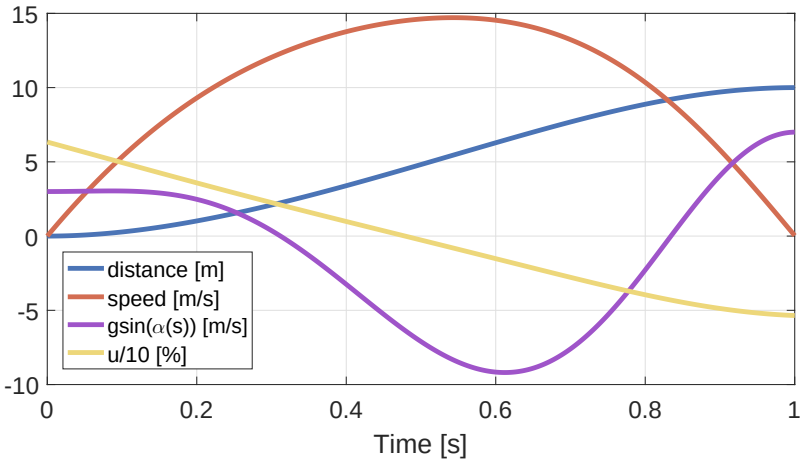

Figure 8.2: Results of the FEV case study.

where $\nu_1 \geq 0$ and $\nu_2 \geq 0$ are penalty parameters. The merit function (8.19b) has a cost term that defines the fuel consumption, a penalty term related to the violation of the state equality constraints (8.10c), and a penalty term related to the augmented inequality constraint (8.10f). Indeed, these two constraints are the only constraints that may be violated at iteration i of the dual problem (8.16), and thus have a contribution in the merit function (8.19b). This concludes the SQP and dual decomposition approach presented in this section, where by formulating (8.10) as a convex SQP subproblem (8.13), we could form the dual problem (8.16), which solves the vehicle energy management problem (8.10).

8

8.4. Results

In this section, we show the results of two simulation studies where the Eco-driving problem is present. In the first simulation study, we will use the SQP approach presented in Section 8.2 to replicate the results of the Eco-driving problem for a full-electric vehicle (FEV) detailed in [13]. In the second simulation study, we consider an energy management problem for a series-hybrid electric vehicle, and solve this with the approach presented in Section 8.3. The results of this simulation are comparable to the results presented in [16], yet not exactly the same, due to slightly different models that are used.

Table 8.1: Full Electric Vehicle Parameters

$p_0 = 3$	$v(t_0) = 0$	$\sigma_r = 0.1$	$\gamma_0 = 0$
$p_1 = 0.4$	$v(t_f) = 0$	$\sigma_v = 10^{-3}$	$\gamma_1 = 10^3$
$p_2 = -1$	$s(t_0) = 0$	$\sigma_u = 1$	$\gamma_2 = 2\times10^3$
$p_3 = 0.1$	$s(t_f) = 10$	$t_0 = 0$	$t_f = 1$

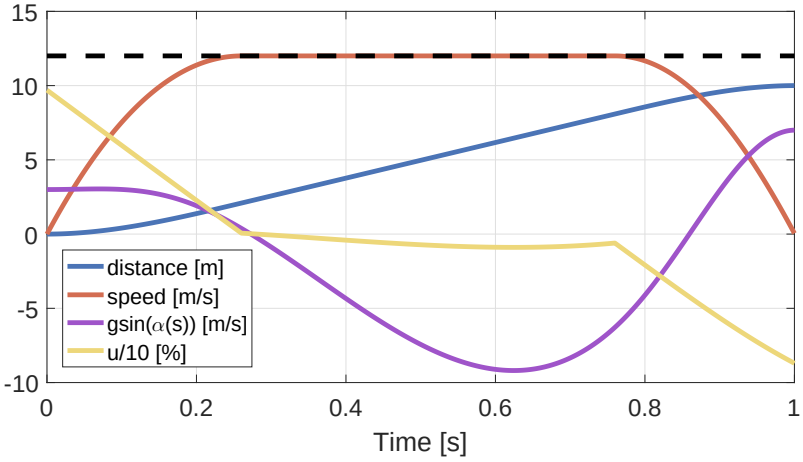

Figure 8.3: FEV case study with state constraints. The black dotted line represents the maximum speed constraint.

8.4.1. Full Electric Vehicle

The full electric vehicle simulation study as presented in [13] has a powertrain consisting of an electric motor (EM) and a high-voltage battery (HVB). However, in this case study, the HVB is not considered, i.e., it is assumed that the HVB has infinite energy storage and no power limitations, which makes it a simple but representative example for eco-driving. Furthermore, the optimal control problem given in [13] does not consider input and state constraints. This follows from the fact that [13] applies Pontryagin's Maximum Principle, in which it is hard to introduce state and input constraints. We solve the eco-driving problem presented in [13] using the discretization approach as presented in Section 8.1, with $\tau = 0.0005$, and SQP, as presented in Section 8.2. We also show that with the SQP approach, adding state and input constraints becomes trivial. In Fig. 8.2, the results of the FEV simulation study, without state and input constraints are shown, in which we see that the initial and final state constraint are satisfied. We further note that the speed curve is not symmetrical, due to the road profile; close to where the slope is steepest, speed is maximized, as is expected. The cost as defined by the discrete-time objective function by the merit function (8.5b) is $J = 1227247.8$, which differs by 0.1% to the cost obtained in [13]. This small difference may be caused due to numerical inaccuracies and the finite sampling time. It is interesting to note that since global optimality and uniqueness of the solution is guaranteed form Chapter 8, the solution obtained with this approach is identical the solutions the presented in [13]. As an illustration to the ease of adding state and input constraints, in Fig. 8.3, the results of the simulation study with a maximum speed constraint of 12 m/s are shown. We observe that with a cost of $J = 1511796.5$, by adding this constraint, the cost becomes higher than without state constraints, as is expected.

8.4.2. Series-Hybrid Electric Vehicle

In this simulation study, we consider the Series-Hybrid Electric Vehicle (SEHV) case study presented in Section 8.3. We solve the case study in a 'forward' and 'backward' simulation using the approach presented in Section 8.3. The term 'forward' and 'backward' refer to way in which the longitudinal vehicle dynamics differential equations (8.1c) are treated. That is, in 'backward' simulation, the differential equations are treated as 'quasi-static' equations, i.e., the states v and s are given a priori and in 'forward' simulation, the differential equations are treated 'dynamically', i.e., the states remain decision variables. We will refer to 'forward' optimization as solving the vehicle energy management problem with eco-driving (8.10), and refer to 'backward' optimization as solving (8.10) as an energy management problem without eco-driving, where the vehicle trajectory information, i.e. speed v_k and distance s_k for all $k \in \mathcal{K}$, are given. We further solve the 'forward' optimization problem with the SQP (8.13), although without applying dual decomposition, which leads to a Quadratically Constrained Quadratic Program (QCQP), which we will refer to as the 'direct' method, to validate the dual decomposition method. We refer to the SQP and dual decomposition approach presented in Section 8.3 as the 'distributed' method. To show additional capabilities of the SQP approach, we show an example where we introduce time-varying minimum and maximum speed constraints.

We base our case study on the work done in [16], in which a convex optimization approach is taken to solve the SEHV case study, where it is formulated a second-order cone program. Due to the chosen problem formulation, the authors in [16] have opted for a piece-wise linear EM model, linear EGU model and a quadratic HVB model. Furthermore, the authors in [16] define the optimization problem in the space domain, for which the physical interpretation of some parts of their problem formulation is not easy to understand. As we have defined the SEHV case study in the time domain, we do not face this issue. To have somewhat comparable results, we fit the parameters of our quadratic EM model using a least-squares fitting tool. We further approximate the linear EGU model with a quadratic EGU model by choosing the quadratic coefficient $\gamma_{egu,2}$ in (8.11c) sufficiently small. The parameters used for the simulation study are shown in Table 8.2. We remark here that the upper and lower bounds for the state and input variables specified in Table 8.2 are defined for all $k \in \mathcal{K}$.

Table 8.2: Series Hybrid Electric Vehicle Parameters

$\gamma_{em,0} = 0.5856$	$m = 15950$ kg	$s_K = 21000$ m
$\gamma_{em,1} = 1.005$	$g = 9.81$ m/s^2	$x_{hvb,0} = 11988$ kJ
$\gamma_{em,2} = 5.052\times10^{-4}$	$c_d = 0.7$	$x_{hvb,K} = x_{hvb,0}$
$\gamma_{egu,0} = 38$	$c_r = 0.0007$	$\overline{v}_k = 22.22$ m/s
$\gamma_{egu,1} = 2.52$	$A_f = 7.54$ m^2	$\underline{v}_k = 16.67$ m/s
$\gamma_{egu,2} = 2\times10^{-5}$	$\rho_A = 1.184$ kg/m^2	$\overline{x}_{hvb,k} = 22680$ kJ
$\gamma_{hvb,0} = 0$	$v_0 = 19.44$ m/s	$\underline{x}_{hvb,k} = 7560$ kJ
$\gamma_{hvb,1} = -1$	$v_K = v_0$	$\overline{u}_{hvb,k} = 92.4$ kW
$\gamma_{hvb,2} = 1.671\times10^{-3}$	$s_0 = 0$ m	$\underline{u}_{hvb,k} = -92.4$ kW

The simulations are done for 1080 s over a distance of 21km with a step size τ = 5 s, which gives an optimization horizon K = 216. In 'backward' optimization, the speed is given by a constant speed of v_k = 70 km/h for all $k \in \mathcal{K}$, and in 'forward' optimization the initial and final velocity are given, while over the trajectory the speed is allowed to vary by 70 $\pm$ 10 km/h. We choose $R_{hvb} = H_{hvb}$ for the HVB dual problem g_{hvb}, as it has a convex quadratic objective function and linear constraints. As the EGU dual problem g_{egu} also has a convex quadratic objective function and linear constraint, it may be solved as a QP problem, and thus we may choose $R_{egu} = H_{egu}$. However, we will show that, because the quadratic term H_{egu} is small in magnitude for the dual problem g_{egu}, it is beneficial to tune $R_{egu} \succeq 0$, such that convergence of the dual problem (8.16) is improved. The EM dual problem g_{em} has a nonconvex quadratic objective function and nonlinear constraints, and thus we are restricted to choose an $R_{em} \succeq 0$. Specifically, we choose $R_{em} = 0.02\left[\begin{smallmatrix} 0 & 0 \\ 0 & I \end{smallmatrix}\right]$. As initial conditions for the 'forward' optimization, we choose the solutions of the 'backward' optimization. For the termination of the dual problem (8.16), we choose $\delta_{\text{tol}} = 10^{-3}$ in (8.19a) and $\nu_1 = 10^3$, $\nu_2 = 10^4$ for the penalty parameters of the merit function. In Fig. 8.4, the simulation results for 'backward' and 'forward' optimization using the 'distributed' method, and 'forward' optimization using the 'direct' method are given. It can be seen that the results for 'forward' optimization using the 'direct' method and 'distributed' method are almost the same, which validates the dual decomposition approach. In the 'forward' optimization results, we see that between 0 and 2 km, where the slope becomes negative, the vehicle reaches the lower speed bound. This action allows the available potential energy from the road profile, between 2 and 13 km, to be maximally converted to kinetic energy; the vehicle speed is maximized in this interval. After 13 km, the road gradient becomes positive and speed is minimized such that the final speed constraint is met. Therefore, we can see that as a result of having the speed as a decision variable, in the 'forward' case, the EGU may provide less power over the course of the trajectory, and noticeably less braking power is applied, when it is compared to the 'backward' case. The fuel consumption of the 'backward' and 'forward' simulation cases are 23.41 l/100 km and 22.31 l/100 km respectively. Thus, by including the eco-driving problem into the vehicle energy management problem, approximately 4.7 % decrease in fuel consumption is achieved. This is compared to the fuel consumption obtained in [16], which are 24.35 l/100 km and 23.98 l/100 km for the 'backward' and 'forward' case respectively. This is a 1.54 % decrease in fuel consumption between the 'backward' and 'forward' case. We may explain this difference in fuel consumption savings largely due to the different models used.

Finally, the convergence of the combined SQP and dual decomposition approach presented in Section 8.3 is shown in Fig 8.5. We see that the number of iterations for the dual problem (8.16) is greatly reduced by tuning R_{egu}, even though $R_{egu} = H_{egu} = 2 \times 10^{-5}$ yields a convex problem. Specifically, The dual problem (8.16) converges after 1003 iterations with $R_{egu} = 0.002$ and converges after around 21000 iterations with $R_{egu} = H_{egu}$. We refer to convergence as the point where the dual problem may be terminated according to the tolerance specified by (8.19a), although we have not terminated the dual problem at these specified

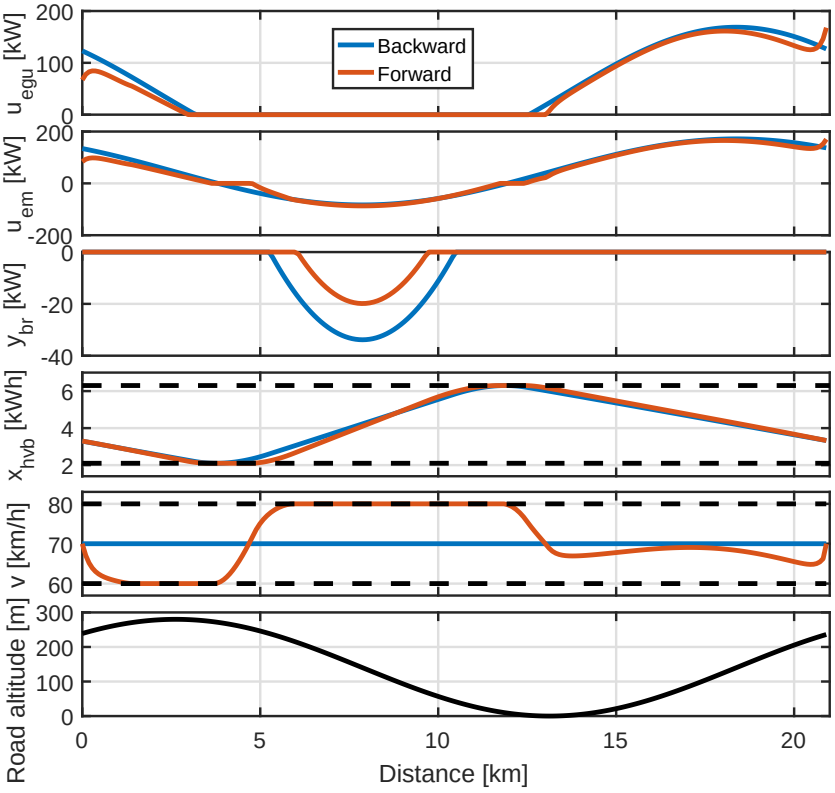

Figure 8.4: Backwards vs forwards optimization. The dotted lines represent minimum and maximum state constraints.

iterations for the purpose of illustration. This shows the additional advantage of regularization, which is the potential to improve convergence, whereas we have used regularization for the EM dual problem g_{egu} to enforce convexity. However, from Fig. 8.5 we also see that we sacrifice robustness for speed of convergence by choosing $R_{egu} = 0.002$, where its graph shows more unstable behavior. However, this is not an issue as long as the required tolerances are reached for the termination of the dual problem.

8.5. Conclusions

In this chapter, we have unified the eco-driving and CVEM in a single optimal control problem formulation. This has broken the dependency of CVEM on a power request known a priori, and it has improved the energy savings that the isolated eco-driving approach can provide. The solutions to this problem have obtained using a scalable distributed optimization algorithm, which is based on a Sequential

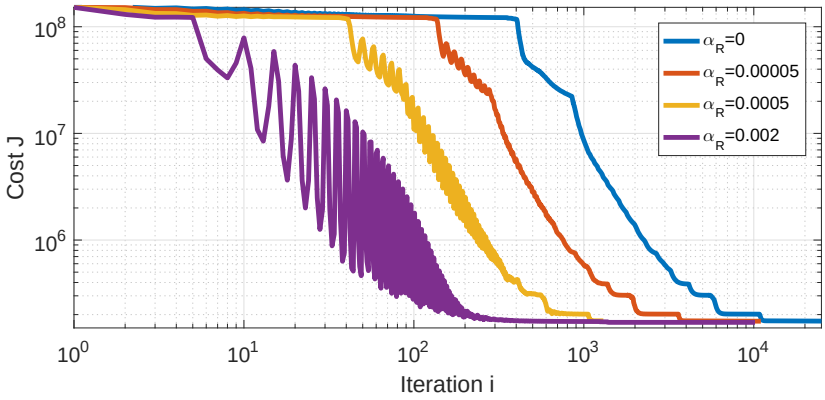

Figure 8.5: Convergence of the SQP and dual decomposition approach.

Quadratic Programming (SQP) algorithm with Thikonov regularization embedded in a dual decomposition scheme. We have done so by formulating a CVEM with eco-driving problem as a convex SQP problem, and applying dual decomposition to solve a dual problem. We have considered two case studies for the eco-driving problem. In the first case study, we have solved the eco-driving problem for a Full Electric Vehicle using the SQP algorithm and have shown that the algorithm yields a very similar result as the benchmark problem set in [13], and shown that adding state constraints is trivial using SQP. In the second case study, we have solved an energy management problem with eco-driving for a Series-Hybrid Electric Vehicle with the SQP algorithm and dual decomposition. We have shown that using our approach, we have had the opportunity to use more representable powertrain models than in [16], and as a result have the potential to save more fuel by incorporating eco-driving to the energy management problem.

References

[1] T. Romijn, M. Donkers, J. Kessels, and S. Weiland, *A dual decomposition approach to complete energy management for a heavy-duty vehicle,* in *Proc. Conference on Decision and Control* (2014).

[2] J. van Schijndel, M. Donkers, F. Willems, and W. Heemels, *Dynamic programming for integrated emission management in diesel engines,* IFAC Proceedings Volumes (2014).

[3] T. M. Padovani, M. Debert, G. Colin, and Y. Chamaillard, *Optimal energy management strategy including battery health through thermal management for hybrid vehicles,* Proc. IFAC World Congress (2013).

[4] S. Ebbesen, P. Elbert, and L. Guzzella, *Battery state-of-health perceptive en-*

ergy management for hybrid electric vehicles, IEEE Trans. Control Syst. Tech. (2012).

[5] Z. Khalik, T. Romijn, M. Donkers, and S. Weiland, *Effects of battery charge acceptance and battery aging in complete vehicle energy management,* Proc. IFAC World Congress (2017).

[6] J. Kessels, J. Martens, P. van den Bosch, and W. Hendrix, *Smart vehicle powernet enabling complete vehicle energy management,* in *Proc. IEEE Vehicle Power and Propulsion Conference* (2012).

[7] D. P. Bertsekas, *Dynamic programming and optimal control*, Vol. 1 (Athena Scientific Belmont, MA, 1995).

[8] L. V. Pérez, G. R. Bossio, D. Moitre, and G. O. García, *Optimization of power management in an hybrid electric vehicle using dynamic programming,* Math. Comput. Simulation (2006).

[9] T. Pham, J. Kessels, P. van den Bosch, R. Huisman, and R. Nevels, *On-line energy and battery thermal management for hybrid electric heavy-duty truck.* in *Proc. American Control Conference* (2013).

[10] N. Murgovski, L. Johannesson, J. Sjöberg, and B. Egardt, *Component sizing of a plug-in hybrid electric powertrain via convex optimization,* Mechatronics (2012).

[11] T. Romijn, M. Donkers, J. Kessels, and S. Weiland, *Complete vehicle energy management with large horizon optimization,* in *in Proc. Conference on Decision and Control* (2015).

[12] T. van Keulen, B. de Jager, and M. Steinbuch, *Optimal trajectories for vehicles with energy recovery options,* Proc. IFAC World Congress (2011).

[13] N. Petit and A. Sciarretta, *Optimal drive of electric vehicles using an inversion-based trajectory generation approach,* Proc. IFAC World Congress (2011).

[14] G. Heppeler, M. Sonntag, U. Wohlhaupter, and O. Sawodny, *Predictive planning of optimal velocity and state of charge trajectories for hybrid electric vehicles,* Control Engineering Practice (2017).

[15] E. Hellström, J. Åslund, and L. Nielsen, *Design of an efficient algorithm for fuel-optimal look-ahead control,* Control Engineering Practice (2010).

[16] N. Murgovski, L. Johannesson, X. Hu, B. Egardt, and J. Sjöberg, *Convex relaxations in the optimal control of electrified vehicles,* in *Proc. American Control Conference* (2015).

[17] J. Nocedal and S. J. Wright, *Sequential quadratic programming* (Springer, 2006).

[18] P. T. Boggs and J. W. Tolle, *Sequential quadratic programming,* Acta numerica (1995).

[19] L. Etman, A. A. Groenwold, and J. Rooda, *First-order sequential convex programming using approximate diagonal qp subproblems,* Structural and Multidisciplinary Optimization (2012).

[20] S. Boyd and L. Vandenberghe, *Convex Optimization* (Cambridge University Press, Cambridge, 2004).

III

Experimental Results and Conclusions

9

A Shrinking Horizon Approach to Eco-driving for Electric City Buses: Implementation and Experimental Results

This chapter presents an efficient shrinking horizon implementation to solve the eco-driving problem. The efficient implementation is demonstrated on a case study of a fully electric bus, driving on an inner-city public transport route. Because the bus drives on designated bus lanes, meaning that it has little interaction with other traffic, and because it has frequent and predictable stops, this case will have a good energy consumption savings potential. An energy consumption reduction of 11.43% *is achieved on a simulation study for the case that the vehicle is fully autonomous and a reduction of* 6.94% *is achieved experimentally for the case that the driver is 'coached' using a driver assistance system.*

This chapter is based on **P.6**.

Eco-driving aims to find a velocity profile that minimizes the energy consumption of a vehicle covering a given route on a fixed amount of time. In Chapter 2, the eco-driving problem was formulated as an optimal control problem (OCP) and it was shown that it as only a global optimal solution. Moreover, a sequential quadratic program (SQP) was used to find the solution to the eco-driving OCP. The results were presented only using a simulation study. In this chapter, the problem formulation and optimization method proposed in Chapter 2 are used to design an online shrinking horizon implementation of eco-driving. Moreover, experimental results that shows its potential to reduce the energy consumption are presented. As a case study, a fully electric city-bus is used on an inner-city public transport route. We consider an ideal scenario for eco-driving, where the city bus drives on designated lanes, meaning that it has no interaction with other traffic, and has frequent and predictable stops.

First, an efficient online implementable algorithm of the solution strategy described in Chapter 2 is presented. In this efficient algorithm, the solution to the state-space model is substituted into the objective function and constraints, as is often done in model-predictive control, leading to a significant reduction of the number of decision variables, when compared to the formulation presented in Chapter 2. This implementation is also be used in a so-called shrinking horizon fashion. A shrinking horizon is needed because at every time instant, the optimal control input is recomputed for a shorter time horizon, due to the fact that the time and distance to the next bus stop is smaller than during the previous time instant. We will present two results: the first being a simulation study for the case that the vehicle speed is exactly controlled (i.e., assuming a fully automated vehicle), and the second being an experimental study for the case that the driver is 'coached' using a driver assistance system that interacts with the driver through a human-machine interface. Both studies will show that the energy consumption of the bus can be reduced significantly.

The remainder of this chapter is organized as follows. In Section 9.1, the eco-driving and the solution strategy of Chapter 2 are briefly summarized. In Section 9.2, the real-time shrinking horizon implementation of this solution strategy is presented. Section 9.3 presents simulation results for the case that the vehicle speed is controlled in an automated fashion. Section 9.4 presents experimental results in case the driver is coached using a driver assistance system. Finally, conclusions are drawn in Section 9.5.

9.1. Eco-Driving Control Problem

In this section, we introduce the continuous-time eco-driving problem and the discrete-time solution approach presented in [1]. This solution approach will serve as a basis for our proposed efficient real-time implementation.

9.1.1. Continuous-Time Formulation

Let us revisit the eco-driving problem of Chapter 2. In eco-driving, we aim to minimize the total energy consumed by a vehicle over a given time interval $[t_0, t_f]$ and trajectory $s(t) \in [s_0, s_f]$ for a road grade $\alpha(s) \in \left[-\frac{\pi}{2}, \frac{\pi}{2}\right]$, which depends on the position s. This can be formulated as a continuous-time Optimal Control Problem (OCP) given by

$$\min_{s(t),v(t),u(t)} \quad \int_{t_0}^{t_f} P(v(t), u(t))dt \tag{9.1a}$$

$$\text{subject to} \quad m\frac{dv}{dt} = u(t) - \sigma_d v^2 - mg\gamma(s), \tag{9.1b}$$

$$\frac{ds}{dt} = v(t), \quad \frac{dv}{dt} = a(t), \tag{9.1c}$$

$$s(t_0) = s_0, \quad v(t_0) = v_0, \tag{9.1d}$$

$$s(t_f) = s_f, \quad v(t_f) = v_f, \tag{9.1e}$$

$$\underline{v} \leq v(t) \leq \overline{v}, \tag{9.1f}$$

$$\underline{a} \leq a(t) \leq \overline{a}, \tag{9.1g}$$

where (9.1b) represents the longitudinal vehicle dynamics of a vehicle with mass m, aerodynamic drag coefficient σ_d and rolling resistance and gravity forces, with gravitational constant g, where the latter two are combined in

$$\gamma(s) = c_r \cos(\alpha(s)) + \sin(\alpha(s)), \tag{9.2}$$

where c_r describes the rolling force coefficient. Furthermore, the non-negative velocity is bounded by (9.1f). In (9.1g), we have also included bounds on the acceleration, which can be done without compromising the uniqueness of the solution claimed by [1]. As in Chapter 2 of this thesis, the consumed power in the driveline is assumed to be a quadratic function given by

$$P(v, u) = \beta_0 v^2 + \beta_1 vu + \beta_2 u^2, \tag{9.3}$$

where β_0, β_1 and β_2 are non-negative parameters that describe the contribution of Ohmic and mechanical friction loses in the power consumption.

9.1.2. Discretization

As in Chapter 2 of this thesis, the OCP (9.1) is discretized at times $t_k = k\tau + t_0$, $k \in \mathcal{K} = \{0, \ldots, N\}$, with time steps $\tau = \frac{t_f - t_0}{N}$, for some $N \in \mathbb{N}$ using a forward Euler discretization method. Additionally, the non-linear equality constraint (9.1b) is included in the objective function (9.1a), resulting a Quadratic Programming (QP)

problem, given by

$$\min_{\{a_k,s_k,v_k\}_{k\in\mathcal{K}}} \quad \sum_{k=0}^{N-1} \tau P(a_k,s_k,v_k) \tag{9.4a}$$

$$\text{subject to} \quad s_{k+1} = s_k + \tau v_k, \tag{9.4b}$$

$$v_{k+1} = v_k + \tau a_k, \tag{9.4c}$$

$$s_0 = s_o, \quad v_0 = v_o, \tag{9.4d}$$

$$s_N = s_f, \quad v_N = v_f, \tag{9.4e}$$

$$\underline{v} \le v_k \le \overline{v}, \tag{9.4f}$$

$$\underline{a} \le a_k \le \overline{a}, \tag{9.4g}$$

where $a_k = a(t_k)$, $v_k = v(t_k)$ and $s_k = s(t_k)$, and

$$\begin{aligned} P(a_k,s_k,v_k) =& \beta_0 v_k^2 + \beta_1 v_k \left(m a_k + \sigma_d v_k^2 + mg\gamma(s_k)\right) \\ &+ \beta_2 \left(m a_k + \sigma_d v_k^2 + mg\gamma(s_k)\right)^2 \end{aligned} \tag{9.5}$$

represents the driveline power consumption, now dependent on the acceleration, position and velocity of the vehicle.

9.1.3. Sequential Quadratic Programming for Eco-driving

The uniqueness and global optimality of the solution to the discrete-time OCP (9.4) has been formally shown in Chapter 2. Moreover, it was suggested that Sequential Quadratic Programming (SQP) is a suitable approach to obtain the solution.

In this chapter, we employ the SQP approach presented in Chapter 2. Like in any SQP approach, a nonlinear program is solved by iteratively solving QP approximations of the nonlinear program. For the OCP (9.4), this leads to

$$\{\mathbf{a}^{i+1},\mathbf{x}^{i+1}\} = \underset{\mathbf{a},\mathbf{x}}{\operatorname{argmin}} \sum_{k\in\mathcal{K}} \tau\ P_{QP}(\mathbf{a},\mathbf{x},\mathbf{a}^i,\mathbf{x}^i) \tag{9.6}$$

$$\text{subject to} \quad (9.4b) - (9.4g),$$

for all $k \in \mathcal{K}$, with $P_{QP}(\mathbf{a},\mathbf{x},\mathbf{a}^i,\mathbf{x}^i)$, a second-order approximation of (9.5), given by

$$P_{QP}(\mathbf{a},\mathbf{x},\mathbf{a}^i,\mathbf{x}^i) = \tfrac{1}{2}\begin{bmatrix}\mathbf{a}\\ \mathbf{x}\end{bmatrix}^\top \widehat{\mathbf{H}} \begin{bmatrix}\mathbf{a}\\ \mathbf{x}\end{bmatrix} + \left(\begin{bmatrix}\mathbf{G}_{\mathbf{a}}^i\\ \mathbf{G}_{\mathbf{x}}^i\end{bmatrix}^\top - \begin{bmatrix}\mathbf{a}^i\\ \mathbf{x}^i\end{bmatrix}^\top \widehat{\mathbf{H}}\right)\begin{bmatrix}\mathbf{a}\\ \mathbf{x}\end{bmatrix}, \tag{9.7}$$

where the superscript i refers to the solution of the i-th iteration of the SQP algo-

rithm, and

$$\mathbf{a} = \left[a_0, \dots, a_{N-1}\right]^\top \in \mathbb{R}^N, \tag{9.8}$$

$$\mathbf{x} = \left[s_0, v_0, \dots, s_{N-1}, v_{N-1}\right]^\top \in \mathbb{R}^{2N}, \tag{9.9}$$

$$\widehat{\mathbf{H}} = \operatorname{diag}\left(\widehat{\mathbf{H}}_\mathbf{a}, \widehat{\mathbf{H}}_\mathbf{x}\right) \in \mathbb{R}^{3N\times 3N}, \tag{9.10}$$

$$\mathbf{G}_\mathbf{a} = \left[\frac{\partial P(a_0,s_0,v_0)}{\partial a_0}, \dots, \frac{\partial P(a_{N-1},s_{N-1},v_{N-1})}{\partial a_{N-1}}\right]^\top \in \mathbb{R}^N, \tag{9.11}$$

$$\mathbf{G}_\mathbf{x} = \left[\frac{\partial P(a_0,s_0,v_0)}{\partial s_0}, \frac{\partial P(a_0,s_0,v_0)}{\partial v_0}, \dots, \frac{\partial P(a_{N-1},s_{N-1},v_{N-1})}{\partial s_{N-1}}, \frac{\partial P(a_{N-1},s_{N-1},v_{N-1})}{\partial v_{N-1}}\right]^\top \in \mathbb{R}^{2N}. \tag{9.12}$$

In (9.10), the Hessian matrix is approximated to a diagonal positive definite matrix [1], given by

$$\widehat{\mathbf{H}}_\mathbf{a} = 2\beta_2 m^2 \mathbf{I}_N \in \mathbb{R}^{N\times N}, \tag{9.13}$$

$$\widehat{\mathbf{H}}_\mathbf{x} = \operatorname{diag}\left(\epsilon_s, \max(h_{v_0},\ \epsilon_v),\ \dots \epsilon_s, \max(h_{v_{N-1}},\ \epsilon_v)\right) \in \mathbb{R}^{2N\times 2N}, \tag{9.14}$$

in which $\mathbf{I}_n \in \mathbb{R}^{n\times n}$ is a n-dimensional identity matrix, ϵ_s and ϵ_v are small positive numbers that guarantee the positive definiteness of the Hessian matrix, and

$$h_{v_k} = 2\beta_0 + 6\beta_1\sigma_d v_k + 4\beta_2\sigma_d\left(mg\gamma(s_k) + 3\sigma_d v_k^2\right). \tag{9.15}$$

The gradients of the power consumption (9.5) are considered in (9.11) and (9.12), where

$$\frac{\partial P(a_k,s_k,v_k)}{\partial a_k} = 2\beta_2 m^2\left(g\gamma(s_k) + a_k\right), \tag{9.16}$$

$$\frac{\partial P(a_k,s_k,v_k)}{\partial s_k} = 2\beta_2 mg\frac{\partial\gamma(s_k)}{\partial s_k}\left(ma_k + mg\gamma(s_k) + \sigma_d v_k^2\right), \tag{9.17}$$

$$\frac{\partial P(a_k,s_k,v_k)}{\partial v_k} = 2\beta_0 v_k + 3\beta_1\sigma_d v_k^2 + 4\beta_2\sigma_d v_k\left(mg\gamma(s_k) + \sigma_d v_k^2\right). \tag{9.18}$$

The QP iterations (9.6) repeat until its solution converges. We consider the algorithm to have converged if

$$\left\|\begin{bmatrix}\mathbf{a}^i\\ \mathbf{x}^i\end{bmatrix} - \begin{bmatrix}\mathbf{a}^{i-1}\\ \mathbf{x}^{i-1}\end{bmatrix}\right\|_2 \le \rho, \tag{9.19}$$

where, $\|\cdot\|_2$ is the 2-norm operator, i and $i-1$ represent the current and previous QP solutions, respectively, and $\rho \in \mathbb{R}$ is a given non-negative convergence tolerance.

This approach provides a tractable solution to the eco-driving OCP (9.4). In the next section, we will modify this method to obtain a real-time implementation for the eco-driving problem.

9.2. Real-Time Implementation

To arrive at a real-time implementable algorithm, the computation time needs to be low, such that solutions can be obtained in a shorter time than the sampling period

used in the embedded system. In this section, we will modify the SQP method presented in the previous section to reduce the computation time by means of a reduction on the number of decision variables and the application of a *shrinking horizon approach* that uses a previous solution as *warm-start* for the next optimization problem. This reduction of the number of decision variables does not affect the solution (and its optimality).

9.2.1. Improving Computational Efficiency

In this section, we will reduce the number of decision variables by eliminating the state $\mathbf{x}$ in (9.6). This leads to a significant reduction of the computation time, because the computation time of the QP subproblems scales cubically with the number of decision variables [2]. By eliminating the state $x_k = [s_k \;\; v_k]^\top$ from the QP problems an improvement of the computation time is expected by a factor of $3^3 = 27$, when compared to [1].

In order to reduce the number of decision variables, the longitudinal motion of the vehicle described by the equality constraints (9.4b)-(9.4d) can be recast as a prediction model for instants $k \in \mathcal{K}$ as

$$\mathbf{x} = \Phi x_0 + \Gamma \mathbf{a}, \tag{9.20}$$

where $\Phi \in \mathbb{R}^{2N\times 2}$ and $\Gamma \in \mathbb{R}^{2N\times N}$ are defined by

$$\Phi = \begin{bmatrix} \mathbf{I}_2 \\ A \\ A^2 \\ \vdots \\ A^{N-1} \end{bmatrix}, \quad \Gamma = \begin{bmatrix} \mathbf{0}_2 & \mathbf{0}_2 & \dots & \mathbf{0}_2 \\ B & \mathbf{0}_2 & \dots & \mathbf{0}_2 \\ AB & B & \dots & \mathbf{0}_2 \\ \vdots & \vdots & \ddots & \vdots \\ A^{N-2}B & A^{N-3}B & \dots & \mathbf{0}_2 \end{bmatrix} \tag{9.21}$$

with

$$A = \begin{bmatrix} 1 & \tau \\ 0 & 1 \end{bmatrix}, \quad B = \begin{bmatrix} 0 \\ \tau \end{bmatrix}, \tag{9.22}$$

and $\mathbf{0}_n$ a n-dimensional column vector with all entries zero. For $k = N$, the final state given by (9.4e) can be expressed as the following equality constraint

$$\begin{bmatrix} A^{N-1}B & A^{N-2}B & \dots & B \end{bmatrix} \mathbf{a} = x_N - A^N x_0. \tag{9.23}$$

By substituting (9.10) and (9.20) into (9.7), we remove the dependency on the state $\mathbf{x}$ in (9.7). After removing the constant terms (which do not change the solution), we obtain

$$\mathbf{P_{QP}}(\mathbf{a}, \mathbf{a}^i) = \tfrac{1}{2}\mathbf{a}^\top \left(\widehat{\mathbf{H}}^i_{\mathbf{a}} + \Gamma^\top \widehat{\mathbf{H}}^i_{\mathbf{x}} \Gamma\right) \mathbf{a} + \left(\mathbf{G}^{i\top}_{\mathbf{a}} - \mathbf{a}^{i\top} \widehat{\mathbf{H}}^i_{\mathbf{a}} + \left(\mathbf{G}^{i\top}_{\mathbf{x}} - \mathbf{a}^{i\top}\Gamma^\top \widehat{\mathbf{H}}^i_{\mathbf{x}}\right)\Gamma\right)\mathbf{a}, \tag{9.24}$$

where $\widehat{\mathbf{H}}^i_{\mathbf{a}}$ and $\widehat{\mathbf{H}}^i_{\mathbf{x}}$ are the approximated Hessian respect to acceleration and state, respectively, evaluated in the i-th iteration of the SQP algorithm.

Using the above notation, we obtain the following QP problem with acceleration $\mathbf{a}$ as the only decision variable

$$\{\mathbf{a}^{i+1}\} = \underset{\mathbf{a}}{\operatorname{argmin}} \sum_{k\in\mathcal{K}} \tau\ \mathbf{P_{QP}}(\mathbf{a}, \mathbf{a}^i) \tag{9.25a}$$

subject to (9.23),

$$\underline{v} - \Xi\Phi x_0 \leq\ \Xi\Gamma\mathbf{a}\ \leq \overline{v} - \Xi\Phi x_0, \tag{9.25b}$$

$$\mathbf{1}_N\underline{a} \leq\ \mathbf{a}\ \leq \mathbf{1}_N\overline{a}, \tag{9.25c}$$

where the constraint (9.25b) is obtained by substituting (9.20) in (9.4f) for all $k \in \mathcal{K}$ and considering $\mathbf{v} = \Xi\mathbf{x}$, with a selection matrix $\Xi = I_N \otimes \begin{bmatrix}0 & 1\end{bmatrix} \in \mathbb{R}^{N\times 2N}$, in which the operator $\otimes$ denotes the Kronecker product. Besides, the constraint (9.25c) is directly obtained from (9.4g) for all $k \in \mathcal{K}$ and considering $\mathbf{1}_n \in \mathbb{R}^n$, a n-dimensional column vector with all entries one.

The QP subproblem (9.25) is sequentially solved until it converges, thus finding the global optimal solution to the discrete optimal control eco-driving problem (9.4), with the corresponding convergence criteria defined by

$$\|\mathbf{a}^i - \mathbf{a}^{i-1}\|_2 \leq \rho. \tag{9.26}$$

In practice, a smaller number of decision variables let the optimization problem converges with fewer iterations, which might lead to an additional reduction in computation time.

9.2.2. Considerations for Real-time Implementation

In order to achieve further improvements in terms of computation time, we use an efficient QP solver with *warm-start* and a *shrinking horizon* approach. Shrinking horizon works in a similar way as receding horizon, also known as model-predictive control. At every time instant k, the full optimization problem (9.25) is solved over the horizon N using the actual state x_k as initial value. This leads to a sequence of optimal control inputs $\mathbf{a}$, where only the first a_0 is implemented at time instant k. Now at time t_{k+1} the process repeats, but in contrary to receding horizon control, the control horizon N now becomes 1 time step shorter. The use of shrinking horizon for eco-driving of buses is motivated by the fact that we only need to optimize the vehicle speed until the next bus stop and at every recomputation of the optimal control inputs, the next bus stop becomes nearer.

The fact that the control horizon shrinks makes the optimization problem time dependant. In particular, at time instant k, the eco-driving problem has to be solved over the discrete-time set $\mathcal{K}^k = \{k, \ldots, N\}$. This causes the QP subproblem at time k to become

$$\{\mathbf{a}^{i+1}\} = \underset{\mathbf{a}}{\operatorname{argmin}} \sum_{k\in\mathcal{K}^k} \tau\ \mathbf{P_{QP}}(\mathbf{a}, \mathbf{a}^i) \tag{9.27}$$

subject to (9.23), (9.25b), (9.25c)

where N has become $N-k$ in (9.23) and the matrices in (9.25b) and (9.25c) are modified similarly. The Hessian and gradient matrices in the SQP algorithm also need to be modified *mutatis mutandis*. The shrinking of the horizon is repeated until $N-k < N_{\min}$ for some $N_{\min}$ to avoid unnecessary computations in the last iterations, where not much energy consumption improvement is expected. For this, we apply the first step of the predicted solution, and the remaining part is provided to the solver as initial guess for the next iteration.

9.3. Simulation Study for Electric City Buses

Inner-city public transportation buses, sometimes drive through exclusive lanes to arrive and depart from stops at well defined times. This makes this scenario to have high predictability, which makes it highly suitable for the implementation of eco-driving approaches.

In this section, we will analyze the performance of the solution to eco-driving problem, presented in Section 9.2.1, in the context of electric city buses. The first part of this section shows an identification approach to obtain a control-oriented model for the power consumption of the driveline in an electric bus, which can be used in the real-time optimal eco-driving problem of Section 9.2. Later, this model is used to obtain an optimal velocity profile for an specific driving route and finally, ideal energy savings are calculated with respect to a benchmark velocity profile, that has been obtained from real data logged from a bus driving on a segment of $2.5[km]$ between two bus stops, where the elevation between the highest and the lowest point is less than one meter. Hence, the grade $\alpha(s)$ is considered zero for all s and the rest of its features are given in Table 9.1.

9.3.1. Identification of the Power Consumption Model

The OCP (9.4) considers a simplified control-oriented power consumption model defined by (9.5). For the identification of this model, several realizations over the $2.5[km]$ predefined route are used. This leads to a set of velocity profiles $\{v_k^j\}$, where $j \in \mathcal{J} = \{1, \dots, J\}$ represents the j-th realization of the velocity profile. These velocity profiles are then simulated on a high-fidelity (hi-fi) vehicle model to obtain power consumption profiles $\{\widetilde{P}_k^j\}$ for each given velocity profile. This data can be used to find the parameters β_0, β_1 and β_2 in (9.5) by solving the following constrained least-squares problem

$$\{\beta_0, \beta_1, \beta_2\} = \operatorname{argmin} \sum_{j\in\mathcal{J}} \sum_{k\in\mathcal{K}} \| P(a_k^j, s_k^j, v_k^j) - \widetilde{P}_k^j \|_2^2$$
$$\text{subject to } \beta_0 > 0,\ \beta_1 > 0 \text{ and } \beta_2 > 0, \tag{9.28}$$

Table 9.1: Route characteristics.

$$h(s) : 0[m] \ \big|\ s(t_f) : 2.756[km] \ \big|\ t_f : 211[s]$$

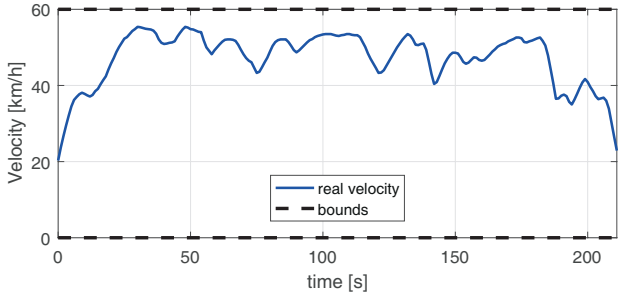

(a) Real velocity profile.

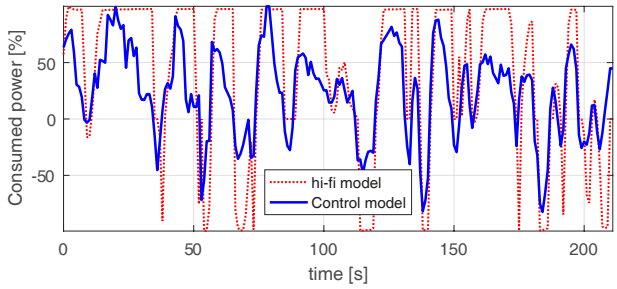

(b) Normalized power consumption.

Figure 9.1: High fidelity and identified control models.

where $P(a_k^j, s_k^j, v_k^j)$ is defined in (9.5). It is important to remark that the hi-fi vehicle model is a *validated* model. Fig. 9.1b depicts the normalized vehicle power consumption, based on a real velocity profile that is shown in Fig. 9.1a. The power consumption described by the hi-fi model is represented by the dotted red line, while the blue line is obtained by identifying the three unknown parameters on the simplified consumption model (9.5).

Although the identified model shows a considerable error with respect to hi-fi model, it is capable to describe a general trend in its behavior. In the last part of this section, we will show that this feature is enough to produce accurate solutions in term of energy savings.

9.4. Assisted Driving Experimental Results

In this section, we will discuss the experimental results obtained by using a driving assistance system that 'coaches' the driver to follow the optimal velocity profile obtained as a solution to the eco-driving problem (9.27). First, we provide details about the case study analysed in this section. Second, the Human Machine Interface (HMI) used to provide visual feedback to the driver is described; and finally, experimental results for the case study are provided and discussed.

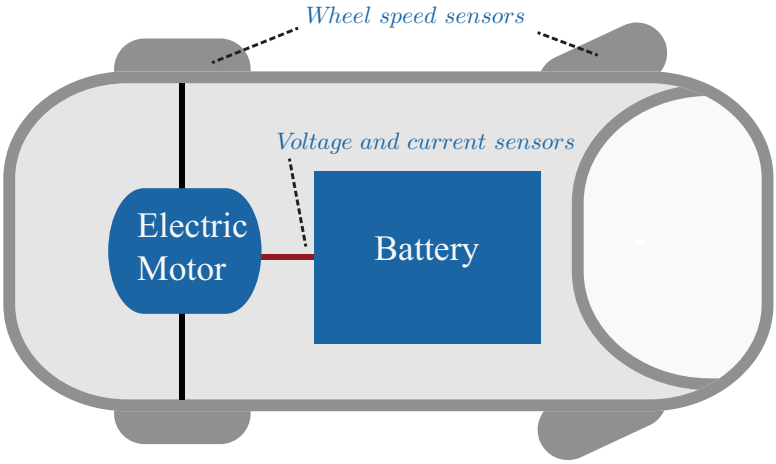

Figure 9.2: Sensors ustilized in the experimatal set up.

9.4.1. Case Study

The experiments have been conducted in the previously selected road, with a distance of $2.5[km]$ that should be covered in $200[s]$, considering a real speed limit of $60[km/h]$. During the experiments, it was registered wind velocity of $30[km/h]$, approximately matching the road direction. The power train layout presented in Fig. 9.2 shows the location of the sensors used for in the experimental set-up. The information provided by the wheel speed sensors and the voltage and battery sensors are read in the through a CAN bus. The power consumed by the vehicle is obtained trough direct measurements of the voltage and current at the battery terminals. The baseline for energy savings is generated by the driver covering the selected road, with the knowledge of velocity bounds and initial and final states. This is compared to the energy consumed while providing visual feedback to the driver and expressed as a percentage ratio of energy savings.

Two drivers have performed the experiments during one day, driving the same bus in both directions. During the experiments, all non-critical safety auxiliary systems where turned off to avoid interference with the results. The power consumption and velocity profiles have been recorded with a sample rate of $1[Hz]$ for data post-processing.

9.4.2. Human-Machine Interface

The Human-Machine Interface (HMI) provides visual feedback to the driver at a specific frequency, based on the solution to the real-time implementation of the eco-driving problem (9.27). The HMI updating frequency should take into account the speed of reaction of the driver. In practice, we the update the HMI at $0.1[Hz]$, which is a frequency considerably smaller than the one used for the real-time implementation of (9.27), i.e. $0.5[Hz]$.

In this case, an external computer manages the HMI that has been developed

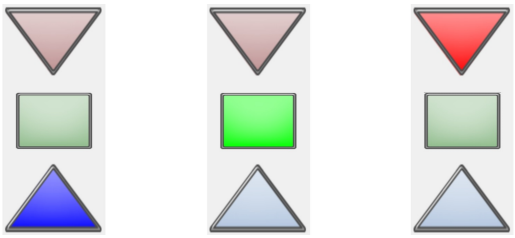

(a) Increase velocity (b) Correct velocity (c) Decrease velocity

Figure 9.3: Human-Machine Interface for velocity feedback

Table 9.2: Experimental energy savings

Wind direction	Driver	Energy savings	Average	Standard deviation
Headwind	Driver 1	1.27%	3.18%	1.09%
	Driver 2	5.09%		1.17%
Tailwind	Driver 1	12.70%	10.70%	1.19%
	Driver 2	8.70%		2.78%
		Total Average	**6.94%**	

in Vector CANoe [3] and depicted in Fig. 9.3. Denoting v_{ref} as the optimal speed and v_{dvr} the current speed, the HMI is updated according to the following rules:

- Increase speed (Fig. 9.3a) : $v_{dvr} < v_{\text{ref}} - 1[\text{km/h}]$.
- Keep current speed (Fig. 9.3b): $v_{\text{ref}} - 1[\text{km/h}] \leq v_{\text{dvr}} \leq v_{\text{ref}} + 1[\text{km/h}]$.
- Decrease speed (Fig. 9.3c): $v_{\text{dvr}} > v_{\text{ref}} + 1[\text{km/h}]$.

9.4.3. Experimental Results

In this section, we will experimentally determine the amount of energy that eco-driving is able to save. Subsequently, we will compare this results with simulations in the hi-fi model with the velocity profiles generated experimentally.

While performing the experiments, a wind velocity of $30[km/h]$ was registered, with a direction approximately matching the selected road. Hence, the experimental eco-driving energy savings are separated for headwind and tailwind driving, and shown in Table 9.2. In average, we obtained 6.94% of energy savings.

Note that the percentages in Table 9.2 were obtained from 20 experiments performed by the two drivers, i.e., four experiments for each wind direction, plus the corresponding baselines. The velocity profiles of two experiments with its baselines are depicted in Fig. 9.4, one for each driver with the specified wind direction.

Table 9.3: Simulated energy savings

Wind direction	Driver	Energy savings	Average
Headwind	Driver 1	6.48%	6.89%
	Driver 2	7.29%	
Tailwind	Driver 1	17.50%	15.96%
	Driver 2	14.42%	
		Total Average	**11.43%**

Here, the blue dotted line represents the baseline and the red line shows the driver behavior when receiving eco-driving feedback.

Tailwind driving saves more energy than headwind. In this case, the difference is approximately a factor of three (see Table 9.2). The difference in energy savings between the drivers can be explained by their own driving style and experience, as well as random disturbances, e.g., changes in intensity and direction of the wind, temperature variations, traffic conditions, etc.

The experimental velocity profiles were logged by Vector CANoe and used as input to the hi-fi vehicle model. Using the same baseline for each driver and wind direction, the simulated energy savings are shown in Table 9.3. Tables 9.2 and 9.3 show correlation between experimental and simulated energy savings, verifying that the hi-fi vehicle model has been validated. Note that in both cases the eco-driving solution to (9.27) reduces the energy consumption.

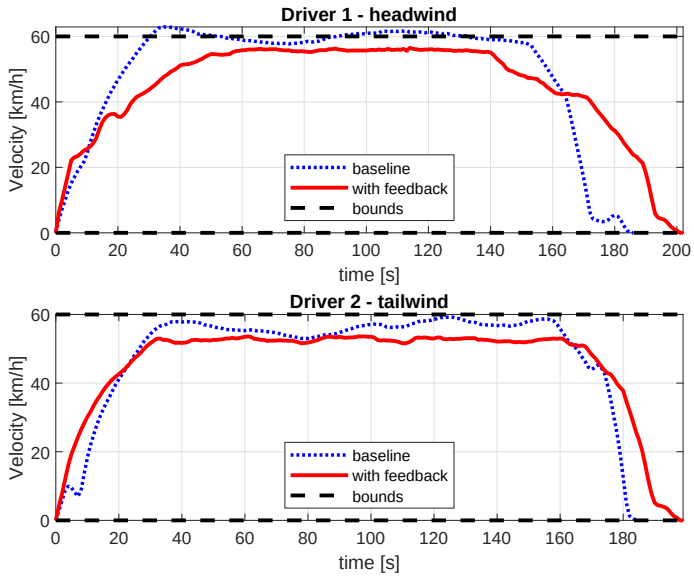

Figure 9.4: Experimental velocity profiles

The mismatch between the simulated energy savings presented in Table 9.2 and the experimental energy savings shown in ables 9.2 is due model uncertainty. Note that the power consumption model (9.3) has a low accuracy since the coefficients β_0, β_1 and β_2 are approximated as constant values. However, these coeffcients are dependent on the motor torque and angular velocity. The use of models that consider this dependency will definitely improve the accuracy of the simulations. However, it is also increase the complexity of the optimal control problem, which is inconvenient for real-time implementation. In practice, the simple model that was used in the experiments was able to produce satisfactory experimental results.

The variability of the energy savings obtained by the different drivers (Table 9.2) was an expected result. We can see the drivers as the actuators of for eco-driving closed-loop control system. Using different actuators with the same control produces different performance in the closed-loop system. This clearly shows that the drivers play an important role for saving energy for this application. Possible method to mitigate this dependency are driver's training, improved human machine interfaces (possibly including haptic feedback), semi-autonomous assistance, etc.

9.5. Conclusions

This chapter has presented an efficient shrinking horizon implementation to solve the eco-driving OCP. The implementation has been demonstrated on a case study of a fully electric bus, driving on an inner-city public transport route. We have shown that the computational performance can be reduced significantly using the proposed implementation. Furthermore, a energy consumption reduction of 11.43% is achieved on a simulation study for the case that the vehicle is fully autonomous and a reduction of 6.94% is achieved experimentally for the case that the driver is 'coached' using a driver assistance system. The obtained results are promising in terms of energy savings by providing feedback to the driver and, at the same time, it has become evident that better results can be achieved by improving the accuracy when following the eco-driving feedback.

References

[1] G. P. Padilla, S. Weiland, and M. C. F. Donkers, *A Global Optimal Solution to the Eco-Driving Problem,* IEEE Control Systems Letters (2018).

[2] M. Diehl, H. J. Ferreau, and N. Haverbeke, *Efficient numerical methods for nonlinear mpc and moving horizon estimation,* in *Nonlinear Model Predictive Control: Towards New Challenging Applications* (2009).

[3] *CANoe – ECU & network testing | vector,* (2020).

10

Conclusions and Recommendations

In this final chapter, the research questions proposed in Chapter 1 are explicitly answered by conclusions linked to the contributions made in the chapters of this thesis. Additionally, recommendations for future research will be given. Finally, the possible implications of the contributions of this thesis will be discussed.

The use of energy management strategies to improve energy efficiency of electrified vehicles is a promising and easily implementable approach that could accelerate the adoption of electric vehicles in the market and, consequently, contribute to clean mobility. This has motivated the development of nonlinear optimal optimal control methods for energy management strategies in this thesis. In this work, we have divided energy management strategies into two groups that are complementary in some degree. The first group is eco-driving, this approach aims to obtain the optimal velocity profile that minimizes the energy consumption of the vehicle. The second group is Complete Vehicle Energy Management (CVEM), which assumes a given velocity profile (or equivalently a given power request) to obtain the optimal power-split among all the subsystems of the vehicle that minimizes the energy consumption.

This chapter is organized as follows. In Section 10.1, the research questions proposed in Chapter 1 are explicitly answered by conclusions linked to the contributions made in the chapters of this thesis. Recommendations for future research are provided in Section 10.2. Finally, the possible implications of the contributions made in this thesis are discussed in Section 10.3.

10.1. Conclusions

For the sake of readability, the research questions presented in Chapter 1 will be repeated in the following paragraphs. Bellow each question, the conclusions of this thesis that address the respective question are detailed.

Main Research Question

Can the current eco-driving and CVEM methods be improved by considering the integration of dynamical features of the systems and the uncertainty of real traffic scenarios such that both higher energy savings and an adequate computational performance are obtained?

This question has been analysed in four different branches, where additional sub-questions were posed. These branches are detailed below.

B.1 Integrating dynamical systems of higher complexity in the CVEM problem

Research Sub-question 1

What modelling frameworks are suitable to formulate CVEM optimal control problems that consider components represented with models of a higher complexity?

The following contributions have addressed this sub-question:

- In Chapter 3, the traditional eco-driving optimal control problem formulation, which often aims to minimize the energy consumption of a vehicle driving on a straight trajectory, has been extended to consider the energy losses that appear while cornering. We deviated from the more common approach to solve cornering effects by limiting centripetal acceleration of the vehicle. Instead, we have proposed a model that approximates cornering forces into the longitudinal axis of the vehicle. The main feature of this model is its simplicity, since it depends only on the geometry of the vehicle and the road. This has eliminated the necessity to estimate parameters that can be dependent on operational operational conditions, i.e., the slip angle. The proposed modeling framework has been used to formulate a general eco-driving optimal control problem formulation that can be used for vehicles driving in both straight and curved trajectories. The proposed modelling framework and optimal control problem formulation have been validated using a high-fidelity model. Furthermore, simulation results have shown improved energy savings for cornering maneuvers in trajectories with large curvatures, which are approximately 8% larger than traditional eco-driving strategies.
- In Chapter 4, we have proposed an energy optimal strategy to coordinate fully autonomous vehicles crossing an intersection. We have demonstrated that the eco-driving problem can be extended such that, for each vehicle in the intersection, it obtains velocity profiles and the intersection crossing order that minimizes the total consumption of energy in the intersection, while avoiding collisions.
- An alternative modelling framework for CVEM based on interconnected port-Hamiltonian systems has been proposed in Chapter 7. In this approach, the subsystems in the vehicle have been represented as dissipative dynamical systems that inherently describe energy losses and changes of internal energy in the subsystem. Thus, we have unified the power-based concepts of energy buffers and power converters in a single dynamical model. Additionally, a systematic approach to formulate a decomposable optimal control problem for CVEM has been proposed, which is useful for distributed static optimization. Simulation results, where the power-based and the port-Hamiltonian approaches were compared, have shown the advantages of the proposed modeling framework. Moreover, it has been shown that the extra freedom obtained by describing power in terms of conjugated variables can capture additional physical features that are impossible with power-based approaches.
- In Chapter 9, we have extended the traditional CVEM modelling framework to consider subsystems with energy buffers described by nonlinear dynamics and power converters defined by quadratic functions dependent on the states and inputs of the subsystems. This framework has enabled the integration of the ecodriving and CVEM problems into a single optimal control problem formulation. This has allowed us to break, in some degree, the strong dependency on a priori information of the driv-

ing cycle that traditional CVEM formulations have. Numerical simulations for a series-hybrid electric vehicle have shown that including eco-driving into the CVEM problem, can approximately decrease energy consumption by 4.7% with respect to a CVEM approach without eco-driving.

Research Sub-question 2

What static optimization methods are appropiate to solve the different configurations of eco-driving and nonlinear CVEM optimal control problems?

The contributions linked to this sub-question are described in the following list.

- In Chapter 2, we have proposed to solve the eco-driving optimal control problem using a sequential quadratic program with a positive definite Hessian approximation, which was obtained from the diagonal elements of the real Hessian matrix. The convergence of the proposed algorithm has been guaranteed since the proposed Hessian approximation satisfies, at every iteration, the theoretical conditions required for convergence of sequential quadratic programs. Consequently, in Chapter 9, we have demonstrated that this optimization method can be used for online implementations of eco-driving. This optimization method was used as the basis for a shrinking horizon implementation that solves the eco-driving problem for a fully electric bus driving a typical city route. Experimental results have shown energy savings of approximately 7% when the driver is assisted by the eco-driving strategy to follow the energy optimal velocity profile.
- In Chapter 4, an energy optimal strategy to coordinate autonomous vehicles crossing an intersection was proposed. For each vehicle, the proposed formulation, aims to obtain the velocity profiles and the intersection crossing order that minimize the aggregated energy consumption subject to safety constraints. The combinatorial nature of the energy optimal conflict resolution problem has been handled using a sequential mixed integer program.
- In Chapter 5, the interconnected nature of CVEM problem was used to propose a separable optimal control problem formulation. The highly structured optimal control problem has been addressed using a primal-dual proximal splitting method to obtain a distributed optimization algorithm for large-scale nonconvex CVEM problems.
- In Chapter 6, we have presented a CVEM stochastic optimal control problem, where realizations of the uncertain driving conditions have been introduced as random constraints in the CVEM formulation. Solutions to this CVEM problem have been obtained using a scenario-based optimization approach in a receding horizon fashion. Thus, we have shown

that this is a tractable method, in which an intuitive tradeoff can be made between computational complexity and robustness depending on the number of scenarios considered.

- In Chapter 8, to achieve the integration of the eco-driving and CVEM problems, we proposed an extension of the CVEM framework that allows for non-linear dynamics. The nonconvex and nonlinear integrated optimal control problem has been solved using a sequential quadratic program with Tikhonov regularization in combination with a dual decomposition approach. Hence, we have obtained a scalable optimization method with satisfactory convergence that solves the integrated eco-driving and CVEM problem.

B.2 Higher effciency

Research Sub-question 3

Under which conditions is it possible to provide guarantees for the global optimality of the solutions to the eco-driving and CVEM prolems?

The following contributions answered this sub-question.

- In Chapter 2, the eco-driving optimal control problem, which is inherently nonconvex, has been analyzed in detail. After, a convenient reformulation and discretization of the problem, a set of physically realistic conditions that guarantee the existence of a unique solution were found. Consequently, we have demonstrated that the solution to the eco-driving optimal control problem is globally optimal.
- In Chapter 5, a deep analysis of the highly structured CVEM optimal control problem has been presented. Taking advantage of obtained insights, we have proven the existence of only multiple global solutions to the CVEM problem under realistic operational conditions.

B.3 Scalability and flexibility

Research Sub-question 4

What optimization method with convergence guarantees can lead to a simple implementation of CVEM strategies maintaining an acceptable numerical performance?

This sub-question was addressed in Chapter 5, where the CVEM problem has been conveniently reformulated such that it is separable in terms of interconnected subsystems and time intervals. A Primal Dual Splitting method has been applied to the reformulated problem to obtain a flexible distributed optimization algorithm. This algorithm breaks down the complexity of the problem into several simpler highly structured coordinated sub-problems, which

has brought a satisfactory scalability as a consequence. Moreover, the implementation of the algorithm has been simplified using spectral methods to automatically select the step-sizes of the optimization algorithm at every iteration. This also has provided a reduced computational time for the convergence of the algorithm. Numerical examples have shown that this method can be approximately 3 times faster than off-the-shelf solvers and it can solve problems with a 100 times larger time horizon. The results obtained have demonstrated that the methodology presented in this work can be used to solve large-scale CVEM problems, thus highlighting the scalability of the algorithm.

B.4 Anticipation and robustness

Research Sub-question 5

Considering real driving conditions, what are the improvements in energy savings for eco-driving and CVEM strategies that exploit available preview information, i.e., historical data and communication networks?

The contributions linked to this sub-question are summarized below.

- In Chapter 4, an energy optimal coordination of autonomous vehicles crossing intersection was studied. In this case, we assumed that I2V and V2V communications provide complete information about of the driving conditions to all the vehicles. Simulation results for this ideal scenario have shown that coordinated autonomous vehicles can reduce energy consumption to approximately 16.2% compared to human driven vehicles without coordination.
- In Chapter 6, the uncertainty produced by real-life conditions has been considered to formulate stochastic optimal control problems for energy management. Solutions to this CVEM problem, known as traffic-aware energy management strategies, have been obtained using a scenario-based optimization approach in a receding horizon fashion. Different alternatives to include traffic information for the generation of scenarios have been explored, i.e., method based on (average) traffic flow information, a method based on Gaussian process regression, and a method that combines both. Simulation results of a case study that considers series-hybrid vehicle have shown a deviation of 0.75% from the optimal consumption with a suitable mix of the available information and 1.79% using variable step-size predictions.

10.2. Recommendations for Future Research

In this thesis, solution methods for nonlinear optimal control problems that emerge from eco-driving and CVEM applications have been studied. In particular, this thesis has contributed to formulate modeling approaches, to prove global optimality

of the solutions, to enhance the scalability of the optimization algorithms and to exploit preview information in the energy management problems to generate anticipative and robust strategies. In this section, some recommendations for possible extensions to the aforementioned topics are given.

10.2.1. Validation of CVEM in a Vehicle Prototype

Part II of this thesis has been devoted to study methods for CVEM formulations. Unfortunately, all these promising approaches have been only validated using numerical simulations. An experimental validation using a prototype vehicle will provide better insight of the online implementability of the proposed approaches and it will allow to asses the energy savings that could be achieved. It would be specially interesting to use the methods presented in Chapter 2 and Chapter 6, to explore the advantages and limitations of an online CVEM implementation that handles the uncertainty in the traffic scenarios. Another promising exploration is the extension of the experimental case study presented in Chapter 9 to consider the integrated eco-driving and CVEM problem formulated in Chapter 8.

10.2.2. Online Parameter Estimation

online implementation of energy management strategies in a receding horizon fashion require knowledge of future disturbances that might affect parameters of the subsystems models, e.g., the ambient temperature could induce changes in the heat and ventilation system model, or alter the rolling resistance coefficient, thus, directly affecting the power request. Therefore, online parameter estimation could become an interesting path to explore, in which parameters that have a large impact on the CVEM strategy could be automatically updated during operation.

10.2.3. Generation of Large-scale Benchmarks for Energy Management Strategies.

Evaluating the performance of online and offline methods for solving energy management requires the use of benchmarks. Traditionally, benchmarks for energy management strategies are generated using dynamic programing. However, due to the "curse of dimensionality", this approach might not be usable by energy management problem formulations with contain a significant number of states and a large time horizon. Taking advantage of the proved global optimality of the solution and the scalable optimization method presented in Chapter 2 and Chapter 5, it is possible to generate relevant benchmarks for large-scale energy management problems, which, to the best of the author's understanding, are scarce in the literature.

10.2.4. Possible Global Optimal Solutions to the Integrated Eco-driving and CVEM Problems

The advantages of integration eco-driving and CVEM problems have been highlighted in Chapter 8. Unfortunately, the optimal control problem is nonconvex, therefore, global optimality of the solutions cannot be directly guaranteed. More-

over, this optimal control problem formulation contains a significant number of states, which limits the use of dynamic programming approaches to obtain global solution to the problem. This motivates the necessity to conduct a deeper analysis on the optimal control problem formulation for integrated eco-driving and CVEM problems. Some light in this path is provided by the fact that the global optimality of the solutions to eco-driving and CVEM have been proved independently in Chapter 2 and Chapter 5, respectively. Moreover, numerical results of the case study presented in Chapter 8 have shown the same cost for multiple solutions. This empirical evidence might imply that the integrated eco-driving and CVEM optimal control problem has only global solutions.

10.2.5. Distributed Optimization Methods for Port-Hamiltonian CVEM

The port-Hamiltonian modelling framework for CVEM introduced in Chapter 7 interconnects each subsystem through ports, in which, a pair of conjugated variables represents power. For instance, the port-Hamiltonian representation of an electric battery considers the current and the voltage at the terminals as conjugated variables, of which the product describes the power provided by the battery. The relevance of this physically insightful modelling framework has been highlighted in Chapter 7. Moreover, it has been shown that the CVEM optimal control problem can be separable, which allows the use of distributed optimization methods to solve the problem. However, the optimization method for port-Hamiltonian methods have not been addressed in detail. Scalability of the optimization methods is an important topic to consider, since the port-Hamiltonian framework introduces a larger number of decision variables. Therefore, distributed optimization approaches are interesting candidates to be applied to this framework. Numerical conditioning of the optimization problem could be an additional topic of interest. The CVEM problem can consider subsystems with slow and fast dynamics that could yield to ill-conditioned formulations. Therefore, systematic methodologies to solve this limitation are needed.

10.2.6. CVEM with On/off Auxiliaries

The CVEM approaches proposed in Part II of this thesis consider subsystems that are manipulated through a bounded input signal. In practice, many auxiliary subsystems in the vehicle can be only controlled by on/off actions. Therefore, it becomes attractive to explore modelling approaches and solution methods for nonlinear CVEM optimal control methods with mixed integer decisions variables. A solution strategy along the lines of Chapter 4 could be considered.

10.2.7. Optimal Component Sizing

In order to be cost effective, the components of a vehicle should be carefully dimensioned. A large portion of literature has only focused in dimensioning the power train components for hybrid vehicles. However, the holistic nature of the CVEM framework could be applied to component sizing problems. This might imply the necessity to use highly scalable optimization methods and to solve multi-objective

optimization problems that optimize the component size for all the subsystems in the vehicle for higher energy efficiency and reduced production cost.

10.2.8. Eco-routing, Eco-driving and CVEM

Eco-routing aims to plan an energy efficient route for a vehicle. In literature ,this approach has been widely explored. However, the integration with eco-driving has recently appeared. Finding the energy optimal route and velocity profile is a challenging problem that promises big rewards in terms of energy savings. This could be further extended by considering CVEM in the problem formulation. Offline solutions to study the achievable performance and simplifications of the problem for online implementation is an important research direction, where modelling frameworks and optimization methods need to be explored.

10.2.9. CVEM for Fleets

The CVEM framework used in this dissertation could be extended to include cooperation as one its main features. A group of vehicles could potentially be coordinated to increase the collective energy savings. For instance, energy efficient platooning is a promising application where the collaboration between vehicles not only increases energy savings, but also reduces the operational cost. Another example is travel scheduling for a fleet of electric buses where considering eco-routing, eco-driving and CVEM concepts can be used to obtain an energy optimal travelling schedule tha maximizes the driving range of the whole fleet. Solving the conceptual and technical challenges of these aforementioned applications might yield important research directions for the future of energy management strategies.

10.3. Implications

The contributions made in this dissertation have implications in the future research paths of energy management strategies, which have been implicitly discussed in the previous section. The certifications for global optimality of the solutions to eco-driving and CVEM, presented in Chapter 2 and Chapter 5, eliminate the necessity to use dynamic programming approaches to find global solutions to these problems, thus, opening the path to easily generate benchmarks for large-scale energy management problems. The main contribution of this thesis is the extension of the CVEM framework as a globally optimal, highly scalable, anticipative and robust approach for energy management strategies. This has paved the way for future explorations where "cooperation" can be incorporated into the CVEM framework for interconnected (and possibly autonomous) vehicles.

Acknowledgements

The last 4 years have been a wonderful learning journey not only in the scientific path but also in personal experiences. This adventure would have not been the same without the support of many people that have been close to me.

I would like to express my sincere gratitude towards my supervisor Tijs Donkers. Thank you for every effort dedicated to clarifying my doubts, for your guidance and trust. Your (extra) optimism and good sense of humor definitely made each one of our meetings enjoyable. I am grateful for having had the opportunity of doing this PhD under your supervision.

Next, I would like to thank my promotor Siep Weiland for his support during my PhD and master's degree. Thanks for sharing your wisdom. Your natural curiosity and your passion for scientific discussions have always been a source of inspiration.

I also want to express my gratitude to the committee members for their efforts in reading and evaluating my thesis. Prof. Frank Willems, prof. Mark Cannon, prof. Antonio Sciarretta, dr. Sergio Grammatico and dr. Emilia Silvas, your feedback has contributed to improve the quality of my dissertation.

It was very pleasant to work together with the people in the EVERLASTING project. I owe my gratitude to Anouk for being open to support my research inside VDL, many chapters in this thesis would have not been possible without this. Thanks to my fellow PhD candidate Camiel. It was a pleasure to collaborate in a publication within ths project. Moreover, our regular meetings were always insightful. Special thanks to Will from whom I learned the special details that are needed to succeed in a european project. I also enjoyed our conversations during the trips to the many general assemblies we attended.

My gratitude goes also for my students Roshni, Rahul, Aparna, Nikos, Roberto and Meherzad. Supervising you was also an enjoyable learning experience for me. Special thanks to Alfredo, Carmine, Zuan and Juan. Without you I would not have been able to complete this work.

My time at the Control Systems (CS) group has been memorable. Thanks to Henrik, Giuseppe, Karthik, Feye, Amritam and Zuan for the nice coffee breaks. To my office-mates Damin, Tuan, Constantijn, Bahadir, David, Gerben and Cristi thanks for making Flux 5.078 a warm place to be. To the old crew Veaceslav, Alejandro, Marcella, Gullio, Ioannis, Dhruv and Harm thanks for the spontaneous beers at "Het Walhalla" to relieve the tensions of day to day research at CS. My special gratitude to Zuan, who was my first student, later a colleague but mainly he has become a close friend. To all the members of CS who I have not mentioned, thank you for creating a very open and pleasant working environment. Particularly, thanks to Diana and Hiltje not only for supporting our administrative tasks but also for your efforts in making our group a home.

Han pasado ya 6 años desde que deje Ecuador para seguir mi sueño de realizar un doctorado. Los sacrificios no han sido fáciles, pero los resultados son satisfactorios. Mi familia ha sido un punto de apoyo fundamental para alcanzar mis objetivos y esta tesis es dedicada a ellos.

Gracias a mis padres que sacrificaron su tiempo y comodidad para darme la educación necesaria que me ha permitido llegar a este punto en mi vida. Gracias por su consejo e incondicional amor. Espero poder seguir su ejemplo y ser para Gilberto lo que ustedes han sido para mí. Gracias por tener fe en mí.

He sido bendecido con la oportunidad de tener a mis abuelos junto a mi durante todo este tiempo. Gracias por estar siempre orgullosos de mí. Al igual que mis padres ustedes han sido el ejemplo que he tratado de seguir para ser un mejor ser humano. Gracias por todo lo que he aprendido de ustedes. No podría haber llegado tan lejos sin su influencia.

Pamela, gracias por ser mi confidente y consejera. Por el animo que me has dado en los momentos difíciles. Créeme tu has sido parte fundamental en este proceso, esta tesis también lleva parte de ti.

Juan Carlos, son casi 20 años que he tenido la fortuna de considerarte mi amigo. Gracias por el apoyo integral que me has dado en este tiempo. Para mi, es una suerte y un privilegio que hayas estado también en esta etapa de mi vida.

Linda, gracias por salvarme. Tu apoyo incondicional en los momentos más difíciles fue crucial. Tu has sido la fuerza e inspiración que necesitaba para salir adelante. Gracias por ese amor incondicional que has demostrado. Espero poder ser todo lo que tu significas para mí.

Finalmente, Gilberto gracias por ser el motor de mi vida.

Curriculum Vitæ

Paul Padilla was born on 12-03-1983 in Quito, Ecuador. After finishing his bachelor's in electrical engineering in 2006 at Universidad de las Fuerzas Armadas in Ecuador. From 2006 to 2014, he worked at his own company Sigmatron Cia. Ltda. developing several industrial automation projects and 3 in-house products registered as his intellectual property in the Ecuadorian Institute of Intellectual Property (IEPI). In 2014, we won the SENESCYT scholarship from the ecuadorian government and began his master's degree studies in Systems and Control at Eindhoven University of Technology in the Netherlands.
In 2016, he graduated within the Controls Systems group in collaboration with the additive manufacture department at TNO on the proof of concept of advanced actuators (thermal pixels) for thermal control of wafers in lithography machines. In 2016, he started his PhD project at Eindhoven University of Technology of which results are presented in this dissertation.